NASA Contractor Report 3821

Refinement and Evaluation of Helicopter Real-Time Self-Adaptive Active Vibration Controller Algorithms

Mark W. Davis

CONTRACT NAS2-11260
AUGUST 1984

NASA

NASA Contractor Report 3821

Refinement and Evaluation of Helicopter Real-Time Self-Adaptive Active Vibration Controller Algorithms

Mark W. Davis
United Technologies Research Center
East Hartford, Connecticut

Prepared for
Ames Research Center
under Contract NAS2-11260

National Aeronautics
and Space Administration

**Scientific and Technical
Information Branch**

1984

TABLE OF CONTENTS

PREFACE

This investigation was sponsored by the National Aeronautics and Space Administration, Ames Research Center, California, under contract NAS2-11260. The NASA technical representative for this contract was Stephen A. Jacklin of the Low Speed Aircraft Research Branch. The Real-Time Self-Adaptive (RTSA) active vibration controller used as the framework in developing the computerized generic controller studied in this investigation was previously developed and evaluated at the United Technologies Research Center under contract NAS2-10121, "Analytical Design and Evaluation of an Active Control System for Helicopter Vibration Reduction and Gust Response Alleviation." The principal investigator involved in the earlier study was Robert B. Taylor. He was also responsible for laying much of the groundwork and selecting the algorithms to be included in the generic controller for the current investigation. His significant contributions and support are gratefully acknowledged. Charles Niebanck and Kurt Hilzinger, Sikorsky Aircraft, contributed significantly in running the many closed-loop computer simulations and assisting in interpreting the results, as well as performing the separate open-loop nonlinearity study reported in the Appendix. Jan Sniffin, Senior Engineering Assistant, UTRC, was responsible for generating the many plots needed to interpret the results as well as those contained herein. Finally, the author would like to acknowledge the support and advice provided during this investigation by Anton J. Landgrebe, Manager, Aeromechanics Research, UTRC.

SUMMARY

A Real-Time Self-Adaptive (RTSA) controller has been used as the framework in developing a computerized generic active controller that can be used to alleviate helicopter vibration by closed-loop implementation of higher harmonic control. This generic controller gives the capability to readily define many different configurations by selecting and tuning one of three different controller types (deterministic, cautious, and dual), one of two linear system models (global and local), and one or more methods of applying limits on control inputs. The algorithms associated with these controller types have been refined, evaluated, and compared as a step toward selecting the best active controller for alleviating helicopter vibration.

The helicopter simulation used to evaluate these alternative configurations is a nonlinear aeroelastic vibration computer analysis (G400) that models the four-bladed H-34 rotor mounted on the NASA Ames Rotor Test Apparatus (RTA) which represents the fuselage. A representative baseline configuration is defined for each of the three controller types. After proper tuning, all three baseline controllers provide more effective vibration reduction and converge more quickly and smoothly with smaller control inputs than the initial RTSA controller (deterministic with external pitch rate-limiting) similar to the best configurations studied by the United Technologies Research Center in an earlier investigation. Excellent controller performance is demonstrated throughout a range of steady flight conditions representing moderate to high flight speeds and thrust values. Reduction in vibration from 75 to 95 percent is achieved with amplitudes of higher harmonic control (3, 4 and 5 per rev) of less than one degree. Also, good transient performance and vibration alleviation is exhibited in transient maneuvers involving a sudden change in collective pitch; however, some retuning is required.

Predicted results at several different flight conditions indicate that higher harmonic control can have a significant effect on rotor blade stresses and performance. However, the existence of multiple higher harmonic control solutions for low vibration indicates the potential for the selection of control inputs that reduce the impact on blade stresses and performance.

The results of the current investigation indicate no definite advantage to any of the three basic controller types. When a configuration is properly defined and tuned, any of the three controller types can provide excellent performance at the flight simulations considered in this study. It is demonstrated that internal limiting of the control imputs significantly improves the overall performance of the deterministic controller. For the transient maneuvers considered, the global system model provides significantly better performance than the local system model. For all steady flight conditions considered, the behavior exhibited by both the global and local models is very similar.

LIST OF FIGURES

LIST OF FIGURES (Cont'd)

LIST OF FIGURES (Cont'd)

LIST OF FIGURES (Cont'd)

LIST OF FIGURES (Cont'd)

LIST OF FIGURES (Cont'd)

LIST OF TABLES

LIST OF SYMBOLS

$C_{L\alpha}$	lift curve slope, N.D.
C_T	thrust coefficient, N.D.
c	blade chord, m (ft)
D	rotor drag, N (lb)
F_H	vector of cosine and sine components of 4 per rev forcing at the hub
H	row vector of control inputs used in Kalman filter formulation (form dependent on system model, see Eqs. (41) and (50)), rad
I	interharmonic coupling ratio, N.D. (see Fig. A-2)
J	quadratic performance index, N.D. (see p. 23)
J_Z	quadratic vibration performance index (with weighted output parameters only), N.D.
K	vector of Kalman-filter gains, 1/rad or N.D
L	rotor lift, N (lb)
L_{HHC}	local blade lift loading due to higher harmonic control, N/m (lb/ft)
M	covariance matrix of state vector of identified system parameters, $(g's/rad)^2$ or $(g's^2/rad)$ or $g's^2$ depending on matrix element and system model
M_{H4P}	mobility matrix relating 4 per rev fixed system accelerations at the hub to 4 per rev hub forces
M_{RTA}	mobility matrix relating 4 per rev accelerations in the rotor test apparatus to 4 per rev hub forces
m	total number of control parameters (both cos and sin components), N.D.
N	number rotor blades or per rev frequency for an N-bladed rotor, N.D. or 1/rev

P	covariance matrix of state vector of identified system parameters, $(g's/rad)^2$ or $(g's^2/rad)$ or $(g's^2)$ depending upon matrix element and system model, see Eq. (52)
P_{TT}	covariance matrix of jth row of transfer matrix, $(g's/rad)^2$
P_{TZ}	cross-covariance of jth row of transfer matrix and jth element of vector of uncontrolled vibration levels, $(g's)^2/rad$
P_{ZZ}	covariance of jth element of vector of uncontrolled vibration levels, $(g's)^2$
Q	covariance matrix of changes in state vector of identified system parameters, $(g's/rad)^2$
Q_{t_1}	generalized coordinate of first blade torsion mode, N.D.
Q_{v_1}	generalized coordinate of first blade edgewise mode, N.D.
Q_{w_i}	generalized coordinate of ith (i=1, 2, 3) blade flatwise mode, N.D.
R	covariance of measurement noise, $(g's)^2$; or total blade radius, m (ft)
r	blade radius, m (ft)
T	transfer matrix between control inputs and measured outputs, g's/rad
TGA	mobility matrix relating vibration in rotor test apparatus to fixed system hub vibration, N.D.
V	airspeed, m/s (kt)
W	vector of random variables describing system parameter variation (see Eq. (42)), g's/rad or g's

W_Z	weighting matrix in performance index on output (vibration) parameters, $(1/g's)^2$
$W_{\Delta\theta}$	weighting matrix in performance index on rate of change of control inputs, $(1/rad)^2$
W_θ	weighting matrix in performance index on control amplitude, $(1/rad)^2$
X	state vector of system parameters to be identified, g's/rad or g's
Z	vector of measured output parameters including harmonic coefficients of vibration, g's
Z_H	vector of cosine and sine components of 4 per rev accelerations at the hub (fixed system), g's
Z_o	vector of uncontrolled response levels, g's
Z_{opt}	vector of prescribed optimum or desired output (vibration) parameters, g's
Z_{RTA}	vector of cosine and sine components of 4 per rev accelerations in the rotor test apparatus, g's
ZC	vector of output parameters to be controlled (see Eq. 53), g's
α_{HHC}	angle of attack due to higher harmonic control, rad
β	switching function indicative of controller type in generic minimum variance control algorithm (see pp. 22 and 23)
γ	control vector used in learning term for dual controller (form dependent on system model, see p. 18), rad
$\Delta R_+/\Delta R_-$	magnitude of nonlinearity of open-loop response (see Fig. A-1), N.D.

ΔZ	incremental change in response, $Z_i - Z_{i-1}$, g's
$\Delta\theta$	incremental change in control inputs, $\theta_i - \theta_{i-1}$, rad or deg
$\Delta\theta_{max}$	maximum allowable incremental change in control inputs, deg
η	measurement noise, g's
θ	vector of harmonics of control variables, rad or deg
λ	empirical stochastic control constant, N.D.
ρ	air density kg - sec^2/m^4 ($lb\text{-}sec^2/ft^4$)
σ	rotor solidity, N.D.
ϕ	phase angle of open-loop control input, rad or deg
ϕ_Δ	angle of nonlinearity of open-loop response (see Fig. A-1), rad or deg
ψ	rotor azimuth angle, deg
Ω	rotor speed, rad/sec
ω	modal frequency, rad/sec

Subscripts

C	cosine component
c	cautious controller
D	dual controller
Det	deterministic controller
eff	effective value
i	time step or rotor revolution number

j	measurement number
jj	diagonal element of output weighting matrix
S	sine component
t	blade torsion mode
v	blade edgewise mode
w	blade flatwise mode
3, 4, 5	vector or matrix elements corresponding to 3, 4, or 5 per rev control inputs

Superscripts

T	matrix or vector transpose
*	calculated optimum control input

Special Symbols

E{ }	expected value
3P, 4P, 5P	denotes 3, 4, or 5 per rev
(^)	estimated value
| |	denotes amplitude of control input
$\angle$	denotes phase angle

INTRODUCTION

In order for the coming generation of helicopters to reach their full potential, significant reductions in vibration response must be accomplished. Commercial passenger acceptance of the helicopter as a viable alternative to other means of transportation will largely depend upon the perception of low vibration and a "jet-smooth" ride. Commercial utilization of the helicopter is directly impacted by maintenance costs and cruise velocity. Thus, increasingly stringent vibration requirements coupled with the desire for high speed aircraft have made vibration alleviation one of the prime objectives of the helicopter industry.

Many advancements in the reduction of vibration have been achieved in recent years, but the need for further improvements is readily apparent in not only the significant amount of research currently being conducted, but also in the diverseness of the vibration control approaches being pursued. References 1 and 2 represent the renewed interest in understanding the fundamental sources of vibration. By desensitizing the blade to vibratory rotor airloads, it is possible to passively minimize the excitation forces transmitted to the fuselage with a resultant decrease in vibration throughout the aircraft. Recognizing that there will always be some residual level of vibration transmitted to the fuselage, Ref. 3 formulates a method for optimizing more conventional procedures that use passive devices, such as vibration absorbers and isolators, to desensitize critical points in the fuselage to excitation forces transmitted from the rotor. The potential limitation of these methods is that they may not result in vibration alleviation over an extensive range of flight conditions.

In contrast, the use of higher harmonic control in conjunction with optimal control theory potentially allows vibration reduction to be achieved throughout the flight envelope and during transient maneuvers as well. Reference 4 presents an excellent review of past helicopter higher harmonic control work. The alternative algorithms presented for real-time self-adaptive active vibration controllers represent the state-of-the-art. In this vibration control approach, higher harmonic blade root cyclic pitch is used to modify blade airloads which in turn reduce harmonic blade forcing. The higher harmonic blade pitch can be mechanically input through the standard helicopter swashplate configuration. The effectiveness of higher harmonic control in reducing vibration was verified experimentally by open-loop wind-tunnel model testing in Refs. 5 through 7. In Ref. 8, the loop was closed and vibration was reduced by actively adjusting multicyclic pitch amplitudes to minimize vibration based on off-line identification of the relationship between vibration and control inputs. References 9 through 11 successfully combined

the concepts of higher harmonic control with optimal control theory to actively reduce vibration in real-time with on-line Kalman filter identification of system parameters. References 9 and 10 present the results for a numerical simulation using a nonlinear aeroelastic helicopter vibration analysis, while Ref. 11 presents results for experimental testing of a model articulated rotor in a wind tunnel.

Both Refs. 9 and 11 formulated the overall vibration control approach in much the same manner. This approach is characterized by the assumption that the helicopter can be represented by a linear, quasi-static transfer matrix (T-matrix) relationship between the harmonics of vibration and the harmonics of the multicyclic control inputs. In order to account for changes in the T-matrix due to system nonlinearities and variations in flight condition, the T-matrix is identified and tracked on line by a real-time Kalman filter identification algorithm. Higher harmonic control is updated on the order of once every rotor rev based on the results of a real-time minimum variance control algorithm used to minimize a weighted mean square sum of harmonic vibration and control inputs. This is the fundamental approach taken in most of the research being done today.

The major differences in the approach taken by these two references is the controller type and system model used to develop the computer control algorithms. The active controller implemented in Ref. 9 was based upon a deterministic control approach, which assumes that all system parameters are explicitly known, and a local system model with external rate-limiting of control inputs. Reference 11 experimentally tested both a deterministic controller with external rate-limiting and a cautious controller with no limiting other than that due to the stochastic caution term which reflects the degree of uncertainty in the estimation of identified system parameters. Both of the controllers studied in Ref. 11 were based upon a linearized global system model. The results of Ref. 11 indicated that the performance of the cautious controller was significantly less erratic than the deterministic controller with external rate-limiting.

Reference 12 extended the investigation of Ref. 11 and again concluded that the cautious controller exhibited smoother performance than the externally limited deterministic controller. In addition, Ref. 12 also proposed but did not test the performance of a new algorithm involving a stochastic learning term. It was suggested that the inherent system probing caused by this learning in the resultant "dual" controller would enchance system identification and, thus, would enable the dual controller to achieve lower vibration levels than otherwise possible. At the time of this reference, the performance of the dual controller had not been verified either experimentally or theoretically on a helicopter vibration simulation.

Reference 13 considered the influence of errors in the T-matrix estimate on controller stability. Reference 13 also proposed algorithms for varying certain Kalman filter covariances as a function of steady aircraft acceleration in order to reflect changes in the system and/or the level of noise. In Refs. 14 and 15, the effects of system nonlinearities on controller performance are considered. Reference 14 compares the performance of both the deterministic controller with internal rate-limiting and the cautious controller, but uses an arbitrary nonlinear simulation model that has not been derived from a helicopter simulation. In Ref. 15, a nonlinear analytical system model has been developed from data obtained from a nonlinear aeroelastic vibration analysis (G400 computer simulation). This model has been used to analytically consider the effects on controller performance and Kalman filter stabililty. Reference 16 develops a linear multivariable system model based on wind tunnel results. This mathematical model, which is dependent upon flight condition, was used to evaluate the performance of the deterministic controller. The effect of measurement noise, inaccurate initial estimates of model properties, and varying flight speed on overall controller performance were considered. This study is the first study to look at the performance of the deterministic controller with internal rate-limiting of control inputs for a model derived from helicopter response data. While this study showed that internal rate-limiting improved the performance of the deterministic controller, no comparison is made to the cautious controller.

Reference 17 presents the results of the first successful flight test with active higher harmonic control. The results of both open- and closed-loop testing of higher harmonic control are presented for low to moderate forward velocities and fairly moderate transient maneuvers. The closed-loop results are based upon a cautious controller.

While the research outlined above has verified the feasibility, both theoretically and experimentally, of reducing vibration with closed-loop higher harmonic control, little work has been done in terms of refining algorithms or directly comparing the overall performance of the best controller configurations in an attempt to develop an "optimum" algorithm. While Refs. 10 and 11 compared the performance of the cautious and deterministic controllers, external rate-limiting was used for the deterministic controller. Reference 14 compared the performance of both when internal rate-limiting was used in the deterministic controller, but an arbitrary nonlinear simulation was used. Reference 4 thoroughly develops and evaluates the characteristics of almost all the viable algorithms in use today. However, the discussion of these algorithms is fundamentally based on the analysis and numerical simulation of single-input and single-output system models. The first recommendation of this reference is that the results should be verified or modified for the multivariable case.

Therefore, the lack of systematic evaluation and comparison of alternative controllers is not indicative of there being a lack of necessity. Rather, it is most likely due to the difficulty of developing mathematical models to adequately simulate the system dynamics of helicopters. For this reason most of the work done has been experimental wind tunnel tests in which it is expensive and time consuming to fully evaluate alternative algorithms.

The purpose of this investigation is to study, evaluate, and compare the alternative controller configurations that, based on previous individual studies, have been shown either theoretically or experimentally to have the potential for providing effective vibration alleviation. The major objective of this study is to refine and evaluate existing controller configurations in order to more fully understand their capabilities and limitations as well as the effect that various control parameters within the algorithms can have on controller performance.

In this report, many different alternative controller configurations are evaluated and compared at a baseline high speed (150 kt) flight condition. The helicopter simulation used is a nonlinear aeroelastic helicopter vibration computer analysis (G400) that models the H-34 rotor mounted on the NASA Ames Rotor Test Apparatus (RTA) which is representative of a generic helicopter fuselage. Three primary controller types will be investigated: deterministic, cautious, and dual. Each of these types have been identified in previous studies as having the potential to provide effective vibration control. Configurations based on both a local linear system model and a global linear system model for each of these controller types are evaluated and compared. The effect of both external and internal limiting is studied. Internal rate-limiting is studied extensively for the deterministic controllers, since much of the past work that led to conclusions that cautious control is much better than deterministic control was based on an externally limited deterministic controller.

Configurations based upon the three controller types are optimized, and the effect of their internal controller parameters are evaluated at the baseline flight condition. One of the best configurations for each controller type is designated as a baseline controller for evaluation and comparison at several different flight conditions. These conditions include alternate forward velocities and rotor thrusts as well as several simple transient maneuvers involving sudden changes in collective pitch.

The results of this study should be directly applicable in at least two ways to a future proof-of-concept wind tunnel test conducted to refine and develop an "optimum" active vibration controller configuration. First, a few of the best configurations in terms of overall performance have been identified for possible inclusion in such a test. Second, extensive testing

of the effect of various internal control algorithm parameters have been performed. These results should not only provide some guidance in what direction wind tunnel tests might take, but should prove helpful in tuning controllers selected for further development for maximum effectiveness. Finally, potential problem areas such as increased blade stress and degraded rotor performance have been identified and recommendations for future studies have been made. It should be noted that extensive documentation of significant results has been included in this report with the hope that they will prove useful to the practical application of the configurations studied or other alternative algorithms. For the reader more interested in overall results, the following sections should be of primary interest.

ANALYTICAL SIMULATION OF CLOSED-LOOP ACTIVE VIBRATION CONTROL

The vibration control approach is much the same as that documented in Refs. 9 and 10, and consists of three distinct components: (1) a method for mechanically implementing higher harmonic blade pitch; (2) an active controller to calculate and then command the required higher harmonic pitch; and (3) a set of fixed system sensors to provide inputs to the active controller. Together these three components form a closed-loop control system which will minimize vibration of the helicopter. A schematic of the active vibration control system as it is integrated into the rotorcraft is shown in Fig. 1. Each of these components will be discussed separately.

Mechanical Implementation

The vibration control approach uses higher harmonic blade root cyclic pitch which modifies the blade airloads to minimize harmonic blade forcing. As shown in Fig. 1, the higher harmonic pitch is mechanically input through the standard helicopter swashplate configuration. By harmonically oscillating the primary servos (actuators) that support the non-rotating swashplate, harmonic blade pitch motions are induced as the blade pitch links follow the motion of the rotating swashplate.

In order for all the rotor blades to have the same harmonic pitch amplitude and phasing, there is a limitation on the frequency of swashplate oscillation in the non-rotating system. In order to ensure that all blades on an N-bladed rotor are performing the same harmonic pitch oscillations as they travel around the azimuth, the harmonic frequency of oscillation of the swashplate must be N or some integer multiple of N. For example, on a four-bladed rotor, the frequency of swashplate oscillation must be 4/rev or some integer multiple of 4. In the present study, 4/rev swashplate oscillation is used on a four-bladed rotor to create 3, 4 and 5/rev harmonic blade pitch in the rotating system. The 4/rev blade pitch results from symmetric oscillation of the swashplate while the 3 and 5/rev blade pitch results from cyclic oscillation of the swashplate (still at 4/rev) about two orthogonal axes. Reference 18 provides a thorough discussion of the transfer of control inputs from non-rotating to rotating systems.

In summary, the higher harmonic cyclic pitch concept was implemented on a four-bladed helicopter model by oscillating the non-rotating swashplate at 4/rev in collective and cyclic motions to create blade cyclic pitch at 3, 4, and 5/rev. Implementing higher harmonic cyclic pitch in this manner provides maximum utilization of the present swashplate control system.

Sensors

The purpose of the sensors is to provide information to the active controller so that it can calculate and then command the required higher harmonic control inputs. The sensors can be thought of as measuring outputs of the helicopter as it responds to higher harmonic control inputs.

While the controller computer code has been reformulated (as will be discussed later) to allow measured parameters such as rotor torque or blade stresses to be included in addition to vibration measurements, the sensors used in the present study are all linear accelerometers that measure vibration in the fixed system. Since the vibration is measured in the fixed system, the output is predominately 4/rev for the four-bladed rotor, with some 8 and 12/rev content.

In the present study, the aeroelastic simulation is based on a four-bladed H-34 rotor mounted on the Rotor Test Apparatus (RTA) used for testing full scale rotor systems in the NASA-Ames 40' x 80' wind tunnel. The RTA is the structure used to simulate the helicopter fuselage and its coupling to the rotor system. A photograph of a rotor mounted on the RTA in the wind tunnel is shown in Fig. 2(a), while a diagram of the NASTRAN model of the RTA and wind tunnel support structure is shown in Fig. 2(b). The aeroelastic simulation of the coupled rotor and RTA will be discussed in a later section. The sensors are placed at six locations in the RTA and close to the hub in the fixed system as shown in Table 1. The locations of the sensors in the RTA are shown schematically in Figure 3. This schematic is a simplified version of the NASTRAN mathematical model of the RTA and is used only to illustrate sensor locations.

TABLE 1

LOCATION OF ACCELEROMETER SENSORS

<u>Rotor Test Apparatus</u>	
Nose	Lateral
	Vertical
Cross-Beam	Longitudinal
	Vertical
Tail	Lateral
	Vertical
<u>Hub (Fixed System)</u>	Vertical
	Lateral
	Longitudinal
	Pitch
	Roll
	Yaw

Note: Angular accelerations are obtained by combining signals from appropriately placed linear accelerometers.

Active Controller

Three different adaptive controllers (deterministic, cautious, and dual) are implemented in the vibration control approach for achieving minimum vibration in the present study. Furthermore, the exact algorithm used for each of these controllers depends upon which one of two system models is used (local or global). Therefore, six basic controller configurations are considered in this study. The Real-Time-Self Adaptive (RTSA) controller used in Refs. 9 and 10 was based on the deterministic controller and the local system model.

Regardless of which one of the basic controller configurations is implemented, there are three fundamental characteristics of the overall active controller approach used in this study:

(1) The approach is based upon an assumed quasi-static linear transfer matrix relationship, termed the T-matrix, between the vibration response and the higher harmonic control inputs.

(2) The transfer matrix is identified and tracked on-line by a real-time algorithm to account for changes in the transfer matrix due to nonlinearities or transient maneuver conditions.

(3) Higher harmonic control inputs are updated on the order of once every rotor revolution on a full-scale rotor system.

The active controller consists of three primary interrelated algorithms: (1) a real-time minimum variance controller for vibration minimization; (2) a real-time identification algorithm for identifying and tracking system parameters such as the T-matrix relating input HHC to vibration response; and (3) a harmonic analyzer for obtaining real-time harmonic components of measured vibration. A simplified diagram of the active controller as it is implemented in the digital computer simulation in this study is shown in Figure 4. Each of the three primary algorithms will be discussed subsequently. It should be noted that the exact form of the minimum variance control algorithm and the real-time identification algorithm both depend upon the controller configuration used; however, as will be discussed later, the modifications are such that each of the primary algorithms can be programmed in one subroutine with the appropriate modifications made according to the value of only two parameters which indicate the system model and the controller type to be used.

System Model

As indicated above, it is assumed that a quasi-static linear transfer matrix relationship can be defined for the ith rotor revolution (or time step)

between the higher harmonic pitch and the vibration response. The form of this matrix relationship between the inputs and outputs depends upon the system model used to represent the rotorcraft. Both a local and global system model were considered in this study.

The transfer matrix relationship between inputs and outputs for the local model is

$$Z_i = T(\theta_i - \theta_{i-1}) + Z_{i-1} \tag{1}$$

This is the same system assumed in the RTSA controller of Ref. 10. In Eq. (1), T is the n x m transfer matrix (T-matrix) relating output vibration response (Z_i and Z_{i-1}) to input higher harmonic control angles (θ_i and θ_{i-1}). In the present study, Z is a vector of harmonics of vibration (both cosine and sine components) and θ is a vector of the harmonics of multicyclic control in the rotating system (both cosine and sine components of 3, 4, and 5/rev harmonic blade pitch). Note that θ_i is defined relative to the initial value of higher harmonic control, which is usually zero. Thus, the total magnitude of the higher harmonic blade pitch is the sum of θ_i and the initial value. The system model represented by Eq. (1) is termed the local model to indicate linearization of the system T-matrix about the current control point. The control angle is expressed in terms of an incremental update so that the total higher harmonic control angles are the sum of the $\Delta\theta$ inputs for all rotor revolutions up to the ith revolution, assuming an initial value of zero.

In contrast, the global model linearizes the system T-matrix about a zero higher harmonic control input. The matrix relationship between inputs and outputs for the global system model is

$$Z_i = T\,\theta_i + Z_o \tag{2}$$

Here Z_o is the uncontrolled vibration level for zero higher harmonic control.

The choice of the system model to be used in the active controller affects the form of both the minimum variance control algorithm and the real-time identification algorithm. The local model in the present study is based on Eq. (1) and uses the identification algorithm to identify the T-matrix

only. Thus, the minimum variance control algorithm for the local model is based on an estimate of the T-matrix and the actual output parameters from the last rotor revolution. The global model in this study is based on Eq. (2) and uses the identification algorithm to identify both the T-matrix and Z_o. Thus, the minimum variance control algorithm is based on an estimate of the T-matrix and an estimate of the uncontrolled vibration level. The minimum variance control algorithm and the real-time identification algorithm will be discussed in more detail in the next two sections.

Minimum Variance Control Algorithm

The required change in the higher harmonic control inputs for minimum vibration response in the ith rotor revolution is shown in Figure 4 to be calculated by a minimum variance control algorithm. The minimum variance control algorithm is based upon the minimization of a performance index that is the expected value of a weighted sum of the mean squares of the input and output variables. The expected value is used to account for the uncertainty in system parameters.

The minimum variance controller is obtained by minimization of the criteria:

$$J = E\left\{(Z_i - Z_{opt})^T W_Z (Z_i - Z_{opt}) + \theta_i^T W_\theta \theta_i + \Delta\theta_i^T W_{\Delta\theta} \Delta\theta_i\right\} \qquad (3)$$

where

J is the performance index (a scalar)

$E\{\ \}$ denotes expected value

Z is the vector of output parameters including harmonic coefficients of vibration

Z_{opt} is the vector of prescribed optimum or desired output (vibration) parameters

W_Z is a diagonal weighting matrix on output (vibration) parameters

θ is the vector of higher harmonic control inputs

W_θ is a diagonal weighting matrix that constrains the amplitude of control

$\Delta\theta$ is the delta higher harmonic control vector

$W_{\Delta\theta}$ is a diagonal weighting matrix that constrains the rate of change of control inputs

Superscript T denotes vector or matrix transpose (e.g., vector transpose results in a row vector)
Subscript i denotes the ith rotor revolution

The performance index J includes not only the measured output parameters but also the higher harmonic control inputs. Therefore, each output parameter and control input can be individually weighted to make it more or less important than the other elements. Typically the cosine and sine components of a given phasor quantity are weighted equally. Note that the difference between the vector of output variables and a vector of optimum or desired values of the output variables has been included in the performance index. This is to enable the use of output variables in the performance index such as thrust or propulsive force which are not to be minimized but driven to a particular value if possible. Furthermore, the output parameters Z can include scalars as well as phasor quantities having two harmonic components. In the present study, only the harmonic coefficients of the vibration response from selected sensors in the fixed system were used as output parameters; thus, Z_{opt} was a zero vector.

The form of the minimum variance control algorithm is determined by the controller type and the system model used. The effect of controller type will be discussed below for each of the three different controllers used in this study. The final form of the minimum variance control algorithm is also affected by the system model used. However, the approach used for obtaining the minimum variance control algorithm is the same for any particular controller configuration with a given controller type and system model. The form of the performance index must be established by taking the expected value, as indicated in Eq. (3), according to the underlying assumptions of the controller type being considered. For the dual controller, the performance index must also be modified to include the additional term used for system probing. Once the performance index to be minimized has been established, the appropriate expression is substituted for Z_i. For the local model, the expression in Eq. (1) is used. The expression in Eq. (2) is used for the global model.

The minimum variance control algorithm is then obtained by taking the partial derivative of the resulting expression for J with respect to θ_i, and setting it equal to zero.

$$\frac{\partial J}{\partial \theta_i} = 0 \tag{4}$$

The result can be solved for θ_i^*. The superscript * denotes the optimal higher harmonic control input required for minimum variance. An expression $\Delta\theta_i^*$ can be determined by substituting $\theta_i = \Delta\theta_i + \theta_{i-1}$ into the expression for θ_i^*. Alternatively, the expression for $\Delta\theta_i^*$ can be solved for directly, as indicated in Ref. 10, by first substituting for θ_i and setting $\partial J/\partial \Delta\theta_i = 0$.

Clearly, the resulting expressions for the local model will depend upon the measured vibration level from the previous rev, Z_{i-1}. The resulting expression for the global model will depend upon an estimate of the uncontrolled vibration level, Z_o, which is identified along with the T-matrix. The actual algorithms for both the local and global models are discussed below for all three controller types (deterministic, cautious, and dual).

Deterministic Controller

The deterministic controller is based upon the assumption that all system parameters are explicitly known and ignores the fact that only estimates for the T-matrix (and Z_o for the global model) are available from the identifier. With this assumption, the performance index in Eq. (3) becomes

$$J_{Det} = (Z_i - Z_{opt})^T W_Z (Z_i - Z_{opt}) + \theta_i^T W_\theta \theta_i + \Delta\theta_i^T W_{\Delta\theta} \Delta\theta_i \tag{5}$$

For the local model, the solution for the deterministic controller becomes:

$$\theta_i^* = D\,[(T^T W_Z T + W_{\Delta\theta})\,\theta_{i-1} - T^T W_Z (Z_{i-1} - Z_{opt})] \tag{6}$$

or

$$\Delta\theta_i^* = -D\,[W_\theta \theta_{i-1} + T^T W_Z (Z_{i-1} - Z_{opt})] \tag{7}$$

where

$$D = (T^T W_Z T + W_\theta + W_{\Delta\theta})^{-1} \tag{8}$$

The algorithm given by Eqs. (7) and (8) is the same as the RTSA control algorithm applied in Ref. 10 if W_θ and $W_{\Delta\theta}$ are set equal to zero.

For the global model, the solution for the deterministic controller becomes:

$$\theta_i^* = D\,[W_{\Delta\theta}\theta_{i-1} - T^T W_Z(Z_o - Z_{opt})] \tag{9}$$

or

$$\Delta\theta_i^* = -D\,[(T^T W_Z T + W_\theta)\,\theta_{i-1} + T^T W_Z(Z_o - Z_{opt})] \tag{10}$$

where D is again defined as in Eq. (8).

Cautious Controller

While the deterministic controller is based on the assumption that the system parameters are all explicitly known, the cautious controller uses a stochastic approach which recognizes that some of the system parameters are only estimates. The cautious controller accounts for these parameter uncertainties when taking the expected value of the performance function and adjusts the control solution accordingly. This type of controller formulation was suggested and experimentally evaluated in Refs. 11 and 12.

In the cautious controller formulation, it is assumed that θ is explicitly known. Thus, the only parameter uncertainties in the performance index occur in the output parameters Z_i. As can be seen by Eq. (1), the uncertainties in Z_i for the local model are due to uncertainties in the identified T-matrix and measurement noise in Z_{i-1}. However, the cautious controller formulation only accounts for the uncertainties in the identified T-matrix when taking the expected value in Eq. (3). The measurement noise is not included. Thus, the performance index to be minimized by the cautious controller becomes for the local model:

$$J_c = (Z_i - Z_{opt})^T W_Z (Z_i - Z_{opt}) + \Delta\theta_i (P_i \cdot \sum_j W_{Zjj})\ \Delta\theta_i$$
$$+ \theta_i^T W_\theta \theta_i + \Delta\theta_i^T W_{\Delta\theta} \Delta\theta_i \qquad (11)$$

The only difference between this form of the performance index and that for the deterministic controller is the second term involving P_i, which is the covariance of the jth row of the T-matrix. As will be discussed later, P_i is assumed to be the same for each row of the T-matrix and is calculated by the Kalman filter identification algorithm. Recall that a covariance is a matrix of statistical parameters that are indicative of the relative uncertainty in an associated set or vector of random variables. Thus, this additional term in the performance index is clearly dependent upon the uncertainty in the identified T-matrix. As P_i (which is indicative of the uncertainty in the T-matrix) goes to zero, this term vanishes, and the performance index reduces to that for the deterministic controller. The expected effect of this term is similar to the effect of the term involving $W_{\Delta\theta}$. That is, this term also places a constraint on the rate of change of control; however, the rate-limiting effect due to this term will depend upon the uncertainty in the identified T-matrix. As the covariance of the T-matrix increases, the rate of change in control allowed by the cautious controller is reduced.

The minimum variance control solution for the cautious controller with the local model can be obtained by setting $\partial J/\partial\theta_i = 0$, where J is given in Eq. (11). However, this solution can be obtained more simply, since Eq. (11) can be rewritten in the same form as Eq. (5) by defining an effective $W_{\Delta\theta}$ that includes the term $P_i \sum W_{Zjj}$. Thus, by replacing $W_{\Delta\theta}$ by

$$W_{\Delta\theta_{eff}} = W_{\Delta\theta} + P_i \cdot \sum_j W_{Zjj} \qquad (12)$$

in Eqs. (6) through (8), the optimal control solution for the local model of the cautious controller becomes:

$$\theta_i^* = D\ [(T^T W_Z T + W_{\Delta\theta} + \lambda_c \cdot P_i \cdot \sum_j W_{Zjj})\ \theta_{i-1} - T^T W_Z (Z_{i-1} - Z_{opt})] \qquad (13)$$

or

$$\Delta\theta_i^* = -D\,[W_\theta \theta_{i-1} + T^T W_Z\,(Z_{i-1} - Z_{opt})] \tag{14}$$

where

$$D = (T^T W_Z T + W_\theta + W_{\Delta\theta} + \lambda_c \cdot P_{i\bullet} \sum_j W_{Zjj})^{-1} \tag{15}$$

In these equations, note the introduction of the arbitrary constant λ_c which can be used for modification of the control algorithm. This constant can be thought of as an indicator of how much caution is introduced by the cautious controller. As λ_c goes to zero, the cautious controller reduces to the deterministic controller with no caution or modification of control to account for parameter uncertainty.

In the global model, the uncertainties in the output parameters Z_i are due to uncertainties in the identified estimate of both the T-matrix and the uncontrolled vibration level Z_o. The cautious controller formulation accounts for both of these sources of uncertainty when taking the expected value of the performance index in Eq. (3). The new performance index to be minimized by the cautious controller becomes for the global model:

$$\begin{aligned} J_c = {} & (Z_i - Z_{opt})^T W_Z\,(Z_i - Z_{opt}) + (\theta_i^T\ 1)(P_{i\bullet} \sum_j W_{Zjj}) \begin{pmatrix} \theta_i \\ 1 \end{pmatrix} \\ & + \theta_i^T W_\theta \theta_i + \Delta\theta_i^T W_{\Delta\theta} \Delta\theta \end{aligned} \tag{16}$$

As for the local model, the only difference between this form of the performance index and that for the deterministic controller is the additional term involving P_i. However, the additional term here involves θ_i rather than $\Delta\theta_i$. Furthermore, P_i must be defined slightly differently:

$$P_i = \begin{bmatrix} P_{TT} & P_{TZ} \\ P_{TZ}^T & P_{ZZ} \end{bmatrix}_i \tag{17}$$

Here, P_{TT} is the covariance of the jth row of the T-matrix. P_{TZ} is the cross-covariance of the jth row of the T-matrix and the jth element of Z_o. P_{ZZ} is the covariance of the jth element of Z_o. Again, P_i is assumed to be the same for each row of matrix Eq. (2) and is calculated by the Kalman filter identification algorithm for the global model.

This additional term is again dependent upon the uncertainty in identification of system parameters. As P_i (which is indicative of the uncertainty in system identification) goes to zero, this term vanishes, and the performance index reduces to that for the deterministic controller. One of the expected effects of this term is similar to the effect of the term involving W_θ. That is, this term also places a constraint on control magnitude. However, this limiting of total θ due to this term will depend upon the uncertainty in system identification.

The minimum variance control solution for the cautious controller with the global model can be obtained by setting $\partial J/\partial\theta_i=0$, where J is given in Eq. (16):

$$\theta_i^* = D\,[W_{\Delta\theta}\theta_{i-1} - T^T W_Z\,(Z_o - Z_{opt}) - \lambda_c\, P_{TZ}\cdot \sum_j W_{Zjj}] \tag{18}$$

or

$$\begin{aligned}\Delta\theta_i^* = -D\,[&T^T W_Z\,T + W_\theta + \lambda_c\, P_{TT}\cdot \sum_j W_{Zjj})\;\theta_{i-1} \\ &+ T^T W_Z\,(Z_o - Z_{opt}) + \lambda_c\, P_{TZ}\cdot \sum_j W_{Zjj}]\end{aligned} \tag{19}$$

where

$$D = (T^T W_Z\,T + W_\theta + W_{\Delta\theta} + \lambda_c\, P_{TT}\cdot \sum_j W_{Zjj})^{-1} \tag{20}$$

As for the local model, an arbitrary constant λ_c has been introduced to allow flexibility in modifying the cautious controller if desired. By comparing Eqs. (18) through (20) to Eqs. (8) through (10) for the global deterministic controller, it can be seen that two differences occur. First,

W_θ has been replaced everywhere that it occurs in the optimal control solution for the deterministic controller by an effective W_θ

$$W_{\theta_{eff}} = W_\theta + \lambda_c^* P_{TT^*} \sum_j W_{Zjj} \tag{21}$$

Thus, the global model of the cautious controller applies a constraint (as discussed above) on the magnitude of total control angles required, and this constraint is proportional to the covariance of the T-matrix. Second, a constant term appears in the solution which is proportional to the cross-covariance P_{TZ}.

In summary, the cautious controller accounts for parameter uncertainties by modifying the form of the performance index when taking the expected value and adjusting the optimal control solution accordingly. The new terms that arise in the performance index for both the local and global models depend directly upon the covariances calculated by the Kalman filter identification algorithm. If these covariances, which are indicative of the uncertainty in system identification, were to go to zero, these terms would vanish. The overall effect of these new terms is to slow down the controller, or introduce caution due to parameter uncertainty. In the local model, a constraint is applied to the rate of change of control. In the global model, a constraint is applied to the magnitude of control. Note that the cautious controller does not directly improve identification. The impact on identification is indirect through effectively slowing down the controller and allowing more iterations or Kalman filter estimates before reaching a given level of control.

Dual Controller

The last controller type to be considered in the present study is an active adaptive formulation of the controller (Ref. 19), also known as a dual controller (Ref. 20). This formulation of the controller has been proposed in Ref. 12. Both the deterministic and cautious controllers discussed above are passive adaptive controllers that make no use of the fact that the control loop will remain closed in the future. While passive adaptive controllers can account for parameter uncertainties as in the cautious controller above, they do not directly affect identification. An active adaptive controller, on the other hand, attempts to improve long term system identification by actively probing the system while at the same time providing good control.

Optimal dual controller solutions are generally so complex and involve such a large number of variables for practical problems that computer memory and computational requirements make implementation in real time impractical (Refs. 4 and 21). Therefore, the dual controller used in this study is a sub-optimal approach taken from Ref. 20. In this approach, the performance index of Eq. (3) is modified to include a term that is a function of the estimation error and acts as a perturbation signal that allows the controller to actively probe the system. The new form of the performance index is

$$J_D = J - \lambda_D \frac{\det P_{i-1}}{\det P_i} \tag{22}$$

Here det refers to the determinant of a matrix. The reasoning behind this form of the performance index is that the controller attempts to provide good control by minimizing the first term, and attempts to make P_i small relative to P_{i-1} -- that is improve identification -- by minimizing the second term. Thus, the arbitrary constant λ_D provides a compromise between good short term control and the rate of learning as measured by the decrease in size of the parameter covariance matrix (Ref. 20). Typically, the value of λ_D would be selected through trial and error in order to achieve an acceptable tradeoff.

In Ref. 20, it is shown that the second term in Eq. (22) is equivalent to

$$-\lambda_D \frac{\det P_{i-1}}{\det P_i} = -\lambda_D \left[1 + \frac{\gamma_i^T P_{i-1} \gamma_i}{R} \right] \tag{23}$$

where $\gamma_i=\Delta\theta_i$ for the local model and $\gamma_i=(\theta_i^T\ 1)^T$ for the global model. As will be discussed later, R is the covariance of the measurement noise used by the Kalman filter identification algorithm. Note that, when the step of setting $\partial J/\partial\theta_i=0$ is performed, the learning term in Eq. (23) is also quadratic. This allows the minimum variance control solution to be readily found. This is the convenience for using this simple formulation for the dual controller.

By using Eq. (23) in Eq. (22) with $\gamma_i=\Delta\theta_i$, the performance index for the dual controller and local system model becomes

$$J_D = (Z_i - Z_{opt})^T W_Z (Z_i - Z_{opt}) - \lambda_D \cdot \Delta\theta_i^T \frac{P_{i-1}}{R} \Delta\theta_i$$

$$+ \theta_i^T W_\theta \theta_i + \Delta\theta_i^T W_{\Delta\theta} \Delta\theta_i \tag{24}$$

Note that the first term on the right-hand side of Eq. (23) (constant λ_D term) has been dropped since it does not affect the minimum variance control solution obtained when setting $\partial J/\partial\theta_i = 0$.

By noting the similarity between Eqs. (5) and (24), the dual controller solution for the local model can be written immediately by replacing $W_{\Delta\theta}$ in Eqs. (6) through (8) by an effective $W_{\Delta\theta}$

$$W_{\Delta\theta_{eff}} = W_{\Delta\theta} - \lambda_D \cdot \frac{P_{i-1}}{R} \tag{25}$$

The dual controller solution for the local model becomes

$$\theta_i^* = D\left[\left(T^T W_Z T + W_{\Delta\theta} - \lambda_D \cdot \frac{P_{i-1}}{R}\right) \theta_{i-1} - T^T W_Z (Z_{i-1} - Z_{opt})\right] \tag{26}$$

or

$$\Delta\theta_i^* = -D\,[W_\theta \theta_{i-1} + T^T W_Z (Z_{i-1} - Z_{opt})] \tag{27}$$

where

$$D = \left(T^T W_Z T + W_\theta + W_{\Delta\theta} - \lambda_D \cdot \frac{P_{i-1}}{R}\right)^{-1} \tag{28}$$

Clearly, the overall effect of the learning term in the local model is a reduction in the constraint on the rate of change of control proportional to the covariance of the estimated T-matrix. This is the exact opposite effect

to that of the cautious controller with an effective $W_{\Delta\theta}$ given in Eq. (12). Whereas the cautious controller penalizes the control for poor identification by an increase in rate-limiting, the dual controller increases control by a reduction in rate limiting.

By using Eq. (23) in Eq. (22) with $\gamma_i=(\theta_i^T\ 1)^T$, the performance index for the dual controller and global system model becomes

$$J_D = (Z_i - Z_{opt})^T W_Z\ (Z_i - Z_{opt}) - \lambda_D \cdot (\theta_i^T\ 1) \cdot \frac{P_{i-1}}{R} \begin{pmatrix} \theta_i \\ 1 \end{pmatrix} + \theta_i^T\ W_\theta \theta_i + \Delta\theta_i^T\ W_{\Delta\theta} \Delta\theta_i \tag{29}$$

By noting the similarities between Eqs. (16) and (29), the dual controller solution for the global model can be written immediately as

$$\theta_i^* = D\left[W_{\Delta\theta}\theta_{i-1} - T^T W_Z\ (Z_o - Z_{opt}) - \lambda_D \cdot \frac{P_{TZ}}{R}\right] \tag{30}$$

or

$$\Delta\theta_i^* = -D\left[\left(T^T W_Z T + W_\theta - \lambda_D \cdot \frac{P_{TT}}{R}\right)\theta_{i-1} + T^T W_Z\ (Z_o - Z_{opt}) - \lambda_D \cdot \frac{P_{TZ}}{R}\right] \tag{31}$$

where

$$D = \left(T^T W_Z T + W_\theta + W_{\Delta\theta} - \lambda_D \cdot \frac{P_{TT}}{R}\right)^{-1} \tag{32}$$

The covariance P is again defined as in Eq. (17)

It can be seen, by comparing the solution in Eqs. (30) through (32) for the dual controller to that in Eqs. (8) through (10) for the deterministic controller, that two differences occur. First, a constant term of the form $D \cdot \lambda_D \cdot P_{TZ}/R$ appears in the solution. Second, W_θ has been replaced everywhere it appears in the deterministic controller solution for the global model by an effective W_θ

$$W_{\theta_{eff}} = W_\theta - \lambda_D \cdot P_{TT}/R \tag{33}$$

Thus, the learning term in the global model effectively reduces the constraint on control magnitude. Again, this is the exact opposite effect to that of the cautious controller. Whereas the cautious controller reduces control magnitude when identification is poor, the dual control probes the system by increasing control magnitude.

In summary, the dual controller is an active adaptive controller formulation that attempts to improve long term system identification by actively probing the system while at the same time providing good control. In order to do this, a new term is added to the performance index in Eq. (3). The exact form of this learning term depends on whether the local or global model is used; however, in both cases, the learning term depends upon the ratio of the system parameter covariance matrix and the covariance of measurement noise. The overall effect of the dual controller when compared to the deterministic controller is a reduction in the constraint on control. For the local controller, this occurs through a reduction in the effective $W_{\Delta\theta}$ and reduced rate-limiting. For the global model, this occurs through a reduction in the effective W_θ and increased control magnitude. These effects are the opposite to those for the cautious controller. It is the reduction in constraints on control that allows system probing.

General Active Controller Algorithm

Three different control approaches were considered in the present study. In the above discussion of these different approaches, many similarities in the controller solutions were noted. In fact, all three controllers can be programmed into the same algorithm. The appropriate controller is then implemented by setting a parameter β to an appropriate value.

The controller solution for all three controller types can be written for the local system model as

$$\Delta\theta_i^* = -D\,[W_\theta\,\theta_{i-1} + T^T W_Z\,(Z_{i-1} - Z_{opt})] \tag{34}$$

where

$$D = (T^T W_Z T + W_\theta + W_{\Delta\theta} + \beta \cdot \lambda \cdot P_{i-1} \cdot \sum_j W_{Zjj})^{-1} \tag{35}$$

When β is set to zero, the controller solution reduces to that given for the deterministic controller in Eqs. (7) and (8). When β is set to a value of 1, the controller solution reduces to that given for the cautious controller in Eqs. (14) and (15) except that P_{i-1} is shown here rather than P_i. This is due to the fact that P_i is not available from the Kalman filter identification algorithm until after the solution for $\Delta\theta_i^*$ has been obtained. Thus, P_{i-1} is used as an estimate for the covariance of the T-matrix for the ith rev. This is also true of the other system parameters estimated by the Kalman filter. As discussed in Ref. 4, the controller solutions for $\Delta\theta_i^*$ should be based upon the estimated T-matrix for the ith rev. However, this estimate is not available from the Kalman filter identification algorithm until after $\Delta\theta_i$ has been implemented and the resulting Z_i measured. Thus, in practice, the T-matrix identified in the (i-1)th rev is used in the controller solutions as the best estimate available. Finally, when β is set to $(-1/R \sum W_{Zjj})$, the controller solution reduces to that given for the dual controller in Eqs. (27) and (28). A summary of the minimum variance control algorithm for the local model is shown below, along with a summary for the global model.

The controller solution for all three types can be written for the global model as

$$\Delta\theta_i^* = -D \left[\left(T^T W_Z T + W_\theta + \beta \cdot \lambda \cdot P_{TT} \cdot \sum_j W_{Zjj} \right) \theta_{i-1} + T^T W_Z \left(Z_o - Z_{opt} \right) + \beta \cdot \lambda \cdot P_{TZ} \cdot \sum_j W_{Zjj} \right] \tag{36}$$

where

$$D = \left(T^T W_Z T + W_\theta + W_{\Delta\theta} + \beta \cdot \lambda \cdot P_{TT} \cdot \sum_j W_{Zjj} \right)^{-1} \tag{37}$$

The same values for β as those given above are required to obtain the appropriate controller solutions. When β=0, the controller solution reduces to that given for the deterministic controller in Eqs. (8) and (10). When β=1, the controller solution reduces to that given for the cautious controller in Eqs. (19) and (20). Finally, when $\beta=(-1/R \sum W_{Zjj})$, the controller solution reduces to that given for the dual controller in Eqs. (31) and (32). As discussed above for the local model, the values of the covariances and identified parameters (T and Z_o) actually used in the controller solutions are those estimated in the (i-1)th rev since they are the best estimates available. A summary of the minimum variance control algorithm for the global model is shown below.

Summary of Minimum Variance Control Algorithms

a) LOCAL MODEL

$$J = \left(Z_i - Z_{opt}\right)^T W_Z \left(Z_i - Z_{opt}\right) + \Delta\theta_i^T \left(\beta \cdot \lambda \cdot P \Sigma W_{Z_{jj}}\right) \Delta\theta_i + \theta_i^T W_\theta \theta_i + \Delta\theta_i^T W_{\Delta\theta} \Delta\theta_i$$

$$Z_i = T(\theta_i - \theta_{i-1}) + Z_{i-1}$$

$$\partial J / \partial \theta_i = 0$$

$$\Delta\theta_i^* = -D\left[W_\theta \cdot \theta_{i-1} + T^T W_Z \left(Z_i - Z_{opt}\right)\right]$$

$$D = \left(T^T W_Z T + W_\theta + W_{\Delta\theta} + \beta \cdot \lambda \cdot P \Sigma W_{Z_{jj}}\right)^{-1}$$

CONTROLLER	β
DETERMINISTIC	0
CAUTIOUS	1
DUAL	$\frac{-1}{R \Sigma W_{Z_{jj}}}$

b) GLOBAL MODEL

$$J = \left(Z_i - Z_{opt}\right)^T W_Z \left(Z_i - Z_{opt}\right) + \left(\theta_i^T 1\right) \left(\beta \cdot \lambda \cdot P \Sigma W_{Z_{jj}}\right) \begin{pmatrix} \theta_i \\ 1 \end{pmatrix} + \theta_i^T W_\theta \theta_i + \Delta\theta_i^T W_{\Delta\theta} \Delta\theta_i$$

$$Z_i = T\theta_i + Z_o$$

$$\partial J / \partial \theta_i = 0$$

$$\Delta\theta_i^* = -D\left[\left(T^T W_Z T + W_\theta + \beta \cdot \lambda \cdot P_{TT} \Sigma W_{Z_{jj}}\right)\theta_{i-1} + T^T W_Z \left(Z_o - Z_{opt}\right) + \beta \cdot \lambda \cdot P_{TZ} \Sigma W_{Z_{jj}}\right]$$

$$D = \left(T^T W_Z T + W_\theta + W_{\Delta\theta} + \beta \cdot \lambda \cdot P_{TT} \Sigma W_{Z_{jj}}\right)^{-1}$$

$$P = \begin{bmatrix} P_{TT} & P_{TZ} \\ P_{TZ}^T & P_{ZZ} \end{bmatrix}$$

CONTROLLER	β
DETERMINISTIC	0
CAUTIOUS	1
DUAL	$\frac{-1}{R \Sigma W_{Z_{jj}}}$

In summary, three different control approaches are to be considered in this study as an alternative approach to the RTSA controller used in Ref. 10. The first approach to be considered is a deterministic controller which is based upon the same assumptions as the RTSA controller. However, certain modifications have been introduced. The first modification is the availability of a deterministic controller based upon the global system model as well as one based on the local model used in the RTSA controller. Both system models are also used as the basis of algorithms for the other two controller types. However, the anticipated advantages and disadvantages of both system models are primarily related to identification and will be discussed in the next section. The second modification of the deterministic controller is the addition of θ and $\Delta\theta$ to the performance index. While the RTSA controller had $\Delta\theta$ in the performance index, $W_{\Delta\theta}$ was always set to zero, and the capability of internal rate limiting was never utilized. It is anticipated that the use of $W_{\Delta\theta}$ and W_{θ} will improve control over that provided by external limiting for reasons that will be discussed later.

The second control approach to be considered is that of a cautious controller that accounts for parameter uncertainties by modifying the form of the performance index by taking the expected value of the performance index and adjusting the optimal control solution accordingly. The net effect is to constrain control and proceed more cautiously than the deterministic controller. It is anticipated that adding caution to the RTSA controller will improve controller performance by smoothing convergence. As discussed above, the cautious controller should provide somewhat the same effect as adding $\Delta\theta$ or θ to the performance index. The addition of caution will not improve identification directly. Indirectly, it may improve identification in much the same manner as $W_{\Delta\theta}$ and W_{θ} by slowing down the controller with internal limiting, which allows more time for Kalman filter identification. On the other hand, controller turn-off may be a problem as discussed in Ref. 21. If identification suddenly deteriorates with a large increase in P, the controller will make very small control changes which may not provide enough system excitation to allow the identifier to improve its estimate. Further deterioration in identification could cause smaller and smaller control inputs and effectively shut down the controller. This is a potential problem for systems with rapidly time-varying system parameters.

The last control approach to be considered is that of a dual controller. In contrast to both the deterministic and cautious controllers, the dual controller attempts to improve system identification by actively probing the system while at the same time providing good control. This probing action excites the system if identification is poor and should avoid the turn-off phenomenon discussed above for the cautious controller. This might be very important if system properties, which are dependent on flight condition, are

very rapidly time-varying. However, as discussed in Ref. 21, the two tasks of trying to improve system identification and of trying to provide good control are, in general, contradictory. Good identification may require large control inputs, while good control may require small control inputs. Thus, the dual controller must be tuned to compromise between these two tasks. It is anticipated that short term control may be compromised.

Since all three control types have their anticipated advantages and disadvantages, they will all be considered in this study. It should be recalled that all three controller types are based upon a linear system model, regardless of whether a local or global model is used. The nonlinear variation of the T-matrix, as well as variations due to time-varying flight conditions, is accounted for by treating the T-matrix as a time-varying matrix with changes identified and tracked by a real-time identification algorithm. All three controllers use the same Kalman filter identification algorithm, which is discussed in the next section.

Kalman Filter Identification Algorithm

Accurate identification of the T-matrix as well as Z_o for the global model is important for good vibration reduction, since the minimum variance control algorithms all depend explicitly upon the estimates of these parameters. The method used for estimating and tracking the T-matrix for the local model is exactly the same as that used in the RTSA controller presented in Ref. 10. The method used for the global model need be modified only slightly to allow Z_o to be identified as well. The identification is based upon an approach analogous to the Kalman filter for linear multistage processes presented in Ref. 19. The Kalman filter formulation will be discussed below for the local model, followed by a brief discussion of the modifications necessary for the global model.

The Kalman filter formulation for the identification problem is obtained by considering each row of Eq. (1) as a separate identification problem and rewriting this equation in appropriate form. For instance, consider the jth row which can be written as

$$\Delta Z_{ji} = \Delta\theta_i^T \, T_{ji}^T \tag{38}$$

where T_{ji} refers to the jth row of the estimated T-matrix T_i, and Z_{ji} refers to the jth element of the output vector Z_i. The subscript i refers to the ith rotor revolution. One can now define a state vector for each row of the T-matrix as

$$X_{ji} = \left[T_j^T\right]_i \tag{39}$$

Using this state vector representation, Eq. (38) can be rewritten as

$$\Delta Z_{ji} = H_i X_{ji} + \eta \tag{40}$$

where

$$H_i = \Delta\theta_i^T \tag{41}$$

In Eq. (40), η is zero mean white Gaussian measurement noise.

The state vector defined in Eq. (39) represents a row in the T-matrix, and has dimensions m x 1. The state vector is assumed to be a time-varying quantity which must be identified and tracked. It is further assumed that the variations in the T-matrix can be represented by

$$X_{ji+1} = X_{ji} + W_{ji} \tag{42}$$

where W_{ji} is assumed to be a zero mean discrete white random sequence corresponding to the jth row of the T-matrix. W_{ji} is considered to be a random forcing vector which conveys to the mathematical formulation that the T-matrix varies with flight condition. The Kalman filter solution to Eqs. (40) and (42) provides an algorithm for identifying and tracking the T-matrix. The Kalman filter solution for this formulation, as taken from Ref. 19, is:

$$\hat{X}_{ji} = \hat{X}_{ji-1} + K_i(\Delta Z_{ji} - H_i\hat{X}_{ji-1}) \tag{43}$$

$$K_i = P_i H_i^T R_i^{-1} \tag{44}$$

$$M_i = P_{i-1} + Q_{i-1} \tag{45}$$

$$P_i = M_i - M_i H_i^T (H_i M_i H_i^T + R_i)^{-1} H_i M_i \tag{46}$$

where superscript ^ denotes estimated value and subscript i refers to the ith rev.

Before pointing out the very slight modifications required for the global system model, it is appropriate to briefly discuss the parameters contained in this algorithm that have not been defined previously. The scalar quantity R is the covariance of the measurement noise, η. The matrix Q (m x m) is the covariance of forcing vector W, which accounts for changes in state. Matrices M and P (m x m) are both covariances of the state vector X_j and are therefore a measure of the uncertainty in the estimate of the jth row of the T-matrix. The matrix M is the covariance before measurement while the matrix P is the covariance after measurement. Thus, M is dependent only upon the covariance of state from the last revolution and the covariance of changes in state, P_{i-1} and Q_{i-1}, respectively; whereas, P is also dependent upon the covariance of measurement noise R. The covariances M, P, Q and R have all been assumed to be the same for each state vector. Thus, these variables require no subscript j in Eqs. (43) through (46), which have been written for the jth row of the T-matrix. Furthermore, P is a measure of the uncertainty in the estimate of the entire T-matrix.

Equation (43) is a model of the system defined in Eq. (42), with a correction term that is proportional to the difference betwen the measured change in vibration (ΔZ_{ji}) and the predicted change in vibration ($H_i \hat{X}_{ji-1}$) corresponding to the change in higher harmonic control ($\Delta\theta_i$). The proportionality constant or Kalman gain K (defined in Eq. (44)) is essentially the ratio between the uncertainty in the estimated T-matrix and the uncertainty in the vibration parameters. This can be seen by inspection of Eq. (44) where P, the covariance of the state vector, appears in the numerator and R, the covariance of measurement noise, appears in the denominator. When R is large and/or P is small to reflect more confidence in the estimate of the T-matrix than in the measurement of vibration, the state vector (X) will change proportionately less even though there may be a difference between measured vibration and predicted vibration. This demonstrates that the important parameters are P/R and ultimately Q/R, rather than the individual magnitudes. If the T-matrix is a good estimate of the actual T-matrix, then P will essentially be

equal to Q by Eq. (45), and the Kalman gain will be directly proportional to the ratio of Q to R.

In the above identification algorithm, the parameters K_i, M_i, and P_i are calculated automatically once the controller has been started. If the estimate of the T-matrix is good, P will be small. Conversely, if the estimate of the T-matrix is poor, P will be calculated to be large. On the other hand, covariances Q and R must be assigned. The magnitude of the elements of Q should be set in direct proportion to the variability of the actual T-matrix from update to update. If the actual T-matrix varies widely and rapidly, the elements of Q should be large. The magnitude of R should be set proportional to the noise-to-signal ratio. Once Q_o and R_o are assigned, Q and R may be held constant or varied according to some algorithm. In the RTSA controller used in Ref. 10, the covariance Q was held constant and the covariance R was varied according to a simple algorithm involving the performance index from the (i-1)th and ith revs. Due to system nonlinearities and transient response to control inputs, it may be necessary to provide additional algorithms describing the covariances Q and R as variables in order to achieve optimum vibration alleviation. Several alternative algorithms are provided for both Q and R in the active controller configuration used in this study. These algorithms will be discussed in a later section as potential improvements to the active controller configuration. For most of the present study, these algorithms were not activated, and covariances Q and R were held constant.

The above identification algorithm was developed for the local system model. Only a few minor modifications are required for the global system model in order to identify the uncontrolled vibration level Z_o as well as the T-matrix. For the global system model, the jth row of Eq. (2) can be rewritten in the same form as Eq.(38)

$$Z_{ji} = \theta_i^T T_{ji}^T + Z_{oji} \tag{47}$$

where the total control input θ_i is now used. The state vector to be identified now becomes

$$X_{ji} = \left[\begin{array}{c} T_j^T \\ \hline Z_{oj} \end{array} \right]_i \tag{48}$$

Equation (40) becomes

$$Z_{ji} = H_i X_{ji} + \eta \tag{49}$$

where

$$H_i = \left[\begin{array}{c:c} \theta^T & 1 \end{array}\right]_i \tag{50}$$

With these changes, the Kalman filter identification algorithm of Eqs. (43) through (46) can be used to identify both the T-matrix and Z_o with only one slight change. Eq. (43) now becomes

$$\hat{X}_{ji} = \hat{X}_{ji-1} + K_i(Z_{ji} - H_i \hat{X}_{ji-1}) \tag{51}$$

to reflect the difference between Eqs. (40) and (49).

The covariances Q, M and P are now of dimension (m+1) x (m+1) corresponding to the (m+1) x 1 dimension of the state vector to be identified. As already shown in Eq. (17), the covariance P can be written as

$$P = \begin{bmatrix} P_{TT} & P_{TZ} \\ P_{TZ}^T & P_{ZZ} \end{bmatrix} \tag{52}$$

Here, P_{TT} is the covariance of the jth row of the T-matrix. P_{TZ} is the cross-covariance of the jth row of the T-matrix and the jth element of the Z_o. P_{ZZ} is the covariance of the jth element of Z_o. As for the local model, all covariances are assumed to be the same for all rows of the matrix equation in Eq. (2).

The primary advantage expected of the global system model over the local system model is better identification for small changes in control input between updates. This is because the identification algorithm for the local system model is dependent upon $\Delta\theta$ instead of total θ, as is the case for the global system model. This can be seen by comparing Eqs. (41) and (50). Thus, the Kalman gain becomes smaller and the error signal used to calculate a

better estimate of state vector X becomes weaker for small $\Delta\theta$ in the local system model. On the other hand, the local system model may give better control for very nonlinear systems since it linearizes locally about the current control point. Furthermore, the global system requires the identification of another parameter Z_o. Although this can be readily done by the Kalman filter, a measurement is considered better than an estimate, so the minimum variance control algorithms may be less accurate for the global system model. Both alternative system models are included in the active controller configuration and the performance based on both models will be compared in the present study.

Regardless of which system model is used, the Kalman filter identification algorithm requires only the current vibration measurements and error covariances to identify the required system parameters. Therefore, the procedure can be carried out recursively with information from only the present rev and the previous rev. The importance of this characteristic is that implementation can easily be carried out in real time. This is especially important in the control of vibration during transients and maneuvers.

Harmonic Analyzer

As previously mentioned, the sensors used to supply information to the controller are assumed to be accelerometers located in the fixed system. These sensors provide a time history of the vibratory response to the controller. For a four-bladed rotor, the vibration measurements are predominately 4/rev with some 8/rev and 12/rev in a steady state flight condition, provided that all four blades are executing the same motions. The active vibration control system seeks to minimize the 4/rev fuselage motions. A harmonic analyzer is used to extract the 4/rev harmonic coefficients from the analog sensor. In the present study, the controller uses the same harmonic analyzer used in G400. G400 is the nonlinear aeroelastic rotorcraft simulation used in this study and will be discussed later.

Limiting of Control Inputs

The last function performed by the active controller (shown in Fig. 4) is the external limiting of control inputs before implementation in the rotorcraft simulation. This limiting function is performed every control update after the optimal minimum variance control solution is obtained.

The purpose of control limiting is to constrain both the total amplitude of higher harmonic control implemented and the rate of change of higher harmonic control from update to update. There are several reasons for limiting control inputs rather than implementing the optimal control solution required

by the minimum variance control algorithm. In an actual rotorcraft, limiting will be required to keep the rate of change of control inputs and the total amplitude of control inputs within the capability of the actuators used to implement higher harmonic control. The total amplitude of control inputs would also be constrained to satisfy possible mechanical stress and safety considerations.

Beyond the practical aspects of limiting higher harmonic control inputs, rate-limiting was also found in Ref. 10 to be very important to controller performance. This capability is required for starting the recursive controller procedure to enhance controller stability and smooth controller convergence, since parameter estimates may be poor when the controller is started. Rate-limiting may also be required to maintain controller stability and aid in system identification if the system is highly nonlinear.

The limiting of higher harmonic control inputs can be performed in two ways, externally and internally. Limiting can be performed externally (as shown in Fig. 4) with the optimal control solution requested by the minimum variance control algorithm arbitrarily limited to satisfy total magnitude and rate-limiting requirements. This is referred to as external limiting since the limiting of control inputs is done outside the minimum variance control algorithm, which is an unconstrained optimization algorithm, and without regard to optimality. The limits placed on incremental changes in vector magnitude are applied to each control input separately. If the vector magnitude of the incremental change in a control input exceeds the rate limits placed on that input, the cosine and sine components are reduced proportionately in order to maintain the same phase while satisfying rate-limiting requirements. While different rate limits can be applied to each control input, equal rate limits are usually applied. After rate-limiting, the external limiter checks the total magnitude of each control vector and limits the cosine and sine components proportionately in order to maintain the same phase on the input vector while satisfying total magnitude requirements. Again, different limits can be placed on the total magnitude of each input, but usually are applied equally.

It is the externally limited control updates $\Delta\theta$ rather than the "optimal" updates $\Delta\theta^*$ calculated by the minimum variance control algorithm that are implemented in the rotor system. These limited updates and the rotorcraft response to these updates are used as the basis for Kalman filter estimates of system parameters. No information on the optimal updates before limiting is passed to the identifier.

As indicated in the discussion of the minimum variance control algorithm, limiting of higher harmonic control can also be performed internally by placing quadratic terms involving θ and $\Delta\theta$ in the performance index, as shown in Eq. (3). In Eq. (3), the weighting matrix $W_{\Delta\theta}$ constrains the rate of change of control inputs by weighting $\Delta\theta$ more or less heavily. Large elements in $W_{\Delta\theta}$

result in more highly constrained rates of change for the corresponding control inputs. The weighting matrix W_θ constrains the total amplitude of control inputs. Again, large elements of W_θ result in more highly constrained total amplitudes for the corresponding control inputs. Typically, both cosine and sine components of a given harmonic are weighted equally by $W_{\Delta\theta}$ or W_θ.

In Refs. 9 and 10, the RTSA controller used external limiting exclusively to limit control inputs since $W_{\Delta\theta}$ was set to zero. While external rate-limiting was found to be important to controller performance in Ref. 10, it is anticipated that internal rate-limiting will further improve controller performance by taking the desire to constrain $\Delta\theta$ or θ into account at the time the optimal control solution is determined rather than arbitrarily limiting individual control angles after the optimal control solution has already been determined. By externally limiting the control inputs, the characteristic of the control inputs implemented may be different than that required by the minimum variance control algorithm. For instance, the mix of 3, 4, and 5/rev inputs may change, especially if one input is more highly limited than the others. This effect could be especially important for highly nonlinear systems or systems that are quite sensitive to the mix of 3, 4 and 5/rev inputs. In fact, external limiting could be potentially destabilizing for a highly nonlinear system with the resulting controller convergence being very oscillatory.

The external limiting function shown in Fig. 4 may still be required even if internal limiting is found to be better suited to adapting the controller to hardware limitations of the mechanical control system and also for smoothing controller response. The reason for this is that the effect of $W_{\Delta\theta}$ and W_θ is somewhat dependent upon the level of vibration present. If the vibration level is high, a given value of $W_{\Delta\theta}$ or W_θ will not result in as highly a constrained control inputs as it would for low level vibration due to the form of the performance index. Thus, external limiting may be required as a safety check to ensure that safety requirements are satisfied.

Further Potential Improvements to Active Controller

The primary modifications to be made to the RTSA controller and evaluated in the present study have already been outlined. These modifications include the availability of two different system models, local and global; three different controller types, deterministic, cautious, and dual; and internal limiting using $W_{\Delta\theta}$ and W_θ. Two other modifications to be considered and evaluated in this study as potential improvements to the controller configuration are algorithms for a variable output parameter weighting matrix and algorithms for variable Kalman filter covariances Q and R. These modifications are briefly discussed below and conclude the specification of the potential active controller configuration.

Variable Output Weighting Matrix

In Ref. 10, it was found that the vibration weighting matrix W_z can have a significant impact on local vibration levels and overall vibration alleviation. Furthermore, the sensor weighting configuration may also have a significant impact on the solution of the controller. These effects are especially significant if the system is nonlinear and/or the controller achieves substantial vibration reduction in the RTA via vectorial modal cancellation as well as a general reduction in the magnitude of modal excitation. Since nonlinear systems are directionally sensitive, a change in sensor weightings can change the directional sensitivity such that it is possible to achieve at least two completely different controller convergent solutions by changing sensor weightings. If vectorial modal cancellation plays a significant role in the vibration reduction achieved by the active controller, then a change in weighting can also change the phasing of rotor hub loads required for vibration reduction in the more heavily weighted sensor locations. Thus, it may be possible to achieve further vibration reduction at the more heavily weighted sensor locations, but at the possible sacrifice of higher vibration at the less heavily weighted locations.

It may be possible to use this characteristic of the sensor weighting configuration to advantage by implementing a variable weighting matrix to perturbate the controller away from a local optimum. Such a variable weighting algorithm may also be useful in maximizing controller performance at all flight conditions. A variable weighting matrix may be a function of time or of controller performance. Two similar algorithms were considered in this study for varying the diagonal sensor weighting matrix W_z as a function of controller performance. Both algorithms calculate a new vibration weighting matrix based upon the current vibration level with a gain factor that is indicative of the uncontrolled vibration level.

Neither algorithm provides any improvement in controller performance at the baseline flight condition. Furthermore, both cause very oscillatory behavior at the high thrust flight condition. It may be that an appropriate algorithm can be defined to provide better performance in terms of the final solution, but these algorithms are too sensitive to changes in vibration. No results will be presented for these algorithms.

Variable Kalman Filter Covariances

As indicated in the discussion of the Kalman filter identification algorithm, Kalman filter covariances Q and R must be assigned in order to complete the identification algorithm description. In the RTSA controller, the covariance Q was held constant, and the covariance R was varied according

to a simple algorithm involving the performance index. Due to system nonlinearities and transient response to control inputs, it may be necessary to provide algorithms describing covariances Q and R as variables in order to achieve optimum vibration alleviation.

Ideally, R should be varied according to changes in the noise to signal ratio or other factors influencing measurement accuracy. Likewise, Q should be varied according to the variability of the actual T-matrix due to nonlinearities or changing flight conditions. Since it is usually very difficult to numerically describe such phenomena in a practical system, algorithms based upon variables such as aircraft acceleration, rotor thrust, or performance index are usually prescribed, with the hope that these variables are indicative of measurement noise and/or parameter variation. In the present study, several alternative algorithms based upon the performance index are considered for varying either Q or R. All of these algorithms attempt to achieve basically the same behavior in the ratio of Q/R which is indicative of the relative uncertainties in system identification and vibration measurement. If J increases, Q/R is increased to reflect degraded controller performance and relatively more uncertainty in system identification than vibration measurement. If J decreases, Q/R is reduced to reflect good controller performance, good system identification, and relatively more uncertainty in vibration measurement.

In this investigation, it has been found that all of these algorithms are very sensitive to the selection of several different internal parameters required to completely define the algorithm. Each algorithm has been implemented in the deterministic controller at the baseline flight condition, and none improve controller performance, even after several attempts to tune them. In fact, they all tend to have detrimental effects on performance. The use of these algorithms did point out the difficulty of trying to define variable Q and R algorithms based on the performance index. It may be more worthwhile to consider algorithms based upon thrust or some other parameter that is indicative of flight condition. Since these algorithms were so unsuccessful, they were deactivated for most of the present investigation, and covariances Q and R were held constant. No results will be presented for these algorithms.

Controller Initialization

An important characteristic of the active controller configuration defined above is that it operates recursively and, after being initialized and activated, is completely independent of theoretical predictions of helicopter response or flight test measured helicopter response to higher harmonic control. No such information is stored in the computer. The controller must identify and track the response to higher harmonic control and then calculate and command the required control inputs. Once the controller is activated, it

performs its calculations and update functions once every rotor revolution based upon the information from the present rev, ith, and the previous rev, (i-1)th. However, this recursive characteristic of the controller requires that the controller be initialized at the time it is activated in order to satisfy the last rev information requirement.

For a given controller configuration, the initialization process consists of zeroing the $\Delta\theta$ vector; defining Q_o, R_o and P_o in the identification algorithms; and initializing the T-matrix for rev zero. For a production helicopter, the controller will normally be initialized and activated in hover; however, in the present analytical study, the controller is initialized and activated at some steady forward flight condition with the expectation that the controller will converge to a steady set of higher harmonic control inputs. The latter method would probably also be used in a wind tunnel test. In either case, the main concern is to keep the controller stable until new measurements are obtained to update the estimate of parameters.

A value for the initial T-matrix can be obtained from open-loop perturbations of higher harmonic control inputs. This approach was used in the Ref. 10 study of the RTSA controller and represents a good estimate of the initial T-matrix even if the system is nonlinear. However, as will be seen, the T-matrix need not be so well defined, since the controller will identify and track the T-matrix. Thus, the only criterion for defining the initial T-matrix is that it maintain stability and not generate vibration when the controller is activated. In the present study, the initial T-matrix determined from open-loop perturbation at the baseline (150 kt) flight condition is used for all other flight conditions.

The initial values of covariances P, Q, and R must be selected to match the system. The initial value of P (the covariance of the T-matrix estimate) can be set to a large value to reflect uncertainty in the estimates of the T-matrix. The Kalman filter identification algorithm will then automatically calculate a new value of P each update. The initial value of Q (the covariance of changes in the T-matrix) should reflect the best estimate of how rapidly and widely the T-matrix changes with flight condition as control inputs are made. In other words, if the system is quite nonlinear, then the initial value of Q must be made large. In the controller algorithms, this reflects increased uncertainty in parameter estimates which increases the Kalman gain in the process of making new estimates. The initial value of R, the covariance of measurement noise, should reflect the uncertainty in vibration measurements.

Since such knowledge of most systems is somewhat vague, the selection of these covariances usually involves some trial and error along with general

knowledge of the system to optimize their relative magnitudes. Recall from the discussion of the identification algorithm that the relative magnitudes of P/R and Q/R are actually more important than individual magnitudes and should reflect the relative uncertainty in vibration measurements and system identification. In this study, covariances P, Q, and R were varied from their baseline values over a fairly wide range to determine the sensitivity of controller performance to non-optimum tuning of P, Q, and R.

Controller Implementation

The sequence of events (neglecting computational requirements) that occurs within a typical rotor revolution with the controller activated is shown in Figure 5. Once the controller is initialized and activated, the controller performs its calculation of required higher harmonic control and implements the appropriate changes in control inputs once every rotor revolution.

In Figure 5, a step change in higher harmonic control input, $\Delta\theta$, is shown to occur at the start of the ith rotor revolution. The magnitude and phase of the $\Delta\theta$ input commanded at the beginning of this rev are the result of controller calculations made at the end of the (i-1)th rev. As a result of this $\Delta\theta$ input, a transient vibration response of the helicopter occurs due to the transient change in rotor higher harmonic airloads. This transient response is allowed to decay for 3/4 rev before the harmonic analyzer in the vibration controller is activated. This 3/4 rev delay is essentially "dead" time during which the controller must wait, but it is very important to controller performance. If the harmonic analysis is performed earlier, the analyzer would operate on a largely transient signal and pass inaccurate information to the parameter identifier. The result would be an inaccurately identified T-matrix with a resultant degradation in controller performance, since the commanded $\Delta\theta$ inputs would be based on inaccurate parameter estimates passed to the minimum variance control algorithms.

The time that is allowed to pass before the harmonic analysis is performed is certainly arbitrary. The more time allowed for transient decay, the better for controller performance in terms of system identification and accuracy of commanded control inputs; however, this may not be true of overall controller performance when taking into account the time to convergence or the capability to quickly track T-matrix changes and reduce vibration due to transient maneuvers. As the time allowed for transient decay decreases, there is a degradation in controller performance due to inaccurate system identification and inaccurate $\Delta\theta$ commands which in the extreme could increase vibration response. On the other hand, an increase in the time delay allowed for transient decay increases the time between vibration response and commanded

higher harmonic control. At some point, time to convergence to a minimum vibration condition will be longer than for a controller needing to hunt around somewhat due to inaccurate system identification. While keeping the above tradeoff in mind, it is desirable to update higher harmonic control as quickly as possible in order to track any maneuver induced transient changes in the T-matrix, and to reduce the resultant vibration response.

The 3/4 rev allowed for transient decay in Figure 5 is based upon a theoretially predicted transient vibration response to a typical step input of higher harmonic control. Figure 6 shows the transient 4/rev response of the vertical component of hub acceleration to a step input of 0.2 degrees of 3/rev cyclic pitch as predicted by G400. The magnitude of the step input and the conditions present when applied are representative of the conditions present when the controller is first activated at rev 4 in a typical closed-loop simulation. The response shown is representative of the transient response observed in the other components of hub acceleration as well as those for the RTA simulation used in this study. For any given revolution, the vibration level plotted in Figure 6 is the 1/2 peak-to-peak amplitude of acceleration obtained from a harmonic analysis of the last 1/4 rev as shown in Figure 5. As indicated in Figure 6, more than five revs are required for the transient response to completely die out. However, the error introduced by allowing only 3/4 rev for transient decay before performing the harmonic analysis is less than 10 percent of the new steady state vibration level. The earlier the harmonic analysis is performed, the larger the error in the 4/rev content. These results depend upon the nature of the $\Delta\theta$ input, the initial vibration level, and the sensitivity of the particular vibration components to higher harmonic control. However, the results do indicate the importance of the transient response to $\Delta\theta$ inputs. In the present study, the impact of waiting longer than one rev between updates has been considered. It has been decided that a 3/4 rev elapse time and a once per rev update is a good compromise between minimizing the transient effect and minimizing the time between updates. Thus, the once per rev update shown in Figure 5 is used in most of the present study.

Returning to Figure 5, the time history of the vibration response is read into the harmonic analyzer for the last 1/4 rev. The harmonic analyzer supplies the cosine and sine components of each vibration parameter to the parameter identifier. Based upon this vibration response and identified parameters from the last rev, the controller updates system identification, calculates the required higher harmonic control, and commands an updated higher harmonic control input which takes the form of a new $\Delta\theta$ step input implemented at the beginning of the (i+1)th rev. This procedure is repeated recursively throughout the entire flight, including all maneuvers and transients.

The controller implementation shown in Figure 5 and described above is for the idealized simulation used in this study where $\Delta\theta$ inputs are put in as step inputs and the computational requirements of the controller are neglected. The practical considerations of implementing active vibration control in an actual helicopter is discussed in detail in Ref. 10. Clearly, the commanded $\Delta\theta$ input in a practical system would not be a true step and the computational requirements of the controller would either infringe upon the time allowed for transient decay or cause a delay in control commands. Thus, in a practical application, the time allowed for decay for once per rev update would be slightly less than 3/4 rev. Note that it may also be possible to perform certain calculations during a combination of sampling time and transient decay.

Controller Computer Simulation

The previous sections outlined the vibration controller, discussed its separate components, and explained how it is implemented in the closed-loop analytical simulation in the present study. This section discusses the computer simulation of the controller coupled to a rotor mounted on the RTA. The controller simulation was performed on a digital computer by linking an existing nonlinear aeroelastic simulation of the rotorcraft with a computer subroutine that performs all of the functions of the vibration controller as outlined in the previous sections. The nonlinear aeroelastic computer analysis used to represent the H-34 rotor mounted on the RTA and the computer subroutine that performs all the functions of the active controller are discussed below.

Nonlinear Aeroelastic Coupled Rotor - RTA Simulation

The nonlinear aeroelastic analysis used to simulate the coupled rotor and Ames Research Center Rotor Test Apparatus (RTA) is the G400 analysis, documented in Ref. 22. Many improvements have been made to the analysis since the publication of Ref. 22. It can, however, be used for a detailed basic description of the analysis.

This computer analysis performs a time history solution of the differential equations of motion for a helicopter rotor coupled with a flexible body such as a fuselage, or in this case, a wind tunnel test apparatus. The nonlinear equations of motion are solved by using a Galerkin procedure in which the uncoupled normal modes are used as degrees of freedom. The mode shapes and spanwise derivatives of blade pitch angle and nonlinear twist are appropriately combined to describe the coupled blade response to the fully coupled aerodynamic and inertial load distributions. The rotor is coupled to the flexible body at the hub by considering all six hub motion components due to a superposition of as many as sixteen fuselage normal modes, which can be either rigid body or elastic modes. Features of G400 which make it especially

suitable for this study of self-adaptive higher harmonic control include the capability of computing a transient time history which considers the influence of a flexible fuselage and the motion of each individual blade, and its use of nonlinear aerodynamic effects as appropriate.

The H-34 rotor system represented in the simulation has the following basic characteristics:

Type - Fully Articulated

Number of Blades - 4

Diameter - 17.069 m (56 ft)

Blade Chord - 0.417 m (1.367 ft)

Blade Airfoil - NACA 0012

Twist - -8 deg.

Tip Speed - 198 m/s (650 ft/s)

Further physical data on the H-34 rotor system are contained in Appendix I of Ref. 23.

The G400 analysis uses uncoupled natural modes of the individual blades as rotor degrees of freedom. The present simulation includes four blade flatwise modes, two edgewise modes, and one torsion mode, which includes the effect of control system flexibility. The natural frequencies of these modes are tabulated below in cycles per revolution for the 198 m/s (650 ft/sec) tip speed:

Mode		Frequency, $\frac{\omega}{\Omega}$
Flatwise	1	1.03
	2	2.65
	3	4.74
	4	7.32
Edgewise	1	0.24
	2	3.31
Torsion	1	7.04

The G400 analysis uses a superposition of normal vibration modes to represent the fuselage or other flexible body such as the RTA to which the rotor is attached. This study uses normal vibration mode data from an existing NASTRAN mathematical model provided by NASA. The mathematical model includes not only the RTA structure itself, but also the wind tunnel support struts and balance frame structure. A diagram of the NASTRAN mathematical model is shown in Fig. 2(b). The routine execution of the NASTRAN normal modes analysis provides natural frequencies, generalized masses, and mode shapes at grid points throughout the structure of the RTA, balance frame, and struts.

Six normal modes were chosen to represent the RTA and wind tunnel support structure in the G400 analysis. These were chosen by examining the translational acceleration mobility at the rotor head of a total of 24 NASTRAN modes in the longitudinal, lateral, and vertical directions at the rotor blade passage frequency of 14.78 Hz. The six modes having the highest mobilities in any of the three translational directions were utilized in the G400 analysis. The modal properties of the six chosen modes are provided in Tables 2 and 3. Descriptive names and natural frequencies are summarized below:

Mode Description	Frequency (Hz)
Strut Fore-Aft	4.327
Strut Lateral	5.410
Module Nose Vertical	8.321
Module Vertical Bending	14.61
Shaft/Transmission Vertical	15.31
Shaft Lateral	28.33

While G400 considers the influence of the flexible RTA, as represented by the above modal properties, in calculating transient time histories, the version available for this study provides vibration levels at the hub only. Accelerations at various locations in the RTA are not directly available. Therefore, provision has been made in the controller subroutine for a linear transformation to calculate accelerations in the RTA from accelerations at the hub (fixed system). This linear transformation can be written as

$$Z_{RTA} = TGA * Z_H \tag{53}$$

where Z_{RTA} is a vector of the cosine and sine components of 4 per rev acceleration at the six locations in the RTA (see Table 1) and Z_H is a vector of the cosine and sine components of 4 per rev acceleration of the six motions at the hub (see Table 1).

TABLE 2. MODAL REPRESENTATION OF ROTOR TEST APPARATUS AT HUB

Mode No.	Freq. Hz	Generalized Mass kg $\left(\frac{lb-s^2}{in}\right)$	x	y	z	Modal Vector at Hub					
						θ_x		θ_y		θ_z	
						rad/m	(rad/in)	rad/m	(rad/in)	rad/m	(rad/in)
1	4.33	10669. (60.9)	1	.0030	-.2333	-.0004	(-.000009)	.1911	(.004854)	-.0010	(-.000025)
2	5.41	7321. (41.8)	-.0018	1	-.0010	-.0804	(-.002041)	-.0003	(-.000007)	-.2259	(.005738)
3	8.32	8199. (46.8)	1	.0004	-.7072	.0001	(.000003)	.9185	(.02333)	.0001	(.000004)
4	14.61	81711. (466.2)	1	-.0029	.5119	.0022	(.000057)	.6185	(.01571)	.00005	(.000001)
5	15.31	48217. (275.1)	-.7689	.0014	1	-.0004	(-.000009)	-.6102	(-.0155)	.0007	(.000018)
6	28.33	3763. (21.5)	.0031	1	-.0003	-1.7893	(-.045448)	.0066	(.000168)	.3039	(.007718)

TABLE 3. MODAL REPRESENTATION OF ROTOR TEST APPARATUS AT SENSOR LOCATIONS

Mode No.	Freq. Hz.	RTA MODAL VECTOR					
		Nose Lateral	Nose Vertical	Cross-Beam Longitudinal	Cross-Beam Vertical	Tail Lateral	Tail Vertical
1	4.33	.0044	- .5475	.7378	-.0830	-.0029	.0696
2	5.41	1.3471	- .0006	-.0015	.0244	-.2627	- .0008
3	8.32	.0009	-2.2659	-.2656	.0203	.0001	.1634
4	14.61	-.0009	- .0250	.4356	.7637	.0018	-1.5102
5	15.31	.0022	1.7121	-.1898	.7949	-.0006	.0442
6	28.33	.3071	.0064	.0003	.1403	-.0986	.0013

The linear transformation matrix TGA can be determined from the following relationship

$$TGA = M_{RTA} * \text{INVERSE}\ (M_{H4P}) \tag{54}$$

where M_{RTA} and M_{H4P} are mobility matrices calculated via a modal steady-state forced vibration analysis using the NASTRAN model provided by NASA Ames Research Center. M_{H4P} is the matrix relationship between 4 per rev forces and 4 per rev accelerations at the hub:

$$Z_H = M_{H4P} * F_H \tag{55}$$

Likewise M_{RTA} is the matrix relationship between forces at the hub and accelerations in the RTA:

$$Z_{RTA} = M_{RTA} * F_H \tag{56}$$

Z_H and Z_{RTA} are as defined above and F_H is a vector of the cosine and sine components of 4 per rev forcing at the hub. M_{H4P} and M_{RTA} consider an equivalent viscous structural damping coefficient of 5 percent of critical.

The above procedure is mathematically correct; however, with a limited number of modes included in the analysis, the practical validity is constrained. It is implicitly assumed that the rotor hub acceleration vector Z_H contains only those motions that result from steady state 4 per rev excitation of the natural modes included in the analysis. If the Z_H vector includes other motions or transient effects due to a limited sample length, errors can be obtained when calculating Z_{RTA} by Eq. (53). This difficulty was evidenced by the appearance in TGA of certain off-diagonal elements having unreasonably large values. These basically result from inverting the M_{H4P} mobility matrix for a limited number of modes. These large elements cancel if the Z_H vector is consistent with modal steady-state excitation by a reasonable but arbitrary set of F_H components. On the other hand, it was evident that small variations in Z_H from an idealized modal Z_H will cause large errors in Z_{RTA}. Therefore, the large off-diagonal TGA elements were arbitrarily removed in order to obtain reasonable RTA accelerations.

This does not compromise the results of this active control study since they pertain to controller behavior. It merely represents RTA accelerometer responses that are somewhat different from those that would result from

a superposition of modal responses at those points. These differences are equivalent to an arbitrary re-selection of transducer locations in the RTA or to differences that might be expected between calculated and experimental data.

Vibration Controller Subroutine

This section briefly describes the computer simulation of the vibration controller defined previously. The vibration controller was formulated into an independent subroutine named CONTRL which is linked to the G400 aeroelastic simulation of the rotorcraft. The subroutine CONTRL is formulated in much the same manner as that defined in Ref. 10 for the original RTSA controller, but with appropriate modifications to include the new capabilities described above. Figure 7 shows a schematic of subroutine CONTRL including the interface with the G400 analysis. Note that the active controller consists of all the subroutines occurring between the first dashed line shown in this figure and the return to G400. Together, these subroutines perform all the active controller functions shown in the lower part of Fig. 4. As can be seen in Figure 7, this subroutine CONTRL implements the alternative controller configurations by setting various input parameters or flags in subroutine VARCON to dictate which system model, controller type, and other alternative modifications are to be used.

During the time history solution process in G400, the time integration step is normally set to an equivalent of 5 degrees of rotor azimuth. In the last quarter rev (270 to 360 degrees azimuth), the time varying hub accelerations as computed by G400 are passed to a harmonic analyzer to simulate analog sensor signals. This step initiates the active controller functions. The harmonic analyzer in the form of subroutine HARM calculates the cosine and sine components of the 4/rev vibrations and stores them in a vibration vector, Z. At the end of the 360 degrees azimuth calculation and, immediately after the call to HARM, CONTRL is called by the G400 main program and the active vibration controller is entered. The information passed when CONTRL is called is the vibration vector, Z, and a control vector containing the cosine and sine components of higher harmonic control inputs from the last rev. This step initiates the remaining active vibration controller functions which are simulated by additional subroutines in CONTRL. Note that no measurement noise has been included in this simulation. If it were to be considered, noise could be added to the harmonically analyzed vibration mesurements at this point, as was done in the study reported on in Refs. 9 and 10.

It should be pointed out that the time varying accelerations could have been just as easily passed to subroutine CONTRL via a storage matrix. The harmonic analysis could then have been performed by a harmonic analyzer within CONTRL. In this manner, all the active controller functions would have been performed by subroutine CONTRL; however, it was decided, for convenience only, to use the same subroutine used in G400 to perform the harmonic analysis.

Each case of the coupled G400/controller simulation begins with an initial settling period to allow initial numerical transients in the G400 time history solution to die out. During this settling period, which lasts a selected number of revs as indicated by input parameter NDELAY, the controller is left inactive and subroutine CONTRL returns control immediately back to G400 with no update in initial control inputs. After this settling period, the controller is activated and the simulation proceeds as follows.

On the first rotor rev of active control, the subroutine INITAL is called to initialize all of the required parameters. As discussed above, this includes the setting of initial values for the T-matrix and covariances P, Q, and R. At this time subroutine PRINT1 (not shown in Figure 7) prints the initial system data. In subsequent calls to CONTRL, these two subroutines are skipped, and the parameters from the previous rev are used as required by the recursive identification algorithm.

At this point, subroutine CONTRL linearly transforms the vector of the cosine and sine components of the 4/rev vibration response calculated in G400 to a new vector of parameters that are to be controlled or minimized. This linear transformation can be written as

$$ZC = TGA \cdot Z \tag{57}$$

where TGA is the linear transformation matrix and ZC is the vector of parameters to be controlled. It is the vector ZC that is actually used to form the performance index to be minimized by the minimum variance control algorithm. The reason for this step in this simulation is that G400 does not, as discussed previously, directly calculate the vibration response in the RTA even though the modal interaction between the RTA and the rotor is taken into account when calculating the hub response. Thus, the vibration response passed to subroutine CONTRL is for the hub. It is then assumed that the vibration response in the RTA can be formed by the above linear transformation. In a practical application, the RTA response would be directly measured and passed to the controller. If it were the hub response that were to be minimized, the TGA matrix would simply be set to the identity matrix, rather than that defined in Eq. (53). Note that the use of a TGA matrix to calculate RTA vibrations is equivalent to controlling hub vibrations with a non-diagonal weighting matrix.

After establishing the vector of parameters to be controlled, the controller is ready to identify the required system parameters using the Kalman filter identification algorithm as discussed previously. In order to implement the identification algorithm, the covariances Q and R must be defined.

If these covariances are to be held constant, subroutine PARID is called to perform all the functions of the Kalman filter identification algorithm using the initial values of Q and R supplied by INITAL. As indicated earlier, several alternative algorithms are to be considered for varying Q and R as functions of the performance index. If one or both of these covariances is to be varied, then the appropriate subroutine QVAR and/or RVAR is called to update the covariances immediately before calling PARID. The primary purpose of PARID is to identify and track the system parameters required by the minimum variance control algorithm. For the local model, the T-matrix relating vibration response to higher harmonic control inputs must be identified. For the global model, the uncontrolled vibration level, Z_o, must also be identified.

Before calculating the required higher harmonic control inputs, the sensor weighting matrix, W_z, must be established. In the present study, two alternative algorithms for varying W_z as a function of controller performance are considered. If W_z is to be varied, the updated weighting matrix is calculated in subroutine ZWT. Otherwise, W_z is held constant at its initial value. If algorithms were to be considered for varying W_θ or $W_{\Delta\theta}$, a subroutine to perform this function would also be called at this point. Once all system parameters have been updated, subroutine VARCON is called to apply the minimum variance control algorithm to calculate the optimum change in higher harmonic control inputs $\Delta\theta^*$ required to minimize the performance index. The exact form of the minimum variance control algorithm implemented by VARCON is dependent upon the controller type and system model. As shown in Figure 7, the controller configuration is defined by the values of parameters IOPT and IBETA. IOPT is set to 1 for the local model and 0 for the global model. IBETA is set to 0 for a deterministic controller, to +1 for a cautious controller, and to -1 for a dual controller.

The end product of VARCON is a computed optimum $\Delta\theta^*$ for updating the higher harmonic control vector; however, before the higher harmonic control inputs are updated and commanded, they must be limited to satisfy any external constraints placed on these inputs. This function is performed in subroutine LIMIT. If the calculated optimum $\Delta\theta^*$ is larger than allowed due to hardware limitations or other reasons, $\Delta\theta$ is limited to the prescribed amplitude while maintaining the same phase as $\Delta\theta^*$. Subroutine LIMIT then calculates the new higher harmonic control input to be implemented in G400 by adding $\Delta\theta$ to the total θ from the previous rev. Finally, subroutines PRINT2 and PRINT3 (not shown in Figure 7) print the results for the current rev. Having performed all its functions, subroutine CONTRL passes the new θ vector back to G400 which then continues its time history solution with the updated higher harmonic control vector.

CLOSED-LOOP ANALYTICAL RESULTS

Analysis and evaluation of the active vibration controller were performed by linking the G400 helicopter simulation with the active vibration controller subroutine CONTRL and operating them in closed-loop fashion, as discussed in the last section. During the course of this study, three controller types were investigated: deterministic, cautious, and dual. Both a local and global system model were investigated as the basis for the primary controller configuration for each controller type. In addition to investigating these primary controller configurations, several internal controller parameters and minor variations in controller configuration were also investigated. These are summarized in Table 4.

TABLE 4

CONTROLLER PARAMETERS INVESTIGATED

- Kalman filter covariances
  P, Q, R
- Minimum variance control parameters
  - Control angles and limits
    θ, $\Delta\theta$
  - Weighting
    W_Z, W_θ, $W_{\Delta\theta}$
  - Stochastic control constant (Cautious, dual)
    λ
- Sensors
  - RTA
  - Rotor hub

The closed-loop analytical study of the controller was generally divided into four parts. First, controller performance for all configurations was investigated at a baseline high speed steady state operating/flight condition. Note that the terms operating and flight condition will be used interchangeably throughout the report even though the simulation considered is for a rotor/RTA coupled system in the wind tunnel. Second, controller performance was investigated at additional steady flight conditions having alternate forward velocities or rotor thrusts. Third, selected controller configurations were investigated during several transient maneuvers. Finally, controller performance was evaluated for additional minor modifications to controller configurations.

The following discussion of the closed-loop analytical results is divided in somewhat the same manner. The baseline controller configurations is presented for each of the three controller types. These baseline configurations can be assumed to be the basis of all results presented for the closed-loop active control study, unless otherwise stated. A summary of overall controller performance for each of these baseline configurations is then presented for the baseline high speed flight condition. Each of the three controller types is then discussed with an emphasis on how controller performance is affected at the baseline flight condition by various controller parameters and variations in controller configuration. The effectiveness of active vibration control at various forward velocities and rotor thrusts is presented. Where applicable, the characteristic performance of specific controller types or system models is discussed at these alternate flight conditions. Controller performance during several transient maneuver conditions is then covered. Throughout this discussion, a comparison is made between the three controller types (deterministic, cautious, and dual) and between the two system models (global and local).

Controller Performance at Baseline High Speed Flight Condition

A steady high speed moderate thrust flight condition was selected as the baseline condition for studying and optimizing controller performance for each controller type. This flight condition had a forward velocity of 77.2 m/s (150 kt) and a nominal value of 0.06 for C_T/σ. The resultant vibratory response for this flight condition was fairly mild with RTA accelerations on the order of 0.2g's with no higher harmonic control or other vibration treatment.

This flight condition was used for the initial study of all modifications made to the RTSA controller. Any modification that failed to show a potential for improving controller performance at this flight condition was not considered further at more severe flight conditions. Much of the testing at the

baseline flight condition focused on the initial study of controller performance, the optimization of controller configuration, and the investigation of controller parameters for each of the three types of controllers.

Baseline Controller Configurations

Based upon the analytical investigation of controller performance at the baseline high speed flight condition, a baseline controller configuration was selected for each of the three controller types. Each of these configurations showed the best overall performance at this flight condition for a given controller type. The characteristics of each of these baseline controllers are presented in Table 5 below.

TABLE 5

BASELINE CONTROLLER CONFIGURATIONS

	Deterministic	Cautious	Dual
System Model	Global	Global	Global
Sensors	RTA	RTA	RTA
Kalman Filter Identifier			
Covariances			
P_o $(g's/rad)^2$	100.	100.	100.
Q_o $(g's/rad)^2$	.001	.001	.001
R_o $(g's)^2$	.001	.001	.001
Minimum Variance Optimizer			
Time between update (rev)	1	1	1
External Control Limits			
θ_{max} (deg)	none	none	none
$\Delta\theta_{max}$ (deg/rev)	none	none	0.2
Stochastic Control Constant (λ)	0.0	1.0	0.01
Weighting in Perf. Index			
Sensors, W_z $(1/g's)^2$	1.0	1.0	1.0
Control Magnitude, W_θ $(1/rad)^2$	0.0	0.0	0.0
Change in Control, $W_{\Delta\theta}$ $(1/rad)^2$	1000.	0.0	0.0

All three of the baseline configurations in this table are identical except for controller type, the arbitrary stochastic control constant related to controller type, and the external limits and internal weighting specifications placed on $\Delta\theta$. Thus, other than the fundamental differences in controller algorithms due to controller type, the only difference in the three baseline controllers is the manner in which limiting of control inputs is implemented.

All three of the baseline controllers are based upon the global system model. As will be discussed later, the selection of the global model was made arbitrarily since the performance of each of the controllers was quite good with both the local and global models. There was no significant advantage of one model over the other. All three of the baseline controllers also use the same Kalman filter configuration with the same initial values for P, Q, and R. Furthermore, all three baseline controllers hold Q and R constant at their initial values while varying P according to the Kalman filter algorithm discussed previously.

All three controllers actively control the vibration levels from the sensors located in the RTA (see Table 1); the output from each of these sensors is weighted equally at unity. The time between control updates is one rotor revolution. Thus, the output from these sensors is harmonically analyzed, the system parameters are identified, and new control inputs are calculated every rotor revolution.

All three controllers place limits on the control inputs, but do so in different ways. None of the baseline controllers externally limit the overall magnitude of control, θ, or internally weight θ via W_θ in the performance index. The baseline deterministic controller slows the rate of change in control inputs between updates by internally weighting $\Delta\theta$ with $W_{\Delta\theta}$ in the performance index. In this baseline deterministic controller, all three control inputs (3, 4 and 5 per rev) are weighted equally at 1000 $(1/\text{rad})^2$. This value does not represent a 1000 to 1 ratio of importance in keeping $\Delta\theta$ small and in reducing vibration. Rather, weighting matrices W_z and $W_{\Delta\theta}$ account for differences in units and relative magnitudes of vibration and control parameters in the terms contained in the performance index (Eq. (3)) as well as the relative importance of these parameters. No external limits are applied to $\Delta\theta$.

The baseline cautious controller neither applies external limits to $\Delta\theta$ nor internally weights $\Delta\theta$ with $W_{\Delta\theta}$. Rather, the cautious controller inherently slows down the implementation of new control inputs via the stochastic term discussed previously. Since the global model is used, this term effectively acts as a variable weighting on θ in the performance index which is dependent upon the uncertainty in system identification.

The baseline dual controller applies external limits on the rate of change of control in order to allow the inherent perturbations in control inputs due to its stochastic term in the performance index without allowing short term control to be compromised too severely. The baseline dual controller externally limits the change in control between updates to a maximum of 0.2 degrees for each of the control inputs.

These baseline controller configurations can be assumed to be the configurations used for all results presented in this report (unless otherwise stated). The performance of these baseline controllers at the baseline high speed (150 kt) flight condition are discussed below.

Vibration Reduction

Figures 8(a) and 8(b) present the G400 simulation results for the three baseline controller configurations operating closed-loop at the baseline high speed flight condition. Each of the three sets of curves in Figs. 8(a) and 8(b) represents the response of one of the best configurations, achieved by tuning appropriate parameters within the controller algorithms, for each of the three controller types when using the global system model. The specific tuning values used for each controller in these figures have been presented previously in Table 5.

Figure 8(a) shows G400 predicted time histories of the vibration performance index J_Z and one typical component of vibration in the RTA (Cross-Beam vertical) after the controller is activated at the fourth rotor revolution. Figure 8(b) shows the time history of the amplitude of each of the higher harmonic control inputs (3, 4, and 5 per rev) commanded by the three controllers. Since the vibration performance index plotted in Fig. 8(a) is a weighted sum of the squares of all the vibration components being actively controlled, it is a good indicator of overall controller performance in reducing vibration. Note that the vibration performance index plotted is not the same as the performance index actually minimized by the minimum variance control algorithms, (e.g., Eq. (3)), since none of the weighted quadratic terms involving θ or $\Delta\theta$ are included. While these terms are important to overall controller performance and stability, they are not indicative of vibration reduction achieved by the active controller. Unless otherwise stated, all plots of the performance index in this report are actually the vibration performance index J_Z having vibration terms only.

Figure 8(a) shows that all three controller types do an excellent job of reaching a new steady vibration level that is greatly reduced from the baseline vibration level. After the controller is activated at rev 4, the vibration performance index J_Z immediately starts to decrease for all three controller types. After only two revs and 0.55 seconds elapsed time of active

control, both the deterministic and cautious controllers achieve and maintain at least a 90 percent reduction in the performance index. The limited dual controller requires about 5 revs or 1.4 seconds of active control to achieve the same overall vibration level. By rev 10, all three controllers have essentially converged to a value of the performance index that is only 3 percent of the baseline value. The elapsed time between rev 4, when the controller is activated, and rev 10 is about 1.6 seconds.

The predicted vibration level in the RTA is represented in Fig. 8(a) by the vertical component at the cross-beam sensor location. The vibration level at this location also decreases abruptly after rev 4 for the deterministic and cautious controllers. By rev 7, these two controllers have achieved at least a 65 percent reduction in this vibration component. The limited dual controller does not achieve this level of vibration until rev 10. In fact, due to system probing by the dual controller, the vibration level at this location actually increases in the first 3 revs, even though the overall vibration level is being reduced, as indicated by a reduction in the performance index. By rev 15, all three controllers have reduced the vertical cross-beam vibration level to less than 0.041g, which is less than 30 percent of the baseline value of 0.14 g.

Note that, at rev 9, both the deterministic and cautious controllers achieve a level of vibration at this sensor location that is quite a bit lower than that achieved at convergence. Thus, these controllers have somewhat sacrificed the reduction in vibration at this location in order to achieve a lower value of the performance index, which is effected by not only the vibration level at each sensor location but also the $\Delta\theta$ and θ terms (see Eq. (3)). If this is unacceptable, the vibration weighting matrix, W_Z, can be changed to alter the relative importance of selected vibration parameters.

Figure 8(b) shows the time history of 3, 4, and 5 per rev cyclic pitch amplitudes as commanded by the three controllers. For the deterministic and cautious controllers, the initial change in 3/rev cyclic pitch is about 0.12 degrees in the first rev, while changes in 4 and 5/rev are on the order of 0.15 degrees. The corresponding reduction in the vibration level in this first step is substantial, as noted above. After the first rev of active control, the deterministic and cautious controllers gradually increase the amplitude of all three control inputs, while further reducing the vibration level. The vibration at the six RTA sensor locations remains fairly steady after rev 15. At this point, the 3/rev cyclic pitch amplitude is still rising very slowly, on the order of 0.002 degrees per rev. However, the 5/rev input

is fairly steady and the 4/rev input slowly starts to decrease at about 0.002 degrees per rev. Thus, after 15 revs, both the deterministic and cautious controllers are trying to further reduce vibration but, in effect, achieve a fairly steady vibration level by trading off an increase in 3/rev with a decrease in 4/rev cyclic pitch. These changes are so gradual that the 3/rev cyclic pitch increases by only 0.025 degrees between rev 30 and rev 50. As will be discussed later, the deterministic and cautious controllers did not exhibit this same tendency to command ever so slightly increasing and/or decreasing control inputs at the baseline flight condition when large values of P_o were specified.

In contrast to the deterministic and cautious controllers, the dual controller exhibits a tendency to probe the system by perturbating the higher harmonic cyclic inputs. This tendency is clearly evident in the cyclic pitch amplitudes shown in Fig. 8(b) for the dual controller. As expected, this probing initially results in a slight degradation in short term control as can be seen in both the cross-beam vertical vibration component and the performance index. After identification improves, system probing diminishes and the final controller solution is every bit as good as that of the deterministic and cautious controllers. As will be discussed later, the dual controller's tendency to probe the system has been somewhat inhibited in the controller configuration represented in Figs. 8(a) and 8(b) by an application of external rate limits of 0.2 degrees per rev. Without these limits, the perturbation in control inputs used to probe the system are much larger and result in much worse short term control; however, the unlimited dual controller still manages to remain stable and to converge to a very good final solution.

The change in the vibration level at all six sensor locations in the RTA is shown in Fig. 9 for all three controllers. In this figure, a comparison is made between the 4 per rev vibration levels at rev 4 without any higher harmonic control and at rev 30 where the controllers have essentially converged to a steady level of reduced vibration. All three controllers have substantially reduced vibration at all sensor locations except the two locations that had very low initial levels of vibration without any higher harmonic control. The low levels of vibration at these two sensor locations have been maintained. Reductions in vibration for the four primary components are between 75 and 90 percent for all three controllers.

Also shown in Fig. 9 are the fixed system hub vibrations. Note that the three angular accelerations have been multiplied by 0.305 m (1 ft) so that all six hub vibrations are presented in the form of g's. The two primary contributors (vertical and longitudinal components) have been reduced by all three controller types. A substantial 75 percent decrease in the longitudinal

component has been achieved while a more modest 20 percent reduction has been achieved in the vertical component. The other four components, which were small initially, remain at about the same order of magnitude. The substantial reduction in the largest component along with less or no reductions in the other five components indicates that the reductions in vibration in the RTA have been achieved by a combination of reduced forcing at the rotor hub and vectorial cancellations of modal contributions to RTA vibrations. It has been found in this investigation that more substantial overall reduction in hub vibrations can be achieved by the use of hub sensors rather than RTA sensors. However, further reduction in RTA vibrations is not necessarily obtained unless proper phasing of the hub vibrations is also obtained. Indeed, certain RTA vibrations increased substantially even with decreased hub forcing when only hub sensors were used at the baseline flight condition.

Finally, the amplitudes and phases of higher harmonic control required to achieve the vibration reductions shown in Fig. 9 are shown in Fig. 10 for the three controllers. Note that the phases shown in this figure have been transformed such that $0 \leq \underline{/\theta_3} \leq 120°$, $0 \leq \underline{/\theta_4} \leq 90°$, and $0 \leq \underline{/\theta_5} \leq 72°$, as allowed by the periodic nature of the control inputs. All three controllers require amplitudes on the order of 0.3 degrees for all three cyclic pitch harmonics which are quite reasonable for this high speed flight condition. Figure 10 also shows that all three controllers converge to about the same control solution. Furthermore, the very slow changes in control occurring after convergence in the performance index has been achieved may eventually lead to exactly the same solutions. However, this need not be the case; as will be discussed later, many different control solutions can result in essentially the same vibration levels in the RTA.

Rotor Blade Stresses

Another area of concern that is affected by higher harmonic control is cyclic rotor blade stresses. Since higher harmonic cyclic pitch affects rotor blade airloads, it is expected that some changes in blade stresses will accompany changes in vibrations. Figure 11 shows the 1/2 peak-to-peak blade bending stresses and torsional moment along the blade span for the baseline flight condition with no higher harmonic control and for the deterministic controller at rev 30 with optimum higher harmonic control. Clearly, there is a significant increase in all the vibratory moments and stresses, but especially in the torsional moment. The effect of the cautious and dual controllers is almost identical to that shown in Fig. 11 for the deterministic controller. This is expected since the total control vector at rev 30 is similar in magnitude and phase for all three controllers. The percent increase in peak bending stresses and torsional moment is presented for critical locations along the blade for all three controllers in Table 6.

TABLE 6

PERCENT INCREASE IN MAXIMUM ROTOR VIBRATORY MOMENTS AND STRESSES FOR BASELINE FLIGHT CONDITION AT REV 30

	Deterministic	Cautious	Dual
Flatwise (0.394R)	13.3	14.4	17.2
Edgewise (0.265R)	52.5	52.0	50.6
Torsional (0.079R)	167.	174.	197.

The increase in 1/2 peak-to-peak torsional moment is almost 200 percent near the blade root. The inboard edgewise bending stress increases by slightly over 50 percent. The inboard flatwise bending stress increases by about 15 percent. These increases are most certainly significant from the standpoint of blade life. For a new aircraft or significant model change, increases in loads such as those indicated in this study would have to be accounted for in the design of the rotor blade. These increased loads must also be considered in any proof-of-concept wind tunnel or flight test to demonstrate the higher harmonic control concept.

An alternate approach is to include terms representative of blade stresses, appropriately weighted, in the performance index J. In so doing, it seems possible to maintain or reduce certain stress levels, without compromising vibration reduction, by reducing airloads induced by interharmonic coupling with properly phased higher harmonic control inputs. For this to be accomplished, parameters from the rotating system (e.g., rotor blade stresses, rotating blade root shears) must be added to the performance index to ensure that reductions in vibration are achieved via properly phased higher harmonic control inputs and modal cancellations of small quantities rather than large quantities. More will be said in regard to this later.

While such an approach was not pursued in the present study, certain results did indicate such an approach might be feasible, and it should be seriously considered in the future. It is not desirable to have to monitor blade stresses (or any other parameter in the rotating system) on a production aircraft, but in future analytical or wind tunnel test investigations such an approach would provide valuable information on the higher harmonic control

phenomenon as well as the capabilities of the closed-loop active controller to operate with numerous output parameters which may represent conflicting criteria. Furthermore, it may be possible to compute blade stresses or other parameters in the rotating system indirectly via a state estimator rather than by direct measurement. Such an approach may then be applicable to a production aircraft.

Rotor Performance

Another area of concern that is affected by higher harmonic control is rotor performance. Due to aerodynamic interharmonic coupling in forward flight, it is possible, as predicted by linear aerodynamic theory, for 3 and 4 per rev higher harmonic control inputs to create 1 and 2 per rev airloading, which can alter the trim condition and, thus, rotor performance. The extent that rotor performance is affected at the baseline flight condition is shown in Table 7. This table compares key trim and rotor performance parameters for the baseline flight condition with no higher harmonic control inputs to those with higher harmonic control being provided by one of the three controller types.

TABLE 7

EFFECT OF HIGHER HARMONIC CONTROL ON ROTOR PERFORMANCE AT BASELINE FLIGHT CONDITION

	No HHC	Deterministic		Cautious		Dual	
Thrust N (lb)	36735 (8255)	37202 (8360)	+1.3%	37224 (8365)	+1.3%	37273 (8376)	+1.5%
Torque N-m (ft-lb)	25139 (18542)	26374 (19453)	+4.9%	26403 (19474)	+5.0%	26514 (19556)	+5.5%
Prop Force N (lb)	4001 (899)	3983 (895)	-0.4%	3978 (894)	-0.6%	3961 (890)	-1.0%
Equiv. L/D	10.26	9.37	-8.7%	9.34	-9.0%	9.23	-10.0%

Note: Rotor Performance Parameters with higher harmonic control are those occurring at rev 30

At the baseline (150 kt) flight condition, the application of higher harmonic control has caused an increase in required torque on the order of about 5 percent for all three controller types. This increase in required torque is accompanied by an increase of about 1 percent in rotor thrust. In actual flight, any impact of higher harmonic control on rotor thrust would be accounted for by adjustment of collective pitch. For this particular flight condition, a direct power penalty is being paid for the implementation of higher harmonic control to reduce vibration by all three controllers (exclusive of any increase in power necessary to operate the control system). Ideally, it would be desirable to implement higher harmonic control without any increase in required power. It may be possible, in future studies, to accomplish this by including in the performance index an appropriately weighted term that is proportional to rotor torque.

In addition to the changes in rotor torque and thrust, the implementation of higher harmonic control has caused a decrease in both propulsive force and equivalent L/D. The propulsive force has decreased by less than 1.0 percent for all three controllers. The equivalent L/D has decreased by almost 10 percent. This is within the accuracy of the performance analysis for which constant inflow and steady aerodynamics were assumed for this study.

Effect of Internal Controller Parameters on Performance at the Baseline High Speed Flight Condition

In the previous section, overall results were presented for three baseline controllers at the baseline high speed steady flight condition. All three controllers demonstrated excellent effectiveness in quickly achieving substantial reductions in RTA vibrations with low multicyclic control inputs. Each baseline configuration was determined by testing many different controller configurations and optimizing controller performance at the baseline high speed flight condition for each one of the three controller types being investigated in this study. In optimizing controller performance, the characteristics considered most important were stability, time to convergence, overall reduction in vibration, and amplitude of control inputs commanded by the controller.

In the process of optimizing controller performance and establishing the baseline controller configurations, much has been learned about the effect that various controller parameters (e.g., λ, $W_{\Delta\theta}$, W_{θ}, and $\Delta\theta_{max}$) can have on controller performance. The effect of important parameters on the characteristic performance of each controller type at the baseline flight condition will be discussed throughout the remainder of this section. Furthermore, the performance of controller configurations based upon the local system model will be presented and compared to the performance of corresponding configurations based on the global model.

Deterministic Controller

One of the most important considerations in controller performance is stability. In Ref. 10, external rate-limiting of control inputs was found to be very important to stability and performance for the deterministic controller. In this investigation, rate-limiting has also proven to be very important to the deterministic controller's stability and performance for not only the local system model, which was used for the RTSA controller in Ref. 10, but also for the global system model. However, it has been found that stability and performance of the deterministic controller is improved dramatically for both system models by the use of internal rate-limiting with $W_{\Delta\theta}$ and the weighted quadratic $\Delta\theta$ term placed in the performance index in Eq. (3), rather than external rate-limiting with $\Delta\theta_{max}$.

External Rate-Limiting

In Figs. 12 and 13, controller performance at the baseline flight condition is shown for an unlimited deterministic controller based on a global system model and a local system model, respectively. Other than the local system model being used in the latter and no limits being placed on control inputs, the configuration of both controllers is exactly the same as the baseline deterministic controller presented in Table 5. Clearly, the time histories of the performance index and the amplitude of 3 per rev cyclic pitch presented in these figures show that both controllers are unstable. The time histories of 3 per rev cyclic pitch magnitude, which are indicative of 4 and 5 per rev control as well, are highly oscillatory and increase to extremely high magnitudes. The time histories of the performance index are also very oscillatory, oscillating violently between vibration reduction and magnification.

Figures 14 and 15 show the effect of applying various amounts of external rate-limiting to the same two controllers. Note that the sharp break that occurs in the 3 per rev cyclic pitch at rev 29 in these figures is due to the control inputs being held constant during the last rev to allow transients to decay before the final vibration analysis is performed. This is done in all the closed-loop simulations, but is most apparent here since convergence has not been achieved. Equal limits are applied to the incremental changes of each of the three control inputs. These limits are applied after the minimum variance control algorithm has calculated a set of optimal changes in control, as shown in Fig. 4. With a limit of 0.5 degree placed on the change in control between updates, the behavior of the deterministic controller is still very oscillatory and unacceptable for both system models. By further restricting the limits to 0.2 degree between updates, controller stability and performance have been improved in both controllers to the extent that the oscillatory behavior has been reduced substantially. Furthermore, once the

controllers are activated a reduced vibration level is maintained. After 10 revs, both controllers maintain at least a 45 percent reduction in the performance index compared to the initial value with no higher harmonic control. By restricting the limits to 0.1 degree per rev, controller performance is smoothed still further; however, the control inputs commanded by both controllers are very high and do not appear to be converging even by rev 30. Furthermore, neither controller can maintain the low levels of vibration achieved between revs 20 and 23. The detrimental effects of large control inputs will be discussed shortly.

While external rate-limiting clearly improves the stability and performance of the deterministic controller with either a local or global system model, performance as shown in Figs. 14 and 15 is still unsatisfactory due to the very high control inputs being commanded for a moderate flight condition and the lack of convergence by rev 30, especially in light of the excellent performance obtained with the three baseline controllers. Part of the problem appears to be that the controller with the particular initial T-matrix supplied is biased towards reducing vibration with large control inputs which are properly phased to produce low vibration in the RTA. Reduced vibration in the RTA can be achieved by a properly phased "mix" of 3, 4, and 5 per rev inputs of large amplitude or of small amplitude, as demonstrated by the solutions just presented for the externally limited deterministic controllers and the solutions presented previously for the baseline controllers. One of the reasons for this is coupling between 3, 4, and 5 per rev control inputs and vectorial cancellation in going from the rotating system to the fixed system. One possible phenomenon is as follows. The 3 and 5 per rev rotating inplane shears combine to form 4 per rev fixed system hub loads (longitudinal, lateral, pitching moment, and rolling moment). Reduced fixed system shears can result from small differences between either large rotating shears or small rotating shears. Since 3 and 5 per rev control inputs directly affect 3 and 5 per rev rotating shears, 3 and 5 per rev higher harmonic control inputs can tend to cancel each other. Thus, a particular mix of control inputs with large amplitudes can have essentially the same overall effect on vibration in the fixed system as an appropriate mix of inputs of small amplitude. Further coupling can take place due to modal cancellation in the RTA for a given set of fixed system hub loads. Thus, many solutions in terms of the amplitude and phase of 3, 4, and 5 per rev may exist for a given vibration level in the RTA, as will be demonstrated later.

It is not clear as to why the controller with this particular initial T-matrix, which is obtained by perturbating control inputs around zero higher harmonic control, is biased toward large amplitude control solutions; however, that appears to be the case. It may be due to the use of fairly large amplitudes (1.0 degree) for perturbation of each of the control inputs. When the controller has no limits or very large limits placed upon the rate that inputs can be implemented, the controller quickly implements large changes in control

inputs, which causes two problems. First, larger transients occur due to large changes in control inputs, and these transients take longer to decay. Thus, the controller is working with larger errors in system measurements which causes it to perceive certain vibration levels in the RTA and effects of implemented control angles on vibration that are erroneous. This, in turn, leads to changes being made to the T-matrix that may not be appropriate. Furthermore, the controller is more sensitive to perceived errors in the T-matrix, and the corresponding changes to the T-matrix are increased due to increased Kalman gains caused by larger control inputs or changes in control inputs. Thus, even if the system is completely linear, large control input implementation can lead to oscillatory behavior and instability. The second effect is that nonlinearities and changes in the T-matrix increase at large amplitudes of control. Clearly, this second effect aggravates the first.

When the limits placed on $\Delta\theta$ are made smaller, the transient effects are lessened and the controller is given more of a chance to measure vibration response and identify and track system parameters more accurately. Thus, performance is improved. However, external limits do nothing to directly remove the bias to go to large control inputs. They simply slow down the rate that the controller proceeds. Indirectly, rate-limiting allows more time for identification to remove this bias with changes in the T-matrix. However, as $\Delta\theta_{max}$ becomes smaller, less information is received by the identifier in order to make changes in the T-matrix. Thus, the bias to go to solutions with high amplitudes of control inputs tends to remain as can be seen in the time history for 3 per rev cyclic pitch and a value of 0.1 degree for $\Delta\theta_{max}$ in Figs. 14 and 15.

It is possible to overcome some of these effects encountered with more restrictive limits by specifying higher initial values of P and Q. With the resulting increase in Kalman gains, the controller becomes more sensitive to errors in predicted vibration levels and makes larger corresponding changes in the T-matrix. The effect of increasing P_o and Q in an externally limited deterministic controller is shown in Fig. 16. This figure shows the time history of 3 per rev cyclic pitch amplitude and the performance index for a deterministic controller with local system model having values of 1000.0, 100.0, 0.001, and 0.2 for P_o, Q, R, and $\Delta\theta_{max}$, respectively. The substantial increases in P_o and Q have allowed substantial changes in the T-matrix to be made which allows a solution having at least an 85 percent reduction in the initial performance index to be reached with control inputs on the order of 0.8 degree or less. The limit of 0.2 degree placed on incremental changes in 3, 4, and 5 per rev control inputs allows the controller to remain stable. However, the controller is very skittish as evidenced by the oscillatory behavior in both control inputs and performance index even after "convergence"

has been achieved. This skittishness could result in instability if large changes in system parameters were encountered due to change in flight condition, transient, etc.

It should be noted that the controller represented by the response in Fig. 16 has essentially the same configuration as the RTSA controller studied in Ref. 10. The only differences are the initial tuning of P_o, Q, R, and $\Delta\theta_{max}$ and a constant covariance R. For the results shown in Fig. 16 as well as all other results presented in this report, R is held constant. In Ref. 10, the controller used a very simple algorithm to vary R as a function of the performance index. The response shown in Fig. 16 is the best performance that can be obtained with the local deterministic configuration without any of the modifications being investigated in this study. Extensive experimentation with the tuning of P_o, Q, R, and $\Delta\theta_{max}$ were required to achieve performance this good.

Figure 17 compares the performance of two deterministic controllers with external rate-limiting. The dashed curve represents the local deterministic controller with high P_o and Q just discussed. The solid line represents a global deterministic controller with values of 100.0, 0.001, 1.0, and 0.1 for P_o, Q, R, and $\Delta\theta_{max}$, respectively. R has been raised such that identification is somewhat inhibited due to low Kalman gains. Thus, changes made in the T-matrix are small. The difference in performance between these two controllers is not a matter of local versus global model, but is a matter of differences in tuning of P_o, Q, R, and $\Delta\theta_{max}$. The intent of this and the next several figures is to demonstrate the phenomenon of cancellation of inplane rotating shears and the differences that exist between these two solutions due to the differences in the magnitude of control inputs implemented.

Figure 18 compares the RTA vibration levels achieved by these two controllers at rev 30 to the initial values present with no higher harmonic control. Both controllers have achieved substantial reductions in vibration. The higher harmonic pitch amplitudes commanded at rev 30 by these two controllers are shown in Fig. 19. Considering the substantial differences in multicyclic pitch amplitudes required by these two controllers, the vibration levels achieved in the RTA are surprisingly similar.

Figure 20 compares the 3 and 5 per rev rotating lateral shears, the 4 per rev longitudinal and lateral fixed system hub shears, and the performance index for these two controllers. The baseline values of these parameters without higher harmonic control and those values achieved by the baseline deterministic controller with internal rate-limiting ($W_{\Delta\theta}$) are also shown

for reference. This figure is indicative of the phenomenom of cancellation between 3 and 5 per rev control inputs and rotating shears as discussed above.

The large 3 and 5 per rev inputs commanded by the global deterministic controller having low Kalman gains have caused large increases in 3 and 5 per rotating lateral shears. The increase in the 5 per rev rotating shear is especially large at almost 14 times the baseline value. On the other hand, the moderate 3 and 5 per rev inputs of the local deterministic controller having high Kalman gains has actually reduced the 3 per rev rotating lateral shear slightly. At the same time, it has increased the 5 per rev component by almost 6 times the baseline value, but this is almost half the value resulting from the global model. In comparison, the small control inputs commanded by the baseline deterministic controller with internal rate-limiting ($W_{\Delta\theta}$) have resulted in a significant decrease in the 3 per rev rotating shear and a comparatively moderate increase in the 5 per rev rotating shear.

These significantly different sets of 3 and 5 per rev rotating shears combine to form hub fixed system components that are fairly close in magnitude. The resulting 4 per rev fixed system longitudinal shears are almost equal in magnitude while the resulting magnitudes of 4 per rev lateral shears are fairly close considering the huge differences in the rotating shears. With modal cancellation in the RTA, these fixed system shears, in turn, result in similar vibration levels in the RTA as indicated by the performance indices in Fig. 20 and the actual vibration at each sensor location in Fig. 18.

Some of the consequences of achieving reduced vibration in the RTA via large control inputs and corresponding large rotating shears rather than small inputs and small rotating shears is shown in Figs. 21 and 22. Figure 21 shows 3, 4, and 5 per rev harmonic components of the blade response of the first two flatwise modes. As expected, the blade response resulting from the high amplitude control inputs is substantially higher than the response resulting from the moderate amplitude control inputs. As a consequence, the 1/2 peak-to-peak bending moments and stresses are significantly higher for the control inputs of high amplitude ($\theta_3 = 2.6° \angle 120°$, $\theta_4 = 2.6° \angle 34°$, $\theta_5 = 2.1 \angle 24°$), as shown in Fig. 22. This is especially true of the edgewise stress and the torsional moment. The effect of the high ampliutde control inputs on rotor performance is summarized in Table 8.

TABLE 8

EFFECT OF CONTROL INPUT AMPLITUDE ON ROTOR PERFORMANCE AT BASELINE FLIGHT CONDITION

	No HHC	Moderate Amplitude (~0.8 deg)		High Amplitude (~2.5 deg)	
Thrust N (lb)	36735 (8255)	36971 (8308)	+0.6%	33638 (7559)	-0.8%
Torque N-m (ft-lb)	25139 (18542)	26488 (19537)	+5.4%	31262 (23058)	24.4
Prop. Force N (lb)	4001 (899)	3974 (893)	-0.7%	3431 (771)	-14.2%
Equiv. L/D	10.26	9.20	-10.3%	5.61	-45.3%

Just as for blade response and stresses, the detrimental effect of control inputs of high amplitude on rotor performance is much more severe than that of control inputs of low amplitude. However, note that the effect on rotor thrust is still relatively small.

The above results clearly indicate that higher harmonic control inputs can have detrimental effects on blade stresses and rotor performance. Furthermore, these effects tend to become much more severe as the amplitudes of the control inputs increase. As far as the controller is concerned, the above two solutions are equally as good since the performance indices are almost equal. It has no way of knowing that it is better to seek out solutions that reduce vibration while degradating as little as possible other performance criteria, such as blade stresses or rotor performance, that do not appear in the performance index. As discussed above, it may be possible to direct it to such solutions by including appropriate criteria in the performance index in addition to vibration response. In so doing, it might even be possible to achieve improvements in these other criteria. In lieu of that, one might use the weighted term for control inputs in the performance index. By adjusting W_θ, a compromise can be reached in the desire to reduce vibration and the desire to keep the magnitude of control as small as possible. Internal limiting of the total magnitude of control via W_θ will be discussed shortly. First, however, controller performance with internal rate-limiting

will be discussed and compared to the results just presented for external rate-limiting.

Internal Rate-Limiting

As already mentioned, the use of internal rate-limiting dramatically improves the stability and performance of the deterministic controller. This is quite apparent when comparing the performance of the baseline deterministic controller, which uses internal rate-limiting, to the results just presented for the deterministic controller with external rate-limiting. Recall that internal rate-limiting refers to the use of a quadratic term involving $\Delta\theta$ in the performance index which penalizes for large incremental changes in control (Eq. (3)). Thus, the controller calculates a solution which takes into account the desire to minimize vibration with relatively small changes in control.

Figures 23 through 25 summarize the overall results for both the baseline deterministic controller with internal rate-limiting and one of the best deterministic controllers with external rate-limiting. The baseline deterministic controller has the configuration specified in Table 5, while the externally limited controller is the same as that used for Fig. 16. Thus, the externally limited deterministic controller has the same configuration as the baseline; except that $W_{\Delta\theta}$ is set to zero (no internal rate-limiting), $\Delta\theta_{max}$ is set to 0.2 degree per rev (external rate-limiting), P_o, Q, and R have been significantly retuned to optimize performance for this flight condition, and the local system model is used. As discussed above, this externally rate-limited deterministic controller is essentially the same as the RTSA controller used in Ref. 10 and the results shown here are the best that could be obtained with significant experimentation and tuning of P, Q, R, and $\Delta\Theta_{max}$.

Figure 23 clearly demonstrates the dramatic improvement in stability and performance provided by internal rate-limiting. The internally limited controller is completely stable with very little oscillation present in the time histories at this flight condition. The externally rate-limited controller is quite oscillatory and skittish. While stable at this flight condition, this controller would tend to be unstable for sudden changes in flight condition due to the high values used for P and Q in the identification algorithm.

As for performance, the internally rate-limited controller significantly improves controller performance according to every criteria dealing with vibration reduction. First, the initial reduction in overall vibration achieved in the first step of active control is significantly greater, even though slightly smaller magnitudes of 3, 4, and 5 per control inputs were used. Over 40 percent reduction in the performance index is achieved in the first step of active control with cyclic pitch magnitudes between 0.13 and 0.18 degree for the internally rate-limited controller. Only a 16 percent

reduction is achieved by the externally rate-limited controller with all three control inputs at their limits of 0.2 degree for the first rev. Second, the time to convergence is much shorter for the baseline internally rate-limited controller. Convergence occurs at about rev 10 for this baseline controller after being activated at rev 4. "Convergence" for the externally rate-limited controller occurs at about rev 25. If the same relaxed criteria were used for the baseline controller, convergence can be said to occur even more quickly at rev 6 after only 2 revs of active control. Third, the internally rate-limited controller achieves significantly greater overall reduction in vibration in the RTA as can be seen in the performance index in Fig. 23 (97 percent reduction versus 85 percent) and the accelerations at each sensor location in Fig. 24 (e.g., 95 percent reduction in Cross-Beam Longitudinal vs 73 percent). Finally, these reductions in vibration are achieved with smaller control inputs as can be seen in Fig. 25.

The main reason for the dramatically improved performance achieved by the internally rate-limited controller is that the minimum variance control algorithm takes directly into account, via $W_{\Delta\theta}$ and the weighted quadratic $\Delta\theta$ term in the performance index, the desire to implement relatively small changes in the control inputs when trying to minimize a certain state of vibratory response. Thus, the bias to achieve vibration reduction via large control inputs is immediately alleviated and the controller searches on the very first step for a solution that minimizes both vibration and the change in control inputs. Every step thereafter, the controller is directly trying to compromise between vibration reduction and implementation of small changes in the control inputs.

The difference in solutions for these two controllers is shown in Fig. 26 where the amplitude and phase of the 3, 4, and 5 per rev control inputs at rev 4 and rev 30 are presented graphically in polar plots. The solutions shown for rev 30 in the bottom half of this figure correspond to those shown (in terms of amplitude only) in Fig. 25. Note that the phase differences between the 4 per rev inputs are not as large as they might appear at first glance, since phase shifts involving integral multiples of 90 degrees for this 4-bladed rotor result in identical 4 per rev inputs. For the externally limited controller, all three inputs have been arbitrarily limited at rev 4 to 0.2 degree while maintaining the same phase calculated by the minimum variance control algorithm. As can be seen by the long dashed vectors, which are not drawn to scale, the minimum variance control algorithm calculated very large magnitudes for these vectors based on the initial T-matrix and measured vibratory response supplied.

This is an inherent problem with the externally limited controller. That is, external limiting is not taken into account when calculating the solution

needed to minimize vibration. Rather, the solution is calculated using an unconstrained optimization algorithm under the assumption that any set of control inputs is acceptable. Then, after the fact, arbitrary limits are applied to the calculated optimum solution. Even if the T-matrix relationship is accurately identified and applicable not only in the region of the current control point but also in the region of the newly calculated control point, this arbitrary limiting can cause problems. By limiting each control input separately, the "mix" of 3, 4, and 5 per rev inputs can be changed. Although the phase of the calculated change in components is maintained, the proportionality in amplitudes is not. It is very possible that the large calculated change in one input (e.g., 3/rev) is highly limited while the small change calculated in another input does not exceed the limits being applied and is implemented as calculated. Clearly, such a situation can result in a change in the mixture of control inputs, both amplitude and phase. Such a change could cause less vibration reduction to be achieved or even an increase in vibration if the system is fairly nonlinear and very sensitive to the mixture of 3, 4, and 5 per rev control inputs.

In contrast, the baseline deterministic controller takes directly into account the desire to minimize changes in control inputs. As a result, the minimum variance control algorithm calculates a completely different solution at rev 4 from that calculated by the externally limited controller as can be seen in Fig. 26. While the magnitudes of the control inputs are about the same, the phases are completely different. Presumably, these phases are the optimum phases for minimizing vibration with inputs of this order of magnitude, if the initial T-matrix is accurate. Consequently, this internally limited controller achieves a much greater reduction in the performance index with this first step of active control, even though its inputs are somewhat smaller than those commanded by the externally limited controller. By rev 30, completely different solutions have been reached by the two controllers, although both have been very successful in reducing overall vibration in the RTA.

As just shown, the use of internal rate-limiting dramatically improves controller performance by taking into account the desire to achieve additional vibration reduction each rev with as small a change in control inputs as possible. The tradeoff in minimizing vibration and restricting the rate of change in control is represented by the diagonal weighting matrix $W_{\Delta\theta}$. As explained in the discussion of controller configurations, this matrix takes into account differences in dimensions, magnitudes, and relative importance of minimizing change in each control input relative to minimizing vibration. Figure 27 shows the effect of this parameter on controller performance at the baseline high speed flight condition. In this figure, the time history of 3 per rev cyclic pitch amplitude and the performance index are shown for the

baseline deterministic controller having various values of $W_{\Delta\theta}$. Throughout the current investigation, each control input has been weighted equally. Thus, the values shown for $W_{\Delta\theta}$ were applied equally to all three control inputs.

As can be seen in Fig. 27, the weighting placed on $\Delta\theta$ in the performance index, $W_{\Delta\theta}$, has a significant impact on controller performance. In fact, the value used for $W_{\Delta\theta}$ affects all the important characteristics of controller performance: stability, time to convergence, vibration reduction, and final control solution reached at convergence. For very small values of $W_{\Delta\theta}$, the controller performance is very similar to the unlimited and lightly limited deterministic controller performances shown in Figs. 12 through 15. However, one important difference is readily apparent in Fig. 27. Even the very oscillatory controller with weighting of 1.0 for $W_{\Delta\theta}$ is close to convergence by rev 30. While not shown since the magnitude of control inputs implemented are completely off the scale after the very first rev of active control, the 3 per rev control input has converged at a value of 3.76 degrees by rev 25. Thus, even minimal internal rate-limiting allows the controller to converge, although a control solution with very large values of 3, 4, and 5 per rev inputs is reached. Recall that the controllers with relaxed external limits never did converge. The capability for controllers with only small internal rate-limiting to converge when controllers with more restrictive external limits could not is most likely due to the phenomenon of arbitrary external limits changing the mix of total control inputs implemented, as discussed above.

At the other extreme, very high values for $W_{\Delta\theta}$ cause slow, although smooth, convergence to a reduced vibration level. The convergence of the controller with the highest value of $W_{\Delta\theta}$ shown in Fig. 27 is so slow as to make the controller almost ineffective.

In between these two extremes, moderate values for $W_{\Delta\theta}$ result in very effective controllers. The baseline deterministic controller having a value of 1000.0 for $W_{\Delta\theta}$ can be seen to have the best overall performance of those shown in Fig. 27 for the baseline flight condition. The optimum value for $W_{\Delta\theta}$ depends upon flight condition since the rate-limiting achieved by a given value for $W_{\Delta\theta}$ depends upon the level of vibration present. While this could prove to be somewhat of a problem, the results in Fig. 27 indicate that the controller is fairly insensitive to the exact value of $W_{\Delta\theta}$. In fact, a wide range of values of 2 to 3 decades for $W_{\Delta\theta}$ results in very effective controllers at the baseline flight condition. Furthermore, the baseline deterministic controller has proven to be very effective at many different flight conditions considered in this study without any adjustment of $W_{\Delta\theta}$, as will be discussed later.

The effectiveness of the baseline deterministic controller in reducing vibration with various values for $W_{\Delta\theta}$ is shown in Fig. 28 where the acceleration at rev 30 is shown for each of the RTA sensor locations. All but the highest value of $W_{\Delta\theta}$ have resulted in essentially the same vibration levels. Even the lowest value for $W_{\Delta\theta}$ has resulted in substantial reductions in vibration after initially oscillatory behavior.

The effect of $W_{\Delta\theta}$ on the final control solution is shown in Fig. 29. As expected, the magnitudes of the control inputs at rev 30 generally decrease as $W_{\Delta\theta}$ increases. These completely different solutions all result in very similar reduction in vibration in the RTA. Thus, by taking into account the desire to minimize incremental change in control amplitudes, the controller calculates a properly phased mix of control inputs that reduce vibration.

The effect of these control inputs on maximum peak-to-peak stresses is shown in Fig. 30. This figure shows the maximum 1/2 peak-to-peak flatwise and edgewise bending stresses and torsional moment. As discussed before, the general trend is to higher stresses as the magnitudes of the multicyclic inputs increase, which corresponds to a decrease in $W_{\Delta\theta}$. All except the most lightly weighted controller have about the same effect on rotor performance at the baseline flight condition as that presented in Table 7 for the baseline deterministic controller. The very large control inputs commanded by the lightly weighted controller cause severe degradation of rotor performance, as is expected.

One final observation should be made about the behavior demonstrated by the deterministic controller with internal rate-limiting. As can be seen in Fig. 27, all the effective controllers have a tendency to command very slight changes in control in an attempt to achieve further reduction in vibration even after convergence has been reached at a fairly steady level of vibration in the RTA. In terms of 3 per rev cyclic pitch shown in Fig. 27, this takes the form of a very slight but steady increase in amplitude. The source of this drift may be any number of things. It may be indicative of the tendency exhibited by the externally rate-limited controller to try to further reduce vibration with large control inputs that effectively cancel to achieve about the same low vibratory response in the RTA. Such a tendency is fought by the internal rate-limiting, which becomes more restrictive as vibration is reduced since the same $W_{\Delta\theta}$ gives relatively more importance to rate-limiting than for reducing vibration. This tendency to drift may also be an effort to better identify the T-matrix. Since convergence in the performance index is reached so quickly and with such small control inputs, little change in the T-matrix has been obtained by convergence. Errors in the T-matrix may cause the controller to hunt, while at the same time, the increased importance of $W_{\Delta\theta}$ inhibits this tendency. As will be pointed out later, raising P_o

allows the identifier to be more sensitive to errors in the T-matrix and does eliminate this slight tendency to drift.

Whatever the cause, the changes can be seen to be very slight even with the large scale used in Fig. 27. However, if the tendency to drift to higher amplitudes of control were significant or bothersome at other flight conditions, it can be alleviated by implementing a small or moderate internal weighting on the total magnitude of control inputs via W_θ. If the tendency to drift is due to a tendency to achieve vibration reduction by cancellation between proper mixes of large inputs, internally weighting only one input (e.g., 5 per rev control) may alleviate the drifting. As will be discussed in the next two sections, both methods do eliminate this tendency to drift at this flight condition. Use of W_θ to internally limit total magnitude of control is discussed in the next section.

Internal Limiting of Total Control Magnitude

Internal limiting of the total magnitude of control inputs also dramatically improves the stability and performance of the deterministic controller in much the same manner as internal rate-limiting. Internal limiting of total control inputs is achieved via a quadratic weighted term in the performance index involving W_θ and θ. This term penalizes for large amplitudes of multicyclic pitch. Thus, the controller calculates a control solution which tries to minimize both vibration and the total magnitude of control inputs. The apparent bias to calculate large control inputs to achieve vibration reduction is removed.

The effect of W_θ on overall controller performance is shown in Figs. 31 through 33. Figure 31 shows the time history of the performance index and 3 per rev cyclic pitch amplitude for various values of W_θ. The vibratory response in the RTA and the multicyclic control amplitudes commanded at rev 30 are shown for these values of W_θ in Figs. 32 and 33, respectively. The results presented in these figures represent the response of a deterministic controller with no rate-limiting at the baseline flight condition. The controller is based on the global system model, and the tuning of P, Q, and R is the same as that for the baseline deterministic controller with internal rate-limiting. The indicated values of W_θ are used by the controller to equally weight both the cosine and sine components of all three multicyclic control inputs.

Figure 31 shows that controller performance is oscillatory and that the controller is still somewhat biased to large control inputs when W_θ is small. This is to be expected since no other limiting is present except that resulting from the internal limiting of total control magnitudes. Thus, as

W_θ goes to 0, the configuration of the controller approaches that of the unlimited global deterministic controller represented in Fig. 12. Clearly, even the smallest value of W_θ shown in Fig. 31 substantially improves controller performance relative to that of the original deterministic controller with no limiting or with external rate-limiting. Even this light internal weighting of control magnitude allows the controller to remain stable, to quickly reduce vibration, and to converge to a steady level of reduced vibration.

As the value of W_θ is increased, the bias to implement larger control inputs is completely removed, and convergence to a final solution is very rapid and smooth. Figure 33 shows that, in general, the magnitudes of the final control inputs decrease as W_θ increases. However, as W_θ is increased, the controller does not simply calculate new control solutions having smaller amplitudes, but the same phases. Rather, the controller calculates a completely different set of control inputs based on the need to minimize both vibration and the weighted control magnitudes. Both the magnitude and phase of the control inputs are changed in an attempt to reduce vibration as much as possible without paying an excess penalty in the form of larger weighted control amplitudes. This can be seen clearly in Fig. 34, which shows the magnitude and phase of both the initial and final control inputs for two different values of W_θ. Thus, for small to moderate values of W_θ, the controller is still able to achieve about the same reduction in overall vibration with smaller but properly phased control inputs, as can be seen by the final performance index in Fig. 31 and the final vibratory response in the RTA in Fig. 32. However, these two figures also show that, at some point, the value of W_θ becomes large enough that the desire to hold down the magnitude of control inputs becomes more important than minimizing vibration, and the controller becomes less effective at reducing vibration. For the highest value of W_θ shown, the controller simply cannot command large enough amplitudes for 3, 4, and 5 per rev cyclic pitch to be able to reduce overall vibration to the same level as that of the other controllers. The exact effect of particular values of W_θ is dependent upon the flight condition and the corresponding level of vibration present. Just as for internal rate-limiting via $W_{\Delta\theta}$, the relative importance of maintaining small control inputs for a given value of W_θ increases somewhat as vibration is reduced.

Figure 35 once again points out the general trend between vibratory blade stresses and the size of multicyclic pitch inputs. This figure shows that the maximum 1/2 peak-to-peak blade bending stresses and torsional moment generally increase with increase in control amplitude. Torsional moment is by far the most sensitive to changes in amplitude. The same can be said for the detrimental effect on rotor performance. As the multicyclic pitch amplitudes

increase, rotor drag tends to increase with an accompanying increase in required torque. Thus, as mentioned previously, it is desirable to reduce vibration with control inputs that are as small as possible, although it may be possible to reduce vibration, blade stresses, and detrimental effects in rotor performance by properly phased multicyclic control inputs obtained with appropriate additional terms in the performance index.

The overall performance of the deterministic controller with internal limiting of total control magnitude is compared to that of the deterministic controller with internal rate-limiting and with external rate-limiting in Fig. 36. The performances shown are the best achieved with the particular controller configuration represented. Clearly, the two deterministic controllers with internal limiting of control inputs, either incremental changes or total magnitudes, substantially improve the performance of the original deterministic controller with external rate-limiting. Both internally limited controllers converge quickly and smoothly to virtually identical vibration levels at each sensor location in the RTA, even though quite different control solutions have been reached. While Fig. 36 shows that the final 3 per rev cyclic pitch control inputs are about the same magnitude for these two controllers, significant differences in phase exist between the two solutions for all three higher harmonic inputs, and a relatively large difference in 5 per rev magnitude also exists. Table 9 presents the amplitudes and phases of the final control solutions (rev 30) calculated by these three controllers. Note that the phases shown in this table have been transformed such that $0 \leq \angle\theta_3 \leq 120°$, $0 \leq \angle\theta_4 \leq 90°$, and $0 \leq \angle\theta_5 \leq 72°$.

TABLE 9

FINAL CONTROL SOLUTIONS FOR DETERMINISTIC CONTROLLER WITH EXTERNAL OR INTERNAL LIMITING PLACED ON CONTROL INPUTS AT BASELINE FLIGHT CONDITION

Limiting	θ_3	θ_4	θ_5
$\Delta\theta_{max}$ = 0.2 deg/rev	$0.58°\angle 20°$	$0.48°\angle 60°$	$0.73°\angle 41°$
$W_{\Delta\theta}$ = 1000 $(1/rad)^2$	$0.28°\angle 37°$	$0.26°\angle 74°$	$0.31°\angle 41°$
W_θ = 10 $(1/rad)^2$	$0.24°\angle 15°$	$0.27°\angle 41°$	$0.52°\angle 27°$

Aside from the different solutions being achieved at convergence, there are several rather subtle differences between the performance of the deterministic controller with internal limiting on total control magnitudes (W_θ) and the performance with internal rate-limiting ($W_{\Delta\theta}$). The limiting of total θ does not restrict the incremental changes in control between updates. Thus, relatively large changes in control inputs can occur between updates even though relatively small overall magnitudes are being maintained. For instance, on two consecutive revs, the 3 per rev cyclic pitch may be of about the same moderate magnitude but of completely different phase. Thus, the difference vector representing the incremental change between updates would be fairly large. As demonstrated in the first few revs of active control in Fig. 36, these fairly large changes cause somewhat more oscillatory behavior initially in both control inputs and vibration performance index than exhibited by the controller with internal rate-limiting on incremental changes. As convergence is approached, these relatively large changes cease and convergence occurs quickly.

The effect of $W_{\Delta\theta}$ and W_θ on rate of convergence and controller effectiveness at convergence is also slightly different. The value of $W_{\Delta\theta}$ significantly affects rate of convergence as can be seen in Fig. 27. As $W_{\Delta\theta}$ increases, smaller incremental changes in control are allowed and the time required to reach a certain level of control increases. Thus, reductions in vibration tend to take longer to achieve. However, the effectiveness in reducing vibration at "convergence" is relatively unaffected. Even the largest value of $W_{\Delta\theta}$ shown in Fig. 27 appears to be approaching, although very slowly, a control solution that achieves the same level of vibration reduction as the other more effective controllers shown in this figure. In contrast, the value of W_θ has very little effect on rate of convergence if it is sufficiently large enough to prevent undue oscillatory behavior. As W_θ increases in Fig. 31, convergence to a smaller level of control is quickly achieved. In the limit as the value of W_θ goes to infinity, the controller would achieve convergence instantaneously but with no change in control and no reduction in vibration. Clearly, the effectiveness in reducing vibration at convergence is affected significantly by the value of W_θ.

For values of W_θ greater than a certain magnitude, the controller can no longer command large enough signals to achieve as large a reduction in vibration. While internal rate-limiting slows down the rate that inputs can be implemented according to the magnitude of $W_{\Delta\theta}$, it does not limit the total magnitude of control that can be commanded. It may take awhile, but any level of higher harmonic control inputs required to minimize the performance index can be reached. Thus, as already observed, the controller with internal rate-limiting tends to slowly implement small changes in control in an attempt

to further reduce vibration. In contrast, the controllers with total weighting converge quickly to an allowable level of control and exhibit no tendency to drift, as can be seen in Fig. 31. This level of control represents the tradeoff between vibration reduction and minimum control inputs. While further reduction in vibration may be possible with only slight increases in control magnitude, such an increase would result in a higher value of the performance index due to the increased penalty term involving θ and W_θ. Note that the performance index referred to here is the complete performance index shown in Eq. (3) including penalty terms on θ and $\Delta\theta$, and not just the vibration performance index as plotted in Fig. 31.

Due to these subtle differences in the effect of $W_{\Delta\theta}$ and W_θ on controller performance, the deterministic controller tends to be a bit more sensitive to values of W_θ than $W_{\Delta\theta}$. This is due to the fact that values of a given magnitude for W_θ begin to compromise overall effectiveness in reducing vibration at convergence, whereas comparable values for $W_{\Delta\theta}$ may start to slow convergence somewhat, but not enough to significantly compromise overall performance. Nonetheless, a fairly wide range of W_θ results in very effective controller performance.

Effect of Control Input Mix

The results presented to this point for the deterministic controller with internal limiting of total θ have all been for equal weighting on each of the three multicyclic control inputs. It is also possible to operate the controller with each of the control inputs weighted differently. This proved to be useful in this analytical study for exploring certain aspects of controller performance.

For instance, it was shown above that very effective vibration reduction in the RTA can be achieved by either a set of small or a set of large control inputs of appropriate phase. In Fig. 20, it was shown that the large control inputs caused large inplane rotating shears, as indicated by the 3 and 5 per rev lateral shears, and that small control inputs caused relatively small inplane rotating shears. When combining to form the 4 per rev fixed system hub loads, the 3 and 5 per rev lateral and longitudinal rotating shears tended to vectorially cancel, if properly phased, to give about the same magnitude of fixed system longitudinal and lateral hub shears and about the same vibration state in the RTA. It has been hypothesized that the unsatisfactory behavior of the original deterministic controller configuration with external rate-limiting is due to the tendency for large control inputs to effectively cancel and to the apparent bias with the initial T-matrix supplied for reducing vibration via a set of large control inputs. Due to the phenomenon just described, it was felt that 3 and 5 per rev control might be the drivers

involved, since both directly affect 3 and 5 per rev rotating shears. If this is the case, then the performance of the original deterministic controller configuration should be improved by inhibiting or eliminating either 3 or 5 per rev control so that they do not tend to fight each other.

To check this hypothesis, the deterministic controller was run at the baseline flight condition with no limiting other than internal limiting of the total magnitude of either 3 or 5 per rev control. This can be accomplished by placing finite values along the diagonal of matrix W_θ corresponding to either θ_3 or θ_5, and zeros elsewhere. Moderate values would inhibit control and very large values would essentially eliminate the weighted control inputs.

It has been found that inhibiting or eliminating either 3 or 5 per rev control does indeed improve the performance of the original deterministic controller. This is demonstrated in Fig. 37 where the time histories of the vibration performance index and 3 per rev cyclic control are presented for three different controllers in which 5 per rev control is essentially eliminated by a very large value of $W_{\theta 5}$ (1×10^5). The solid curve represents a controller with no rate-limiting of any kind. Thus, the performance of this controller can be compared directly to the performance shown in Fig. 12 for the unlimited global deterministic controller. The only difference between these two controllers is that 5 per rev control has been eliminated from the controller represented in Fig. 37. Otherwise, they are both unlimited and have the same tuning.

Clearly, elimination of 5 per rev control has substantially improved performance. While the controller with no 5 per rev control exhibits fairly oscillatory behavior, it remains stable and finally begins to converge after 15 to 20 revs of active control. Furthermore, at convergence, vibration in the RTA and, thus, the vibration performance index have been reduced almost as effectively as with the baseline deterministic controller having 3, 4 and 5 per rev control and internal rate-limiting. These reductions in vibration are achieved with reasonable magnitudes of 3 and 4 per rev control on the order of 1.0 degree or less. In contrast, the unlimited controller using all three control inputs shown in Fig. 12 is completely unstable and commands ever increasing magnitudes of control. Thus, elimination of 5 per rev control has, in fact, eliminated the tendency at this flight condition to calculate solutions with very high magnitudes of control.

Although the unlimited controller shown in Fig. 37 remains stable and converges to a very satisfactory final solution, the oscillatory behavior indicates the need for rate-limiting to improve overall performance. Also shown in Fig. 37 are two controllers having no 5 per rev control but using

rate-limiting. This figure shows that either external ($\Delta\theta_{max}$ = 0.2 deg/rev) or internal ($W_{\Delta\theta}$ = 1000 (1/rad)^2) rate-limiting significantly improves performance by greatly reducing the oscillatory behavior of the unlimited controller. In so doing, rate-limiting allows the controller to converge more quickly (even though control inputs are implemented more slowly) and to achieve a slightly better level of overall vibration in the RTA with significantly smaller 3 and 4 per rev control inputs.

While both internal and external rate-limiting significantly improve performance, it is important to point out some differences between these two methods of rate-limiting. While removing the tendency to calculate very large control inputs has allowed the externally rate-limited controller to provide excellent performance, internal rate-limiting still provides somewhat better performance than external rate-limiting. Convergence is achieved more quickly and smoothly with internal rate-limiting. This is most likely due to the change in control "mix" that occurs with external limiting when arbitrarily limiting control inputs as separate quantities outside the minimum variance control algorithm. Taking into account the desire to implement small control changes within the minimum variance control algorithm inherently provides better performance than external limiting. This is true even for this moderate flight condition and this better behaved control configuration having only 3 and 4 per rev control. As previously shown, internal rate-limiting starts exhibiting significant improvements in performance over external rate-limiting when the situation is not so well behaved. Regardless of the cause of the difficulties encountered when all three control inputs are used, internal rate-limiting provides excellent performance, and the performance achieved with external rate-limiting is unsatisfactory. Internal rate-limiting should also provide significantly better performance at more severe flight conditions where increased nonlinearities or extreme sensitivity to the "mix" of 3, 4, and 5 per rev control exist.

One final point should be made in regard to Fig. 37. Note that neither rate-limited controller has any tendency to drift after convergence is achieved. That is, elimination of 5 per rev control has inhibited the tendency, which is exhibited by the baseline controllers in Figs. 8(a) and 8(b), to continue to trade off changes in control inputs in an attempt to further reduce vibration after convergence has already been achieved in the performance index.

As mentioned above, elimination of 3 per rev control also improves controller performance significantly by presumably eliminating the coupling between 3 and 5 per rev control and the tendency to calculate high magnitude control inputs. In fact, eliminating 3 per rev control resulted in less oscillatory behavior without any other limiting than did the elimination of 5

per rev control. It also should be noted that 3 or 5 per rev control need not be entirely eliminated to achieve the same improvements in controller performance. Simply weighting either 3 or 5 per rev control inputs with a moderate value of W_θ eliminates the tendency at this flight condition to calculate solutions with large control inputs. These results indicate that coupling between 3 and 5 per rev inputs is indeed a source of the unsatisfactory behavior exhibited by the original deterministic controller configuration with external rate-limiting. However, elimination of 4 per rev control also improves controller stability and performance. This tends to indicate that the coupling effect between 3 and 5 per rev control mentioned above is not the only coupling phenomenon. In fact, since elimination of 3 or 4 per rev control results in a less oscillatory behavior than elimination of 5 per rev control, a coupling between 3 and 4 per rev control may be more important than that discussed above.

Therefore, it is still not clear as to the exact driver of the tendency to alleviate vibration with appropriately phased control inputs of large magnitude when 3, 4, and 5 per rev control are all implemented. However, at this flight condition, elimination of any one of the control inputs essentially "decouples" the system and eliminates this tendency. As a result, controller stability is improved such that rate-limiting is no longer required at this flight condition, although rate-limiting can still improve overall controller performance significantly. At more severe flight conditions, rate-limiting will most likely be required for stability as well.

Results obtained by eliminating or inhibiting various control inputs points out another very important aspect of controller performance. As mentioned previously, many significantly different control solutions can result in very effective vibration reduction in the RTA. This is shown in Figs. 38 through 40. Figure 38 shows the final control solutions occurring at rev 30 for several different controllers operating at the baseline high speed flight condition. Each solution is shown as a polar plot of the amplitude and phase of the 3, 4, and 5 per rev control inputs commanded. Figures 38(a) through (c) represent the solutions for deterministic controllers in which internal limiting on total θ has been used to separately eliminate 3, 4, and 5 per rev control, respectively. Figure 38(d) represents the control solution for the baseline deterministic controller having 3, 4, and 5 per rev control and internal rate-limiting. Figure 38(e) represents the control solution for a deterministic controller with 3, 4, and 5 per rev control and very light internal rate-limiting. Figure 38(f) is the only figure that does not represent the control solution for only one controller. Rather, Fig. 38(f) represents the final solution for three deterministic controllers in which

internal limiting on total θ has been used to eliminate all but one of the multicyclic control inputs.

Clearly, all the solutions shown in Fig. 38 represent a completely different "mix" of amplitude and phase of 3, 4, and 5 per rev control inputs. Each solution either has one or two control inputs eliminated and/or exhibits significantly different amplitudes and phases than that of the baseline controller shown in Fig. 38(d). It is interesting to note that elimination of one or two of the three standard control inputs generally results in slightly larger magnitudes required for the remaining control input(s) in order to achieve the same vibration reduction. Despite the significant differences in the control solutions, each of these controllers has been very effective at reducing overall vibration in the RTA, as indicated by at least a 95 percent reduction in the vibration performance index. The resulting vibration at each of the sensor locations for these solutions is shown in Figs. 39 and 40. Figure 39 shows the vibration response for the control solutions shown in Figs. 38(a) through (d), and Fig. 40 shows the response for control solutions shown in Figs. 38(d) through (f). The baseline RTA vibration levels without higher harmonic control are shown in both figures for reference as is the response of the baseline controller having the solution shown in Fig. 38(d).

Figures 39 and 40 show that essentially the same vibration levels at each location in the RTA have been achieved by these completely different solutions. While minor differences do exist at each individual sensor location, these differences are for the most part insignificant, especially in light of the completely different solutions that cause them. Furthermore, once the sum of the squares of the magnitude of vibration at each location is calculated to form the vibration performance index, little difference exists. However, differences do exist in the 1/2 peak-to-peak blade moments and stresses and in rotor performance, although not shown here. Certain of these solutions result in significantly reduced stresses and/or detrimental effect on rotor performance when compared to the baseline solution, while others result in a larger degradation in blade stresses and/or performance. While no general trends or conclusions, other than the general correlation between large control inputs and large detrimental effects on blade stresses and/or rotor performance, can be drawn from these results, they do highlight two important aspects of controller performance that should be explored.

First, the controller does not care what set of control inputs are achieved at convergence as long as the performance index is being minimized. If other criteria are of concern (e.g., blade stresses or required rotor torque) and it is desirable to try to meet these criteria or at least not compromise them too severely, the controller must be guided to more acceptable solutions. The only way of doing this with the particular unconstrained

minimization algorithm being used is to place an appropriately weighted term in the performance index that penalizes for violating or not meeting the corresponding criterion. In the results just presented, weighting matrices W_θ and $W_{\Delta\theta}$ have been used to guide the solution in one way. For instance, it has been clearly shown that W_θ can be used to guide the controller to a solution that maintains all inputs at reduced levels or that inhibits or eliminates one particular input. Since there is the general correlation between large control inputs and large stresses, the weighted θ term in the performance index can be looked upon as a penalty on high stress solutions. Clearly, any additional term in the performance index raises the possibility of compromising reduction in the original parameters of interest (e.g., vibration) for better satisfaction of the associated criterion. This was shown in Figs. 31 through 33 for sufficiently high W_θ. However, the results just presented, demonstrate the effectiveness of the controller in reducing vibration in the RTA with significantly different control solutions. This capability to reduce vibration with different control "mixes" highlights the possibility that better control solutions may be achieved in terms of blade stresses and/or rotor performance without unduly compromising vibration reduction.

Effect of Kalman Filter Covariances

Tuning of the initial values of the Kalman filter covariances (P, Q, and R) can have a significant effect on controller performance depending upon the controller configuration and the flight condition. As discussed previously, the performance of the deterministic controller with external rate-limiting can be changed significantly by tuning of P_o, Q, and R. In contrast, the baseline deterministic controller with internal rate-limiting is fairly insensitive to tuning of these covariances. In fact, excellent controller performance is maintained for P_o in the range of 1.0 to 10000, R in the range of 0.001 to 1.0, and Q in the range of 0.001 to 10.0.

If P_o, Q, and R are adjusted in order to essentially eliminate identification due to extremely low Kalman gains, the deterministic controller with internal rate-limiting exhibits excellent performance that is very similar to that of the baseline controller with identification, as can be seen in Fig. 41. This is due the flight condition being fairly linear, especially at small magnitudes of control. Since internal rate-limiting allows the controller to converge to a solution having very small multicyclic control inputs, the linear T-matrix relationship between vibration measurements and control inputs is still applicable. Thus, lack of identification and non-optimal tuning of P_o, Q, and R have only a minor effect on controller performance at this flight condition. This is not true at more nonlinear flight conditions or in maneuvers changing from one flight condition to another.

It is also not true at this flight condition if the tendency to calculate large control inputs is not eliminated (e.g. by internal rate-limiting or internal limiting of total θ), and the controller allows these high amplitude solutions to be achieved, where the T-matrix is no longer valid. This is the case, for example, when $W_{\Delta\theta}$ is small or external rate-limiting is used. In such a case, identification and optimal tuning of identifier covariances become important. This can be seen in Fig. 42 which shows the performance of both a local and global deterministic controller with external rate-limiting ($\Delta\theta_{max}$ = 0.2 deg/rev) when identification is inhibited at the baseline flight condition. Without identification both controllers exhibit extremely poor performance. The local model is unstable. Compare this to the performance shown in Fig. 16 for a local model having the same external limiting, but high Kalman gains that result in a very sensitive identifier. The global model with inhibited identification is stable, since it bases calculations on the identified Z_o vector as well as an identified T-matrix. Without identification, T and Z_o do not change, and the global controller always calculates the same solution. The controller proceeds to this solution as quickly as the rate-limiting allows. Figure 42 clearly shows that this particular large magnitude solution when reached does not result in any reduction in the performance index. If these controllers were not biased to high magnitude solutions, they would most likely be relatively insensitive to non-optimal tuning of the identifier as well.

Local System Model

Unless otherwise stated, all the results presented above for the deterministic controller are for the global system model. These results and the accompanying discussion are generally applicable to the local system model as well. It has been found in this investigation that the performance of the deterministic controller at steady flight conditions is very similar for both system models when the same overall configuration is used (e.g., internal limiting) and similar tuning of internal parameters is specified (e.g., $\Delta\theta_{max}$, $W_{\Delta\theta}$, P_o, Q, R).

Figures 43 through 45 compare the overall results at the baseline flight condition for a local deterministic controller with internal rate-limiting to those for the baseline deterministic controller specified in Table 5. The overall configurations are the same; however, tuning of P_o and Q are somewhat different. For the local model, P_o and Q are 1000.0 $(g's/rad)^2$ and 100.0 $(g's/rad)^2$, respectively. Covariance R is the same as that shown in Table 5 for the global model. Figure 43 compares the time histories of the performance index and 3 per rev cyclic pitch. Clearly, the performance of both models in terms of minimizing the performance index is virtually identical. The time histories of 3 per rev cyclic pitch show some minor

differences. This particular local controller holds steady control inputs after convergence in the performance index is achieved. The global model shown tends to try to reduce vibration further by making small changes in control inputs. As discussed previously, the small changes in all three control inputs tend to cancel so that about the same RTA vibrations and performance index are maintained. This tendency to "drift" and the differences in the time histories of 3 per rev cyclic pitch are greatly exaggerated in this figure due to the enlarged scale.

Figures 44 and 45 show the very similar control solutions and RTA vibration response achieved by both controllers at rev 30. Actually, the very minor differences shown in Figs. 43 through 45 are not due to the difference between local and global system models, but to differences in tuning of P_o, Q, and R. The local controller shown has high values for P_o and Q so that the identifier is very sensitive to errors in the T-matrix. When similar tuning is specified for the global model, the 3 per rev cyclic pitch time history is virtually identical to that shown for the local model. This is the type of minor differences caused by different tuning of identifier covariances that were discussed above for the deterministic controller with internal rate-limiting at the baseline flight condition.

The similarity in performance for both the local and global system models is seen in the results for all three controller types and all steady flight conditions investigated. Thus, there will not be a great deal of emphasis placed on the results for the local model. As in the discussion here for the deterministic controller, the results for the local model will only be covered when appropriate.

Deterministic Controller Summary (Baseline Flight Condition)

In summary, all the results at the baseline flight condition demonstrate that the baseline deterministic controller is very effective in reducing vibration when an appropriate configuration is defined. With either internal rate-limiting and/or internal limiting of total magnitude, the deterministic controller with appropriate tuning of internal parameters exhibits excellent stability and performance. Convergence to a solution with significantly reduced vibration in the RTA is achieved quickly and smoothly. The reduced vibration in the RTA can be achieved with quite small control inputs.

It has been found that controller performance with internal limiting on either $\Delta\theta$ or θ significantly improves performance over that of the original deterministic configuration, which used external limiting. While $\Delta\theta_{max}$, P_o, Q, and R could be defined for this particular flight condition to make the

original controller fairly effective in reducing vibration, performance of the original configuration is unsatisfactory when compared to the performance of the deterministic with the modification of internal limiting. Furthermore, performance with the original configuration is very sensitive to tuning of internal parameters ($\Delta\theta_{max}$, W_θ, P_o, Q, and R).

Finally, higher harmonic control tends to have a detrimental effect on rotor blade stresses and rotor performance. However, these detrimental effects are generally correlated to the magnitude of the multicyclic pitch amplitudes and can be reduced by achieving vibration alleviation with the smallest control inputs possible. Use of internal limiting has shown to be very effective in doing this. Furthermore, it has been shown that essentially the same vibration reduction can be achieved with a multitude of significantly different control solutions having various effects on stresses and rotor performance. These results indicate that it may be possible to guide the controller to better solutions that effectively reduce vibration, but have a minimal detrimental effect on other criteria by adding appropriate terms to the performance index. These last remarks pertain also to the cautious and dual controllers which will be discussed next.

Cautious Controller

In Figs. 8 through 10 and the accompanying discussion, it was demonstrated that the baseline cautious controller has very similar performance characteristics at the baseline flight condition as the baseline deterministic controller with internal rate-limiting. Thus, the addition of the stochastic term to the performance index in Eqs. (11) and (16), which converts the deterministic controller to a cautious controller, dramatically improves controller performance over that of the original deterministic configuration in much the same manner as the addition of internal rate-limiting and/or internal limiting of total magnitude in the deterministic controller. This is as expected since, as discussed in relation to Eqs. (11) through (21), the cautious term for the local model has a form similar to that of the weighted $\Delta\theta$ term that provides internal rate-limiting. For the global model, the cautious term has a form similar to the weighted θ term that provides internal limiting on total control magnitude.

Thus, these stochastic terms of caution are expected to effectively provide additional internal rate-limiting and total θ limiting in the local and global models, respectively. However, since these terms are proportional to the varying covariance matrix of the estimated T-matrix rather than the constant diagonal matrices used for $W_{\Delta\theta}$ or W_θ, the weighting placed on $\Delta\theta$ or θ is dependent upon the uncertainty in identified system parameters, and some differences in performance are expected.

Effect of Stochastic Control Constant (λ)

Recall that the stochastic cautious term for both system models is proportional to $\lambda \cdot P_i \cdot \sum W_{z_{jj}}$. As discussed previously, P_i for the local model is the covariance of the estimated T-matrix. For the global model, P_i is defined as in Eq. (17) and includes the covariances and cross-covariances for the estimated T-matrix and Z_o. Thus, in either model, P_i is a matrix of statistical parameters that indicates the relative uncertainty in the estimated parameters being identified by the Kalman filter algorithm. The stochastic control constant λ is an arbitrary constant used to give some flexibility to modify the cautious control algorithm if desired.

For a given controller with a particular initial covariance matrix P_o and constant vibration weighting matrix W_z, the stochastic control constant λ is indicative of the amount of "caution" introduced by the cautious controller. Figure 46 shows the effect of λ on the performance of the cautious controller at the baseline high speed flight condition. In this figure, the time histories of the vibration performance index and 3 per rev cyclic pitch are shown for the baseline cautious controller with several different values of λ. Recall that the baseline cautious controller is based on the global model.

Clearly, λ has a significant effect on controller performance. As λ goes to zero, the cautious controller becomes very oscillatory and unstable with performance similar to that of the unlimited or lightly limited deterministic controller, as is expected since the cautious control algorithms degenerate to those of a deterministic controller for λ equal to zero. For small finite values of λ that are greater than some minimum allowable magnitude, controller performance is oscillatory, but stability is maintained, effective control solutions are reached, and substantial reductions in vibration are obtained. At the other extreme, very large values of λ cause very slow, but smooth, convergence to a reduced vibration level. The rate of convergence for the largest value of λ shown in Fig. 46 is so slow as to make the controller practically ineffective. However, it does appear that convergence to the same minimum vibration levels achieved by more effective controllers may eventually be reached.

In between these two extremes, a wide range of values for λ result in very effective controllers. The baseline cautious controller, which has a value of 1.0 for λ, can be seen to have the best overall performance of those shown in Fig. 46 for the baseline flight condition. The optimum value of λ for a given flight condition obviously depends upon the nominal magnitude of the elements in P_i and the vibration weighting matrix. For a given controller, the optimum value of λ depends upon the flight condition since the

limiting achieved by the weighting placed on θ for the global model and $\Delta\theta$ for the local model depends upon the level of vibration present. However, Fig. 46 indicates that the cautious controller is somewhat insensitive to the exact value of λ. Furthermore, the baseline cautious controller has been used effectively in this investigation at many different flight conditions without adjustment of any internal parameters, including λ.

The effectiveness of the baseline cautious controller (λ=1.0) in reducing vibration in the RTA was shown in Fig. 9. All of the effective controllers shown in Fig. 46 achieve essentially the same vibration level at rev 30 at each sensor location in the RTA as those shown for the baseline cautious controller in Fig. 9, despite the obvious differences in control solutions. The magnitude of 3 per rev control shown at rev 30 in Fig. 46 is indicative of the general effect of λ on the final control solution. For a given controller and flight condition, the magnitude of the control inputs at convergence generally decreases as the specified value of λ increases. This is expected since the weighting on θ ($\Delta\theta$ for the local model) increases with increase in λ. Figure 46 also shows that there are exceptions to the trend for any given control input and range of λ. One of the reasons for this, other than just converging to a particular local solution, is that the weighting matrix on θ (or $\Delta\theta$ for the local model) depends upon the covariance matrix P_i multiplied by a scalar constant. In contrast to W_θ or $W_{\Delta\theta}$, P_i is not a diagonal matrix, although the diagonal terms are dominant. Furthermore, once the controller is initialized, P_i is automatically calculated by the Kalman filter identification algorithm (e.g., Eq. (46)) during each controller update. Thus, after a few updates, the diagonal elements may or may not be of the same magnitude, and one control input may be weighted more heavily than another for a given convergence sequence.

In comparing the results shown in Fig. 46 to those shown in Fig. 27, the performance of the cautious controller with the global system model is almost identical to the performance of the global deterministic controller with internal rate-limiting. Note that corresponding controllers in these figures having elements of the same order of magnitude along the diagonal of the weighting matrix also have virtually the same performance, as indicated by the time histories shown. For example, the baseline cautious controller is initialized with a value of 100.0 for each element along the diagonal of P_o. The trace of the vibration weighting matrix, $\sum W_{zjj}$, is 12.0 since the sine and cosine components of each of the six RTA vibration sensors is weighted equally with a value of 1.0. Thus, when activated, the baseline cautious controller (λ=1.0) has a weighting matrix with diagonal elements equal to 1200.0 as calculated by $\lambda \cdot P_o \cdot \sum W_{zjj}$. As already shown in Figs. 8(a) and 8(b), this baseline cautious controller has virtually the same performance as the baseline deterministic controller, which has values of 1000.0 along the

diagonal of $W_{\Delta\theta}$. The same can be seen to be true for the other values of λ. Since P_o and W_z remain the same, the range of λ shown in Fig. 46 for the global cautious controller corresponds very closely to the range of $W_{\Delta\theta}$ shown in Fig. 27 (except for the lowest values of λ and $W_{\Delta\theta}$).

This similarity between the performance of the cautious controller based on the global system model and the deterministic controller with internal rate-limiting is somewhat surprising, since the stochastic term for the global model results in an effective weighting on θ, not $\Delta\theta$, as discussed above and shown in Eq. (21). Thus, it was expected that the performance of the global cautious controller would be more similar to the performance, shown in Fig. 31, for the deterministic controller with internal limiting on total θ. It is the local cautious controller that is expected to have performance characteristics similar to the internally rate-limited deterministic controller, since the stochastic term for the local model results in effective weighting on $\Delta\theta$, as shown in Eq. (12). Indeed, the local cautious controller does have performance characteristics almost identical to those of the global cautious controller and, therefore, to the deterministic controller with internal rate-limiting as well.

The main reason that the global cautious controller behaves more like a rate-limited controller than a controller with limiting on total θ is that the effective weighting matrix on total θ depends directly on P_i. As already pointed out, P_i is calculated automatically at each controller update according to the Kalman filter algorithm. Since P_i is indicative of the uncertainty in system identification, the magnitude of its elements tends to decrease, as active control proceeds, due to improved system identification. Thus, internal weighting on total θ generally decreases as convergence is approached. This decreased weighting on total θ allows the controller to try to reduce vibration further by calculating larger control inputs. The result is the characteristic "drift" noted in the internally rate-limited deterministic controller. As a result, an increase in λ slows the rate of convergence somewhat for the cautious controller, but does not appear to affect its ability to eventually achieve the same reductions in the vibration. This is the same effect $W_{\Delta\theta}$ has on the deterministic controller.

In contrast, the weighting on total θ due to W_θ is held constant. As discussed previously, the relative importance of maintaining small control inputs due to the constant W_θ increases as vibration decreases. Thus, the deterministic controller with weighting on total θ tends to converge to a steady control solution, which represents the optimum tradeoff between reducing vibration and reducing the magnitude of control. An increase in W_θ, if its magnitude is larger than some minimum value, generally results in less effective vibration reduction due to more emphasis placed on maintaining small

control inputs than on reducing vibration. As will be discussed in the next section, the global cautious controller begins to perform like a deterministic controller with internal weighting on total θ when P_i remains essentially constant (e.g., inhibited identification).

As for the deterministic controller with internal rate-limiting, elimination of 3 or 5 per rev control in the cautious controller tends to alleviate the slight "drift" in control that occurs at convergence. As will be discussed in the next section, raising P_o to make the identifier more sensitive to errors in the estimated system parameters also eliminates this slight drift, just as it did for the internally rate-limited deterministic controller.

Effect of Kalman Filter Covariances

The baseline cautious controller is fairly insensitive to the tuning of the Kalman filter covariances (P_o, Q, and R) at the baseline flight condition. Due to the fairly linear nature of the flight condition at the small magnitudes of control commanded by the baseline cautious controller, excellent controller performance is maintained for P_o in the range of 1.0 to 10000.0 $(g's/rad)^2$, R in the range of 0.001 to 1.0 $(g's)^2$, and Q in the range of 0.001 to 10.0 $(g's/rad)^2$. However, some clarification is necessary when talking about the effect of P_o on controller performance, since P_i not only affects identification in the cautious controller, but also directly affects the effective weighting placed on θ or $\Delta\theta$.

In the range of P_o just cited, controller performance is affected significantly if the value of λ is not also adjusted accordingly. For a constant value of λ, the nominal value of elements in P_o have about the same effect as the effect of λ discussed in the last section. For small P_o, the control inputs are lightly weighted and the controller tends to command large control inputs. For large P_o, the control inputs are weighted very highly which results in very slow convergence similar to that shown in Fig. 46 for large λ.

However, if λ is adjusted accordingly to maintain about the same level of weighting on control inputs as that used in the baseline cautious controller, excellent controller performance is achieved for the cited range of 1.0 to 10000.0 $(g's/rad)^2$ for P_o. For example, if elements along the diagonal of P_o are reduced to 1.0 $(g's/rad)^2$ from the baseline value of 100.0 $(g's/rad)^2$, then adjustment of λ to a value of 100.0 maintains essentially the same controller performance as that for the baseline controller. Since the same nominal weighting on control inputs is maintained, the controller converges to a fairly small control solution, the T-matrix changes very little, and controller performance is not hurt by the small Kalman gains. On

the other hand, if P_0 is increased to 10000.0 $(g's/rad)^2$ and λ is reduced to 0.01 to maintain about the same level of weighting on control inputs, the identifier is very sensitive to errors perceived in the estimated system parameters, and the slight "drift" noted above is eliminated.

Therefore, an important parameter is $\lambda \cdot P_0$ for a given controller with some specified vibration weighting matrix. If $\lambda \cdot P_0$ is maintained at about the same level as that for the baseline controller, controller performance at this baseline flight condition is fairly insensitive to changes in P_0 since small control inputs are commanded and only small changes in the T-matrix must be tracked. This may not be true for very nonlinear flight conditions or flight conditions requiring large control inputs to minimize vibration.

Degradation in controller performance for the global system model does become noticeable if P_0, Q, and R are adjusted to essentially eliminate identification due to extremely low Kalman gains. This is shown in Fig. 47 where the performances of two cautious controllers, which have the Kalman filter system identifier essentially turned off, are compared to the performance of the baseline controller having optimal tuning for P_0, Q, and R. System identification is inhibited in both these controllers by specifying very large values of R while keeping $\lambda \cdot P_0$ at its baseline value. The Kalman filter can make essentially no changes in system parameters since the Kalman gains, which are proportional to P_0/R, are so small. Clearly, the effectiveness of the global cautious controller in reducing vibration has been compromised. The reduction in the vibration performance index is only 77 percent compared to over 97 percent reduction achieved by the baseline controller. The degradation in performance is not due, however, to poor identification of system parameters. This can be seen by the performance shown in Fig. 47 for the local cautious controller with no identification, which is essentially the same as that of the baseline controller with identification. As mentioned earlier, only very small changes occur in the T-matrix relationship between vibration outputs and control inputs over the small range of inputs commanded by these controllers at this flight condition. Thus, lack of identification due to non-optimal tuning of P_0, Q, and R has only minor effects on the cautious controller based on the local system model.

Therefore, the degradation in the performance of the global cautious controller with no identification is not due to poor identification of system parameters since it commands small control inputs on the same order of magnitude as those commanded by the local cautious controller. Rather, the degradation in controller performance is due to little or no change occuring in P_i. Since essentially no identification is allowed to take place due to non-optimal tuning of the identifier, little information is gained about system properties. As a result, the identifier maintains about the same P_i

matrix indicating that the relative uncertainty in system parameters has not been reduced from that specified initially. This causes the effective weighting placed on total θ in the performance index to remain nearly constant. It was pointed out in the last section that the global cautious controller performed more like a deterministic controller with internal rate-limiting than with internal limiting on total θ due to the reduction in P_i that occurs with improved system identification. However, without identification, P_i remains nearly constant, and the global cautious controller can be expected to perform more like the deterministic controllers shown in Fig. 31 with constant internal limiting on total θ. Indeed, the global cautious controller with no identification shown in Fig. 47 has essentially the same performance as that shown in Fig. 31 for W_θ equal to 1000.0 along the diagonal. The effective weighting matrix for the global cautious controller has diagonal elements of 1200.0.

In contrast, the local cautious controller without identification performs like a deterministic controller with constant $W_{\Delta\theta}$ weighting matrix. Thus, as long as $\lambda \cdot P_i \cdot W_{z_{jj}}$ applies enough weighting on $\Delta\theta$ to guide the controller to a control solution with small amplitudes, lack of identification does not significantly affect the performance of the local cautious controller at this flight condition, as is shown in Fig. 47.

Local System Model

Unless otherwise stated, all the results presented above for the cautious controller are for the global system. These results and the accompanying discussion are generally applicable to the local system model as well. Any significant differences have already been noted. It has been found in this investigation that the performance of the cautious controller, at steady flight conditions, is very similar for both system models when similar and near optimal tuning of internal parameters is specified (e.g., P_o, Q, R, and $\lambda \cdot P_o$).

Figures 48 through 50 demonstrate the similarity in overall controller performance for both system models. The configuration used for the global model is the baseline configuration specified in Table 5 for the cautious controller. The tuning of the local cautious controller is somewhat different, but $\lambda \cdot P_o$ is the same. Clearly, the performance based on both system models is nearly the same in every respect. Almost identical levels of substantially reduced vibration are achieved at each of the RTA sensor locations. These reductions in vibration are achieved with almost the same control solutions, and time to convergence is virtually the same. The only significant difference between the performance of these two controllers is the tendency for drift in the control inputs exhibited by the baseline controller

with global model after convergence is reached in the vibration performance index. The local model does not exhibit this tendency; however, this difference is a matter of the tuning of P_o, Q, and R. The local model shown has high values for P_o and Q so that the identifier is very sensitive to errors in the T-matrix. When similar tuning is specified for the global model, while maintaining the value of $\lambda \cdot P_o$, the tendency to drift is eliminated, and the performances of the two controllers are virtually identical.

Cautious Controller Summary (Baseline Flight Condition)

In summary, the cautious controller has proven very effective in reducing vibration at the baseline high speed flight condition. When appropriately tuned, both the local and global system models form the basis of controllers that exhibit excellent stability and performance. Convergence to a solution with significantly reduced vibration in the RTA is achieved quickly and smoothly, and the required inputs for achieving these reductions are quite small. With near optimal tuning, the controller, based on either the local or global model, performs much like the baseline deterministic controller with internal rate-limiting. The effective weighting matrix on control inputs depend directly upon $\lambda \cdot P_o$ which has much the same effect as $W_{\Delta\theta}$ on controller performance. However, the effective weighting matrix for the cautious controller varies with time since P_i is calculated by the Kalman filter identifier at each controller update. Generally, the magnitude of elements in P_i and, thus, the effective weighting matrix decrease as system identification improves. For this reason, the global cautious controller behaves much like a rate-limited controller, even though it effectively weights total θ in the performance index. Finally, the cautious controller is fairly insensitive to tuning of internal parameters (λ, P_o, Q, and R) at this fairly linear flight condition. Even quite non-optimal tuning of these parameters results in significantly better performance than that of the original deterministic configuration with external rate-limiting. However, it must be kept in mind that P_o directly affects both the identification algorithm and effective weighting placed on control inputs. For this reason the cautious controller is somewhat more sensitive to tuning than the deterministic controller having either form of internal limiting. If P_o is changed significantly, λ may have to be adjusted to maintain effective controller performance by maintaining appropriate weighting on control inputs.

Dual Controller

In Figures 8 through 10, it was shown that the baseline dual controller is very effective in reducing vibration with small control inputs at the baseline flight condition. However, it was also noted that the dual controller has very different performance characteristics than those already discussed in

some detail for the deterministic and cautious controllers. This is due to the stochastic learning term that is added to the performance index in Eq. (22). This term acts as a perturbation signal that allows the controller to actively probe the system in order to improve system identification at the same time it is providing control.

The stochastic learning term has the exact opposite effect to that of the weighting terms placed on control inputs by the baseline deterministic and cautious controllers, since this learning term tends to reduce the constraints on control inputs. While the cautious controller penalizes control (when poor system identification is indicated) by limiting control inputs, the dual controller actively tries to improve identification by providing more information to the identifier in the form of large control and vibration changes.

Therefore, the system probing used by the dual controller tends to compromise short term control and may lead to instability. As will be discussed in the next section, some form of rate-limiting is required to ensure that the detrimental effect on short term control is not too severe.

Effect of Rate-Limiting

Figures 51 through 53 show the overall performance for three different dual controller configurations. The first configuration shown is that of the baseline dual controller presented in Table 5. The other two configurations are the same except for the limiting of control inputs. The second configuration uses internal rate-limiting ($W_{\Delta\theta}$ = 5000) rather than the external rate-limiting used in the baseline controller, and the third configuration is completely unlimited allowing the controller to actively probe the system at will. While all three controllers converge to excellent final solutions, the time histories presented in Fig. 51 show the significant differences in short term control.

The time history of 3 per rev cyclic pitch shown in Fig. 51 for the unlimited dual controller clearly demonstrates the active probing that results from the stochastic learning term included in the performance index. In the first four revs of active control, the resulting perturbation in control inputs is quite large, and the resultant short term control is unacceptable. For instance, after the first rev of active control, the performance index has increased tremendously to a value that is over forty times the baseline value before any higher harmonic control is implemented. In the second rev of active control, the performance index increases further to a peak value that is almost sixty times the baseline value. This corresponds to increases in the vibration level at each of the RTA sensor locations to values that are 6 to 12 times their baseline values. Representative of these increases in

vibration is the increase in the vertical vibration component at the cross-beam sensor location from 0.14 g's just before activating the controller to 1.3 g's after two revs of active control. Thereafter, the unlimited dual controller begins to reduce the performance index fairly steadily, even though it is still probing the system with fairly large perturbations of the control inputs. As system identification improves, the size of the perturbations caused by the learning term decrease from the very large initial perturbations to almost no perturbations at convergence. This is due to the stochastic learning term being proportional to $\lambda \cdot P_{i-1}/R$ as shown in Eq. (23). As system identification improves, P_{i-1} decreases while λ and R are held constant.

By convergence, the unlimited dual controller achieves a steady control solution that is very similar to and equally effective in reducing vibration as that achieved by the baseline controller. Figure 52 shows the similarity in the higher harmonic pitch amplitudes for these two solutions. Furthermore, there is only a few degrees difference in phase between any one of the control inputs for the two solutions. Figure 53 shows that essentially the same substantially reduced vibration levels have been reached in the RTA. Recall that the deterministic controller is completely unstable and diverges at this flight condition when no rate-limiting is applied. Thus, the inherent probing by the dual controller allows the controller to converge to a very good solution.

Despite the excellent final solution and reductions achieved in the RTA, the overall performance of the unlimited dual controller is unacceptable due to the severe detrimental effects on short term control, not to mention the impracticality of the large changes in control commanded in the first four revs. While the stochastic control constant λ can be adjusted to try to achieve a better tradeoff between short term control and system probing for improved identification, the unlimited dual controller is very sensitive to the value specified for λ. In fact, all other values used for λ in the unlimited dual controller resulted in worse performance than that shown in Fig. 51. An increase in λ results in even worse short term control and less effective vibration reduction as well. A decrease in λ results in better short term control, but eventually, divergence of the controller.

Clearly, rate-limiting is required to achieve adequate controller performance in terms of improved stability and short term control. Figure 51 shows that excellent controller performance can be achieved by both external or internal rate-limiting; however, internal rate-limiting tends to inhibit or eliminate the inherent probing of the dual controller. Furthermore, controller performance is very sensitive to the relative weighting specified for $W_{\Delta\theta}$ and the effective "negative" weighting due to the learning term. If

$W_{\Delta\theta}$ is too small, the controller tends to have the same problems as the unlimited dual controller. If $W_{\Delta\theta}$ is nearly equal in magnitude to the probing term, the controller tends to perform like a deterministic controller with no limiting or light rate-limiting. Thus, performance is oscillatory and/or very large control solutions are calculated. Finally, if $W_{\Delta\theta}$ is made large enough to improve stability and short term control, it tends to remove the probing nature of the dual controller. While performance is excellent, even better performance has been demonstrated with much simpler configurations, such as the baseline deterministic controller with internal rate-limiting, that are much less sensitive to tuning of internal parameters.

On the other hand, Fig. 51 shows that external rate-limiting allows some system probing to occur while still providing excellent overall performance. If more system probing is desired, the external limits can be relaxed with the expected penalty of relatively poor short term control. The external rate-limiting used in Fig. 51 is 0.2 deg/rev and the excellent overall performance of this baseline dual controller has already been discussed and compared to that of the baseline deterministic and cautious controllers. While this amount of rate-limiting severely limits the system probing when compared to the unlimited controller, this limited amount of system probing must still have a fairly large effect since convergence to an excellent steady solution is achieved. Recall that a deterministic controller with the same tuning of P_o, Q, and R and the same amount of external rate-limiting has very unsatisfactory behavior, as was shown in Fig. 14 ($\Delta\theta_{max}$ = 0.2 deg/rev). This externally rate-limited deterministic controller never really converges and is not nearly as effective in reducing vibration.

Effect of Stochastic Control Constant λ

Recall that the stochastic learning term implemented by the dual controller is directly dependent upon $-\lambda \cdot P_{i-1}/R$ and results in effectively a "negative" weighting on total θ in the global model and $\Delta\theta$ in the local model. The result is a reduction in constraint on control inputs and active probing of the system by the controller, as demonstrated in Fig. 51. As discussed previously, P_i for the local model is the covariance of the estimated T-matrix. For the global model, P_i is defined as in Eq. (17) and includes the covariances and cross-covariances for the estimated T-matrix and Z_o. For both system models, R represents the covariance of the measurement noise. Thus, the learning term is directly dependent upon the ratio between the relative uncertainty in the estimated system parameters (T and/or Z_o) and the uncertainty in the measured vibration parameters (Z_i). The stochastic control constant λ is an arbitrary constant used to give some flexibility to modify or tune the dual control algorithm.

While system probing tends to improve system identification, Fig. 51 clearly shows that it also tends to compromise short term control. Thus, the dual controller, in order to be useful, must achieve an acceptable tradeoff between long term system identification and short term control. The stochastic control constant λ represents this tradeoff. This constant must be selected to tune the dual controller by reaching an acceptable compromise between good short term control and the rate of learning. Figure 54 shows the effect of λ on the performance of the dual controller at the baseline high speed flight condition. In this figure, the time histories of the vibration performance index and 3 per rev cyclic pitch are shown for the baseline dual controller with several different values of λ. Recall that the baseline dual controller is based upon the global system model and implements external rate-limiting with $\Delta\theta_{max}$ = 0.2 deg/rev.

Clearly, λ has a significant effect on the dual controller's performance. The baseline dual controller (λ=0.01) exhibits the best overall performance. As λ is decreased from the baseline value, short term control improves somewhat, but long term control worsens. The lowest value shown for λ results in the best short term control, but the controller eventually goes unstable. As λ increases over that for the baseline controller, controller performance becomes unacceptable. In just the small change from the baseline value of λ to that of the next higher value, the tendency to probe the system completely dominates to the point that not only is short term control severely compromised, but the controller goes unstable, despite external rate-limiting. It is not clear what is happening at the highest value of λ, but the same type of behavior has been exhibited at high values of λ for the unlimited dual controller as well. Apparently, the learning term becomes so large that it dominates the performance index and the minimum variance control algorithm breaks down.

Figure 54 indicates the extreme sensitivity of the dual controller to tuning of internal parameters. Even for this fairly mild flight condition, only a very small range of values for λ results in acceptable performance. Tuning of the controller is further complicated by the fact that two important internal parameters used to tune the Kalman filter identification algorithm (P_o and R) also play an important role in the learning term and significantly affect the tuning of the minimum variance control algorithm. Thus, tuning of λ, P_o, Q, R, and $\Delta\theta_{max}$ to achieve the best tradeoff between system probing and short term control for optimum dual controller performance may be extremely difficult for new flight conditions. Much of this increased sensitivity to tuning is probably due to the increased importance of matching identifier tuning to system probing and tuning of the minimum variance control algorithm. Clearly, making large control changes with continually poor system identification can quickly degenerate in an unstable controller.

Local System Model

Figures 55 and 56 demonstrate the similarity in dual controller performance for both the global and local system models when similarly tuned. Figure 55 compares the time histories of the vibration performance index and 3 per rev cyclic pitch amplitude for two unlimited dual controllers based upon local and global models, respectively. The tuning of both controllers is identical; the only difference between these two controllers is the system model used as the basis of the controller algorithms. Figure 56 compares the time histories for a local dual controller to those for the externally rate-limited baseline dual controller. The controllers are the same except for the system model used. In both figures, controller performance for the local model is essentially identical to that for the global model, as indicated by the very similar time histories of a representative control input and the performance index.

Dual Controller Summary (Baseline Flight Condition)

In summary, the dual controller can be very effective in reducing vibration of the baseline flight condition when an appropriate configuration is defined and properly tuned. It has been found that rate-limiting is essential for maintaining acceptable short term control. Despite the inherent difficulties of external rate-limiting that were discussed in relation to the deterministic controller, external rate-limiting is most appropriate for the dual controller since it allows system probing to occur. Internal rate-limiting, on the other hand, tends to eliminate the inherent probing used by the dual controller to improve system identification, if the internal weighting is made large enough to achieve adequate short term control. For a given configuration, the dual controller is extremely sensitive to tuning of internal parameters. Thus, tuning of the dual controller at other flight conditions may present a significant problem. This is in contrast to the optimum configurations for the deterministic and cautious controllers which are fairly insensitive to tuning. However, as will be discussed later, the dual controller has provided good performance at other flight conditions without retuning. Its performance during certain transients indicates that it may have more potential for performing well during transients, when properly tuned, than perhaps the deterministic and cautious controllers.

Based only on the results at the baseline flight condition, the dual controller does not offer any sufficiently significant improvements in performance to warrant its use. Configurations for both the deterministic and cautious controllers can be defined that give better overall performance than the baseline dual controller. Their short term control performance is significantly better. Furthermore, the minimum variance control algorithm for

the deterministic controller is much simpler and more satisfying, since it is not based on some rather nebulous parameters (λ, P_o, R) that require significant tuning to achieve good performance. The weighting of $\Delta\theta$ and θ with $W_{\Delta\theta}$ and W_θ, respectively, can be related back to the physical system, and one can get a feel for the effect of $W_{\Delta\theta}$ and W_θ. Furthermore, their effect is consistent and does not depend upon the performance of the identifier. Thus, unless the dual controller (and the cautious controller for that matter) provide significantly better performance than the deterministic controller in one way or another, there is no reason to consider them further. Therefore, it is only the anticipated potential for the dual controller to better handle transients and maneuvers that warrants further consideration.

Effect of Forward Velocity on Controller Performance

The effect of forward velocity on controller performance is shown in Figs. 57 through 60. These figures present the results of active control at three different steady flight conditions having forward velocities of 57.6 m/s (112 kts), 66.9 m/s (130 kts), and 77.2 m/s (150 kts). The latter flight condition is the baseline high speed flight condition that has already been discussed. All three flight conditions have about the same thrust level with a nominal value of 0.06 for C_T/σ. The results shown are for the baseline cautious controller, but essentially the same excellent performance is expected from the baseline deterministic and dual controllers as well. It is important to note that these excellent results have been obtained with no retuning of the controller and with the same initial T-matrix (between RTA vibrations and higher harmonic control inputs) developed at the baseline flight condition.

Figure 57 compares the time histories of the vibration performance index and the 3 per rev cyclic pitch amplitude for all three flight conditions. The controller exhibits the same excellent performance characteristics at all three forward velocities. Convergence to an excellent control solution occurs very quickly and smoothly, with about 5 revs required for all three flight conditions.

The change in the vibration level at each of the six RTA sensor locations is shown in Fig. 58 for the two lower forward velocities. These results can be compared directly to those for the cautious controller at the baseline flight condition (150 kts) shown in Fig. 9. Clearly, the controller is very effective at all three velocities in reducing vibration at all sensor locations except those having very low initial levels of vibration without any higher harmonic control (nose lateral and tail lateral). The low levels of vibration at these sensor locations have been maintained if not reduced

slightly. Note that at the lower velocities the controller is starting to achieve reductions in vibration at these locations as well, since the initial vibration levels at these locations are now higher than the reduced vibration levels at the other sensor locations. The controller generally tends to achieve about the same level of vibration at each of the sensor locations.

Figure 59 shows a more direct comparison in the effectiveness of the controller at reducing vibration at the three forward velocities. The longitudinal and vertical cross-beam vibration levels with and without higher harmonic control are shown for all three forward velocities. The vibration performance indices are also shown. As forward velocity increases, overall vibration without any higher harmonic control increases, as expected. This increase is apparent at both representative sensor locations and the vibration performance index, which is indicative of overall vibration. After the active controller has converged to a substantially reduced vibration level, this same trend is again present; vibration at each of the two representative sensor locations and the vibration performance index tend to increase with increased forward velocity. While the controller has reduced vibration substantially, it cannot achieve the same minimum vibration levels at each flight velocity. Apparently, the minimum vibration levels that can be achieved via higher harmonic control are dependent upon the flight condition. Figure 60 shows that about the same percentage reduction is achieved in the vibration levels at the two sensor locations and in the vibration performance index. In any case, substantial reductions in vibration have been achieved at all three flight velocities as indicated by at least a 97 percent reduction in performance index, at least a 95 percent reduction in the longitudinal cross-beam vibration, and at least a 75 percent reduction in the vertical cross-beam vibration.

Finally, Fig. 60 shows that the higher harmonic pitch amplitudes at 3, 4 and 5 per rev required to achieve these substantial reductions in vibration tend to decrease with a decrease in forward velocity. Required higher harmonic pitch amplitudes are on the order of 0.1, 0.2, and 0.3 degree at 57.6 m/s (112 kts), 66.9 m/s (130 kts), and 77.2 m/s (150 kts), respectively. These levels of required control to achieve such substantial vibration reduction at these flight velocities are quite reasonable.

The effect of higher harmonic control on rotor blade vibratory stresses and moments at all three flight conditions is shown in Table 10. This table shows the maximum 1/2 peak-to-peak stresses and moments at critical locations along the blade span before and after higher harmonic control is applied. The percentage increase in stress or moment is also shown for each velocity. As forward velocity is decreased, the relative increases in blade stresses and moments that tend to be associated with the application of higher harmonic

control are reduced. This is most likely due to the smaller amplitudes of control required for vibration reduction. It should be noted that, even with these increases, the blade vibratory stresses and moments are still significantly lower than those at the high thrust conditions without higher harmonic control, which will be discussed in the next section.

TABLE 10 - EFFECT OF HIGHER HARMONIC CONTROL ON MAXIMUM ROTOR VIBRATORY MOMENTS AND STRESSES AT VARIOUS FORWARD VELOCITIES (Baseline Cautious Controller)

	FORWARD VELOCITY								
	57.6 m/s (112 kts)			66.9 m/s (130 kts)			77.2 m/s (150 kts)		
	No HHC	HHC	% Diff	No HHC	HHC	% Diff	No HHC	HHC	% Diff
Flatwise (0.394R) N/cm^2 (lb/in^2)	1669 (2419)	1805 (2617)	+8.2	1950 (2827)	2195 (3182)	+12.6	2363 (3426)	2702 (3918)	+14.4
Edgewise (0.265R) N/cm^2 (lb/in^2)	288 (418)	366 (531)	+27.0	410 (594)	565 (819)	+37.9	640 (928)	973 (1411)	+52.0
Torsion (0.079R) N-m (in-lb)	59.2 (524)	131.9 (1167)	+124.	74.6 (660)	200.1 (1771)	+168.	101.7 (900)	278.8 (2467)	+174.

The effect of higher harmonic control on rotor performance is shown in Table 11 for all three forward velocities. As forward velocity is decreased, the effect on each rotor performance parameter is reduced. The detrimental effects on drag and required torque are significantly reduced. At the 57.6 m/s (112 kts) flight condition, the effect of higher harmonic control on rotor performance is minimal.

TABLE 11 - EFFECT OF HIGHER HARMONIC CONTROL ON ROTOR PERFORMANCE AT VARIOUS FORWARD VELOCITIES
(Baseline Cautious Controler)

	FORWARD VELOCITY								
	57.6 m/s (112 kts)			66.9 m/s (130 kts)			77.2 m/s (150 kts)		
	No HHC	HHC	% Diff	No HHC	HHC	% Diff	No HHC	HHC	% Diff
Thrust N (lb)	36543 (8212)	36606 (8226)	+0.2	37322 (8387)	37505 (8428)	+0.5	36735 (8255)	37224 (8365)	+1.3
Torque N-M (ft-lb)	16702 (12619)	17220 (12701)	+0.6	20768 (15318)	21163 (15609)	+1.9	25139 (18542)	26403 (19474)	+5.0
Prop. Force N (lb)	3071 (690)	3071 (690)	0.0	3645 (819)	3640 (818)	-0.1	4001 (899)	3978 (894)	-0.6
Equiv. L/D	9.42	9.44	+0.2	10.34	10.07	-2.6	10.26	9.34	-9.0

Forward Velocity Variation Summary

In summary, the active controller is very effective in reducing vibration throughout the range of velocities of 57.6 m/s (112 kts) to 77.2 m/s (150 kts). These reductions are achieved very quickly by the controller, even though the same initial T-matrix developed at the high speed flight condition is used throughout the range of velocities and the controller is not retuned. The required control inputs to achieve these reductions in vibration throughout the range of velocities are quite reasonable. As the forward velocity decreases, the required higher harmonic pitch amplitudes also decrease. Finally, the detrimental effects on rotor blade vibratory stresses and rotor performance also decrease with a decrease in forward velocity.

Effect of Rotor Thrust on Controller Performance

The effectiveness of the active controller has also been investigated as a function of rotor thrust. Figures 61 and 62 present a summary of the results of active control for three different steady flight conditions. All three flight conditions have the same forward velocity of 77.2 m/s (150 kts) as the baseline flight condition, but different nominal values of 0.058, 0.08, and 0.085 for C_T/σ. The first flight condition ($C_T/\sigma = 0.058$) is the baseline flight condition that has already been discussed in detail. The last two flight conditions represent more severe flight conditions with increases in rotor thrust over the baseline of 39 and 47 percent, respectively. As can be seen in Fig. 61, increased rotor thrust results in higher baseline (no HHC) vibration levels in the RTA as a direct result of increased hub loads corresponding to a greater rotor disc loading. These figures also show the excellent reduction in vibration achieved by active higher harmonic control at all three thrust conditions.

The highest thrust level ($C_T/\sigma = 0.085$) is especially severe with a significant increase in vibratory response over not only the baseline flight condition but also the other high thrust condition ($C_T/\sigma = 0.08$). Predicted RTA accelerations for this flight condition are on the order of 0.8 to 1.0 g with no higher harmonic control or other vibration treatment. Thus, a relatively small increase in rotor thrust between the two high thrust flight conditions results in a significant increase in vibration. The severity of the highest thrust condition is due to its being well into stall with the constant inflow model used. As will be discussed in the results of the open-loop nonlinearity study, this flight condition is also somewhat more nonlinear and has more interharmonic coupling effects than the baseline flight condition. Furthermore, the T-matrix relationship between vibration response in the RTA and control inputs changes significantly with change in both flight condition and higher harmonic control. Thus, this maximum thrust flight condition should represent a good test of controller performance. For this reason, a comparison of the performance of the three baseline controllers specified in Table 5 will be made at this flight condition, and the results will be covered in somewhat more detail in the following discussion. Comparisons made between the three thrust conditions will be for results obtained by the baseline deterministic controller. It should be noted that these baseline controller configurations have been applied to these high thrust flight conditions without any retuning of the controllers to improve performance. The excellent performance shown in Figs. 61 and 62 will be discussed in some detail in the next subsection entitled: "Vibration Reduction."

Before covering these results, it should be pointed out that the same initial T-matrix, T_o, used to initialize the active controller at the baseline flight condition is also used at the high thrust flight conditions. This

T-matrix was found by open-loop perturbation at the baseline flight condition. Since the system is somewhat nonlinear and sensitive to both the flight condition and the operating control point, such an initial T-matrix can be quite inaccurate for flight conditions other than that at which it was determined. Since the high thrust flight conditions represent more severe conditions than the baseline, it is expected that the linearized relationship between inputs and outputs is also quite different from that at the baseline. A comparison, which will be made later, between the initial T-matrix and one determined at the final optimal control point at the highest thrust condition considered shows that significant differences occur due to change in flight condition and the presence of nonzero higher harmonic control. Thus, activating the controller at these high thrust conditions with the baseline T-matrix is a good test of the controller's capability to remain stable while identification of system parameters is updated. However, it should be noted that, in a production helicopter, the controller will probably be activated and initialized in hover with system identification being updated as the design flight condition is approached. Such a procedure represents a much less severe task for the controller than that required in this analytical study where the controller is activated at some steady forward flight condition with, perhaps, a fairly inaccurate T-matrix.

Vibration Reduction

Figures 61 and 62 directly compare the effectiveness of the baseline deterministic controller in reducing vibration at all three thrust conditions. Figure 61 presents the longitudinal and vertical components of vibration at the cross-beam sensor location and the vibration performance index for all three thrust conditions; a comparison is made between the values of these representative quantities with and without higher harmonic control. As rotor thrust increases, overall vibration without higher harmonic control increases due to larger hub loads resulting from a higher rotor disc loading. A significant increase in vibration occurs between the two high thrust conditions, since the maximum thrust condition is well into stall. This same trend is apparent after the baseline deterministic controller has converged to a substantially reduced vibration level; vibration is still generally higher for higher thrust levels at convergence. While the controller reduces vibration substantially at all three thrust conditions, it cannot reach the same minimum vibration levels. However, the minimum vibration levels achieved at each condition are fairly close considering the significant differences in vibration present without any higher harmonic control.

Figure 62 shows that the controller achieves about the same percentage reductions in the vibration performance index and accelerations at the two representative sensor locations. Clearly, the deterministic controller has achieved substantial reductions in overall vibration at all three thrust conditions, as indicated by at least a 97 percent reduction in the performance

index, at least a 95 percent reduction in the longitudinal cross-beam vibration component, and at least a 74 percent reduction in the vertical cross-beam vibration component.

Figure 62 also shows that larger higher harmonic pitch amplitudes are required for an increase in rotor thrust and corresponding increase in baseline vibration response. Required higher harmonic pitch amplitudes are on the order of 0.3, 0.5, and 0.9 degree at C_T/σ equal to 0.058 (8255 lb), 0.08 (11508 lb), and 0.085 (12053 lb), respectively. These levels of required control are quite reasonable with less than 1.0 degree required for each of the three control inputs at even the highest thrust condition. As will be discussed later, higher harmonic control has a significant effect on rotor performance at the two high thrust conditions. However, the effect on rotor thrust is less than 2 percent for even the highest thrust condition considered, and the resultant thrust level is greater than that without higher harmonic control in each case. Thus, the results just presented should be indicative of the control requirements and potential reductions in vibration that could be achieved if the rotor could be kept in trim in the computer simulation as active control is implemented.

While the overall results just presented for the three thrust conditions are for the baseline deterministic controller, comparable results to those shown in Figs. 61 and 62 could be shown for both the baseline cautious and dual controllers. As shown in Figs. 9 and 10 for the baseline flight condition and Figs. 63 and 64 for the highest thrust condition, the final control solutions and resulting vibration response in the RTA are very similar for all three controller types when appropriate configurations are specified. Figure 63 shows the reductions in vibration achieved by all three controllers at all six sensor locations for the highest thrust condition. Basically the same vibration levels have been achieved by all three controllers, although the reductions achieved by the dual controller are slightly less due to system probing still occurring at rev 30. Figure 64 shows the similarity in the control solutions commanded by all three controllers at the highest thrust condition.

It should be noted that deterministic and cautious controller configurations that are the same as the baseline controllers, except for the use of the local system model, exhibited very similar performance characteristics to the global models used in the baseline controllers. However, the local controllers were slightly more oscillatory indicating that the local system model might be more sensitive to tuning and to the effects of transients and inaccurate vibration measurements.

While Figs. 61 and 62 demonstrate that excellent final reductions in vibration are achieved at all three thrust levels, transient response is somewhat different at the highest thrust level, as can be seen by comparing the time histories for the baseline deterministic controller at all three operating conditions. Figure 65 presents the time histories of the vibration performance index as well as the amplitude of the 3, 4, and 5 per rev control inputs commanded by the baseline deterministic controller at the high thrust condition having a value of 0.080 for C_T/σ. Figure 66 shows the time history of the performance index for all three baseline controllers operating at the highest thrust condition (C_T/σ=0.085) as well as the time history of vibration at a representative RTA sensor location (Cross-Beam vertical). Figure 67 presents the time histories of the amplitude of the 3, 4, and 5 per rev control inputs commanded by all three baseline controllers at this thrust condition. The results shown in these figures can be compared directly to the time histories for all three controllers operating at the baseline flight condition (C_T/σ=0.058) presented in Figs. 8(a) and 8(b).

In Fig. 65 for C_T/σ of 0.08, the deterministic controller exhibits virtually the same characteristics as at the baseline flight condition; reduction of vibration is achieved very quickly and smoothly, with about 5 revs required for convergence in the performance index. In contrast, the behavior of all three controllers is fairly oscillatory at C_T/σ equal to 0.085. This increased oscillatory behavior is exhibited in the time histories for the vibration performance index, the acceleration at a representative RTA sensor location (Cross-Beam vertical), and the amplitude of the 3, 4, and 5 per rev control inputs shown in Figs. 66 and 67. The dual controller exhibits even more oscillatory behavior than both the deterministic and cautious controllers, whose time histories are very similar just as they were at the baseline flight condition. This increased oscillatory behavior in the dual controller is clearly evident in the higher harmonic control inputs and RTA vibrations and is due to increased system probing, which is still evident in the time history of all three control inputs at rev 30.

The increased oscillatory behavior of all three controllers at the highest thrust condition is due to an inaccurate initial T-matrix, increased system nonlinearities, increased sensitivity of the T-matrix to changes in the higher harmonic control operating point, and non-optimal tuning of the controllers at this flight condition. The extent of the changes in the T-matrix relationship between RTA vibration and control inputs that can occur due to change in flight condition and the presence of nonzero higher harmonic control inputs will be discussed briefly in the next section. A more detailed discussion of system nonlinearities will be covered in Appendix A, which presents the results of a separate open-loop study (e.g., no active control) of the extent and sources of system nonlinearities and interharmonic coupling at the baseline and maximum thrust flight conditions (C_T/σ = 0.058 and

0.085). It is sufficient here to say that significant changes in the initial T-matrix estimate must be adapted to by the controllers in converging to an optimal solution at the maximum thrust condition (C_T/σ = 0.085). The significant inaccuracies in the initial T-matrix and the changes that occur with changes in the control inputs cause inaccurate calculations for updates in control by all three controllers and increased system probing by the dual controller. The inaccurate calculations for new "optimal" control solutions cause commanded inputs that may or may not reduce vibration. Depending on the severity of system nonlinearities and the limiting placed on control inputs, this can cause oscillatory behavior similar in nature to that caused by the inherent system probing of the dual controller.

Another significant factor in the somewhat oscillatory behavior of the baseline deterministic and cautious controllers is that they have not been retuned. In particular, $W_{\Delta\theta}$ for the deterministic controller and λ for the cautious controller have not been changed to match the flight condition. As shown in Fig. 61, there is a significant increase in overall vibration in the RTA at the maximum thrust condition compared to the baseline flight condition at which the controllers were tuned. Thus, the effective weighting on the control inputs at the highest thrust condition due to the values of $W_{\Delta\theta}$ and λ determined at the baseline flight condition is significantly reduced; more relative emphasis is placed by the controller on reducing the increased RTA vibrations than on maintaining small changes in control inputs. This is evidenced by initial changes in control commanded at the baseline and maximum thrust conditions. At the maximum thrust condition, initial changes in control on the order of 0.7 degree are commanded by both the deterministic and cautious controllers for 3, 4, and 5 per rev inputs. At the baseline flight condition, initial changes on the order of 0.15 degree are commanded, even though the same values of $W_{\Delta\theta}$ or λ are used. At C_T/σ equal to 0.08, vibration levels in the RTA are higher than those at the baseline flight condition, but the effective weighting due to $W_{\Delta\theta}$ or λ is still high enough to keep initial changes in all three control inputs less than 0.35 degree. Note that these initial changes in control inputs are acceptable for this analytical investigation since stability is maintained; however, in practice, it will be necessary to limit the allowable changes in control inputs that can be implemented in any given rev in order to meet the capability of controller hardware.

The large initial changes in control caused by the non-optimal tuning of the deterministic and cautious controllers at the maximum thrust condition cause two problems. First, the T-matrix is more sensitive to change in control inputs at this flight condition. Thus, larger changes in the T-matrix are more likely to occur with these large changes in control. The controller must track these changes as well as overcome the inaccuracies of the initial T-matrix estimate. Second, the large changes in control cause larger

transients to occur in the vibration response which also take longer to die out. The transients cause less accurate vibration information to be obtained by the harmonic analyzer. This inaccurate vibration information can, in turn, lead to inaccurate updates made to the T-matrix estimate and inaccurate calculations of updates in optimal control required to reduce the perceived vibration. Thus, while larger changes in control inputs give a potential of better system identification since more information is passed to the identifier more rapidly, these changes cannot be so large as to cause completely inaccurate information to be processed. Obviously, the large initial control inputs caused by non-optimal tuning of $W_{\Delta\theta}$ or λ can lead to oscillatory behavior.

Despite the inaccurate initial T-matrix and non-optimal tuning, stability is maintained and convergence is achieved by all three controllers at the maximum thrust condition. Furthermore, no amplification of vibration occurs at any time during convergence, except perhaps during initial transients. However, convergence is slowed somewhat by the oscillatory behavior. All three controllers require about 10 revs (2.7 seconds) to achieve and maintain at least a 90 percent reduction in the performance index as compared to about 2 revs (0.55 seconds) for the same deterministic and cautious controllers at the baseline flight condition. As might be expected after the above discussion, increasing the effective rate-limiting of control inputs via increase in $W_{\Delta\theta}$ or λ for the deterministic or cautious controllers, respectively, improves performance by providing a smoother, less oscillatory convergence. Whether or not convergence is achieved more quickly depends upon the level of weighting placed on control inputs. For heavy weighting, more accurate information is sent to the controller, but the controller takes longer to achieve required levels of control. For light weighting, required levels of control can be reached more quickly, but the control inputs actually commanded may be based on inaccurate information. The oscillatory behavior of the dual controller can also be alleviated by more restrictive rate-limiting; however, in so doing, the inherent system probing of the dual controller is inhibited.

One last point should be made in regard to the time histories shown for the highest thrust condition in Figs. 66 and 67. By rev 20, vibration response and control inputs have smoothed out somewhat for all three controllers. The deterministic and cautious controllers no longer exhibit any oscillatory behavior since the effective rate-limiting of constant parameters $W_{\Delta\theta}$ or λ increases for the reduced vibration levels present. Thus, transient effects are alleviated and these controllers smoothly update control inputs based upon updated system information. At rev 30, both these controllers have the same tendency, which was exhibited at the baseline flight conditions, to continue to command very slight changes in 3, 4, and 5 per rev control after the performance index and RTA vibrations have essentially converged. When allowed to run to 50 revs, these two controllers continue to increase 3 per

rev cyclic pitch amplitude at a nominal rate of 0.01 degree per rev, while decreasing 5 per rev amplitude at a nominal rate of 0.005 degree per rev and holding 4 per rev amplitude almost constant. Between rev 30 and rev 50, the total increase in 3 per rev amplitude and decrease in 5 per rev amplitude is about 0.2 and 0.1 degree, respectively. These changes in control after rev 30 tend to cancel and achieve only slight reductions in the performance index and RTA vibrations relative to the baseline values with no higher harmonic control. For example, between revs 30 and 50, the deterministic controller reduces the vibration performance index from 0.018 to 0.015 and the 4/rev amplitude of vibration at the longitudinal cross-beam sensor location from 0.031 to 0.017 g's. While these changes represent reductions of 17 and 45 percent relative to the values at rev 30, they represent reductions of only 0.13 and 1.9 percent relative to the baseline values. If this tendency to drift proves troublesome, it can be alleviated by implementing some limiting on total θ via W_θ, as discussed for the baseline flight condition.

In contrast to the deterministic and cautious controllers, the dual controller does not appear to have the same tendency to drift after rev 20. Rather, the dual controller causes the control inputs to oscillate around fairly steady nominal values. This oscillation due to system probing, in turn, causes oscillatory behavior in the performance index and RTA vibrations.

Nonlinear Effects

As already noted, the time history of control inputs and the resulting vibratory response are somewhat more oscillatory for all three controllers at the maximum thrust condition than the corresponding time histories at the baseline flight condition. It has been suggested that this oscillatory behavior is partially due to using an inaccurate initial T-matrix which was determined by open-loop perturbation about a zero higher harmonic control operating point at the baseline flight condition. Figures 68 and 69 demonstrate the extent of the changes in the linearized T-matrix relationship between RTA vibration components and higher harmonic control inputs that can occur due to change in flight condition, system nonlinearities, and the presence of non-zero higher harmonic control. These changes must be adapted to by the controller for successful convergence to an optimum solution to occur.

Figure 68 compares two T-matrices determined by open-loop perturbation at two different flight conditions and two different operating control points. The T-matrix shown in Fig. 68(a) has been determined by perturbating about a zero higher harmonic control point at the baseline flight condition. Each column represents the 4 per rev harmonic response in the RTA to a 1.0 degree

input for the cosine or sine component of one of the higher harmonic control inputs. Each element has the dimensions g's per radian. The T-matrix shown in Fig. 68(b) has been determined by open-loop perturbation about the optimal control solution previously determined by the baseline deterministic controller at the maximum thrust condition (C_T/σ = 0.085). Thus, the open-loop perturbations were superimposed on the optimal control point shown for the deterministic controller in Fig. 64. The cosine and sine components of this optimal control point are shown in Table 12. Thus, the T-matrix shown in Fig. 68(a) represents the sensitivity of the vibratory response at each sensor location in the RTA to each of the higher harmonic control inputs at the baseline flight condition before any higher harmonic control is applied. This is the T-matrix used to initialize the controller at all flight conditions considered in this study unless otherwise noted. The T-matrix shown in Fig. 68(b) represents the sensitivity of RTA vibratory response to control inputs near convergence (rev 30) of the baseline deterministic controller at the maximum thrust condition.

TABLE 12

OPTIMAL CONTROL POINT USED FOR OPEN-LOOP PERTURBATION AT THE MAXIMUM THRUST CONDITION

Harmonic	Cosine Component	Sine Component
3	0.89	0.12
4	0.22	0.90
5	-0.69	-0.20

Clearly, these two matrices are completely different. Nearly every element of the T-matrix determined at the optimal control point for the maximum thrust condition has changed extensively from the initial T-matrix used to initialize the controller at this flight condition. Figure 69 shows graphically the extent of these changes for two representative sensor locations (cross-beam vertical and longitudinal). In this figure, vibration response at these two sensor locations to each of the components of higher harmonic control are plotted in polar form. Thus, the vectors in this figure have dimensions of g's per radian and represent the sensitivity of the

vibratory response at these sensor locations to changes in control inputs. Both Figs. 68 and 69 show significant changes in both amplitude and phase of these sensitivities. Furthermore, the changes in sensitivity that occur in going from one flight condition and control point to another are different for each of the three control inputs. For example, the sensitivity to 4 and 5 per rev control has increased significantly at the maximum thrust condition, while the sensitivity to 3 per rev control has decreased. There are also significant differences in the phase shift between vibratory response at the two flight conditions for each control input.

There are several sources of the significant differences in the T-matrices shown in Figs. 68 and 69. A change in flight condition is one major source. One expects significant changes in the relationship between higher harmonic control inputs and vibratory response when a 2.0 degree change in collective pitch, which results in almost a 50 percent increase in rotor thrust, is made. Even larger changes are expected when the resultant high thrust condition is in stall, as is the case at the maximum thrust condition ($C_T/\sigma = 0.085$) shown in these figures. Another major source of changes in the T-matrix at a given flight condition is the variation of the T-matrix with control inputs due to nonlinear effects in system response. The T-matrix shown for the baseline condition is based upon no higher harmonic control being present at the operating point, while the T-matrix shown for the maximum thrust condition is based on an optimal control point having 3, 4, and 5 per rev inputs on the order of 1.0 degree. These nonlinear effects can take on two forms. First, the T-matrix can vary with input amplitude and phase about a local operating point due to nonlinear changes in response to local changes in a particular input. Second, the matrix can vary with change in the local control point. That is, the T-matrix varies with and is dependent upon the total control vector. For example, the sensitivity to 3 per rev control can vary with change in 5 per rev control. Thus, at a given flight condition, the T-matrix can change not only with the amplitude and phase of a particular control input, but with the "mix" of 3, 4, and 5 per rev inputs.

Figure 69 indicates that a certain amount of nonlinearity is present in the vibratory response to higher harmonic control. Since the sensitivities shown are for perturbations about a fixed control point, these nonlinearities are of the first type where the T-matrix varies with amplitude and phase of a given control input about a local control point. In a linear system, the response at a given sensor location would be of the same magnitude for both the sine and cosine components of a given higher harmonic control input. Furthermore, these two components would be exactly 90 degrees out of phase. In Fig. 69, at the baseline flight condition with no higher harmonic control at the operating control point, the sensitivities to sine and cosine

components for a given input are about the same magnitude, and have a phase shift of almost 90 degrees. This indicates that the relationship between RTA vibration and higher harmonic control is fairly linear at the baseline flight condition when zero or small higher harmonic control inputs are implemented. In contrast, the phase differences between sensitivities to cosine and sine components of a given higher harmonic control input are significantly greater or less than 90 degrees at the maximum thrust condition. Furthermore, differences in magnitude are evident. Thus, nonlinearities are evident at this flight condition and optimal control point; however, they appear to be fairly moderate.

A separate open-loop study (e.g., no active control) of system nonlinearities and interharmonic coupling has been performed in addition to the closed-loop simulation of active control. The results of this study are presented in Appendix A. In this study, the response to higher harmonic control was investigated at both the baseline flight condition and the maximum thrust condition. By implementing various amplitudes and phases of 3, 4, and 5 per rev control at different local control points, the change in response due to the change in amplitude, phase, and mix of 3, 4, and 5 per rev control inputs has been determined for both flight conditions. By tracing the response to higher harmonic control from the fixed system vibratory response in the RTA back through the hub vibratory response, rotor blade forces, blade motions, and harmonic airloading, further insight into the extent and sources of nonlinearity and interharmonic coupling has been gained.

As expected, the sensitivity of vibratory response in the RTA to changes in control inputs is highly dependent upon flight condition. The severity of both types of nonlinear effects discussed above are also dependent upon flight condition. At the baseline condition ($C_T/\sigma = 0.058$), 4 per rev vibratory response in the RTA has been found to be fairly linear for separate local perturbations of 3 and 4 per rev control and moderately nonlinear for 5 per rev control. At the highest thrust condition ($C_T/\sigma = 0.085$), RTA response is moderately nonlinear for all three control inputs. However, nonlinear coupling effects are significant at both flight conditions. That is, the sensitivity of vibratory response in the RTA to higher harmonic control inputs (T-matrix) changes significantly in both magnitude and phase with a change in the local control point, even though response at this new control point remains fairly linear at the baseline flight condition and moderately nonlinear at the maximum thrust condition. The linearized T-matrix relationship between control inputs and RTA response is particularly sensitive to the "mix" of 3, 4, and 5 per rev control inputs at the maximum thrust condition. This nonlinear coupling effect at the highest thrust condition is particularly severe for 3 per rev inputs. The major source of these nonlinear effects is the blade modal response, rather than nonlinear aerodynamic effects.

Interharmonic coupling has also been found to be highly dependent upon flight condition and the local control point. Interharmonic coupling of modal blade response is significantly greater than interharmonic coupling of airloads. Furthermore, interharmonic coupling between 5 per rev blade modal response to 3 per rev inputs and between 3 per rev response to 5 per rev inputs can be substantial; whereas, the interharmonic coupling of airloads occurs principally between adjacent harmonics. The interharmonic coupled blade response can be substantially larger than the response at the same harmonic as the input. Thus, interharmonic coupling of blade response significantly increases the potential for high blade stresses resulting from the coupled effect of a given set of higher harmonic control inputs. The source of this interharmonic coupling is the blade flatwise bending mode response. The results of the open-loop study of nonlinearity and interharmonic coupling will be discussed in Appendix A.

Rotor Blade Stresses

The effect of higher harmonic control with the baseline deterministic controller on rotor blade vibratory stresses and moments at the maximum thrust condition is shown in Fig. 70. This figure shows the 1/2 peak-to-peak blade bending stresses and torsional moment along the blade span with and without higher harmonic control at C_T/σ equal to 0.085. The distributions shown are for the control solution commanded at rev 30 by the baseline deterministic controller. As can be seen, the relative increases in stresses and moments are of the same magnitude or lower than those shown in Fig. 11 for the baseline (minimum) thrust condition. Most importantly, the torsional moment is not nearly as sensitive to higher harmonic control at the maximum thrust condition as at the minimum thrust condition. While Ref. 10 also noted that relative increases in blade stresses and moments were smaller as rotor thrust increased, results at C_T/σ equal to 0.08 tend to contradict this trend.

Table 13 shows the maximum 1/2 peak-to-peak stresses and moments at critical locations along the blade span before and after higher harmonic control is applied at all three thrust conditions. The percentage increase in the maximum vibratory stress or moment is also shown. Indeed, the percentage increases in the maximum vibratory bending stresses and torsion moment at the maximum thrust condition are less than those at the minimum thrust condition. The maximum flatwise stress at C_T/σ equal to 0.08 also follows this trend of a lower percentage increase in stress with decrease in rotor thrust; however, the edgewise bending stress and the torsion moment at this thrust condition both show larger relative increases than those at the lower thrust condition ($C_T/\sigma = 0.058$). This may or may not be a matter of a particularly bad mix of control inputs being commanded by the deterministic controller. In any case, the vibratory stresses and moments with higher harmonic control at both C_T/σ equal to 0.058 and 0.08 are significantly lower than those without higher harmonic control at the maximum condition.

TABLE 13

EFFECT OF HIGHER HARMONIC CONTROL ON MAXIMUM ROTOR VIBRATORY MOMENTS AND STRESSES FOR VARIOUS ROTOR THRUSTS (Baseline Deterministic Controller)

	Rotor Thrust, C_T/σ								
	0.058			0.08			0.085		
	No HHC	HHC	% Diff	No HHC	HHC	% Diff	No HHC	HHC	% Diff
Flatwise (0.394R) N/cm^2 (lb/in^2)	2363 (3426)	2678 (3882)	+13.3	2878 (4172)	3204 (4646)	+11.4	4228 (6130)	4451* (6452)	+5.3
Edgewise (0.265R) N/cm^2 (lb/in^2)	640 (928)	976 (1415)	+52.5	1134 (1644)	2072 (3004)	82.7	2137 (4548)	4851 (7033)	+54.6
Torsion (0.079R) N-m (in-lb)	102 (900)	271 (2400)	+167.	138 (1228)	426 (3774)	+207.	500 (4424)	713 (6310)	+42.6

*Maximum flatwise bending stress at maximum thrust condition with higher harmonic control occurs at blade spanwise location of 0.265R and has value shown.

If increases in blade stresses caused by higher harmonic control throughout the flight regime are of the same magnitude as those at the maximum thrust condition, blade life would have to be considered. This may lead to the necessity for redesigning the rotor blade or limiting control inputs to acceptable levels while accepting less than maximum possible reduction in vibration. However, certain results of the current study indicate that it may be possible to guide the controller to acceptable solutions in terms of blade stresses by placing appropriately weighted terms in the performance index that are indicative of increases in blade stresses and moments. With proper weighting, a tradeoff in reducing vibration and maintaining acceptable blade stress can be reached. With such a term to guide the solution, it may even be possible to maintain acceptable stress levels without severely sacrificing reductions in vibration. As discussed previously, the weighting matrix W_θ has been used in this study to guide the controller to many significantly different solutions that achieve about the same substantial reductions in RTA vibrations but have significantly different effects on rotor blade vibratory stresses.

The blade stress distributions for one such solution are shown in Fig. 71 for the highest thrust condition. This solution is the result of W_θ being used to eliminate 5 per rev control in the baseline deterministic controller. As can be seen in Fig. 71, the resulting control solution achieved by the controller with only 3 and 4 per rev control causes almost no increase in the flatwise bending stress and the torsion moment and only about a 20 percent increase in edgewise bending stress. Furthermore, the resulting vibratory response in the RTA is less at all sensor locations, except nose lateral, than those shown in Fig. 63 for the baseline deterministic controller having all three control inputs. The resultant vibration level at the nose lateral sensor location is about the same as the very small initial value present without higher harmonic control. Thus, eliminating 5 per rev control at the maximum thrust condition allowed a much more acceptable control solution, in terms of blade stresses, to be reached and even a slightly lower overall vibration response in the RTA. However, elimination of 5 per rev control at the baseline flight condition did not result in significant reductions in blade stresses. No generalization, such as inhibiting or eliminating 5 per rev control for better all around control solutions, can be made. It does indicate that it might be possible to generally guide the controller to much better control solutions while achieving excellent vibration reduction with an appropriate term in the performance index.

For this approach to work, it may be necessary to include parameters, such as blade stresses or rotating blade root shears, from the rotating system in the performance index to ensure that reductions in vibration are achieved via properly phased higher harmonic control inputs and modal cancellations of

small blade loads rather than large loads. This approach should be seriously considered in future studies. While it is not desirable to have to monitor blade stresses (or any other parameter in the rotating system) on a production helicopter, such an approach in future analytical and/or wind tunnel investigations will provide valuable information on the higher harmonic control phenomenon and its effect on blade stresses. Based on the results of such an investigation, it may be possible to define parameters in the fixed system that can be used to predict blade stresses or other parameters in the rotating system via a state estimator, rather than direct measurement. Such an approach may then be applicable to a production aircraft.

Rotor Performance

The effect of higher harmonic control on rotor performance is shown in Table 14 for all three rotor thrust conditions. As rotor thrust is increased, the effect on each rotor performance parameter increases. The change in rotor thrust from trim is less than 2.0 percent for all three thrust conditions. It should be noted that collective and 1 per rev cyclic pitch were kept constant at these steady flight conditions. It is recognized that in practice, any impact of higher harmonic control on rotor forces and moments (thrust, propulsive force, etc.) would be accounted for by retrimming the helicopter, which would also have an effect on required torque. The detrimental effects on propulsive force, and required torque increase significantly at the high thrust conditions. This is believed to be due to the rotor being near stall at C_T/σ equal to 0.08 and well into stall at C_T/σ equal to 0.085, when using constant inflow. Thus, such severe effects on rotor performance are not expected at normal operating conditions. However, the effects shown at the baseline flight condition ($C_T/\sigma = 0.058$) are significant enough to cause concern. As discussed for rotor blade stresses, it may be possible to guide the controller to a better control solution in terms of rotor performance by including in the performance index an appropriately weighted term that is indicative of rotor torque. While the severity of the maximum thrust condition as predicted by the constant inflow simulation may or may not be real, the simulated flight condition still represents a good test of the ability of the controller to remain stable and reduce vibration for a severe flight condition.

TABLE 14

EFFECT OF HIGHER HARMONIC CONTROL ON ROTOR PERFORMANCE FOR VARIOUS THRUST CONDITIONS (Baseline Deterministic Controller)

	Rotor Thrust, C_T/σ								
	0.058			0.08			0.085		
	No HHC	HHC	% Diff	No HHC	HHC	% Diff	No HHC	HHC	% Diff
Thrust N (lb)	36735 (8255)	37202 (8360)	+1.3	51211 (11508)	51749 (11627)	+1.0	53636 (12053)	54659 (12283)	+1.9
Torque N-m (ft-lb)	25139 (18542)	26374 (19453)	+4.9	30167 (22250)	33076 (24396)	+9.6	35690 (26324)	41765 (30805)	+17.0
Prop. Force N (lb)	4001 (899)	3983 (895)	-0.4	4481 (1007)	4290 (964)	-4.7	2617 (588)	1998 (449)	-23.6
Equiv. L/D	10.26	9.37	-8.7	11.11	9.10	-18.0	6.61	5.19	-21.5

Thrust Variation Summary

In summary, the active vibration controller has proven to be very effective in reducing vibration throughout the range of rotor thrust from C_T/σ equal to 0.058 (8255 lb) to 0.085 (12053 lb). All three baseline controllers, which have been tuned at the minimum thrust baseline flight condition (C_T/σ = 0.058), achieved substantial reductions in RTA vibrations at the maximum thrust condition despite the significant differences shown to exist between the inaccurate initial T-matrix and the T-matrix applicable at the optimal control point reached at convergence. Reductions on the order of 75 to 95 percent have been achieved in all the dominant vibration components. These reductions have been achieved with higher harmonic control amplitudes at 3, 4, and 5 per rev of less than 1.0 degree throughout the range of thrust considered. These control requirements agree with other published theoretical

and experimental results and are quite reasonable for the flight conditions considered. While retuning of the baseline controllers is not necessary to achieve these excellent reductions in vibration at convergence, overall controller performance can be improved by retuning, if desired. By tuning the controllers for the maximum thrust condition, convergence can be reached more smoothly and perhaps more quickly. Furthermore, it may be possible to attain the same vibration reductions at the two high thrust conditions with even smaller control inputs by using more appropriate weighting on θ and $\Delta\theta$ in the performance index. The results presented here for various rotor thrusts and those presented above for various forward velocities indicate that very effective active vibration control can be achieved over a wide range of flight conditions. By tuning or optimizing the controller for fairly severe flight conditions (e.g., a high thrust condition), it should be possible to ensure optimum performance for these flight conditions while maintaining more than satisfactory performance at less severe flight conditions.

While the relative increases in vibratory rotor blade stresses resulting from higher harmonic control are smaller at the maximum thrust condition than at the other two thrust conditions, these increases are still significant and will have to be considered in terms of their impact on blade life. However, a potential for control inputs that does not increase blade stresses has been demonstrated. Detrimental effects on rotor performance previously noted at the baseline flight condition are significantly worse at the two high thrust conditions. These significant increases are most likely due to these two high thrust conditions being near and well into stall before higher harmonic control is even implemented. It is not anticipated that such severe effects will be encountered at normal operating conditions. However, the detrimental effects that occur at the baseline flight condition still warrant study into the effect of higher harmonic control on rotor performance. Methods should be studied for guiding the controller to better control solutions in terms of other important parameters such as blade stresses and required rotor torque.

Controller Performance During High Speed Transient Maneuvers

Each of the three baseline controllers has been evaluated during several simulated transient maneuvers. While these simulated maneuvers are very simple in nature, they represent the first step in evaluating the performance of an active vibration controller at anything other than steady operating or flight conditions. Each of these maneuvers represents a sudden change in rotor thrust via a sudden change in collective pitch during an otherwise steady flight condition. For all but one of these transient maneuvers, the initial steady flight condition is the baseline flight condition having a forward velocity of 77.2 m/s (150 kts) and a value of 0.058 for C_T/σ. After the sudden change in collective pitch, the resulting steady flight condition, once all transients subside, is one of the high thrust conditions just discussed (C_T/σ = 0.08 or 0.085). Thus, these transient maneuvers can be considered to be simple simulations for various pullups. The last maneuver considered is just the opposite; the initial flight condition is the maximum thrust condition and the final flight condition, after a sudden decrease in collective pitch, is the baseline flight condition. For every one of these transient maneuvers, the active vibration controllers not only remain stable, but converge to an excellent control solution having about the same substantially reduced RTA vibration levels as those presented previously for the corresponding steady flight conditions.

1.0 Degree Increase in Collective Pitch

Figure 72 shows the response of all three baseline controllers to a 1.0 degree step increase in collective pitch. While this "step" increase in pitch is actually a very sharp ramp spanning one one-hundredth of a rotor revolution, it is effectively a step since it occurs during the dead time allowed for transient decay. In this figure, the time histories of 3 per rev cyclic pitch and the vibration performance index are shown to represent higher harmonic control commanded in response to the transient maneuver and overall vibration response, respectively.

The simulated maneuver is as follows. At rev 1, the baseline flight condition (V = 77.2 m/s, C_T/σ = 0.058) is initialized and numerical transients are allowed to settle out. At rev 4, the controllers are activated and allowed to reduce vibration at the steady baseline flight condition until the end of rev 18, where the controllers have essentially converged to a steady minimum level of vibration. Thus, the simulation and response shown for the first 18 revs are identical to that shown in Figs. 8(a) and 8(b) for the steady baseline flight condition. The 1.0 degree step increase in collective pitch occurs at the beginning of rev 19 after the controller has finished updating the control inputs based upon vibration measurements in rev 18. The

resulting final flight condition, after all transients die out, is the same as the high thrust flight condition with a value of 0.08 for C_T/σ discussed in the last section. After allowing transients to decay for 3/4 rev, the vibration response is harmonically analyzed for 1/4 rev, and this information is passed to the controller at the end of rev 19. At the beginning of rev 20, the controller makes its first update in control in response to the transient maneuver. Thus, one complete rev has passed without the controller being able to respond with an update in control. After rev 20, the controller actively reduces vibration just as it did for the steady flight conditions, and no further transients or maneuvers are encountered.

The solid line shown in this figure represents a simulation of open-loop higher harmonic control for the transient maneuver just described. As can be seen by the 3 per rev cyclic pitch, a steady level of higher harmonic control is implemented from the beginning of the simulation. These inputs are the same as those previously determined, by closed-loop active control at the steady baseline flight condition, to be the optimum set of higher harmonic control inputs for minimizing vibration at this flight condition. After the transient maneuver occurs, no change in control is made since the loop is open. Thus, any changes occurring in the performance index after rev 19 for the open-loop simulation are due to transients in the vibration response of the system to a step input. Note that the performance index, after all transients die out, will remain at about the level shown at rev 30, as will be shown later for an equal but much more gradual increase in thrust. The final performance index (0.063) attained by open-loop control is significantly lower than the baseline value for zero higher harmonic control at the new high thrust condition (0.319). However, it is substantially higher than that achieved by the active controller.

In contrast, the three baseline active vibration controllers have been very effective in not only converging to an excellent control solution that minimizes vibration at the new steady high thrust condition, but also in minimizing transient effects. The active controllers immediately begin updating control and reducing vibration at the beginning of rev 20. This is long before induced transients have died out, as can be seen by the open-loop response with no active control. While vibration increases significantly during the 1 rev dead time inherent to a 1 rev update, the peak value of the vibration performance index for closed-loop active control (0.043) is 60 percent and 32 percent lower than the peak and final values for open-loop control, respectively. This corresponds to reductions in peak values of vibration at all six RTA vibration sensors of between 33 and 45 percent. Furthermore, the peak value of the vibration performance index is over 85 percent lower than the baseline value of 0.319 that would occur at the final

high thrust condition if zero higher harmonic control was implemented. Finally, the peak value of the performance index is held to a value that is almost 60 percent lower than the initial value for the baseline flight condition with zero higher harmonic control, despite the fact that the final flight condition, even without transient effects, was shown in Fig. 61 to be a more severe flight condition. Thus, all three baseline controllers maintain vibration levels below that of the initial flight condition with no higher harmonic control despite transient effects and the increase in severity in the final flight condition.

Since the magnitudes of the vibration response and the performance index at and near peak response are based upon the harmonic analysis of vibration signals having significant transient effects, the calculated vibration levels and performance indices are most likely in error to some degree. However, it is felt that the trends just cited are indicative of the improvement in the vibration response to this transient maneuver that has been achieved by the active controllers. Thus, all three active controllers remain stable, immediately reduce vibration when allowed to update control, and minimize the transient effects to the point allowed by the 1 rev update. It may well be possible to reduce the peak vibration levels even further by shortening the time between updates, since the vibration controller could then start actively trying to reduce vibration sooner. However, the tradeoff is the increased transient effects on the harmonically analyzed vibration signals. As the time between updates is decreased, the errors in the harmonically analyzed vibration components will increase. Since the harmonic analysis of the vibration response is used in updating system identification and in calculating new control inputs, these errors can significantly degrade controller performance. At some point, the time allowed for transient decay and for sampling of data for harmonic analysis will become so short that worse control is obtained than that resulting from longer dead times. While 1 rev between updates resulted in excellent controller performance at all flight conditions studied, the effect of less time between updates should be studied further.

In addition to reducing the peak vibration response, all three baseline controllers converge very quickly and smoothly to a steady minimum vibration level in the RTA. Note that, as discussed previously, the minimum levels of vibration that have been achieved at the new high thrust condition are somewhat higher than those achieved at the initial moderate thrust condition, as indicated by the steady levels of J before and after the transient maneuver. The deterministic and cautious controllers exhibit very similar behavior during this transient maneuver and have very similar time histories for all three control inputs and all six RTA accelerations. Furthermore, both of these controllers reached almost identical levels of vibration in the RTA at convergence. These final levels of vibration are almost identical to those reached by the deterministic and cautious controllers at the equivalent steady

high thrust condition. Note that the reason that the final vibration performance index appears to be larger at convergence in Fig. 72 for the transient maneuver than in Fig. 65 for the same steady flight condition is the much smaller scale used in Fig. 65 to accommodate the large initial value for this high thrust condition with no higher harmonic control. The active controller never allows the vibration performance index to reach these levels, even during the transient. Figure 73 shows the final RTA vibration levels achieved by these two controllers and compares them to the vibration levels that would be present at the initial and final flight conditions in this transient maneuver if no higher harmonic control were implemented. Also shown in this figure is the final RTA vibration response achieved by the open-loop controller. The final control solutions commanded by these two controllers to achieve these excellent reductions in vibration are very similar to those shown in Fig. 62 for the deterministic controller when applied to the equivalent steady high thrust condition ($C_T/\sigma = 0.08$).

While the dual controller also achieves substantial reductions in vibration, it converges to a completely different solution as clearly shown in Fig. 72 for the 3 per rev cyclic pitch. The final RTA vibration levels are also slightly different from those shown in Fig. 73 for the deterministic and cautious controllers. While slightly lower vibration levels at the small lateral components are achieved, slightly higher levels result for the vertical components at the cross-beam and nose sensor locations. However, the resultant performance index is about the same. Although a different control solution is reached, the dual controller still commands amplitudes of control of less than 0.55 degrees for 3, 4, and 5 per rev.

1.0 Degree Ramp Increase in Collective Pitch

Figure 74 shows the response of both the baseline deterministic and cautious controllers to a transient maneuver that is very similar to the one just discussed. The initial flight condition is the baseline flight condition ($V = 77.2$ m/s, $C_T/\sigma = 0.058$), a total change in collective pitch of 1.0 degree is again initiated at the beginning of rev 19 after vibration at the initial flight condition has been substantially reduced, and the final flight condition is the same high thrust condition with a value of 0.08 for C_T/σ. However, in this simulation, the 1.0 degree change in collective pitch is implemented in ramp fashion with a fairly gradual rate of increase of 0.2 degree per rev. Thus, the transient maneuver requires 5 revs for completion and ends at rev 24.

Due to the rather gradual increase in collective pitch, transient effects in the open-loop controller response are not nearly as noticeable. The vibration performance index with open-loop control gradually and smoothly increases to about the same level as that present at rev 30 for the 1.0 degree step increase in collective pitch, and very little overshoot or oscillation occurs

in the performance index. While transients most likely are occurring in the vibration response, they are small enough that the harmonically analyzed components and, thus, the performance index appears to be changing very smoothly.

Since the active vibration controllers can now track changes in system parameters and update control during the maneuver to the new high thrust condition, transient vibrations are substantially improved over those observed during the step increase in thrust. The deterministic and cautious controllers, again, have very similar performance. At rev 20, which is the first control update after initiation of the transient, both controllers immediately begin reducing the steadily increasing vibration level. Even though the controllers still have the 1 rev of dead time during each rotor rev when thrust and, therefore, vibration is continually increasing, the controllers are able to reduce the peak value of the vibration performance index by 58 percent compared to the peak value achieved during the step increase in thrust. This is over 83 percent lower than the final value reached by the open-loop controller and almost 95 percent lower than the value of the vibration performance index when no higher harmonic control is implemented. In fact, the controllers are able to track these more gradual changes so well that they hold the peak vibration performance index to a value that is only slightly higher than the value for minimum vibration reached at convergence. After rev 24 when the collective pitch and rotor thrust have reached their final steady value, the controllers very quickly reduce vibration to the same minimum vibration levels reached at convergence during both the step increase in collective and the steady high thrust condition. Thus, these baseline active controllers, with no retuning for the transient maneuver, do an excellent job of tracking changes in flight condition and minimizing both transient and final vibration for a 40 percent increase in thrust over a 5 rev time span.

2.18 Degree Step Increase in Collective Pitch

Figure 75 shows the response of all three baseline controllers to a 2.18 degree step increase in collective pitch initiated at rev 19. This causes a 47 percent increase in rotor thrust in going from the initial baseline flight condition ($V = 77.2$ m/s, $C_T/\sigma = 0.058$) to the final maximum thrust flight condition ($V = 77.2$ m/s, $C_T/\sigma = 0.085$). Thus, this simulation is exactly the same as the 1.0 degree step increase except that the final flight condition is the maximum thrust condition. As discussed previously, this final flight condition is well into stall and has significantly higher vibration levels than the other high thrust condition with C_T/σ equal to 0.08. For this reason, the scale in Fig. 75 is much smaller than that in Fig. 72 in order to accommodate the large resulting peak values of the performance index and the higher values of required higher harmonic control at this severe final flight condition. Thus, the first 18 revs of these simulations at the same baseline flight condition appear quite different, but are identical.

Despite the much larger increases in vibration that occur at rev 19 for this step input, all three baseline controllers not only remain stable, but immediately start reducing vibration as soon as the 1 rev dead time is over. The peak values of the performance index with active control are about the same as that for the open-loop controller. This is due to the apparent lack of significant overshoot exhibited in the vibration response to the 2.18 degree step increase in collective pitch, as indicated by the open-loop response for the vibration performance index. This is quite different from the large overshoot that occurred for the 1.0 degree step. This phenomenon may be due to the combination of at least two effects. First, the significantly larger increase in vibration response for this step causes much larger transient effects in the time history of accelerations at each sensor location. This in turn causes large errors in the harmonic analysis. Thus, the values of vibration and the performance index at and near the peak are most likely in error to some degree. Second, the substantial increases in drag due to stall effects at the final flight condition may result in some aerodynamic damping of the vibration response to the step input.

After rev 20, the deterministic and cautious controllers achieve and maintain at least an 80 percent reduction in the performance index relative to peak in just 2 revs. They then quickly and smoothly reduce the vibration levels to the substantially reduced levels achieved during the equivalent steady maximum thrust condition, although slightly different final control solutions are commanded after the transient increase to this flight condition. Again, the behavior of the deterministic and cautious controllers is very similar for this rather severe transient maneuver.

While the dual controller also achieves an 80 percent reduction in the vibration performance index from its peak value in 2 revs, it cannot maintain this level of reduction until rev 29. Due to system probing, the dual controller exhibits more oscillatory behavior than the deterministic and cautious controllers; however, it eventually achieves about the same minimum vibration levels by rev 50.

2.18 Degree Ramp Increase in Collective Pitch

Figure 76 shows the response of all three baseline controllers, again with no change in tuning, to a transient maneuver that has the same initial and final flight conditions as the 2.18 degree step change in collective pitch just discussed. However, this same total change in collective pitch is obtained by a steady increase at a rate of 0.44 degree per rev for 5 revs. The transient maneuver is initiated at rev 19 and is completed at rev 24. Thus, this transient maneuver is very similar to the 1.0 degree ramp increase in collective pitch discussed above, but the rate of increase is over twice as large.

As expected, all three controllers do a much better job of reducing vibration than the open-loop controller for the first four revs of the maneuver since they are tracking system changes and updating control during each rev of the maneuver. Furthermore, during these four revs, the controllers have maintained significantly lower levels of vibration than the peak values experienced due to the step input. In fact, if the maneuver were to end after 4 revs of this ramp input and a total change in collective of 1.76 degrees rather than 2.18 degrees, all three controllers would have reduced the peak value of the performance index by almost 90 percent over that of the step response. However, the ramp continues, and the last 0.44 degree change in collective pitch is implemented between revs 23 and 24. The result is a fairly significant increase in the calculated performance index at rev 24, as indicated in Fig. 76. From there on, performance of each of the three controllers is completely different and fairly poor. Although the cautious and dual controllers eventually converge to excellent control solutions with the same minimal vibration levels achieved at the maximum thrust condition in steady flight, they have peak values of the performance index that are almost as large or larger than those for the closed-loop controller and those experienced for the 2.18 degree step increase in collective pitch. The deterministic controller performance is even worse. Although the peak shown for the vibration performance index is no higher, it appears to be starting to diverge after rev 30. However, there is no way of knowing whether convergence would eventually be achieved since the particular mix of control inputs that occurs at rev 33 causes numerical difficulties in the simulation that cause termination of the computer run.

Clearly, something occurs between revs 23 and 24 to initiate very poor controller performance. As will be discussed later, the performance of each of these controllers during this transient maneuver can be improved significantly with only slight retuning. Before proceeding with that discussion, it is appropriate here to try to explain why this maneuver causes such problems for the controllers.

To explain this, consider the transient maneuver shown in Fig. 77. During this maneuver, the same change in flight condition (e.g., total change of 2.18 degrees in collective pitch) from the baseline flight condition to the maximum thrust condition is implemented even more gradually with a steady rate of 0.218 degree per rev. Thus, 10 revs are required to complete the maneuver. As can be seen in Fig. 77, both the baseline deterministic and cautious controllers perform very well during this maneuver until the end of rev 28. At this point, 9 out of the 10 revs of the ramp input have been completed and a total change of 1.962 degrees has been made in collective pitch. The value of the performance index at this point is just as low as that noted above for

a total change of 1.76 degrees in collective pitch after 4 revs of the maneuver shown in Fig. 76. Thus, even though this point represents a much more severe flight condition, the active controllers have achieved the same low levels of vibration since they have had more time to track changes in system parameters, and smaller changes in collective pitch are made during controller dead times.

Simply put, the controllers have exhibited excellent performance until rev 28 even though most of the total change in collective has been made and a fairly severe flight condition is present. At this point, the last 0.218 degree increase in collective is implemented at the same rate to complete the maneuver at rev 29. Note that this fairly small change in collective pitch causes a fairly large increase in overall vibration. Furthermore, this change may actually be even larger due to transients and errors in the harmonic analysis. This is indicated by the very large change in vibration between revs 29 and 30 even though the maneuver has been completed. It does not appear that this further sudden increase, which occurs after the end of the maneuver, is precipitated by control changes since both the controllers implement changes in control on the order of 0.05 degree for all three control inputs just before this sudden increase in vibration. Thus, due to severe stall effects in the constant inflow model used, a very large increase in vibration occurs in the last 0.5 degree change in collective pitch. This has been verified by running two open-loop steady thrust conditions with no higher harmonic control. At the maximum collective pitch (11.0 degrees), which corresponds to what has been called the maximum or highest thrust condition, the thrust level actually decreases from that achieved with a collective pitch of 10.5 degrees. Furthermore, the vibration response, required rotor torque, rotor drag, and blade stresses all increase significantly in going from the 10.5 degree collective pitch to the 11.0 degree maximum collective pitch. Note, for reference purposes, that the baseline flight condition corresponds to a collective pitch of 8.82 degrees, and the other high thrust condition discussed previously (C_T/σ = 0.08) has a collective pitch of 9.82 degrees.

From the results presented in Fig. 77, it appears that a good part of these severe stall effects occur in the last 0.2 degree increase in collective (e.g., between 10.8 and 11.0 degrees). Thus, in Fig. 77, this sudden increase in vibration with corresponding changes in system parameters causes the controllers to respond with a large change in control which immediately brings vibration back down. However, somewhat oscillatory behavior occurs while the controllers identify the changes in system parameters. As can be seen in Fig. 77, both controllers eventually reach an excellent but completely different control solution that minimizes vibration at the steady final flight condition.

Based on this discussion, it is clear that what is happening in Fig. 76 is the result of severe stall effects as predicted by the constant inflow model. While a more appropriate variable inflow model would most likely result in different vibration response, this simulation provides a good test of controller performance with severe changes occurring very suddenly. In Fig. 76, the controllers, as already pointed out, perform well for the first 4 revs of the transient maneuver. Then, the last rev causes severe problems for the controllers. Note that in this last rev of the maneuver the change in collective is 0.44 degree in ramp fashion to the maximum collective pitch of 11.0 degrees. As just noted, this is the region having the severe stall effects. As further penetration of the stall regime occurs near the completion of this maneuver, a large sudden increase in vibration occurs along with significant changes in system parameters. As discussed in Appendix A, the T-matrix relationship between RTA vibration and higher harmonic control inputs is most sensitive to changes in flight condition and control inputs at the high thrust flight conditions and large control inputs. Thus, it is not surprising that a large increase in the performance index occurs at the end of the transient maneuver since essentially a step change in vibration response occurs during the 1 rev dead time for the controllers. It is actually satisfying that the cautious and dual controllers remain stable and are able to converge fairly quickly to a minimum vibration solution. As discussed in the next section, the deterministic controller can also be tuned to allow convergence to be achieved.

Retuning of Controller Parameters for Improved Performance

While the transient performance of the controllers shown in Fig. 76 are fairly poor compared to the excellent results achieved for the other transient maneuvers discussed so far, it should be noted that all three controllers, assuming the deterministic controller does not go unstable but eventually converges, maintain a level of vibration that is about the same or less than that resulting from the open-loop simulation. Furthermore, these levels are only momentary peaks that occur due to transient effects during controller dead time and are immediately reduced when updates in control are implemented. Also note that peak vibration levels are well below those that would occur if no higher harmonic control were implemented. There are two possible ways to try to improve controller performance for this maneuver simulation. One that should be explored is to decrease the time between updates. If transient effects do not degrade the accuracy of the harmonic analysis too severely, more updates during the maneuver should allow better system identification and faster reduction of vibration. The second way is to retune the controllers to better match the flight condition.

It may be possible to improve controller performance significantly by retuning either the Kalman filter identifier, the minimum variance control algorithm, or both. As discussed above and in Appendix A, fairly large and

rapid changes in system parameters can occur as the rotor enters the stall regime. For example, the sensitivities of RTA vibration response to both changes in flight condition and changes in higher harmonic control inputs are significantly different in this region than at more moderate flight conditions. Furthermore, these sensitivities are dependent upon the mix of 3, 4, and 5 per rev control inputs. Thus, it is likely that a different tuning than that determined at the fairly linear and moderate baseline flight condition will be required to adequately track the type of changes in system parameters that are encountered in the stall regime. Retuning of the Kalman filter identifier for this transient maneuver was not explored in this investigation.

While the Kalman filter identifier may not be optimally matched to this transient maneuver or the stall regime, it may be that the identifer can provide adequate identification for good controller performance if the minimum variance control algorithm is slightly retuned. It is likely that the sudden changes in system parameters that occur when first penetrating the stall regime are much worse than those that occur due to changes in control inputs or further slight changes in flight condition within the stall regime. In addition, the large sudden increases in vibration that occur when entering stall are accompanied by large transients. Once the rotor has penetrated the stall regime and transients have subsided, the identifier may be very capable of providing satisfactory identification. Thus, if the minimum variance algorithm is tuned to maintain good short term control while the identifier is adapting to the sudden changes in system parameters, it may be possible to achieve good overall performance without retuning the Kalman filter identifier. Retuning of the minimum variance control algorithm for improved controller performance at this transient maneuver (0.44 deg/rev ramp increase in collective pitch) has been explored briefly in this investigation. Figures 78 through 80 demonstrate that controller performance can be effected and improved significantly during this maneuver by slightly retuning the minimum variance control algorithm.

One way to improve controller performance for all three controller types is to ensure stability by increasing internal rate-limiting (e.g., increase $W_{\Delta\theta}$). This would be particularly appropriate for the deterministic controller for this simulation. The increased rate-limiting would prevent the controller from making large sudden changes in control in response to the large sudden increase in vibration that occurs at the very end of the transient maneuver. This allows the transients to subside and gives the identifier the chance to adapt to variations in system parameters, before large control updates cause further changes to be tracked. Unfortunately, since $W_{\Delta\theta}$ is held constant, this will cause much slower changes in control and much slower reductions in vibration everywhere else in the flight regime. Thus, only slightly better performance than the open-loop controller is likely to be achieved in the early part of the maneuver, and convergence would most likely be very slow

after the maneuver is completed. However, it may be possible to achieve good overall performance by developing a method of varying $W_{\Delta\theta}$ with flight condition or vibration response. This approach was not pursued in this investigation.

Figure 78 shows the performance of two deterministic controllers in addition to the open-loop controller and baseline deterministic controller shown previously in Fig. 76. Other than the slight differences in tuning of $W_{\Delta\theta}$ and W_{θ}, these controllers have exactly the same configuration as the baseline deterministic controller. The first new deterministic controller shown in Fig. 78 maintains the same $W_{\Delta\theta}$ as the baseline but also implements a weighting on total control (W_{θ} = 100). In so doing, the controller prevents large control inputs from being commanded in response to the large sudden increase in vibration at rev 25, but does not slow down the controller elsewhere. This allows the controller to quickly reduce vibration after the maneuver is completed, but does not help in reducing peak response. Furthermore, the fairly large value of W_{θ} used does not allow the controller to reduce vibration quite as much at convergence as other controllers.

The second new deterministic controller shown in Fig. 78 uses a smaller value of $W_{\Delta\theta}$ than the baseline controller for reduced rate-limiting and no total θ limiting. This allows the controller to make somewhat larger changes in control early in the maneuver when system identification is still good. In so doing, slightly larger reductions in vibration are achieved in the first 4 revs of the ramp increase in collective pitch. Furthermore, these larger changes in control provide more information to the identifier which gives it the potential of better identifying changes in system parameters in the early part of the maneuver. The identifier is better able to adapt to these sudden changes in system parameters due to penetration of the stall regime if system identification is already very good when they occur. In any case, this controller not only converges quickly to substantially reduced vibration levels after the maneuver is completed, but also substantially reduces the peak. Clearly, the price paid for this excellent performance is the very large control inputs commanded and their inherent detrimental effects on other criteria. Furthermore, using this reduced rate-limiting in practice to improve controller performance for a fairly severe transient maneuver is somewhat risky unless additional means are used to ensure stability (e.g., total θ limiting).

Figure 79 shows that the same type of reduction in limiting on control inputs via a smaller λ also provides substantially improved performance in the

cautious controller. Again, the price is large control inputs. Note that this controller converges to steady control inputs.

Figure 80 shows the effect of increasing system probing in the dual controller during this maneuver by eliminating all limiting. Amazingly enough, the unlimited dual controller provides the best performance of all three controllers during this transient maneuver. While it takes slightly longer to reach convergence in J due to significant system probing still occurring at rev 50, it maintains the same reduced peak vibration response and also maintains all three control inputs to magnitudes on the order of 1.0 degree or less. It appears that, if the problems due to initial system probing (which obviously cause totally unacceptable performance at the beginning of this simulation) can be solved, then the unlimited dual controller may have the potential for better performance during transients than the deterministic and cautious controllers. However, using a totally unlimited dual controller is too risky in practice. Thus, it is necessary to see if the same type of performance can be achieved with a practical external limit placed on $\Delta\theta$. It may be that practical rate-limits due to hardware limitations will inhibit the inherent system probing to the extent that the dual controller cannot work successfully.

2.18 Degree Step Decrease in Collective Pitch

Figure 81 shows the performance of the baseline cautious controller during a transient maneuver in which a 2.18 degree decrease in collective pitch is implemented in step fashion at rev 19. The result is a change in the flight condition from the initial maximum thrust condition (V = 77.2 m/s, C_T/σ = 0.085) to the baseline moderate thrust flight condition (V = 77.2 m/s, C_T/σ = 0.058). Clearly, the increase in vibration that occurs during the 1 rev dead time is immediately reduced after the controller is able to respond. Furthermore, the controller very quickly converges to almost exactly the same vibration levels in the RTA as it did for the baseline steady flight condition. It is interesting to note that the controller has converged to a completely steady set of control inputs, whereas it had a tendency to drift at the baseline flight condition. The important point is that the controller is able to determine that the increased vibration occurring at rev 20 requires a decrease in the magnitude of the control inputs at the final baseline flight condition. As demonstrated in the discussion of baseline controller results at the steady baseline flight condition, the controller could have achieved the same reduced vibration levels by finding an appropriate mix of large inputs.

Local System Model

Figure 82 compares the performance of a local deterministic controller to that of the baseline deterministic controller, which is based on the global system model, during a transient maneuver. The transient maneuver is the 2.18 degree step increase in collective pitch which results in a change in the flight condition from the baseline flight condition to the maximum thrust condition, which is in stall. The configuration and tuning of the local model is exactly the same as that of the baseline controller with global model. Clearly, the baseline deterministic controller with global model provides much better performance than that of the local model. The local model is much more oscillatory and requires quite a bit longer to converge. The same can be seen to be true for the local and global cautious controllers shown in Fig. 83 for the same transient maneuver. The global model shown in this figure is the baseline cautious controller, and the local model, again, has the same configuration and tuning. Except for the slightly more oscillatory behavior at the maximum thrust condition, this is the first indication of a difference in behavior between the local and global system models. It is anticipated that these local controllers can be retuned to achieve basically the same performance as the global baseline controllers. However, this may indicate that the local model is somewhat more sensitive to tuning at different flight conditions or perhaps more sensitive to inaccurate vibration measurements due to large transient effects. Perhaps, the local controllers have not been optimally tuned and this did not make a difference at more moderate flight conditions. The only way to answer some of these questions and adequately compare the local and global models is to optimally tune both a local and global controller of similar configuration (e.g., deterministic with internal rate limiting) at a fairly severe but representative flight condition, and then subject these optimally tuned controllers to several fairly severe flight conditions.

Alternate Controller Configurations

Many alternate controller configurations have been investigated in addition to those already presented. Among those considered are several that calculate updates in control based on fixed system hub vibration rather than RTA response and several that allow 2 revs to elapse between control updates rather than 1 rev. The effect of these modifications will be briefly discussed below.

Effect of Hub Sensors

In all the results presented above, vibration was actively controlled at only the RTA sensor locations listed in Table 1 and shown schematically in

Fig. 3. Since these sensors are placed throughout the RTA and measure components of vibration in three orthogonal directions, it is expected that the excellent reductions achieved are also indicative of significant reductions elsewhere in the RTA. However, the reductions achieved at these particular locations may be partially due to modal cancellations occurring in the RTA, which might result in somewhat smaller reductions elsewhere. Thus, it may be possible to attain similar vibration levels at these locations as well as better overall reductions throughout the fuselage by actively controlling the response at remote sensors closer to the source of vibratory excitation in the rotor.

This approach has been implemented at the baseline flight condition by using a deterministic controller to actively control vibration at sensors near the hub in the fixed system. The controller configuration is the same as that of the baseline deterministic controller except that the hub sensors shown in Table 1 are used instead of the RTA sensors. The value of the $W_{\Delta\theta}$ has also been decreased to reflect the significant differences in magnitude of vibration response at the hub and the RTA sensors. All six hub sensors are equally weighted and the procedure followed in the simulation is the same as that described previously. The rationale for this approach is that using higher harmonic control to achieve decreased rotor hub excitations will also result in reduced vibration throughout the RTA. If such an approach is successful, it may be easier to incorporate the adaptive controller into new aircraft since there would be no need to determine critical locations in the fuselage or an appropriate weighting matrix for the many different fuselage sensors.

Figure 84 shows the effect of using hub sensors rather than local sensors in the RTA representing the fuselage. This figure compares the hub and RTA vibration response when the controller is actively controlling either local sensors in the RTA or remote sensors at the hub (fixed system). The resulting vibration levels are compared to the baseline response that occurs when no higher harmonic control is applied. Clearly, the controller is able to reduce overall vibration both at the hub and in the RTA when either set of sensors are used; however, larger overall reductions may be achieved at the sensors being actively controlled than at those simply being monitored. For example, the controller achieves larger overall reductions in vibration at the hub sensor locations when actively controlling these sensors. While one might expect reduced vibration in the RTA as a result of the decreased forcing at the hub, it is readily seen that vibration levels in the RTA are smaller when the RTA sensors are used. Despite the higher vibration levels at the hub, the controller achieves larger reductions in the RTA (when using RTA sensors); which are evidently due to proper phasing of HHC inputs and hub forces with modal cancellation occurring in the fuselage.

These results indicate that the remote hub sensors are probably not a viable alternative to local sensors placed at points of interest in the fuselage, unless the use of equally weighted hub vibrations results in acceptable levels of vibration at all critical points in the fuselage of a particular aircraft. It would probably be easier to tune the weighting matrix directly for a set of local sensors rather than that of the hub sensors in order to determine the best tradeoff in vibration that can be achieved at each of the critical fuselage locations. However, the use of hub sensors can be potentially useful when used in conjunction with local vibration sensors. Since the response of the helicopter to higher harmonic control inputs is nonlinear there is a greater possibility of reaching the optimum solution rather than a local solution if both the amplitude and the phase of the fuselage modal response are controlled. This might be accomplished by including both hub and fuselage sensors (appropriately weighted) in the performance index. The hub sensors work to reduce the amplitude of the fuselage excitation without regard to phase, and the fuselage sensors work to reduce the fuselage response by vectoral cancellation with emphasis primarily on phase. This approach could potentially lead to a vectoral cancellation of small numbers as opposed to a vectoral cancellation of large numbers (fuselage sensors) or uncontrolled response to minimized forcing (hub sensors). If both hub sensors and local fuselage sensors are included in the performance index, this type of control can be implemented and could result in lower hub and fuselage vibrations.

Effect of 2 Rev Update

All the results presented so far have been based upon controller configurations allowing one complete rotor revolution to pass before updating control inputs. As shown in Fig. 5, this allows 3/4 rev for transients to decay and 1/4 rev to perform the harmonic analysis of vibration response. As shown in Fig. 6, allowing only 3/4 rev for transient decay results in a certain amount of error in the harmonically analyzed vibration response supplied to the controller. The errors involved clearly will depend upon the nature of the $\Delta\theta$ input, the flight condition, the initial vibration level, and the sensitivity of a particular vibration component to higher harmonic control. Regardless, the accuracy of information supplied to the controller will be increased by allowing more time for transients to subside before harmonic analysis of the vibration response is performed, unless of course the flight condition changes during this controller dead time. For such a case, changes in vibration will not only be due to variations in control, but to new flight conditions and accompanying transients. Since the accuracy of measured response directly impacts the identification of system parameters as well as the calculation of updated control inputs, the time allowed between updates is critical to overall controller performance.

The effect of increasing time between updates to 2 revs is shown in Figs. 85 through 88. Each of these figures compares the transient response of two different controller configurations at a particular flight condition. The only difference in the configurations in any one of these figures is the use of 1 or 2 revs between controller updates. For a 2 rev update, 1-3/4 revs are allowed for transient decay and 1/4 rev is again used for harmonic analysis. Both a variety of controllers and a variety of flight conditions are represented.

Figure 85 compares the time histories of the performance index and a representative control input amplitude (3/rev cyclic pitch) for deterministic controllers operating at the baseline (150 kt) flight condition. The controller configuration used and the transient response shown for a 1-rev update is exactly the same as that for the local deterministic controller with external rate-limiting ($\Delta\theta_{max}$ = 0.2 deg/rev) shown in Fig. 23. The configuration for a 2-rev update is also the same except for the increased time for transient decay, which clearly has a significant effect upon controller performance. The use of 2 revs between updates smoothes the time histories of both the performance index and the control inputs by allowing more accurate response measurements to be sent to the controller; however, the erratic behavior inherent to external limiting is still apparent at this fairly mild flight condition. Furthermore, the overall performance of the baseline deterministic controller is still significantly better even with a 1-rev update, since larger reductions in vibration are more rapidly achieved with smaller control inputs.

One of the reasons for the significant improvements in performance for this externally rate-limited controller is the erratic behavior and rather large changes in control (on the order of 0.2 degree) still being implemented at rev 30. Figure 86 shows the effect of a 2-rev update on the performance of a much better behaved controller at the same baseline flight condition. Both transient responses shown are for the internally rate-limited baseline deterministic controller having either a 1-rev or a 2-rev update. Due to the small inputs required to minimize vibration and a fairly accurate initial T-matrix, there is little difference in the response for these two configurations at this flight condition. Due to the moderate first step in control inputs, some smoothing of the initial time histories results from the increased time between updates, but the difference is not significant enough to warrant using longer than a 1 rev update for this controller and flight condition.

Figure 87 compares the time histories for the baseline deterministic controller having 1 and 2-rev updates at the maximum thrust condition (C_T/σ=0.085). Substantial differences do exist for this case, especially in the 3/rev cyclic pitch amplitude time histories. The controller converges to

a steady set of control inputs much more smoothly and quickly with 2 revs between updates. This is most likely due to both the large initial change in control inputs, which result in a much larger transient response in the RTA than that caused by comparatively small changes at the baseline condition, and the errors in the initial estimate of the T-matrix, which is the same as that determined and used at the baseline flight condition. By allowing more time for the transient response to die out, more accurate vibration measurements are supplied to the controller each rev for making updates in the T-matrix and calculating new control inputs. Note that the oscillatory behavior in the control inputs due to these effects tend to cancel, and only slightly better performance is achieved in terms of the smoothness and rapidity of convergence of the performance index. Furthermore, both configurations appear to be converging to about the same set of control inputs.

If the controller had been retuned with increased weighting on $\Delta\theta$ in the performance index ($W_{\Delta\theta}$) to reflect increased vibration levels at the new flight condition, smaller initial changes in control would be implemented, and the resultant transient response of the controller would most likely be much smoother. Thus, after retuning the controller for this flight condition, it is expected that only minor differences would again be apparent for the baseline deterministic controller having 1 or 2-rev updates. In practical applications, the controller would not be initialized at such a severe flight condition. Rather, the controller would probably be initialized and activated at a much milder flight condition, perhaps in hover, and allowed to track changes in system parameters and gradually implement larger control inputs as more severe flight conditions are encountered.

While a 2 rev update results in slight improvements in overall controller performance at steady flight conditions, a 1 rev update allows the controller to reduce vibration much more quickly during transient maneuvers, as shown in Fig. 88. Since fewer updates are made during the maneuver shown in Fig. 88 (a total change of 2.18 degrees in cyclic pitch made steadily over 5 revs starting at rev 19), the cautious controller takes longer to reduce vibration. The additional delay in updating control inputs could cause further problems (including the possibility of instability) during extended maneuvers.

As might be expected, the time allowed between updates results in a tradeoff in the ability to smoothly implement control inputs and reduce vibration and the ability to handle transient maneuvers. Since the results of the current investigation indicate that a 1-rev update does not significantly compromise controller performance during steady flight conditions and can significantly improve performance during maneuvers, it appears to give a viable compromise between minimizing errors due to transient vibration effects and minimizing the time between updates for transient maneuvers. However, as previously indicated, the effect of using less than 1 rev between updates should be considered in the future, especially during extended maneuvers.

CONCLUSIONS

A Real-Time Self-Adaptive (RTSA) active vibration controller previously developed and studied at the United Technologies Research Center has been used as the framework in developing a computerized generic controller incorporating a set of improved algorithms. These refined algorithms allow the capability to define many different configurations by selecting one of three different controller types (deterministic, cautious, and dual), one of two system models (local and global), and one or more of several different methods of applying limits on control inputs (external and/or internal limiting on higher harmonic pitch amplitude and rate). The initial RTSA controller configuration was based upon a deterministic controller with local system model and external rate-limiting. A baseline configuration has been defined for each of the three controller types. All three baseline controllers are based on the global system model and tuned for best effectiveness at a high speed (77.2 m/s, 150 kt) operating/flight condition. The baseline deterministic and dual controllers have internal and external rate-limiting respectively. After proper tuning, each of these baseline configurations significantly improves overall controller performance and effectiveness in reducing helicopter vibration compared to the initial RTSA controller. The following are the conclusions from this analytical evaluation study.

- All three baseline controllers provide more effective vibration reduction and converge more quickly and smoothly with much smaller control inputs than the initial RTSA controller.

At the high speed flight condition (77.2 m/s, 150 kt) for the H-34 rotor, all three controllers achieved nearly the same solutions with 3, 4, and 5 per rev control inputs on the order of 0.3 degrees, and reductions in vibration on the order of 75 to 95 percent at all significant vibration sensor locations throughout the wind tunnel Rotor Test Apparatus (RTA) simulating the fuselage.

- The baseline active controllers are effective at a wide range of steady flight conditions of different severities. No distinct advantage in terms of controller performance and effectiveness has been identified for any of the three controller types at the flight conditions considered in this investigation.

Excellent overall performance has been achieved throughout a range of forward velocities from a moderate speed (57.6 m/s, 112 kt) condition to the baseline high speed (77.2 m/s, 150 kt) condition. Excellent overall performance has also been achieved at two high speed, high thrust flight conditions with C_T/σ equal to 0.08 and 0.085 and forward velocities of 77.2 m/s (150 kts). These two high thrust conditions are particularly severe flight

conditions. According to the constant inflow model used, both are at or well into stall even before higher harmonic control is implemented. Reduction in vibration on the order of 75 to 95 percent is achieved at all significant sensor locations throughout the RTA for all steady flight conditions considered. These reductions in vibration are achieved at all flight conditions with amplitudes of 3, 4, and 5 per rev control on the order of 1.0 degree or less. The required amplitudes of control generally decrease with decrease in forward velocity or rotor thrust.

- In addition to steady flight conditions, all three controllers exhibited good performance characteristics for the transient maneuvers investigated.

For the transient maneuvers investigated, involving sudden changes in thrust due to step or ramp changes in collective pitch, the controllers remained stable, maintained peak vibration response well below the levels that would be present without higher harmonic control, and quickly reduced vibration to the same levels achieved at steady flight conditions. Retuning of the controllers was required to achieve satisfactory performance during only one transient maneuver that involves a change in thrust from the baseline high speed (minimum thrust) flight condition to the maximum thrust condition. Due to stall effects at the end of this maneuver, controller performance without retuning was somewhat less than satisfactory. Retuning of the controllers resulted in excellent performance in terms of vibration reduction; however, higher control inputs were commanded.

- All three controllers are very adaptable as demonstrated by their excellent performance at a wide variety of flight conditions.

These controllers have been initialized at all flight conditions with the same initial T-matrix that was determined by open-loop perturbation about a zero higher harmonic control point at the baseline high speed flight condition. Since the maximum thrust condition had a significantly different T-matrix due to stall effects predicted using constant inflow, the controllers had to adapt to errors in the initial T-matrix as well as changes in sensitivity resulting from updates in control inputs. For all steady flight conditions studied, the controllers have been able to adequately identify and update changes in the T-matrix in order to command a set of control inputs that substantially reduce vibration. Furthermore, the excellent performance of these controllers at all steady flight conditions has been achieved without any retuning of the baseline configurations, although there are some indications that overall performance might be improved somewhat by slightly retuning the controllers.

- Significant nonlinear and interharmonic coupling effects can occur at the more extreme conditions.

Results from a separate open-loop study of vibration response to higher harmonic control show that significant nonlinear and interharmonic coupling effects occur at the maximum thrust condition. While vibration response at this flight condition is only moderately nonlinear for changes of any given control input about an otherwise fixed control point, nonlinear coupling effects are significant. That is, the linearized transfer matrix (T-matrix) relating RTA vibration response to higher harmonic control inputs is highly dependent upon the mix of 3, 4, and 5 per rev inputs. Since the minimum variance control solution is directly dependent upon the T-matrix, the controller must adequately adapt to these changes in sensitivity before satisfactory controller performance can be achieved.

- Higher harmonic control can have significant detrimental effects on rotor blade stresses.

Significant increases in rotor blade stresses have been noted at all flight conditions investigated and will have to be accounted for in any proof-of-concept wind tunnel or flight test to demonstrate the higher harmonic control concept. The torsion moment is particularly sensitive to higher harmonic control. These increases in blade stresses are due in part to the significant interharmonic coupling of blade response noted in the open-loop study.

- Significant detrimental effects of higher harmonic control on rotor performance were predicted for the more extreme flight conditions.

Performance effects are insignificant at moderate velocities (e.g., 112 to 130 kt), but tend to increase with increase in velocity and/or rotor thrust. A five percent increase in required torque was noted for the baseline (150 kt) flight condition. Larger effects have been noted at the high thrust conditions. While these results are approximate due to the constant inflow model used, they do point out the potential for rotor performance changes with higher harmonic control.

- Essentially the same vibration reductions can be achieved with a multitude of significantly different control solutions having differing effects on blade stresses and rotor performance.

Multiple control solutions (different levels and mixes of harmonics of control) are possible for achieving low vibration. The detrimental effects on rotor blade stresses and rotor performance tend to increase with increasing magnitude of higher harmonic control inputs, and can be reduced by minimizing vibration with the smallest inputs possible. Use of internal limiting has

been shown to be very effective in doing this. At least one solution was found at the maximum thrust, maximum vibration condition that had nearly the same stresses as those without higher harmonic control. These results indicate that it may be possible to guide the controller to better solutions, by adding appropriately weighted terms to the performance index, that effectively reduce vibration, but have minimal effects on other criteria (e.g., blade stresses and rotor performance).

- Global and local system models result in similar controller performance at steady flight conditions.

It has been found in this investigation that the performance of all three controller types at the baseline and maximum thrust flight conditions is very similar for both the local and global system models when the same overall configuration is used (e.g., controller type, method of limiting) and similar tuning of internal parameters is specified (e.g., P_o, Q, R, $W_{\Delta\theta}$, $\Delta\theta_{max}$). Significant differences in controller performance for the local model have been noted only during the transient maneuvers. Controllers based on the local system model were generally less effective without retuning during transient maneuvers than those based on the global model. While it is anticipated that retuning would result in equally effective performance, these results for transient maneuvers may indicate that the local model is more sensitive to tuning or to errors in system measurements due to transient effects.

- All three active controllers (deterministic, cautious, and dual) are very effective in reducing helicopter vibration. The baseline deterministic and cautious controllers exhibit very similar performance characteristics at most flight conditions. The behavior of the dual controller is somewhat different.

The baseline deterministic and cautious controllers have been found to be rather insensitive to less than optimum tuning. On the other hand, the dual controller, while equally effective in reducing vibration, tends to have slightly poorer short term control and somewhat more oscillatory behavior due to system probing. In addition, the dual controller is quite a bit more sensitive to the tuning of its internal parameters; however, once it was tuned at the baseline flight condition, the dual controller did not require any retuning at most other flight conditions.

RECOMMENDATIONS

Based upon the results presented, several areas requiring further attention have been identified and the following recommendations are made.

- It is recommended that further study of the controllers be conducted at more severe flight simulations.

The results of this investigation have proven the baseline controllers to be very effective at the flight conditions considered. The next logical step is evaluation at many different flight conditions in order to fully explore controller capabilities and limitations. Due to the scope and nature of the current investigation, in which many different configurations and alternative modifications were explored for their potential for improving overall controller performance, only a limited number of simplified flight simulations were made to evaluate the performance of even the best configurations. Furthermore, the computational efficiency required by the large number of computer cases necessitated the use of constant inflow and quasi-steady aerodynamics in the aeroelastic analysis. Thus, it is recommended that further study be conducted at several additional flight simulations. Representative flight conditions should be selected to fully test selected controllers throughout the flight envelope using appropriate aerodynamic models to represent the actual flight conditions as realistically as practical. Variable inflow and unsteady airfoil data should be used in appropriate flight conditions to fully evaluate the effect of higher harmonic control on vibration, rotor blade stresses, and rotor performance. In addition to several low and high velocity and high thrust steady flight conditions, a few simulations should be developed to test controller performance during more extensive transient maneuvers. One of the objectives of this study should be to determine the need for retuning the controller at various flight conditions and maneuvers. If significant retuning is required, it may be necessary to develop some method for varying parameters such as $W_{\Delta\theta}$ to match the flight condition. During the course of this study, the use of more than 1 update per rev should be explored. While it is recognized that such a study requires the number of controller configurations to be held to a minimum, it is recommended that dual controller configurations be included, since the results of the current investigation did give some indication that dual controllers may have the potential for providing better controller performance during extended transient maneuvers. Methods for improving initial start up response should be explored (e.g., variable λ and $\Delta\theta_{max}$). A comparison of controllers at more extensive flight simulations should further answer the question of whether the dual controller concept should be developed. The additional "hands-on" experience gained through such a study will prove useful in tuning the controller for maximum effectiveness and should increase the probability of a successful proof-of-concept wind tunnel test.

- Results of this investigation do not indicate a distinct advantage for any of the three controller types. If the baseline deterministic controller can be shown to have good performance at more extensive, rapidly varying, transient maneuvers, it is recommended that the deterministic controller be selected for final development for a proof-of-concept wind tunnel test.

The deterministic controller is at least as effective in reducing vibration as both the cautious and dual controllers and provides as good or better short term control. Furthermore, the deterministic control configuration is based upon a simpler algorithm that is somewhat easier to tune than those for the cautious and dual controllers. The variables used to tune the deterministic minimum variance control algorithm (e.g., $W_{\Delta\theta}$ and W_{θ}) have some basis in real world hardware that can be used as a guide in their selection for optimum controller performance in practical control systems; whereas, both the cautious and dual controllers contain covariance matrices from the Kalman filter identification algorithm in their minimum variance control algorithms. Not only are these covariances unrelated to pitch control hardware functions, but they usually have to be selected by trial and error in an attempt to optimize the Kalman filter identifier as well. This coupling between the tuning of the minimum variance control algorithm and the Kalman filter identification algorithm is accounted for with the stochastic control constant λ, which is completely lacking in practical significance as well. Furthermore, this coupling can cause the cautious and dual controllers to be harder to tune initially when adapting the controllers to different aircraft. If it is found that retuning of the controllers are required for satisfactory behavior during practical flight maneuvers or more severe steady flight conditions, it may be simpler to develop an algorithm to accomplish this when using the deterministic controller since it does not have this direct coupling between algorithms. Finally, the deterministic controller has proven to be a very stable controller configuration whereas, the dual controller demonstrated a tendency for instability when non-optimally tuned. For these reasons, the cautious and dual controllers would have to exhibit significantly better performance to warrant their selection over the deterministic controller with internal limiting.

- It is recommended that a study be made into the effects of each separate control input as well as the mix of 3, 4, and 5 per rev control on controller performance, blade stresses, rotor performance, system nonlinearities, etc.

The objective of such a study should be to determine if better overall controller performance can be achieved by weighting control inputs unequally. Results of the current study show that certain combinations of control inputs result in various improvements in controller performance, blade stresses,

and/or controller performance at different flight conditions. Some important considerations that should be addressed are 1) sensitivity of blade stresses and rotor performance to each individual control input, 2) nonlinearities associated with each input, and 3) controller performance and effectiveness in reducing vibration when various control inputs are inhibited or eliminated. While the open-loop investigation of nonlinear and interharmonic coupling effects addresses some of these considerations at two particular flight conditions, further study at several different flight conditions is necessary to draw any conclusions on whether equal weighting on 3, 4, and 5 per rev control is indeed the best set of control inputs for optimum overall controller performance in terms of vibration reduction, blade stresses, and rotor performance. Both of the above studies should prove useful to the practical application of active vibration control by providing further insight into the fundamental characteristics of higher harmonic control.

- It is recommended that a study be made into the use of appropriate terms in the performance index to guide the controller to better solutions in terms of blade stresses and rotor performance.

Some of the important considerations in such a study should be 1) the feasibility of such an approach, 2) practical parameters that can be measured readily in a production aircraft, 3) the magnitude of realizable improvements that can be expected in blade stresses and rotor performance, 4) the effect on vibration reduction, 5) the effect on controller performance, 6) the characteristics of the low stress and/or improved rotor performance solutions, 7) the relative weightings required on the vibration parameters, control inputs, blade stresses, and rotor performance parameters, and 8) sensitivity of required weighting matrices to change in flight condition.

For this approach to be successful for blade stresses, it may be necessary to include parameters from the rotating system (e.g., blade stresses or rotating blade root shears) in the performance index to ensure that reductions in vibration are achieved via properly phased higher harmonic control inputs and modal cancellations of small blade loads rather than large loads. While it is not desirable to have to monitor blade stresses (or any other parameter in the rotating system) on a production helicopter, such an approach in future analytical and/or wind tunnel investigations will provide valuable information on the higher harmonic control phenomenon and its effect on blade stresses. Based on the results of such an investigation, it may be possible to define parameters in the fixed system that can be used to predict blade stresses or other parameters in the rotating system via a state estimator, rather than through direct measurement. Such an approach may then be applicable to a production aircraft.

REFERENCES

1. Taylor, R. B.: Helicopter Vibration Reduction by Rotor Blade Modal Shaping. Proceedings of the American Helicopter Society 38th Annual Forum, Anaheim, CA, May 1982.

2. Blackwell, R. H.: Blade Design for Reduced Helicopter Vibration. Journal of the American Helicopter Society, Vol. 28, No. 3, July 1983.

3. Bartlett, F. D.: Flight Vibration Optimization Via Conformal Mapping. Journal of the American Helicopter Society, Vol. 28, No. 1, January 1983.

4. Johnson, W.: Self-Tuning Regulators for Multicyclic Control of Helicopter Vibration. NASA Technical Paper 1996, March 1982.

5. Wood, E. R.; Powers, R. W.; and Hammond, C. E.: On Methods for Application of Harmonic Control. Fourth European Rotorcraft and Powered-Lift Aircraft Forum, September 1978.

6. McHugh, F. J.; and Shaw, J.: Benefits of Higher Harmonic Blade Pitch: Vibration Reduction, Blade Load Reduction, and Performance Improvement. Proceedings of the American Helicopter Society Mideast Region Symposium on Rotor Technology, August 1976.

7. Sissingh, G. J.; and Donham, R. E.: Hingeless Rotor Theory and Experiment on Vibration Reduction by Periodic Variation of Conventional Controls. NASA SP352, February 1974.

8. Shaw, J.; and Albion, N.: Active Control of the Helicopter Rotor for Vibration Reduction. Paper No. 80-68, 36th Annual Forum of the American Helicopter Society, Washington, D.C., 1980.

9. Taylor, R. B.; Farrar, F. A.; and Miao, W.: An Active Control System for Helicopter Vibration Control by Higher Harmonic Pitch, presented at the AIAA/ASME/ASCE/AHS 21st Structures, Structural Dynamics Conference, AIAA Paper 80-0672, May 1980.

10. Taylor, R. B.; Zwicke, P. E.; Gold, P.; Miao, W.: Analytical Design and Evaluation of an Active Control System for Helicopter Vibration Reduction and Gust Response Alleviation. NASA CR-152377, July 1980.

11. Hammond, C. E.: Wind Tunnel Results Showing Rotor Vibratory Loads Reduction Using Higher Harmonic Blade Pitch. Journal of the American Helicopter Society, Vol. 28, No. 1, January 1983.

12. Molusis, J. A.; Hammond, C. E.; Cline, J. H.: A Unified Approach to the Optimal Design of Adaptive and Gain Scheduled Controllers to Achieve Minimum Helicopter Rotor Vibration. Presented at the 37th Annual Forum of the American Helicopter Society, New Orleans, LA, May 1981.

13. Shaw, J.: Higher Harmonic Blade Pitch Control; A System for Helicopter Vibration Reduction. Massachusetts Institute of Technology, PhD Thesis, May 1980.

14. Molusis, J. A.; Mookerjee, P.; and Bar-Shalom, Y.: Evaluation of the Effect of Vibration Nonlinearity on Convergence Behavior of Adaptive Higher Harmonic Controllers. NASA CR-166424, January 1983.

15. Molusis, J. A.: The Importance of Nonlinearity on the Higher Harmonic Control of Helicopter Vibration. Presented at the 39th Annual Forum of the American Helicopter Society, St. Louis, Missouri, May 1983.

16. Chopra, I.; and McCloud, J. L., III: A Numerical Simulation Study of Open-Loop, Closed-Loop and Adaptive Multicyclic Control Systems. Journal of the American Helicopter Society, Vol. 28, No. 1, January 1983.

17. Wood, E. R.; Powers, R. W.; Cline, J. H.; and Hammond, C. E.: On Developing and Flight Testing a Higher Harmonic Control System. Presented at the 39th Annual Forum of the American Helicopter Society, May 1983.

18. Biggers, J. C.; and McCloud, J. L., III: A Note on Multicyclic Control by Swashplate Oscillation. NASA TM-78475, April 1978.

19. Bryson, A. E., Jr.; and Ho, Y. C.: Applied Optimal Control. Blaisdell Publishing Co., Waltham, MA, 1969.

20. Goodwin, G. D.; and Payne, R. L.: Dynamic System Identification, Experiment Design and Data Analysis. Academic Press, New York, 1977.

21. Wittenmark, B.: Stochastic Adaptive Control Methods, A Survey. International Journal of Control, Vol. 21, No. 5, 1975.

22. Bielawa, R. L.: Aeroelastic Analysis for Helicopter Rotor Blades with Time-Variable, Nonlinear Structural Twist and Multiple Structural Redundancy - Mathematical Derivation and User's Manual. NASA CR-2638, October 1976.

23. Niebanck, C.: A Model Rotor Test Data for Verification of Blade Response and Rotor Performance Calculations. USA-AMRDL-TR-74-29, May 1974.

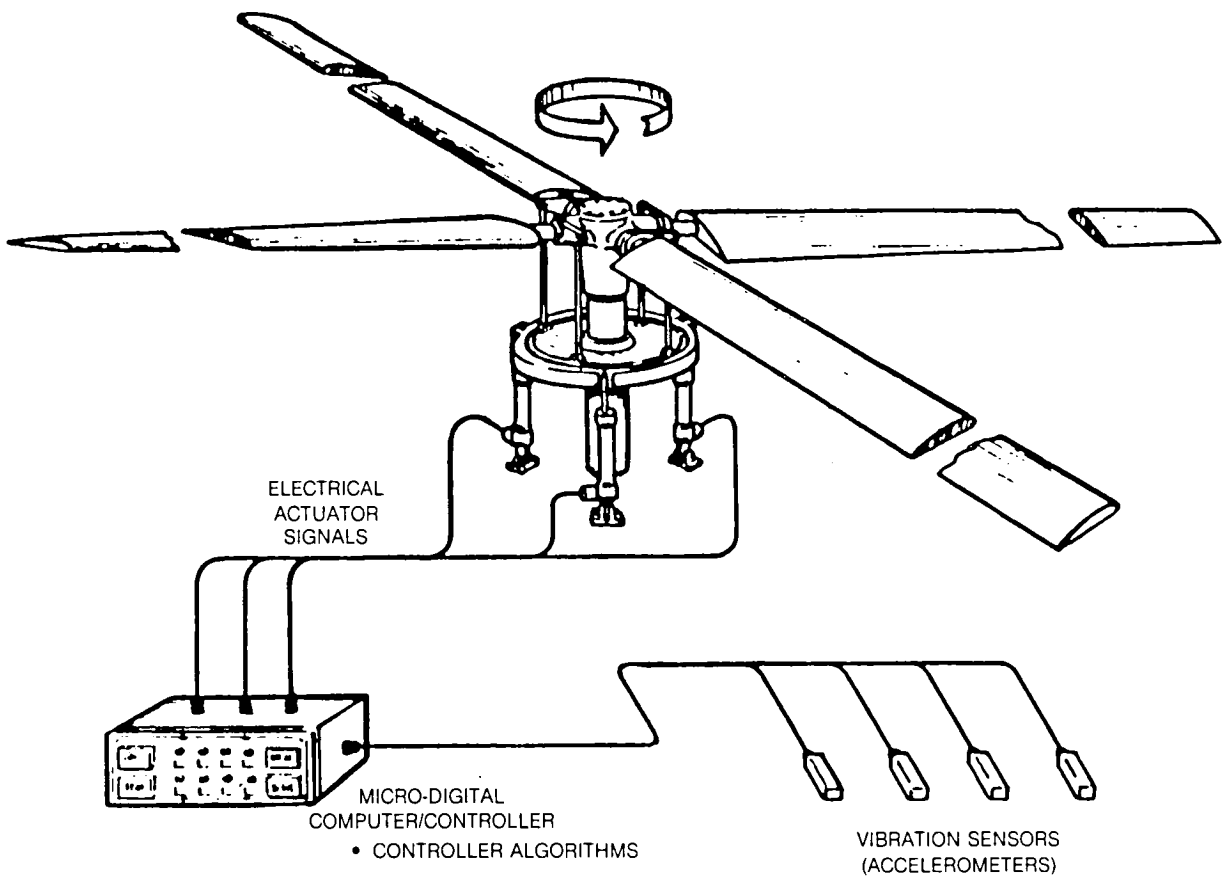

Fig. 1 Schematic of Active Vibration Control Concept

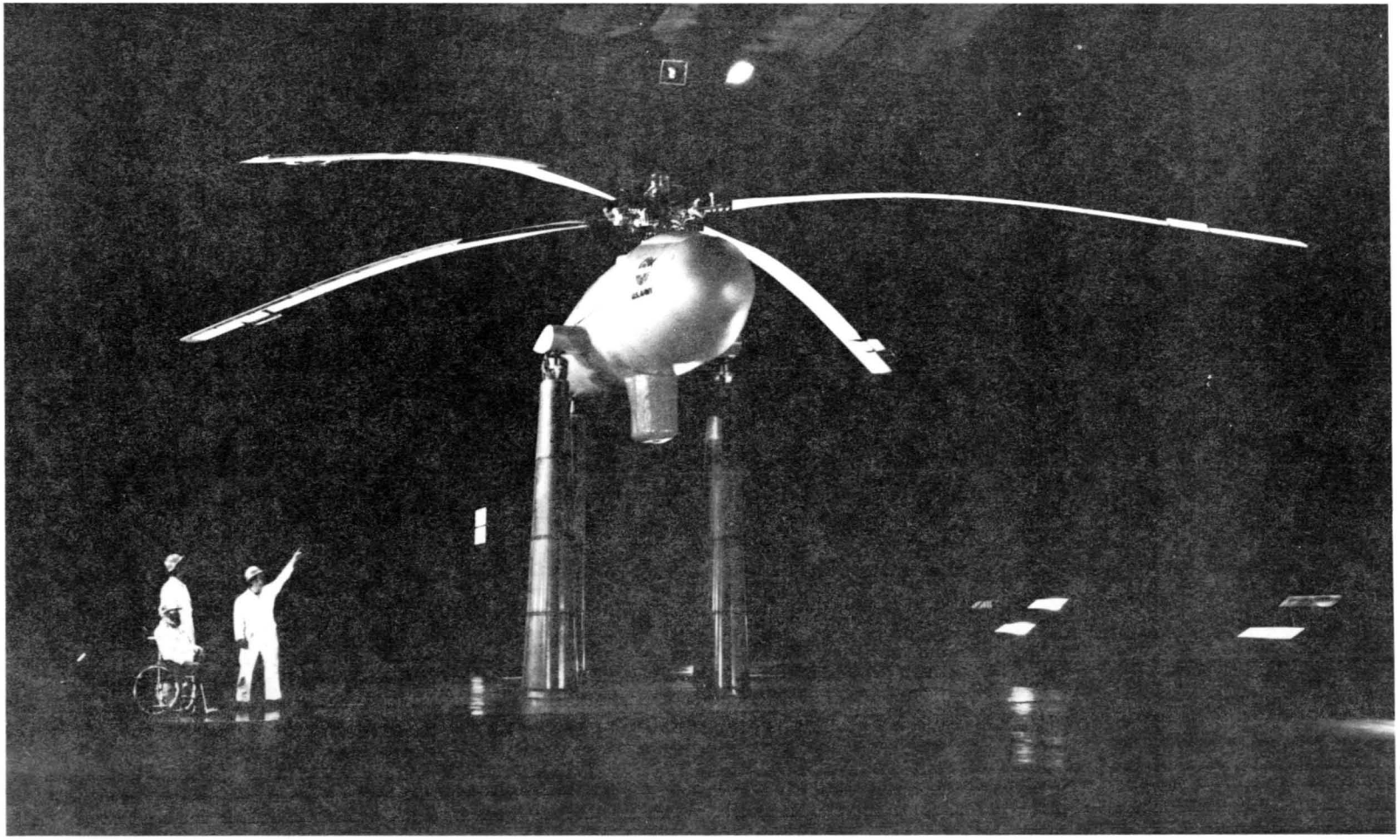

Fig. 2(a) Rotor Test Apparatus in Wind Tunnel

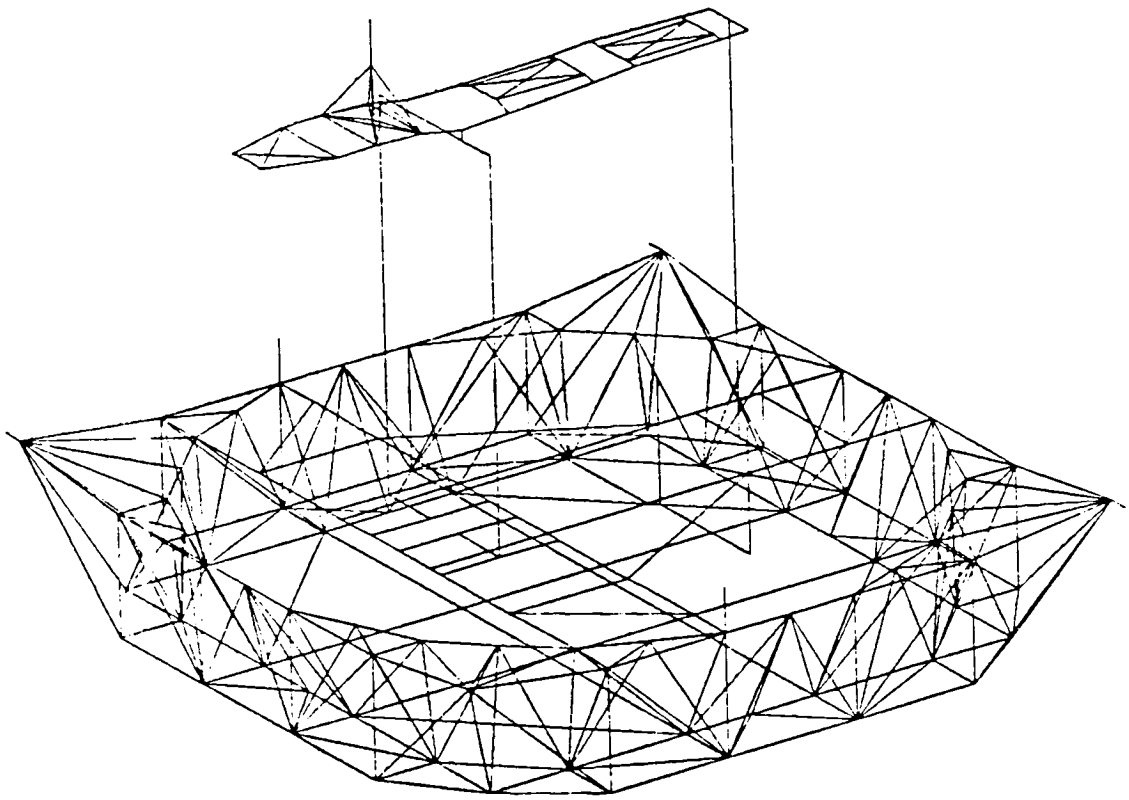

Fig. 2(b) Schematic of NASTRAN Model of Rotor Test Apparatus, Wind Tunnel Support Struts, and Balance Frame Structure

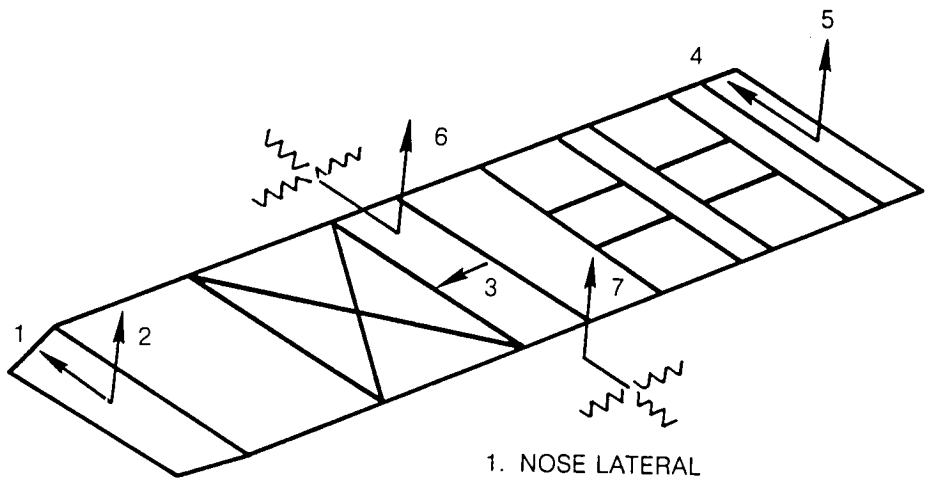

Fig. 3 Accelerometer Locations in Rotor Test Apparatus

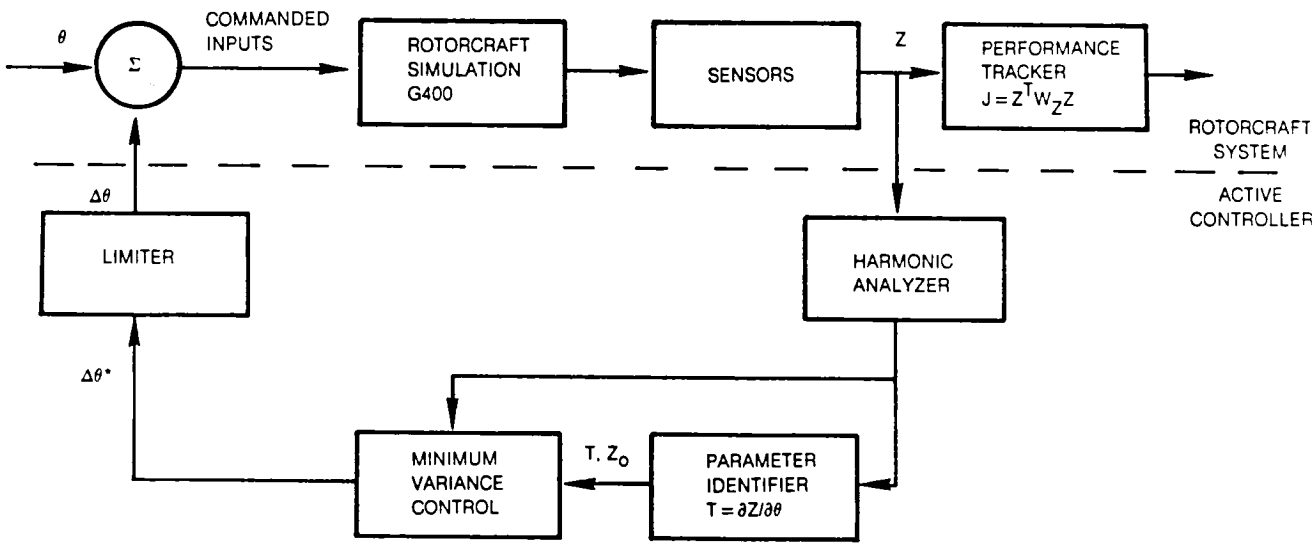

Fig. 4 Computer Simulation of the Closed-Loop Active Vibration Control System

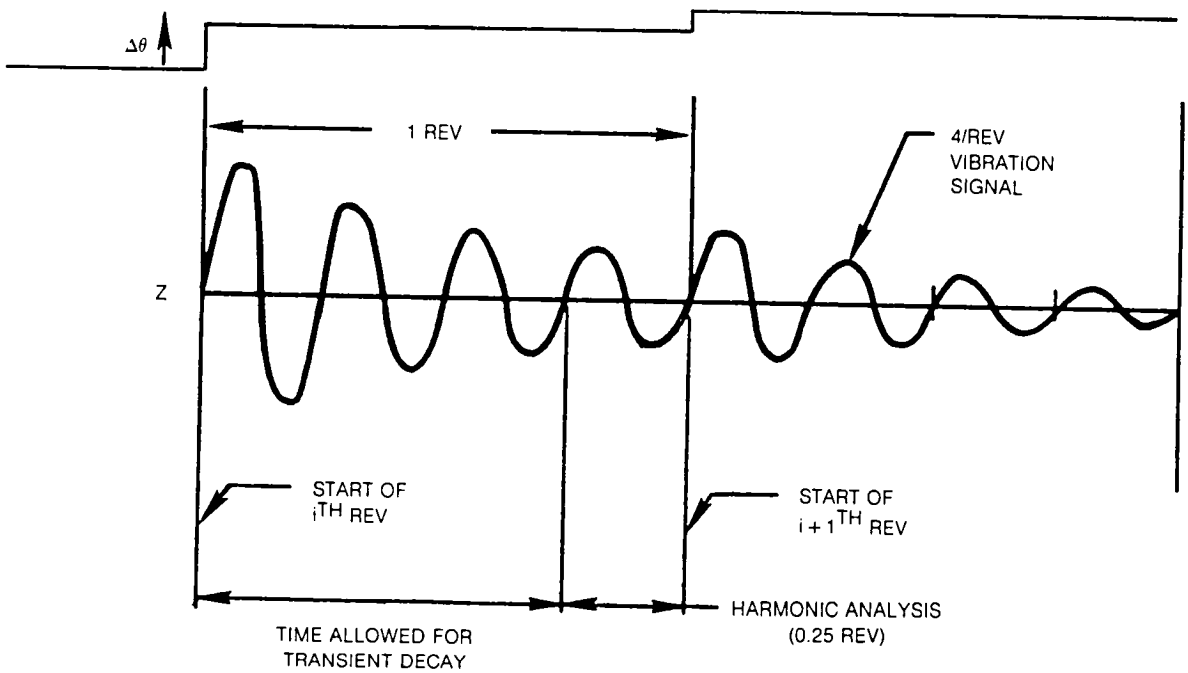

Fig. 5 Sequence of Events Occurring in Active Vibration Control System for One Rotor Revolution

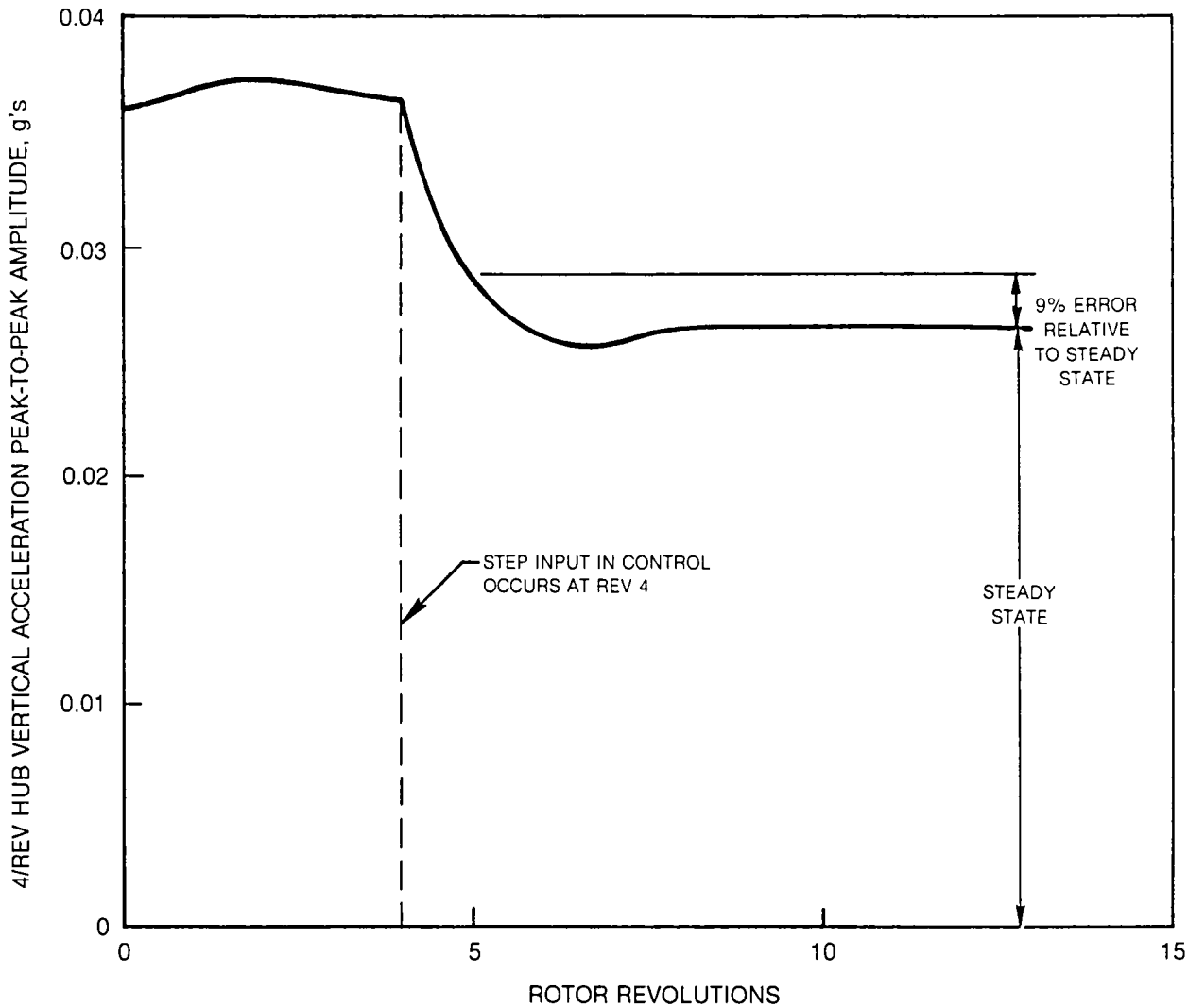

Fig. 6 Transient Vibration Response to Step Input of Higher Harmonic Control

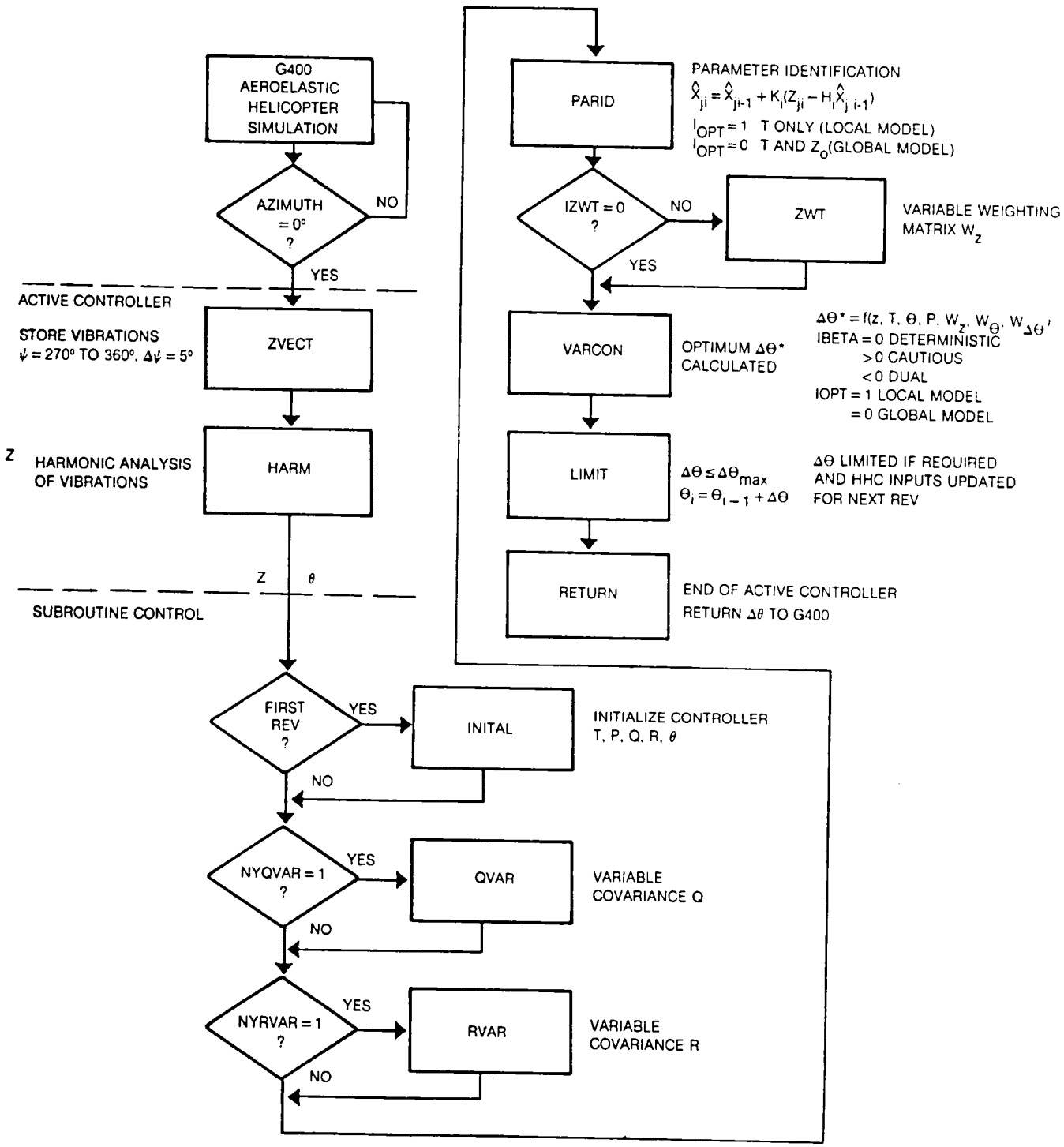

Fig. 7 Flow Diagram of Controller Subroutine

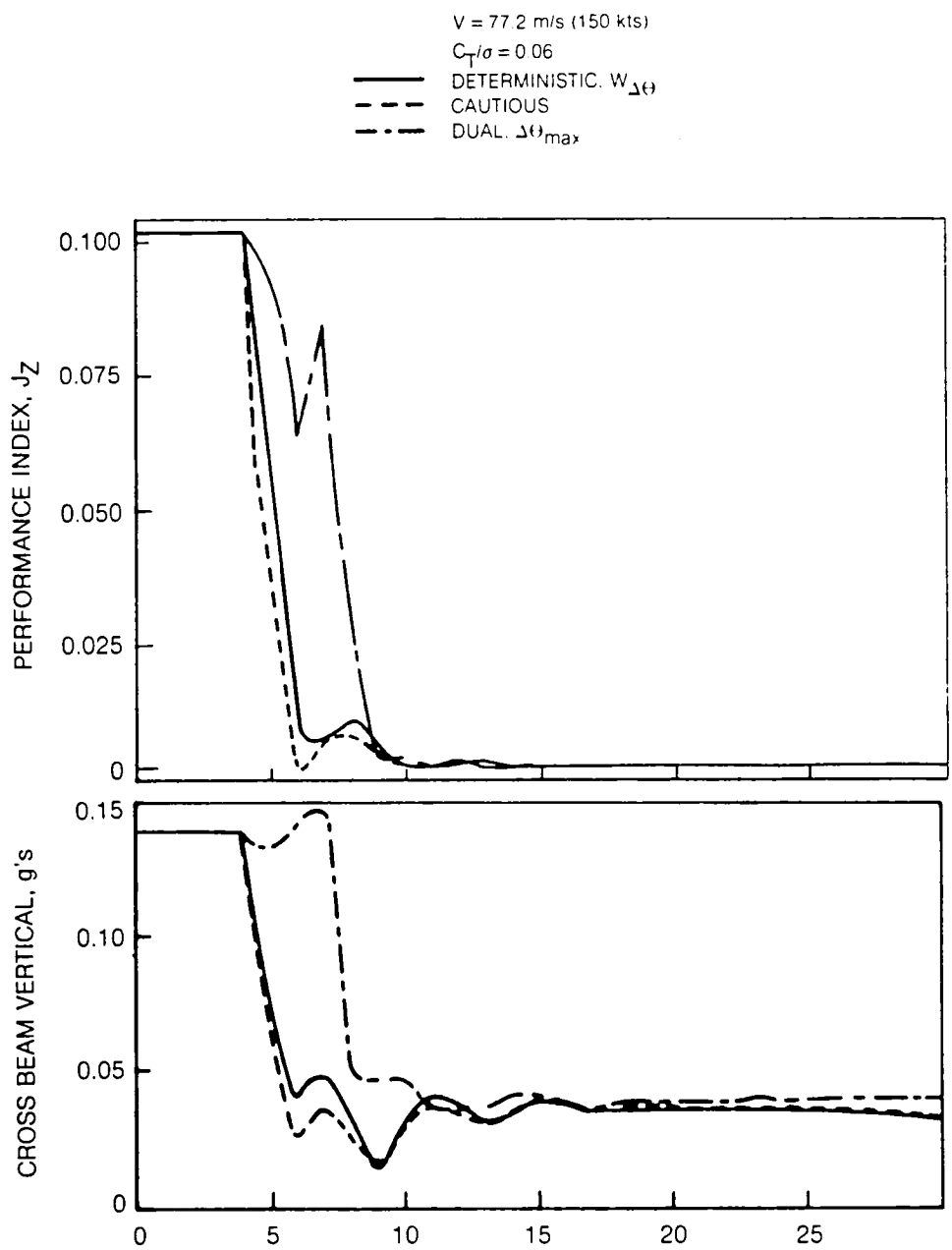

Fig. 8(a) Time History of Vibration Controller at Baseline Flight Condition (Vibration Response)

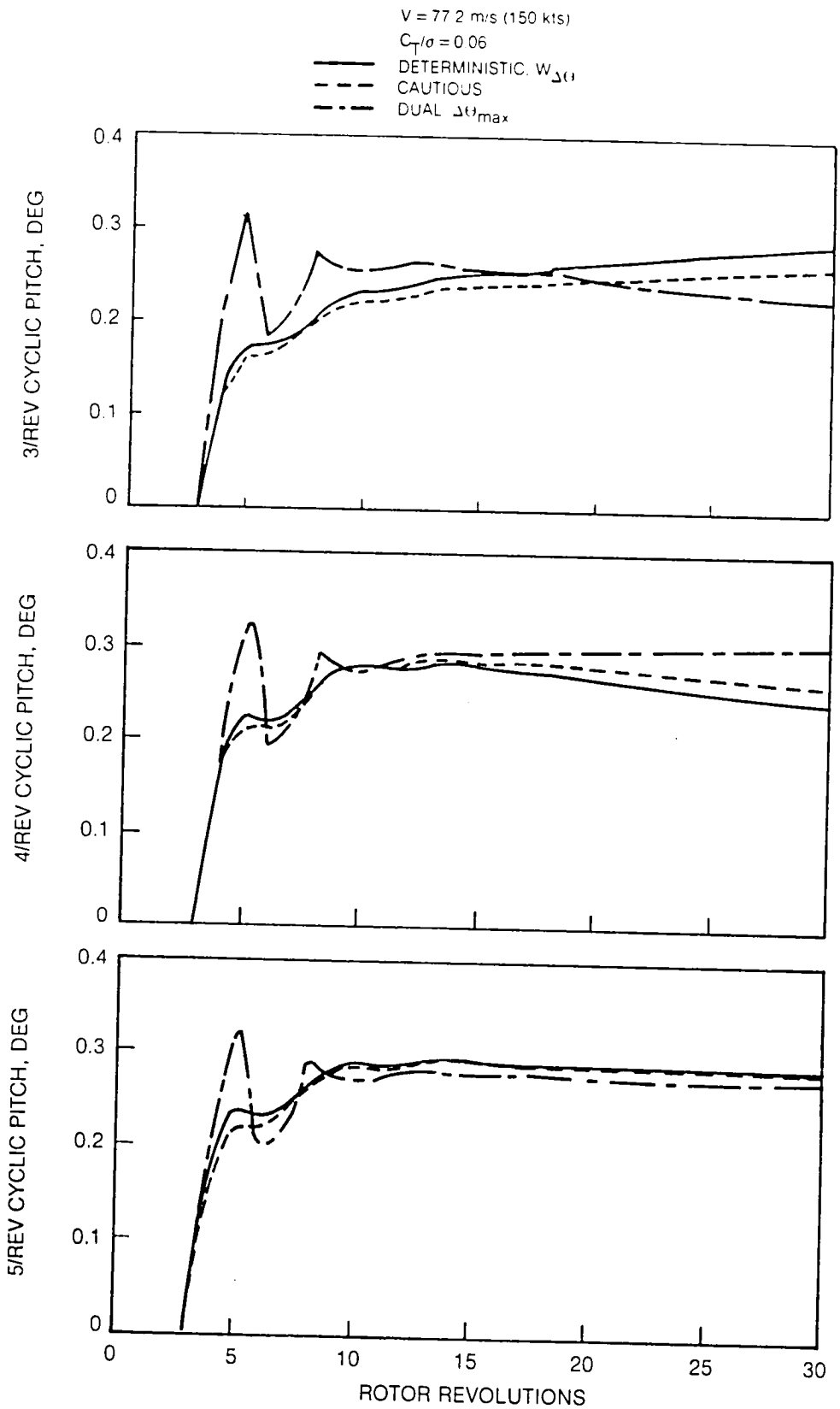

Fig. 8(b) Time History of Vibration Controller at Baseline Flight Condition (Control Inputs)

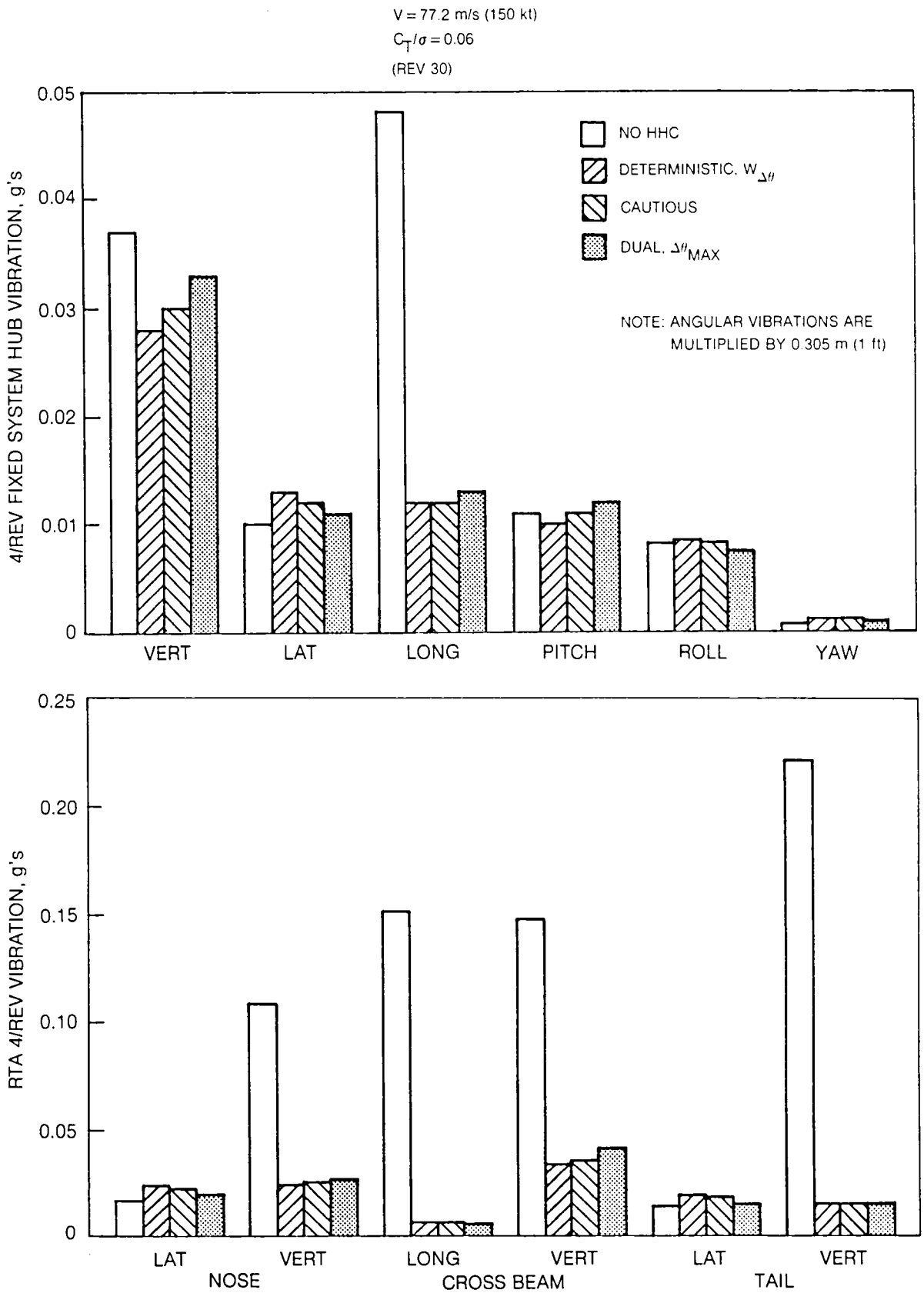

Fig. 9 Effect of Active Control on Predicted 4/Rev Hub and RTA Vibration at Baseline Flight Condition

V = 77.2 m/s (150 kt)
$C_T/\sigma = 0.06$
(REV 30)

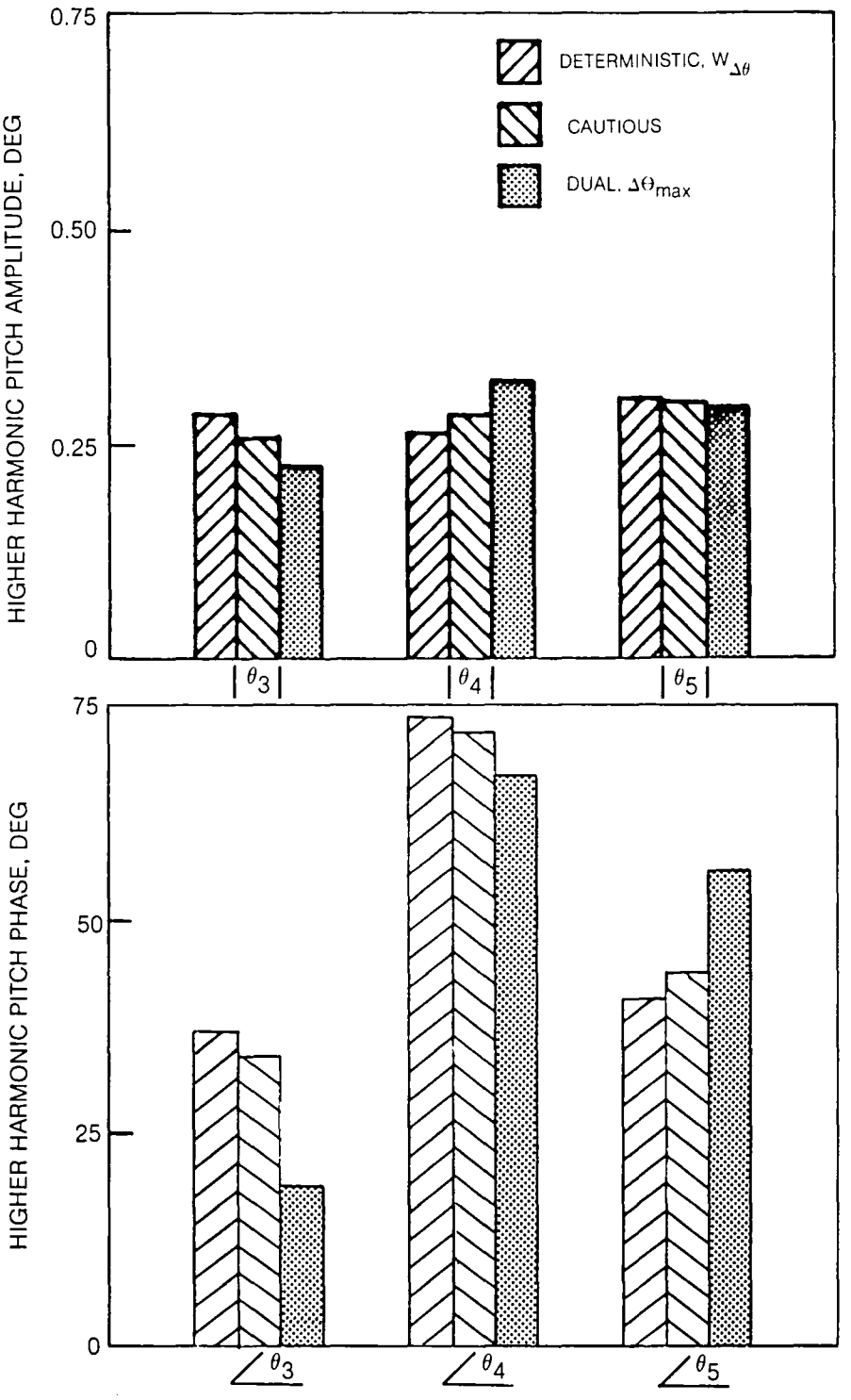

Fig. 10 Higher Harmonic Pitch Required by Baseline Controllers at Baseline Flight Condition

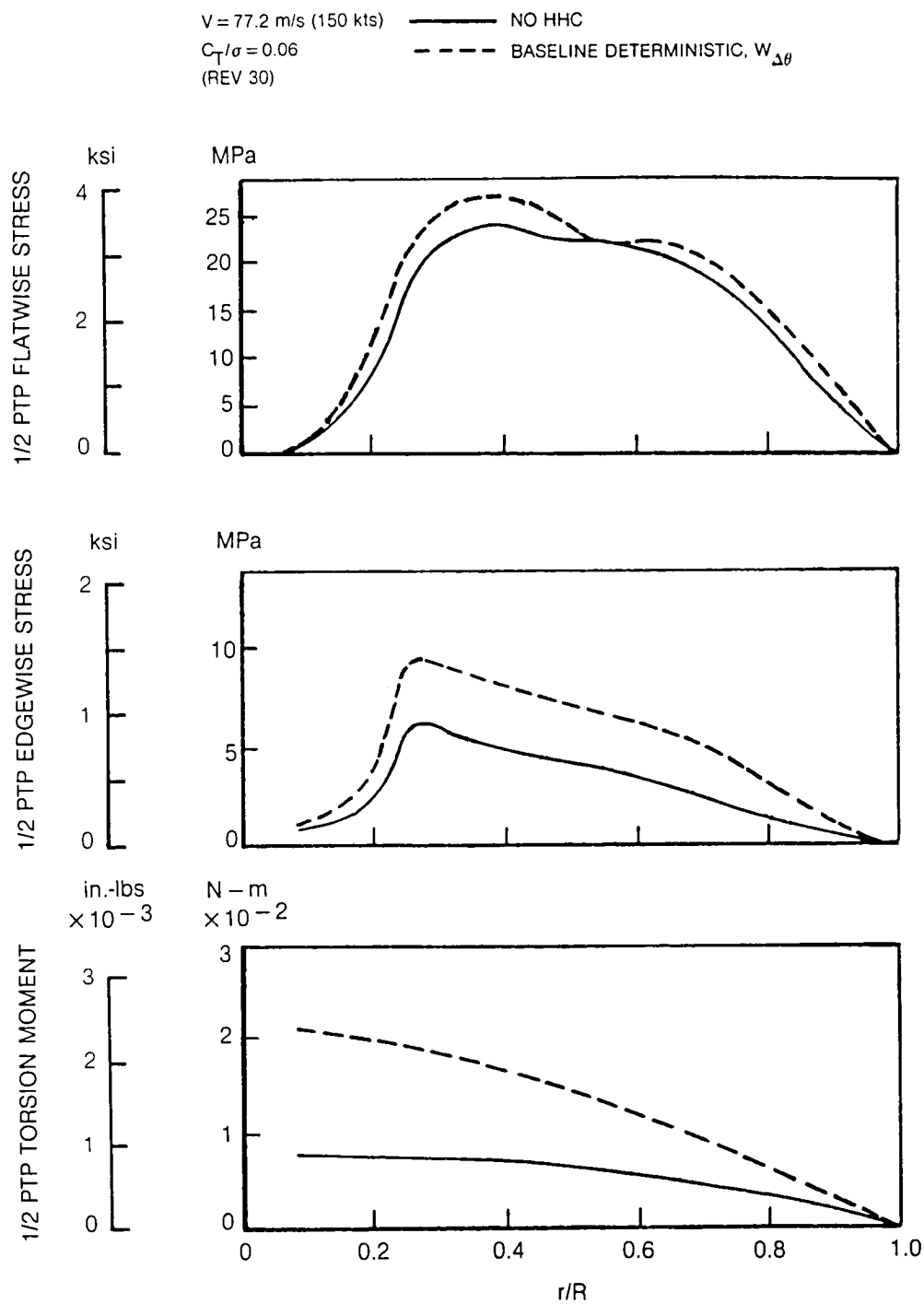

Fig. 11 Effect of Active Vibration Control on Rotor Blade Vibratory Moments and Stresses at Baseline Flight Condition

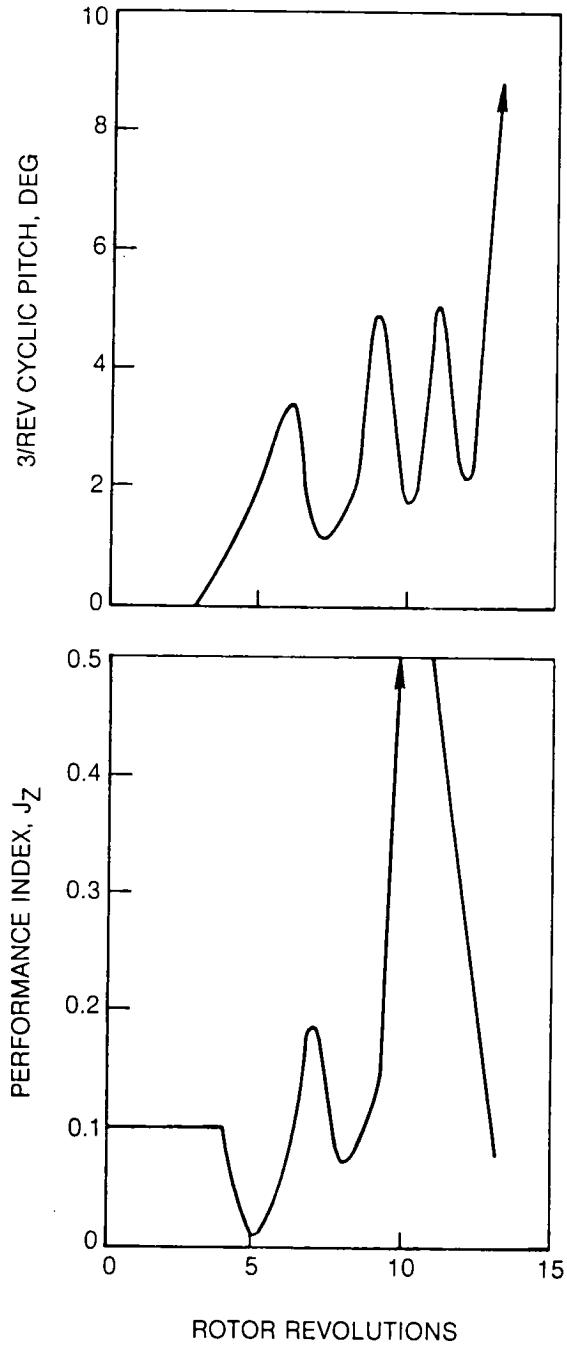

Fig. 12 Deterministic Controller Performance Without Limiting at Baseline Flight Condition (Global Model)

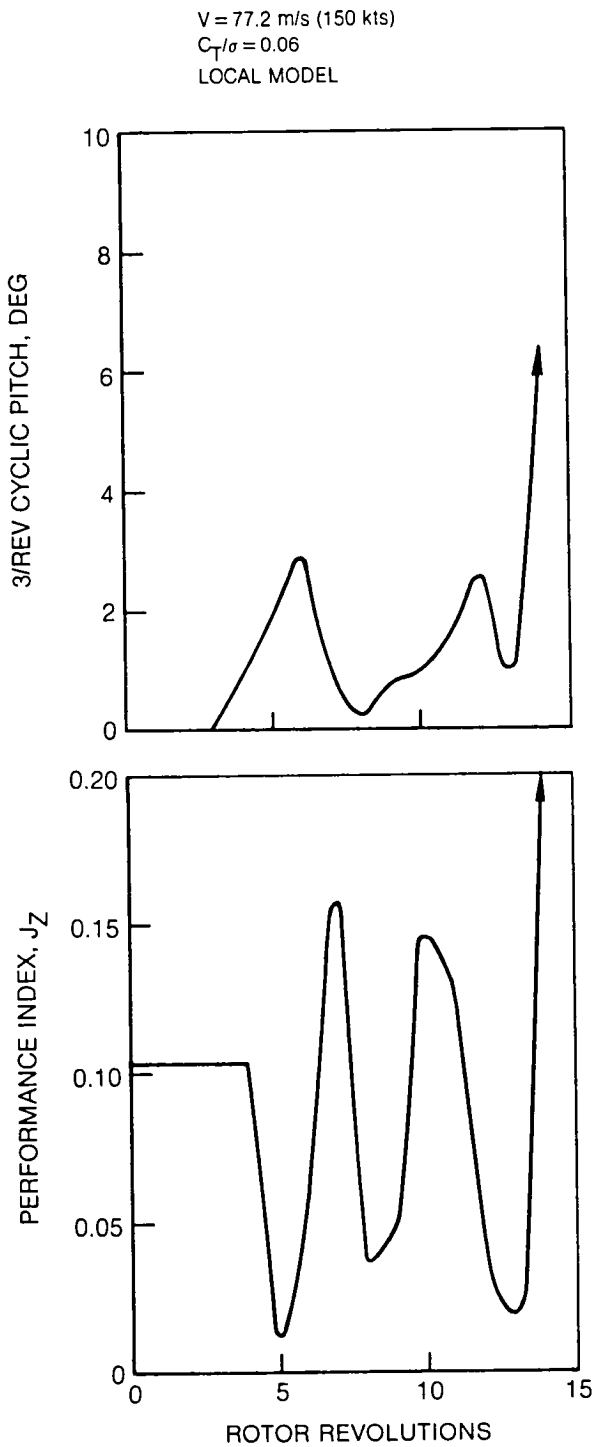

Fig. 13 Deterministic Controller Performance Without Limiting at Baseline Flight Condition (Local Model)

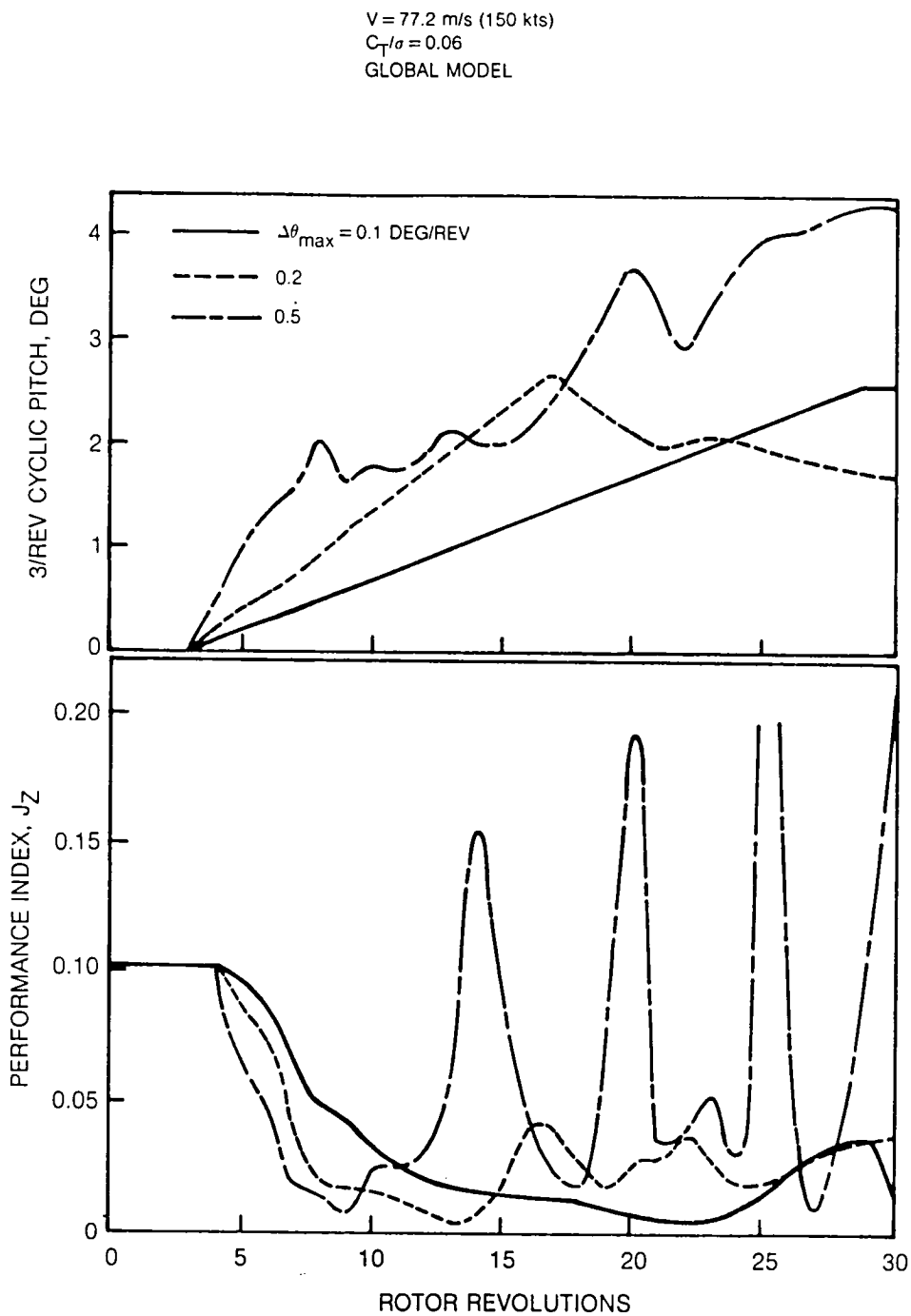

Fig. 14 Effect of External Rate-Limiting on Deterministic Controller Performance (Global Model)

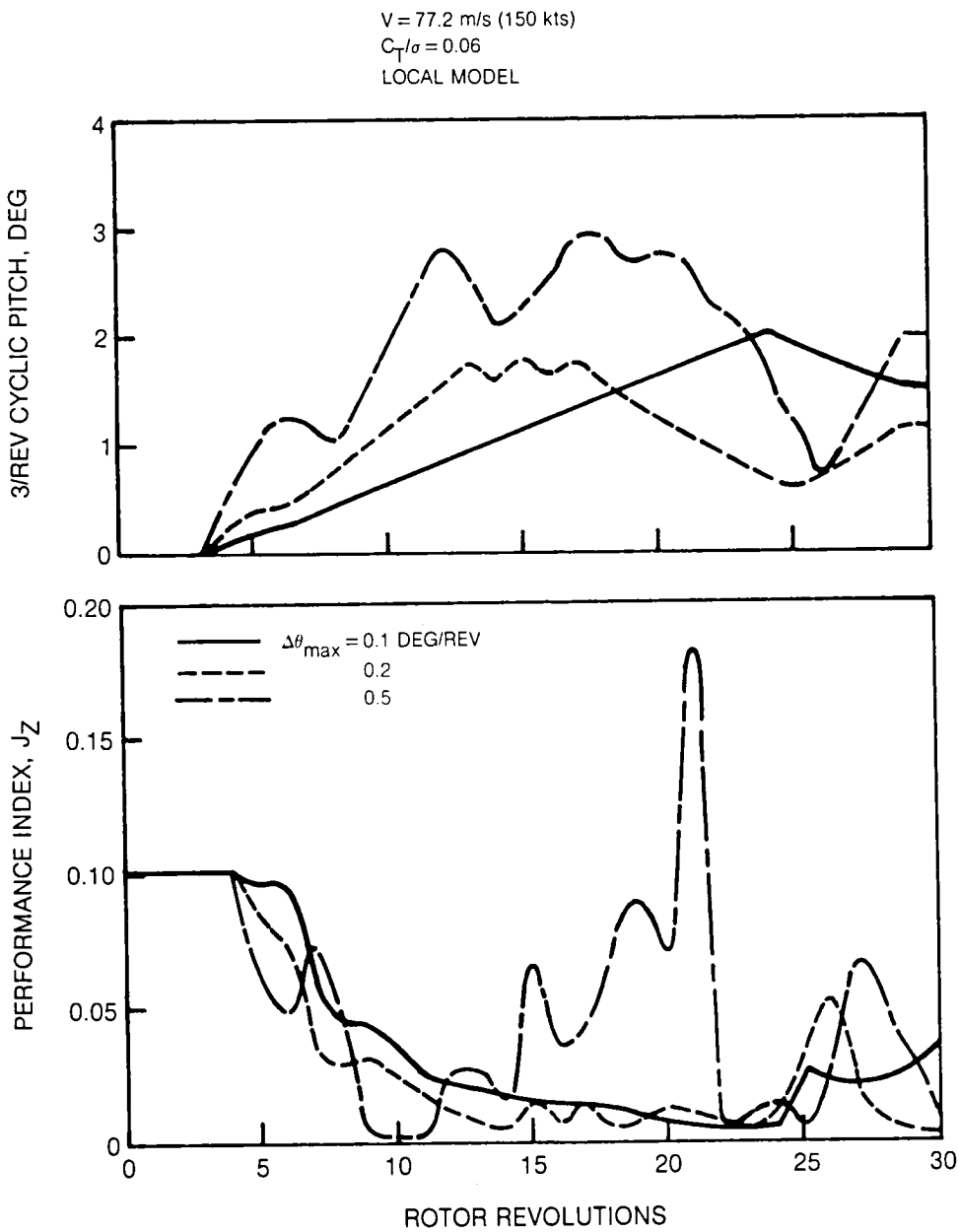

Fig. 15 Effect of External Rate-Limiting on Deterministic Controller Performance (Local Model)

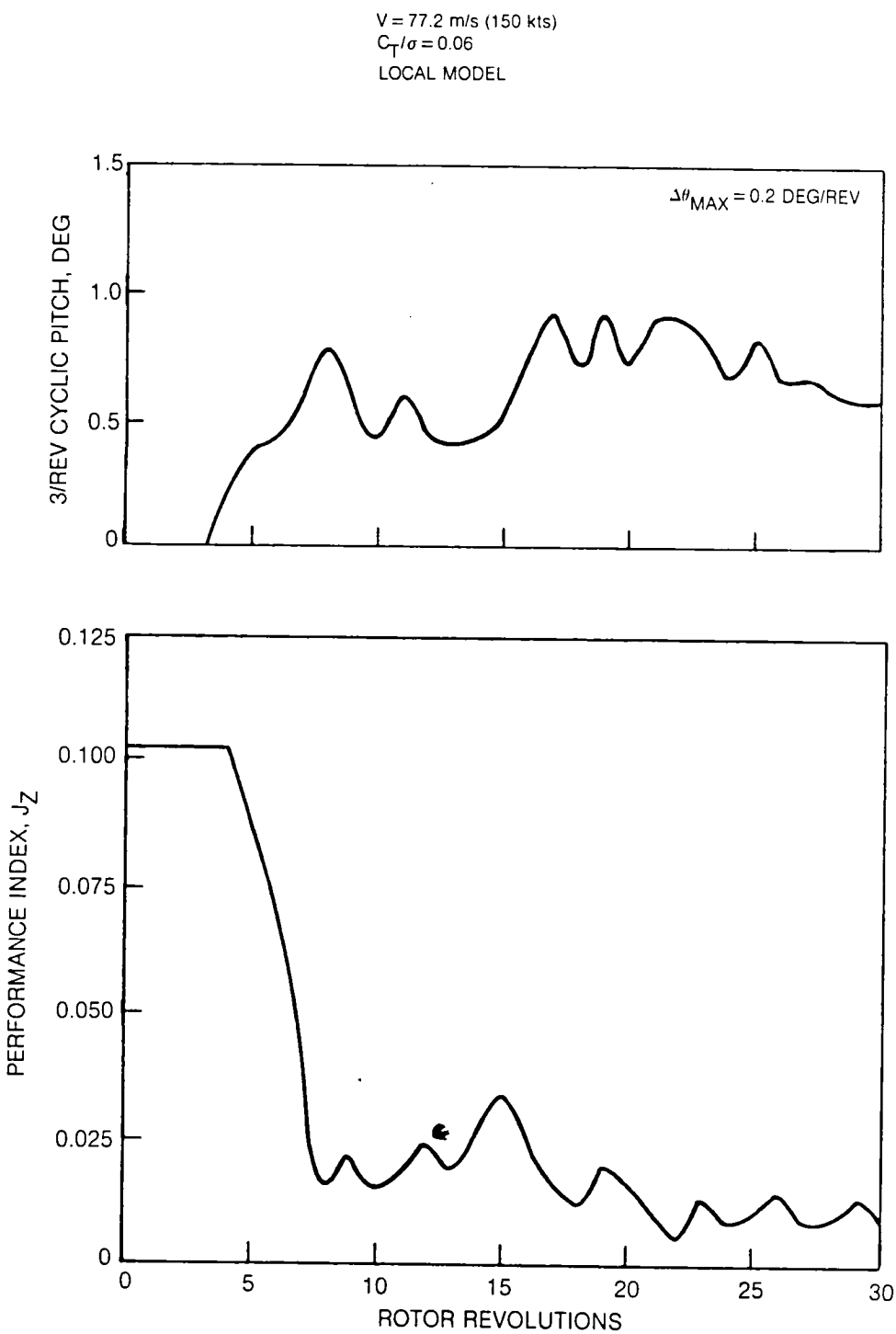

Fig. 16 Deterministic Controller Performance with External Rate-Limiting at Baseline Flight Condition

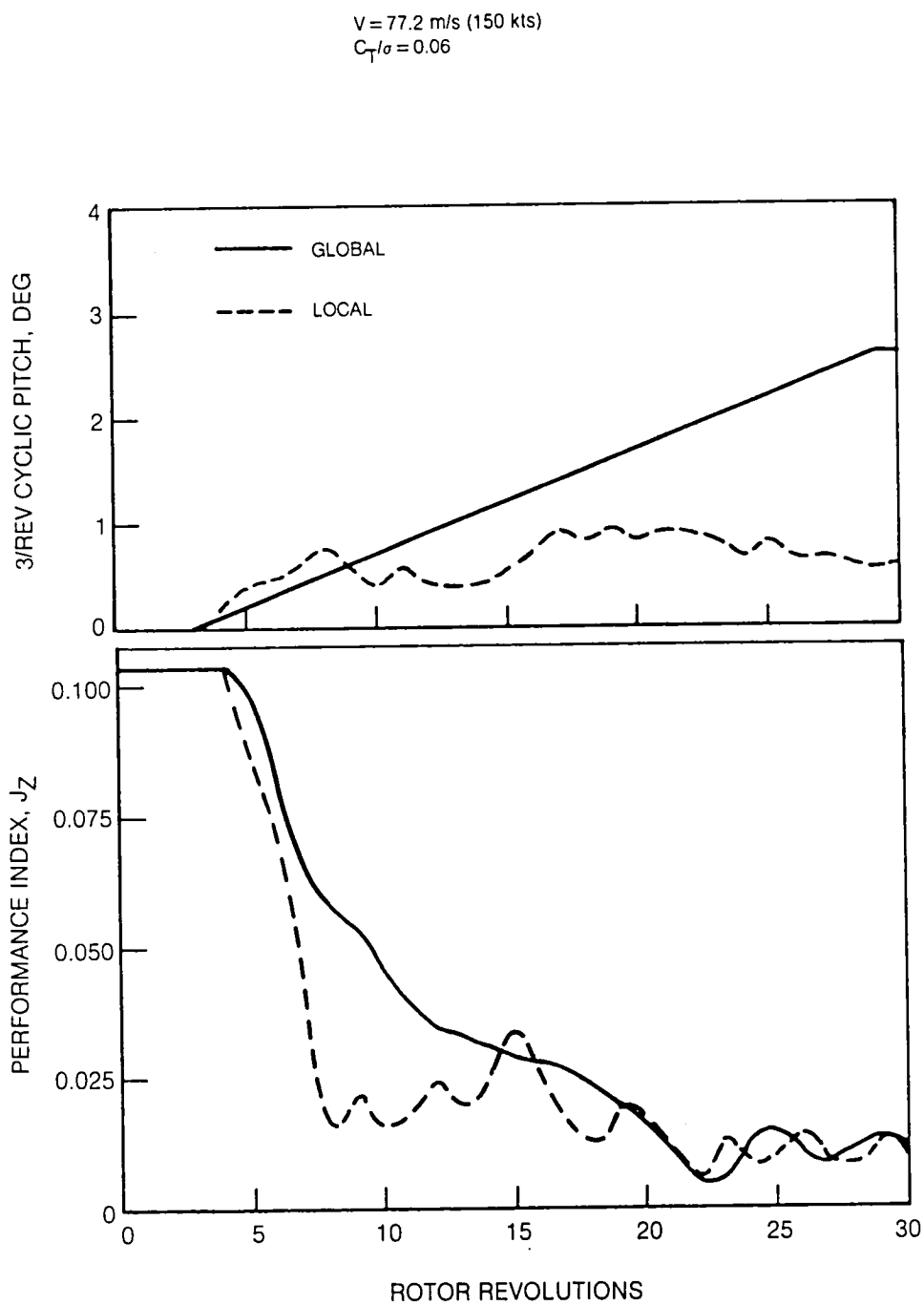

Fig. 17 Deterministic Controller Performance with External Rate-Limiting at Baseline Flight Condition

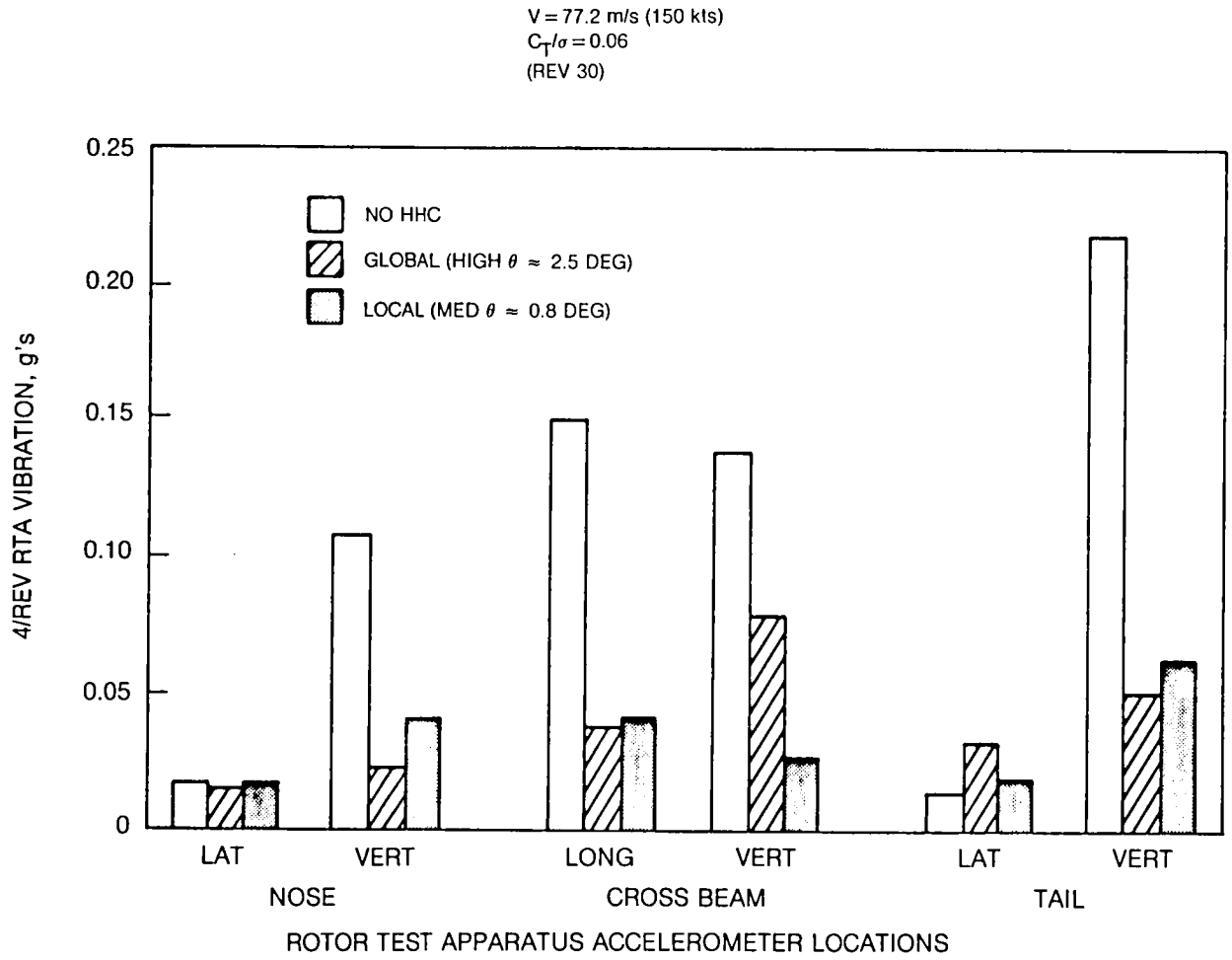

Fig. 18 Predicted 4/REV RTA Vibration with Externally Limited Deterministic Controller at Baseline Flight Condition

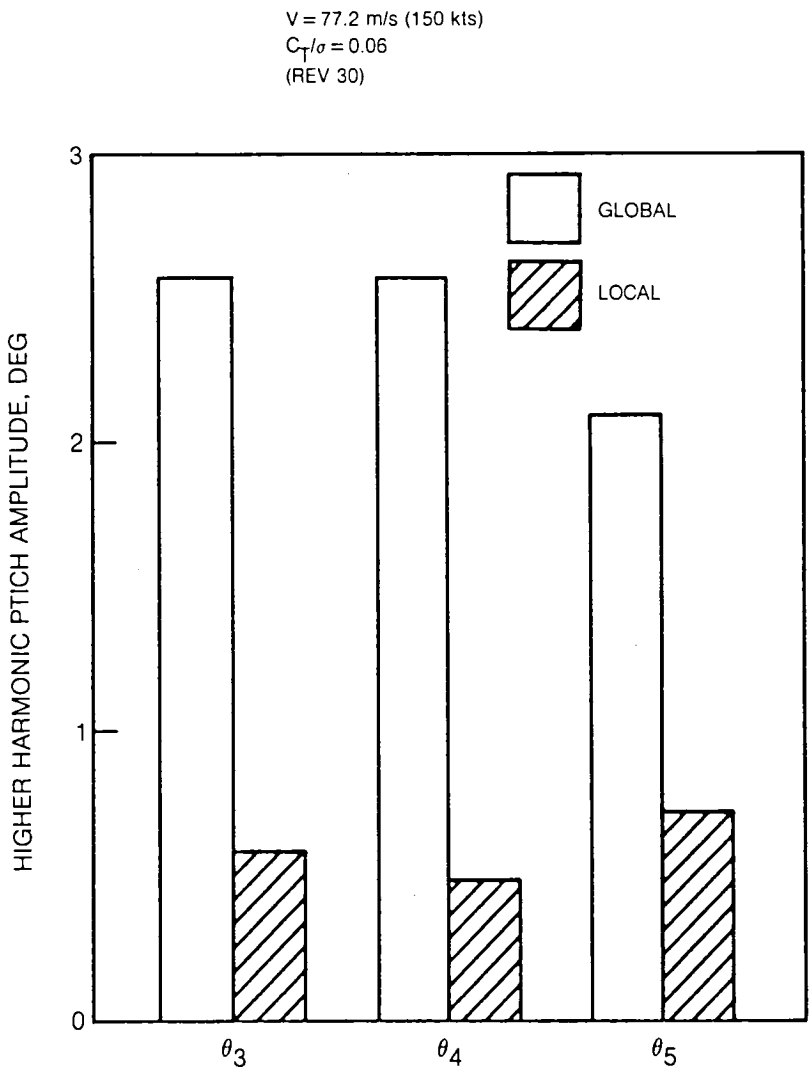

Fig. 19 Higher Harmonic Pitch Amplitude Required by Externally Limited Deterministic Controller at Baseline Flight Condition

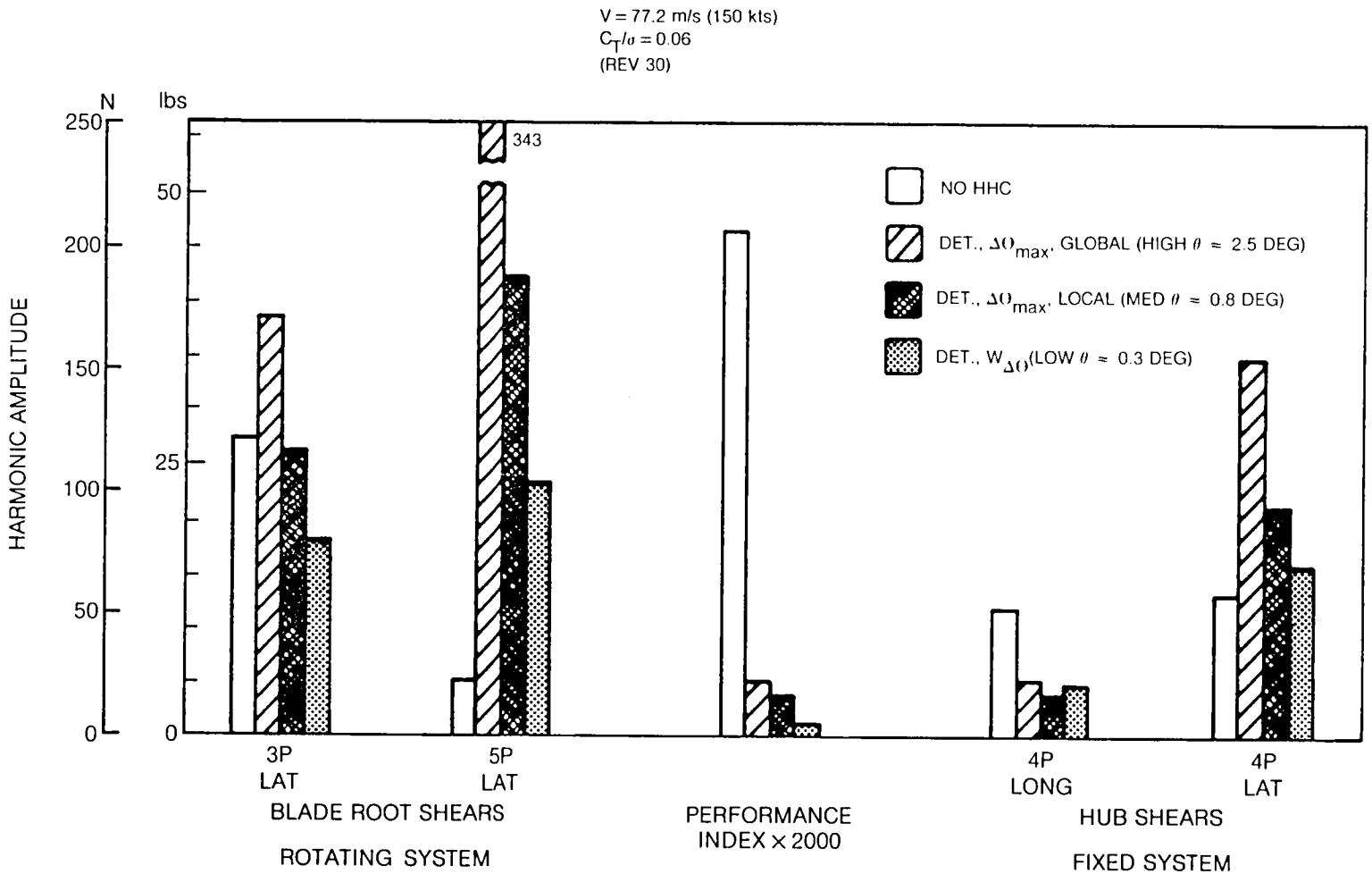

Fig. 20 Effect of Fixed System Sensors on Controller Performance at Baseline Flight Condition

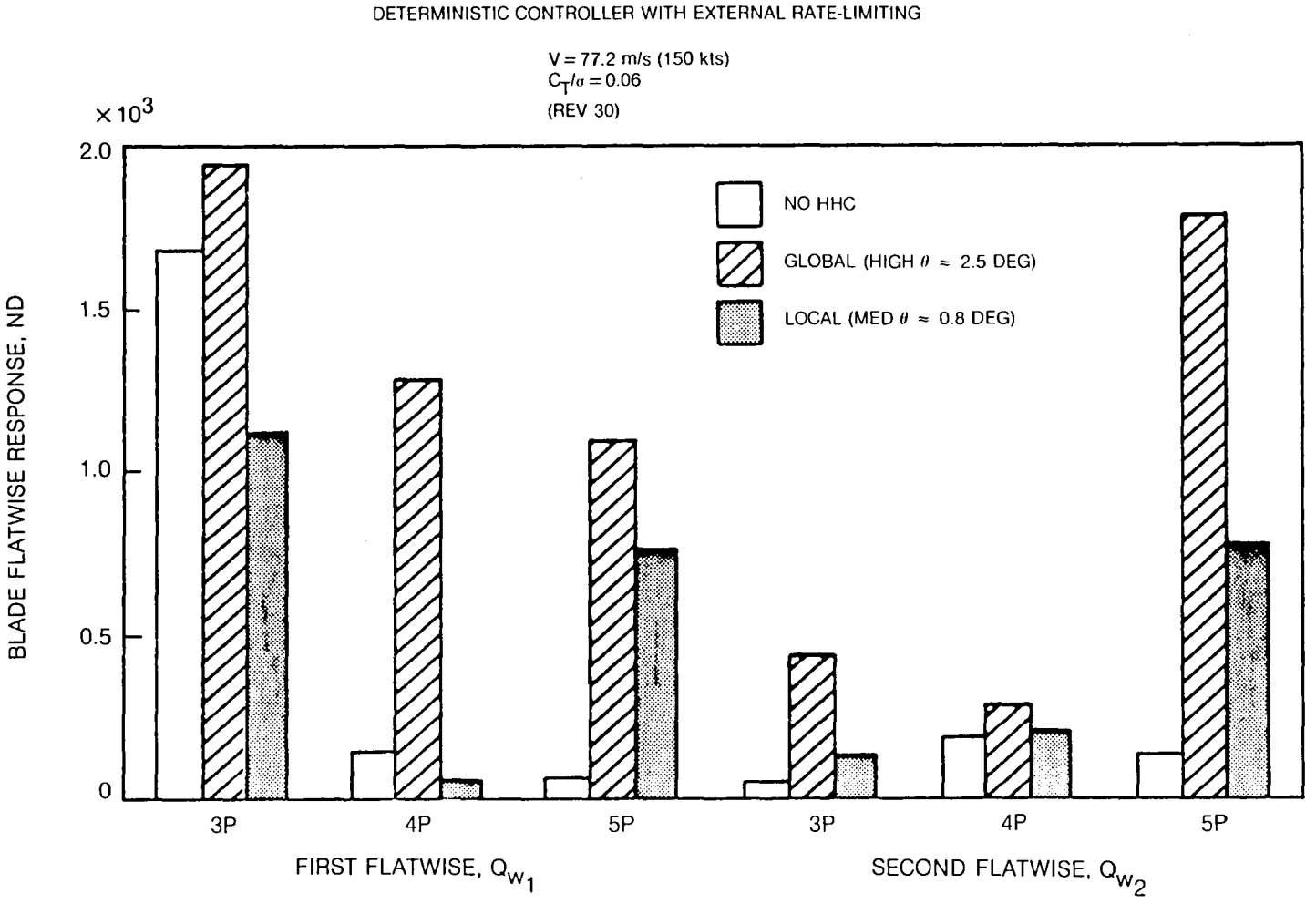

Fig. 21 Effect of Active Control on Blade Modal Response at Baseline Flight Condition

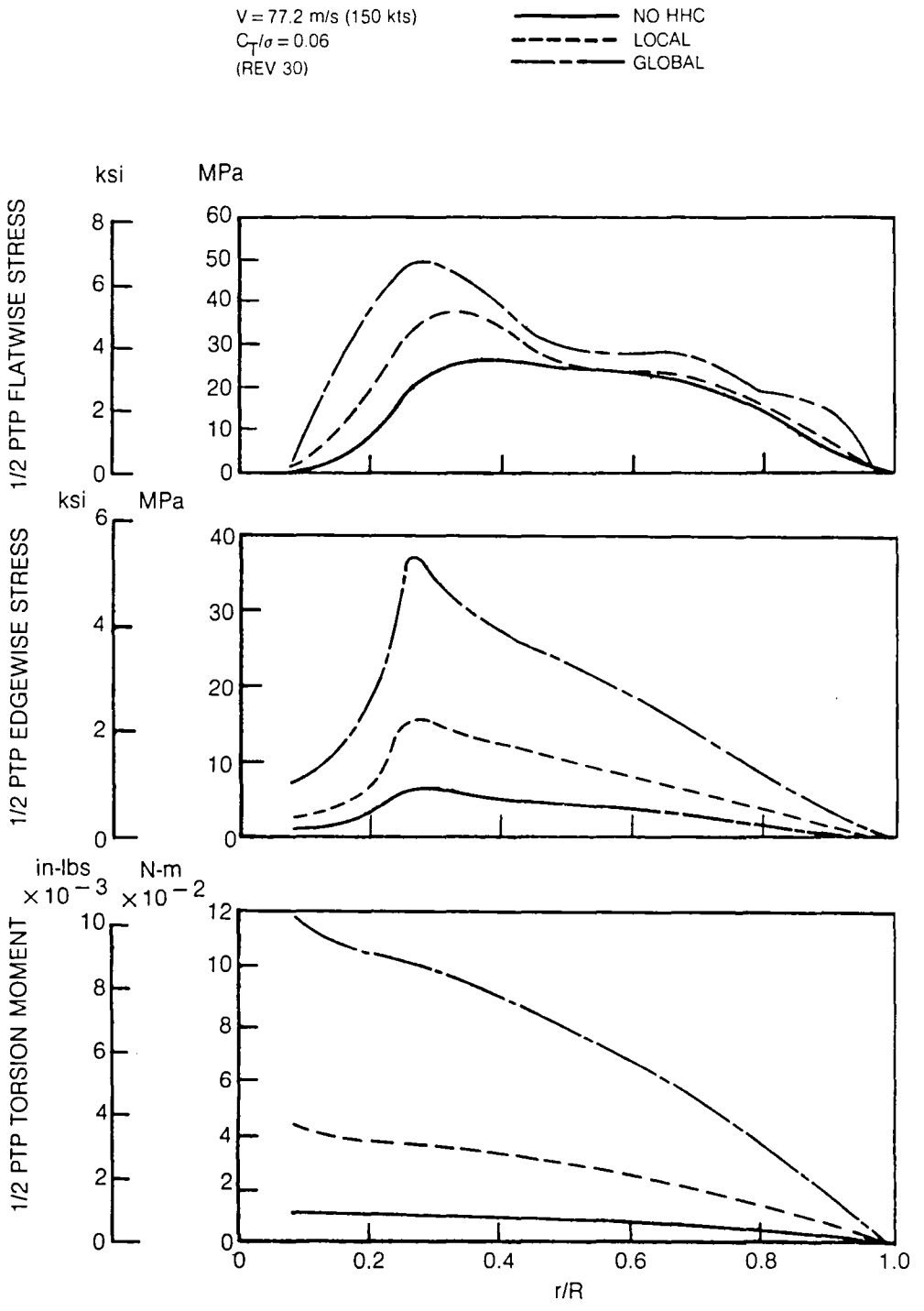

Fig. 22 Effect of Active Vibration Control on Rotor Blade Vibratory Moments and Stresses at Baseline Flight Condition

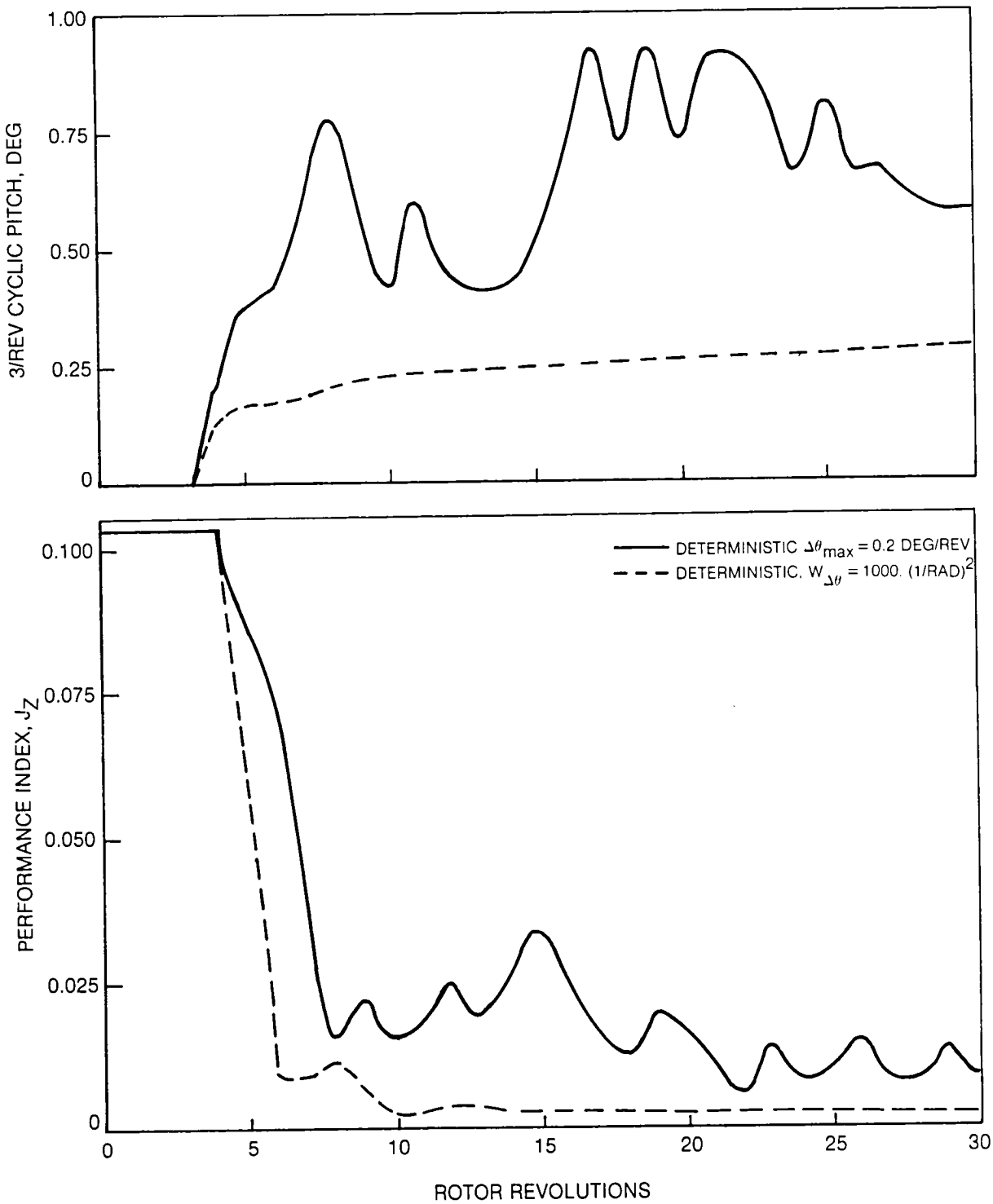

Fig. 23 Comparison of Deterministic Controller Performance with External and Internal Rate-Limiting at Baseline Flight Condition

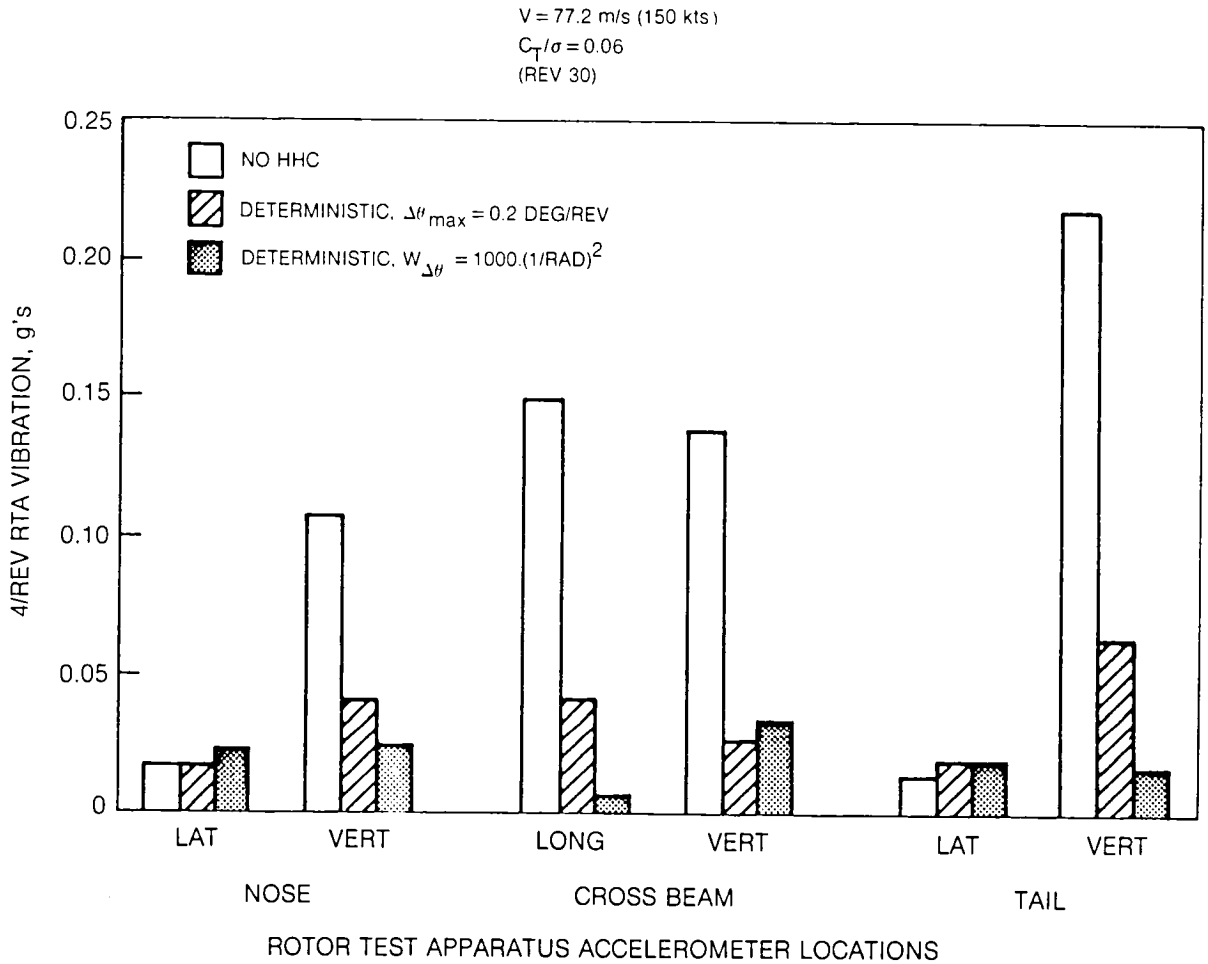

Fig. 24 Comparison of Deterministic Controller Performance with External and Internal Rate-Limiting at Baseline Flight Condition

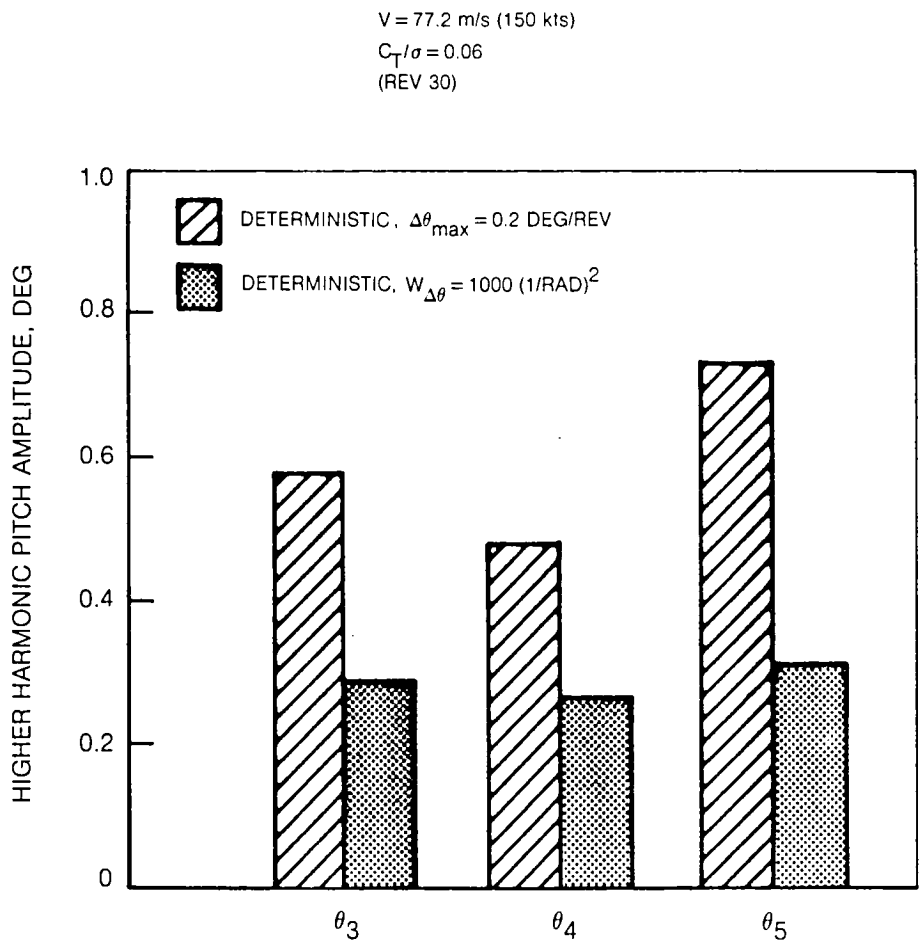

Fig. 25 Comparison of Deterministic Controller Performance with External and Internal Rate-Limiting at Baseline Flight Condition

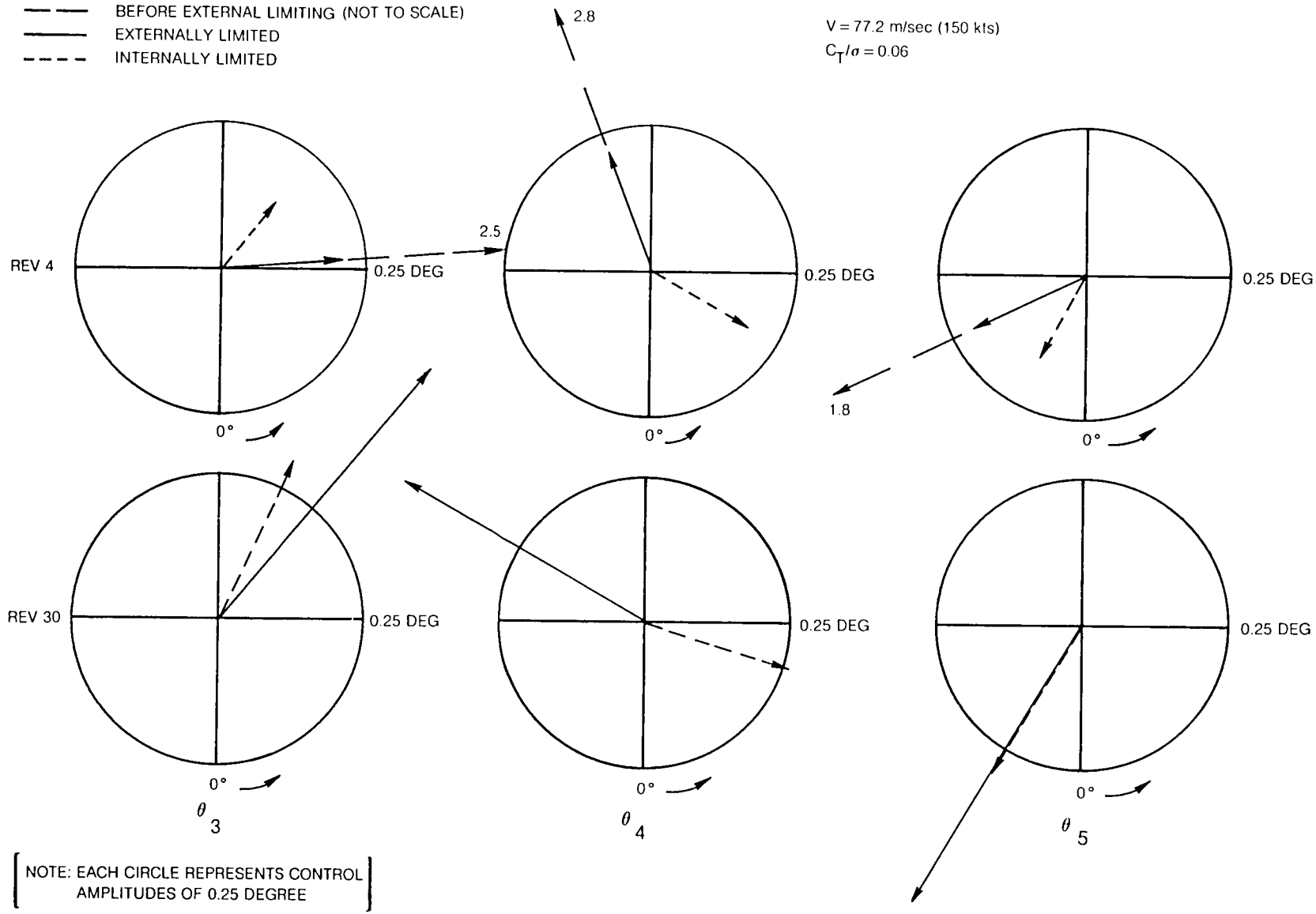

Fig. 26 Effect of Rate-Limiting on Higher Harmonic Control Inputs Commanded by Deterministic Controller at Baseline Flight Condition

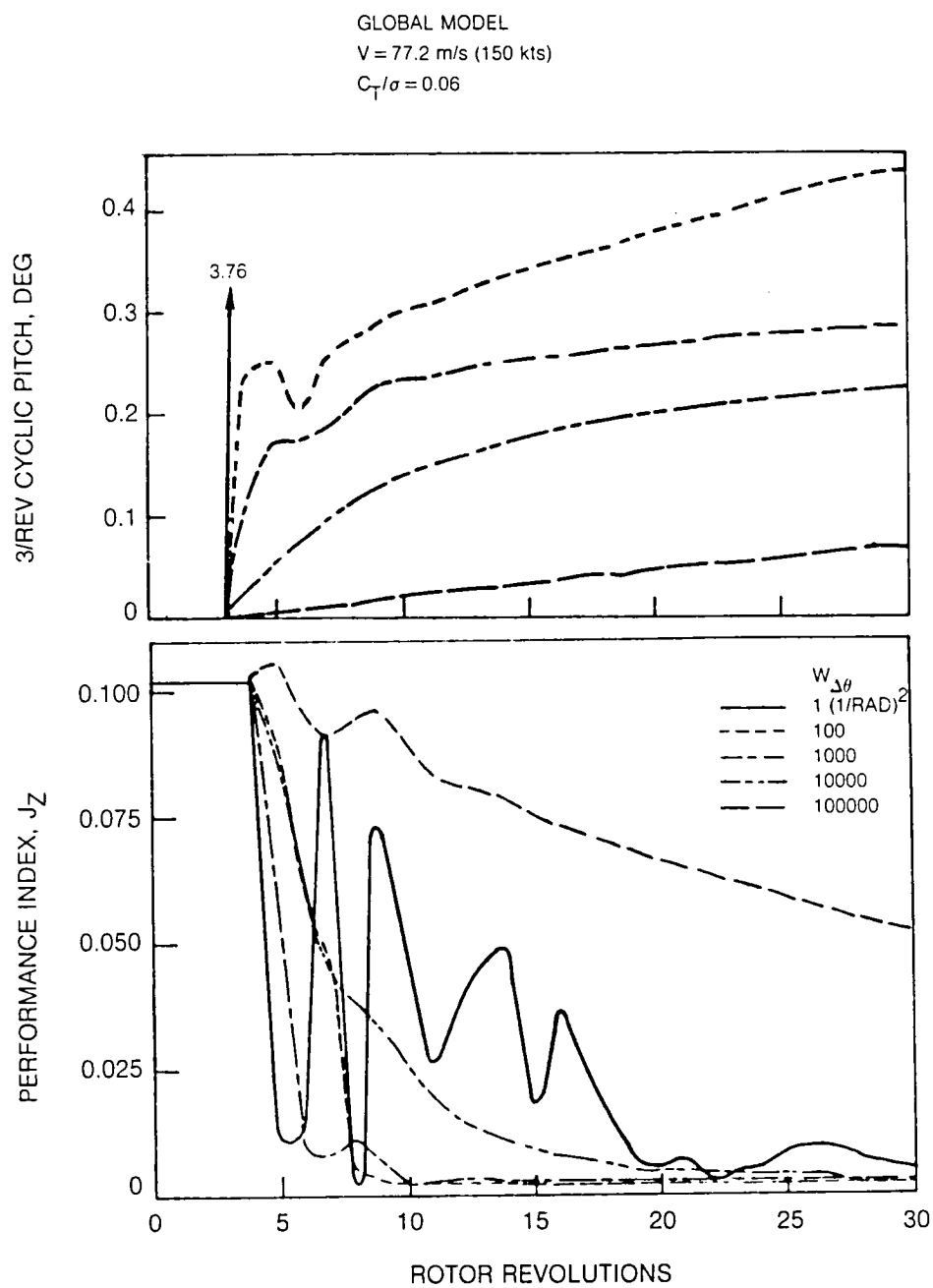

Fig. 27 Effect of Internal Rate-Limiting on Deterministic Controller Performance at Baseline Flight Condition

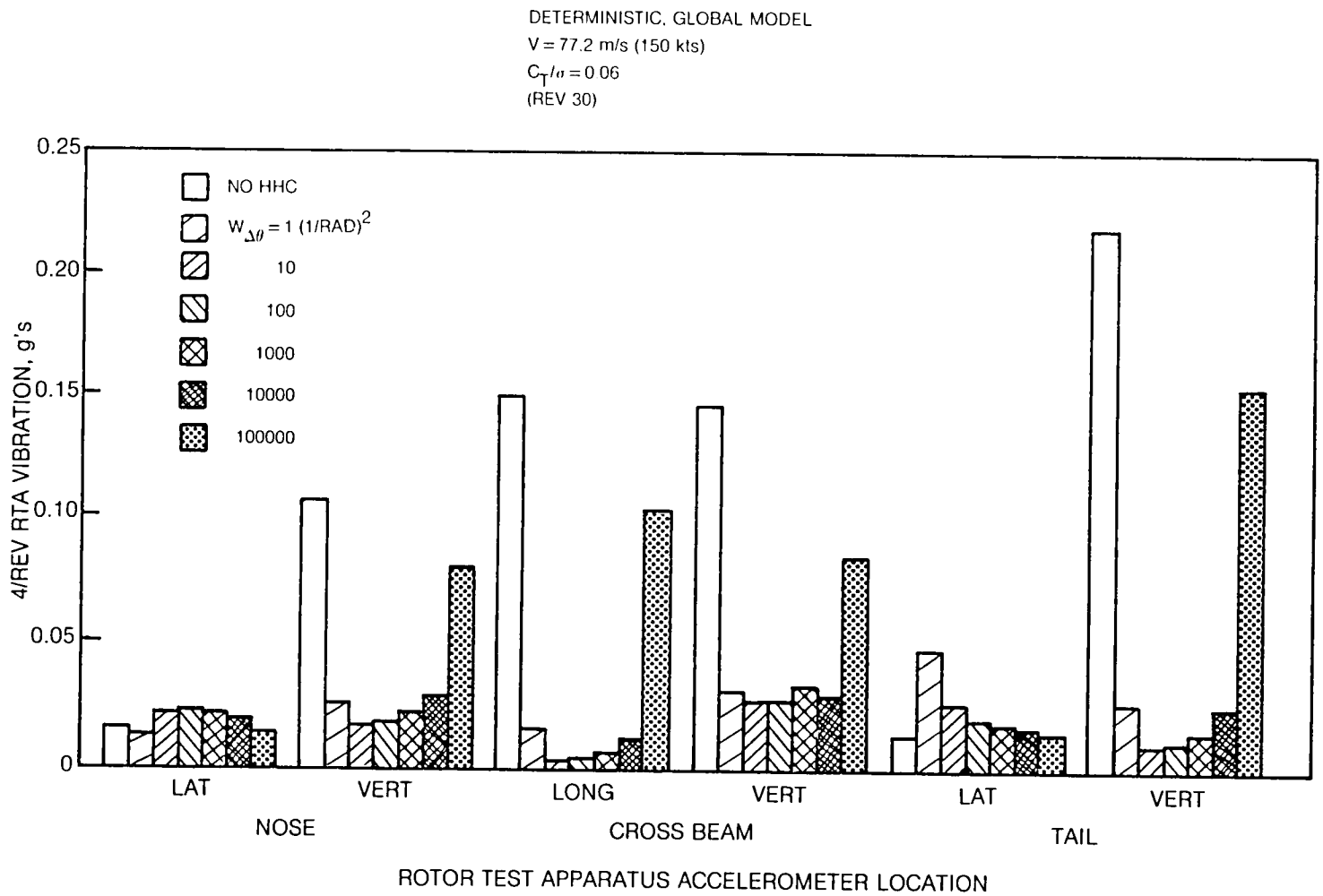

Fig. 28 Effect of Internal Rate-Limiting on Vibration Reduction

HIGH HARMONIC PITCH PHASE

$W_{\Delta\theta}$	$\angle\theta_3$	$\angle\theta_4$	$\angle\theta_5$
1	16	42	24
10	80	53	5
100	32	55	28
1000	37	74	41
10000	30	70	49
100000	26	67	47

DETERMINISTIC, GLOBAL
V = 77.2 m/s (150 kts)
$C_T/\sigma = 0.06$
(REV 30)

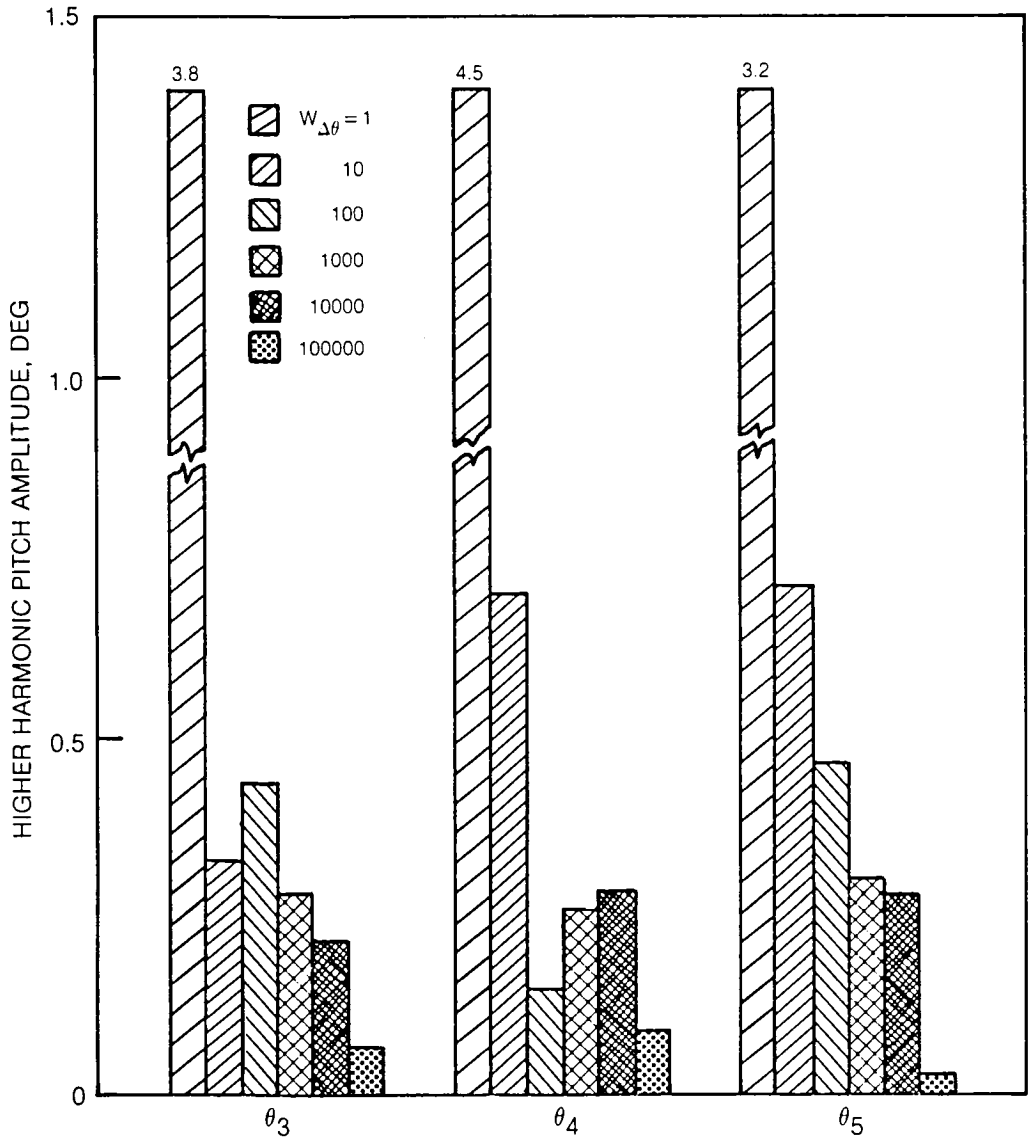

Fig. 29 Effect of Internal Rate-Limiting on Final Control Solution

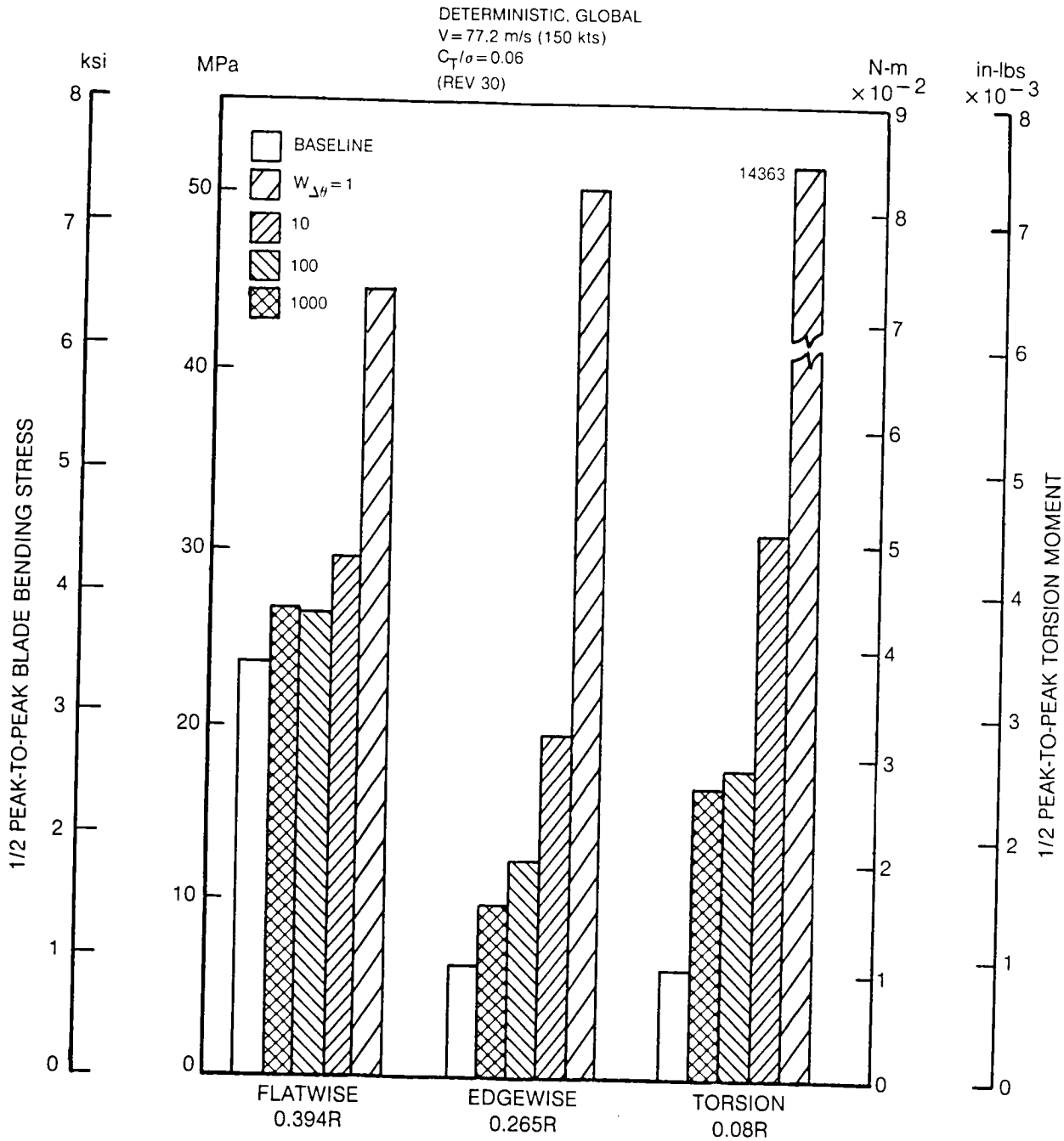

Fig. 30 Effect of Internal Rate-Limiting on Vibratory Blade Stresses and Moments

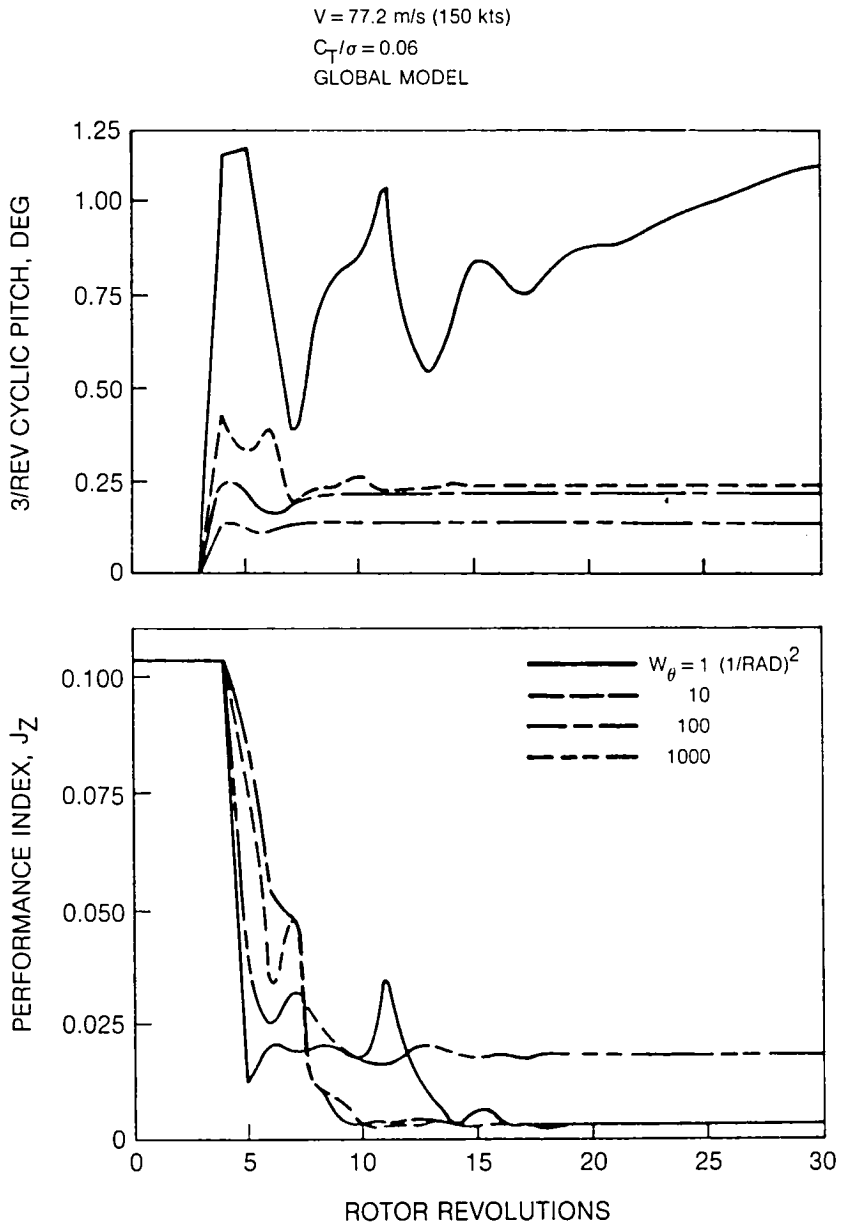

Fig. 31 Effect of Internal Limiting of Total Control Magnitude on Deterministic Controller Performance

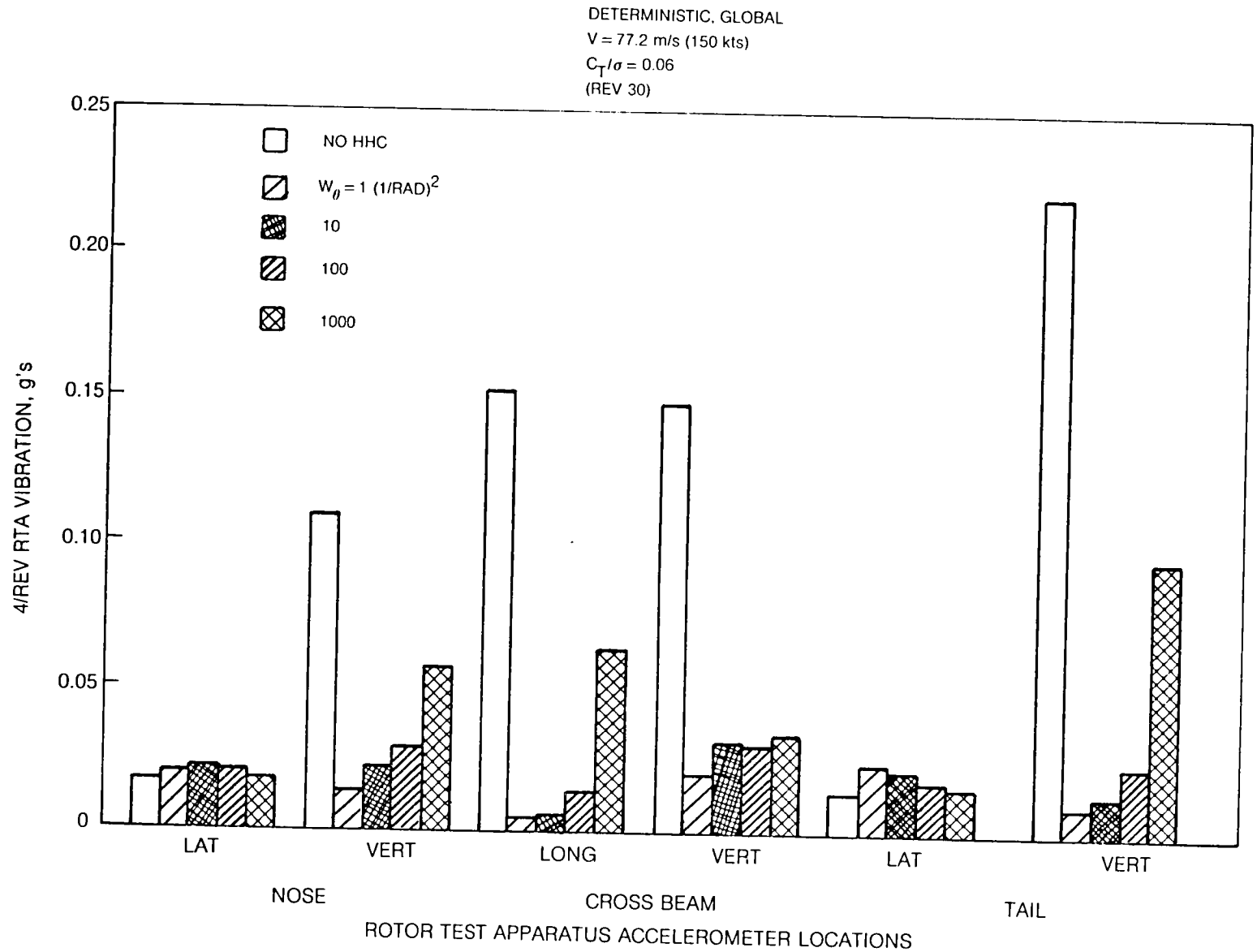

Fig. 32 Effect of Internal Total θ Limiting on Vibration Reduction

	HIGHER HARMONIC PITCH PHASE, DEG			
	W_θ	$\angle\theta_3$	$\angle\theta_4$	$\angle\theta_5$
DETERMINISTIC, GLOBAL	1	116	11	15
V = 77.2 m/s (150 kts)	10	15	41	27
$C_T/\sigma = 0.06$	100	34	73	47
(REV 30)	1000	31	71	51

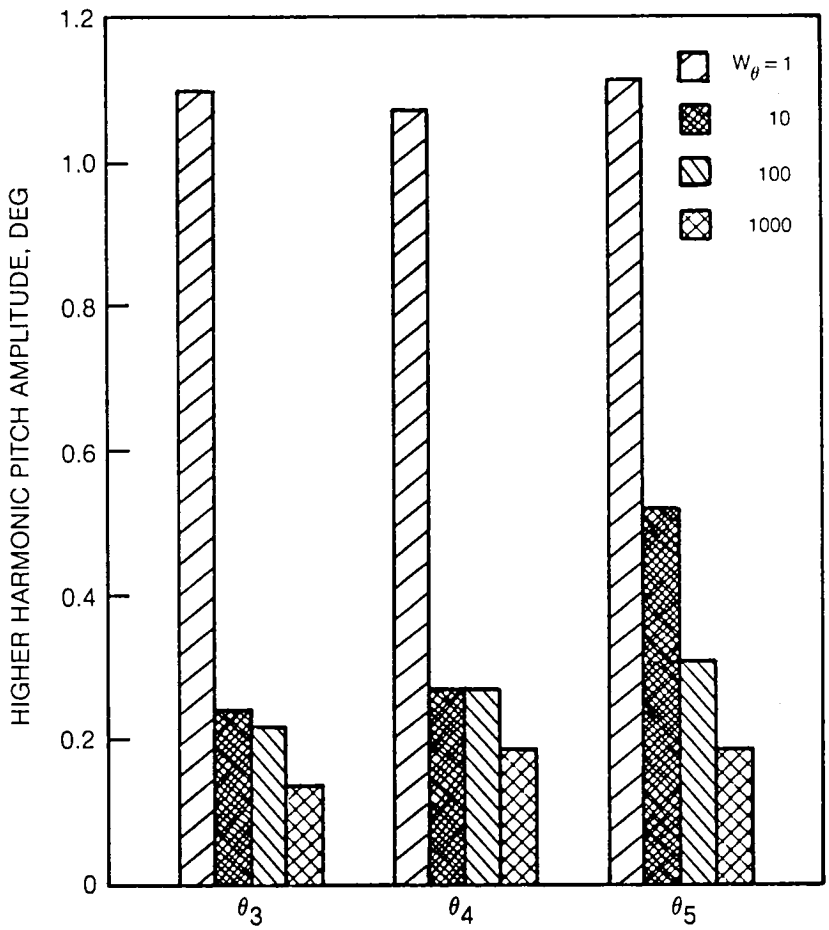

Fig. 33 Effect of Internal Total θ Limiting on Final Control Solution

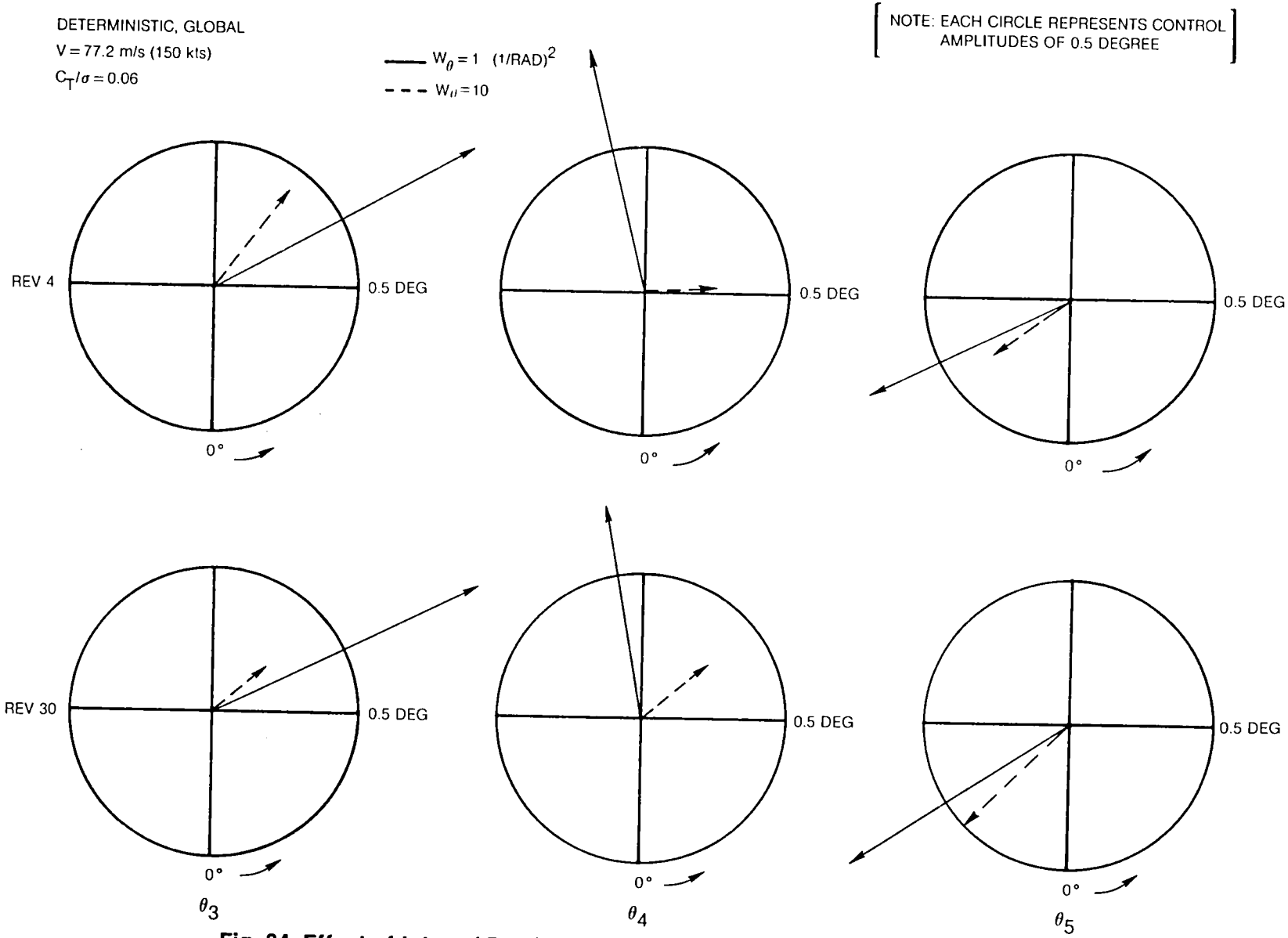

Fig. 34 Effect of Internal Total θ Limiting on Higher Harmonic Control Solution

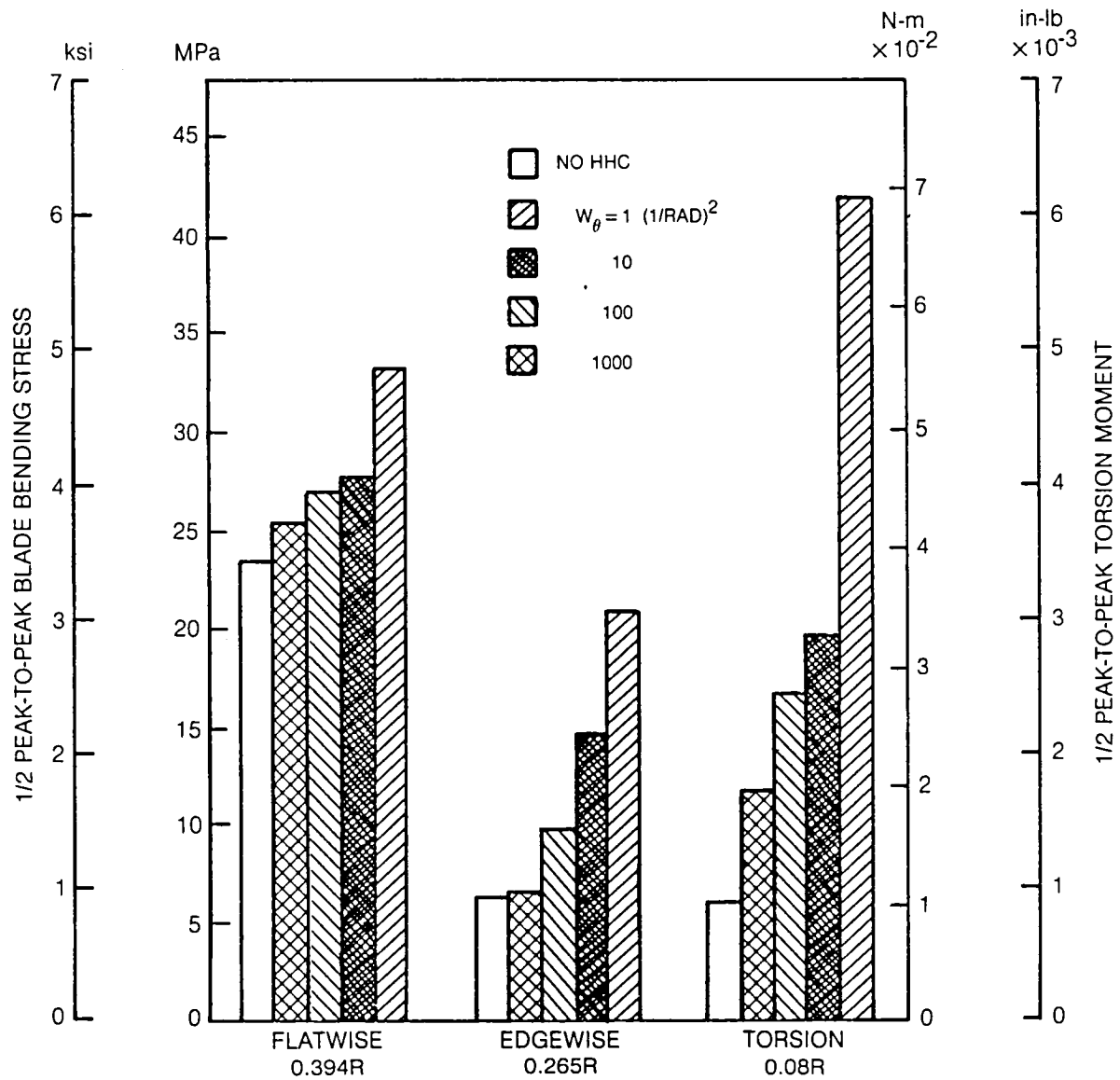

Fig. 35 Effect of Internal Total θ Limiting on Blade Stresses and Moments

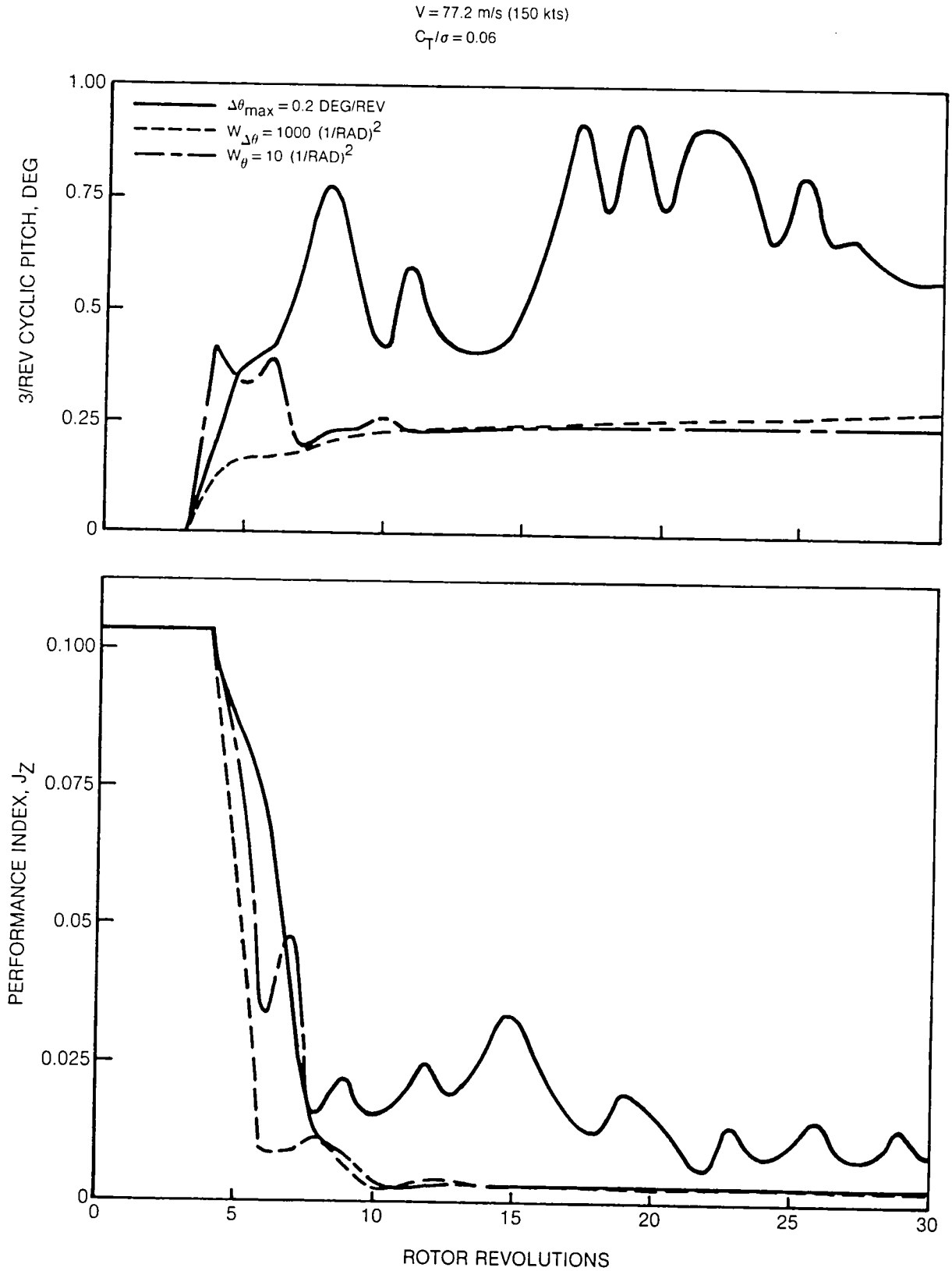

Fig. 36 Deterministic Controller Performance at Baseline Flight Condition

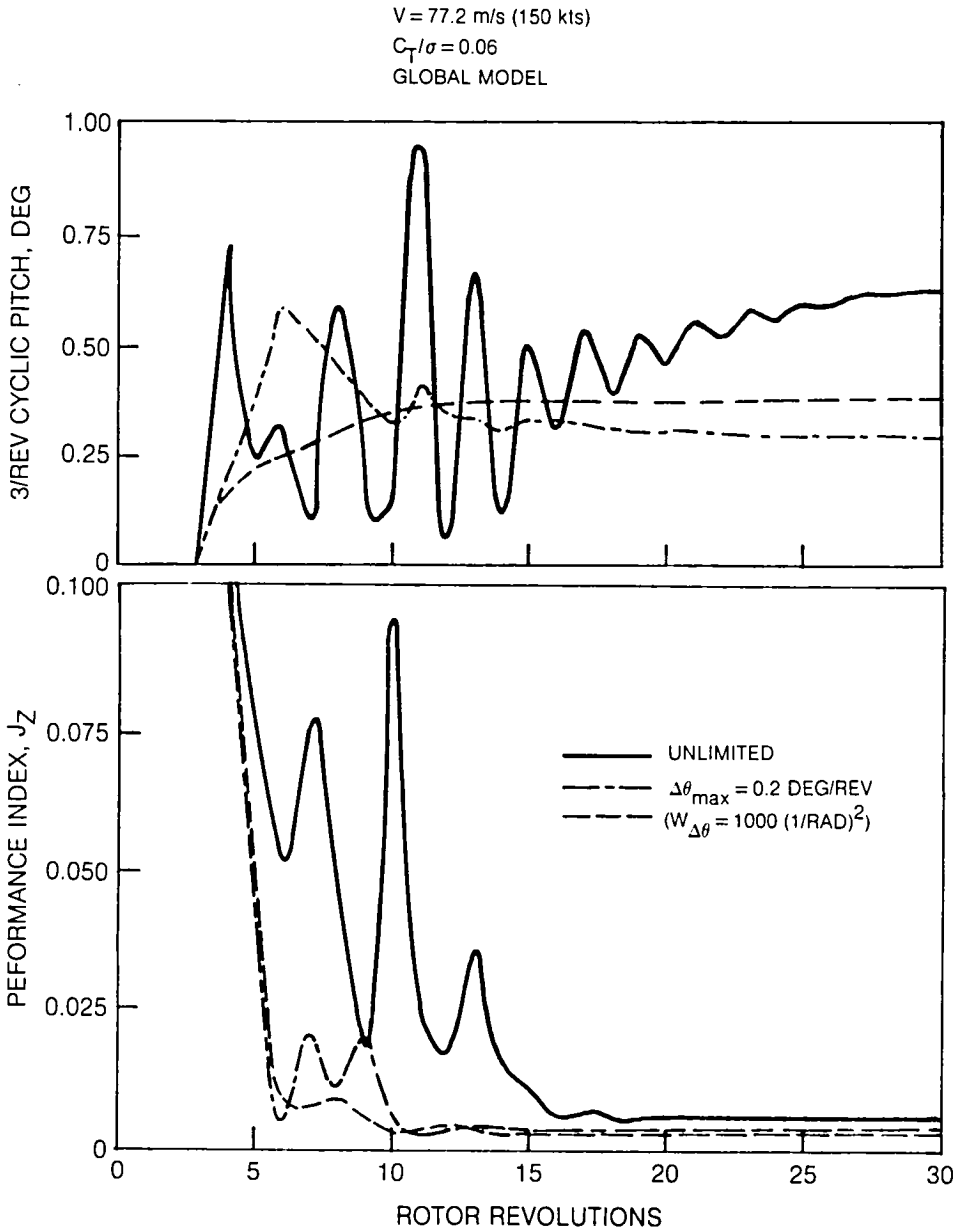

Fig. 37 Deterministic Controller Performance with No 5/Rev Control at Baseline Flight Condition

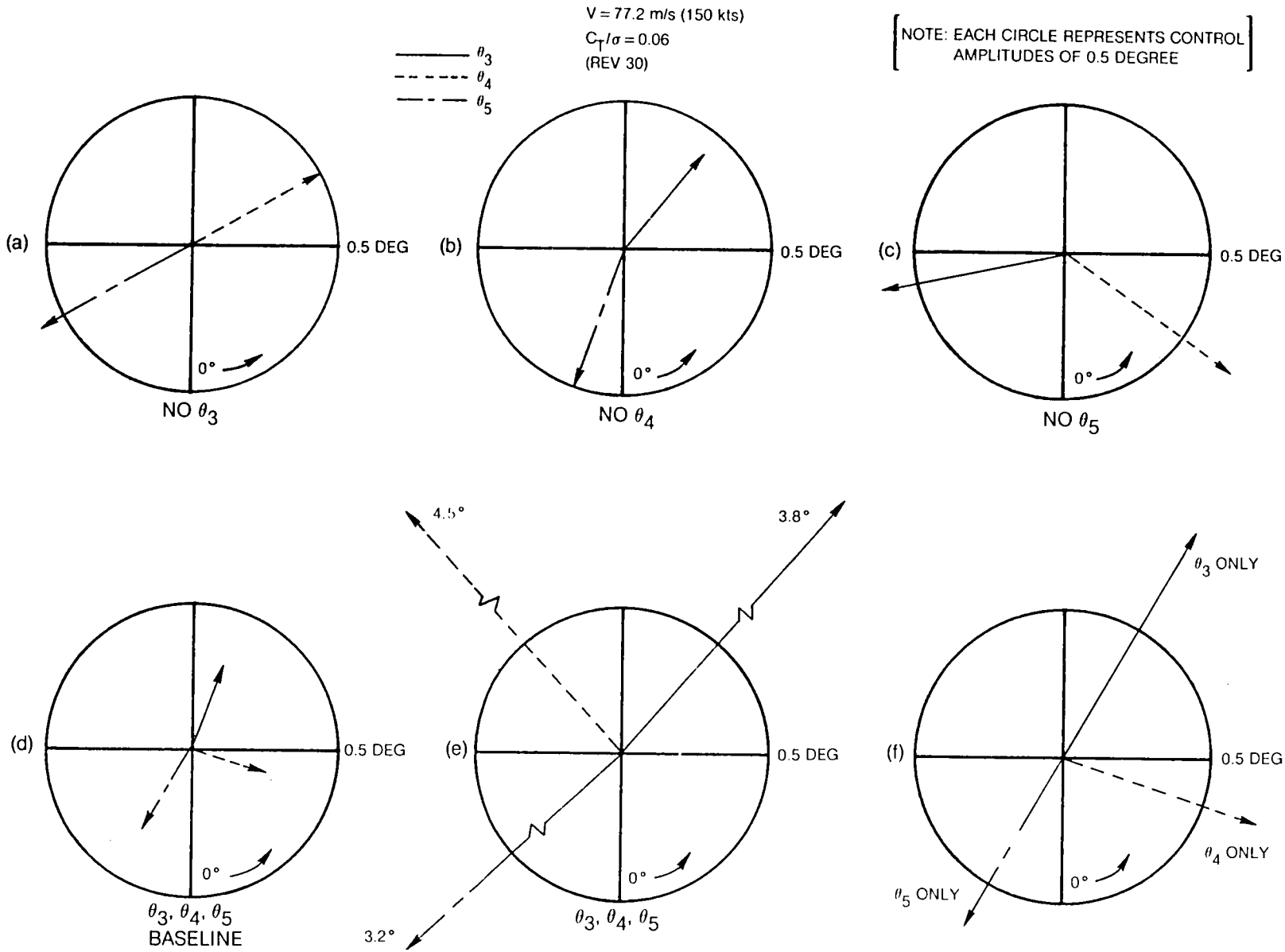

Fig. 38 Comparison of Effective Higher Harmonic Control Solutions for Baseline Flight Condition

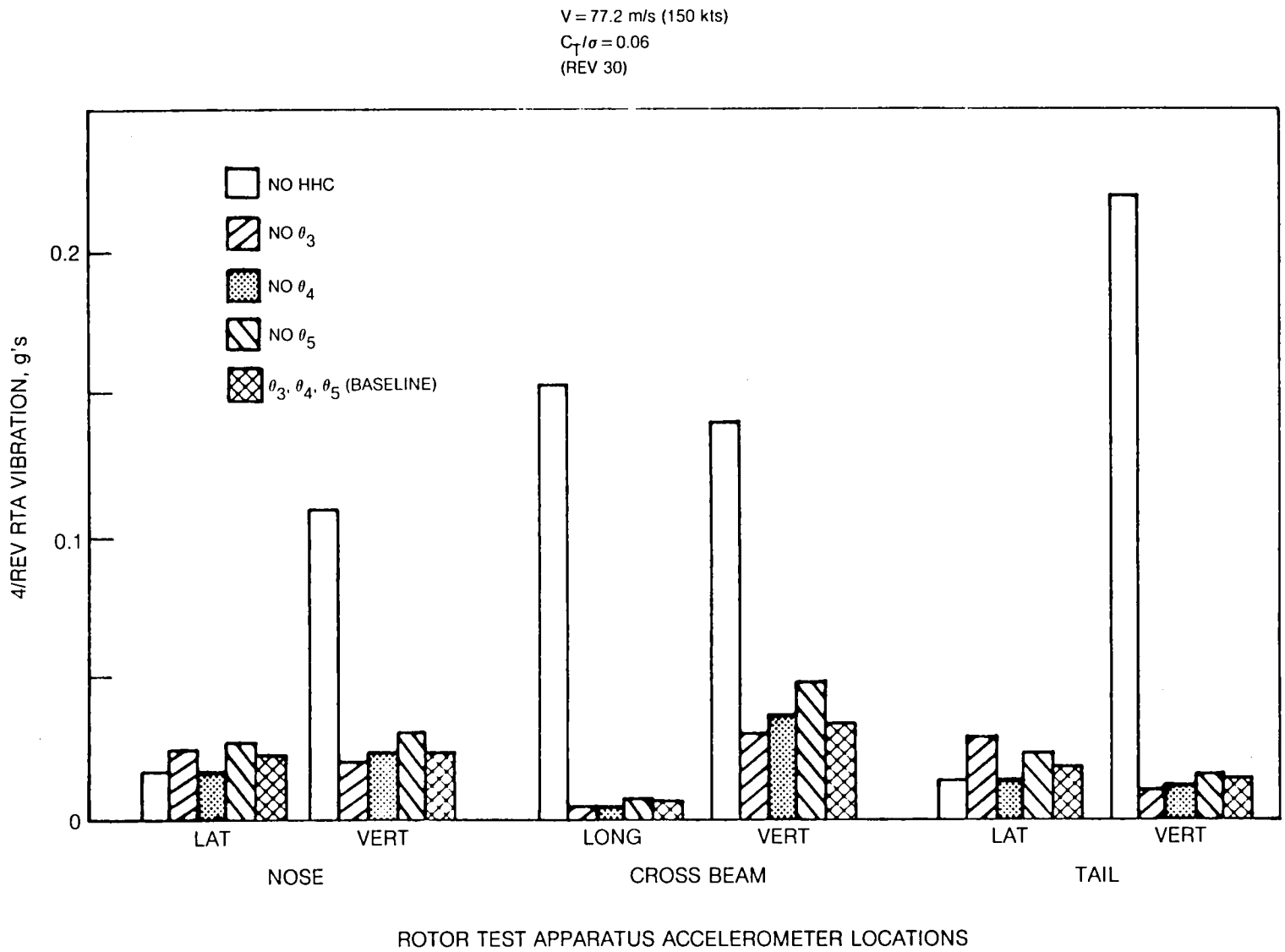

Fig. 39 Comparison of Vibration Reduction for Different Control Solutions at Baseline Flight Condition

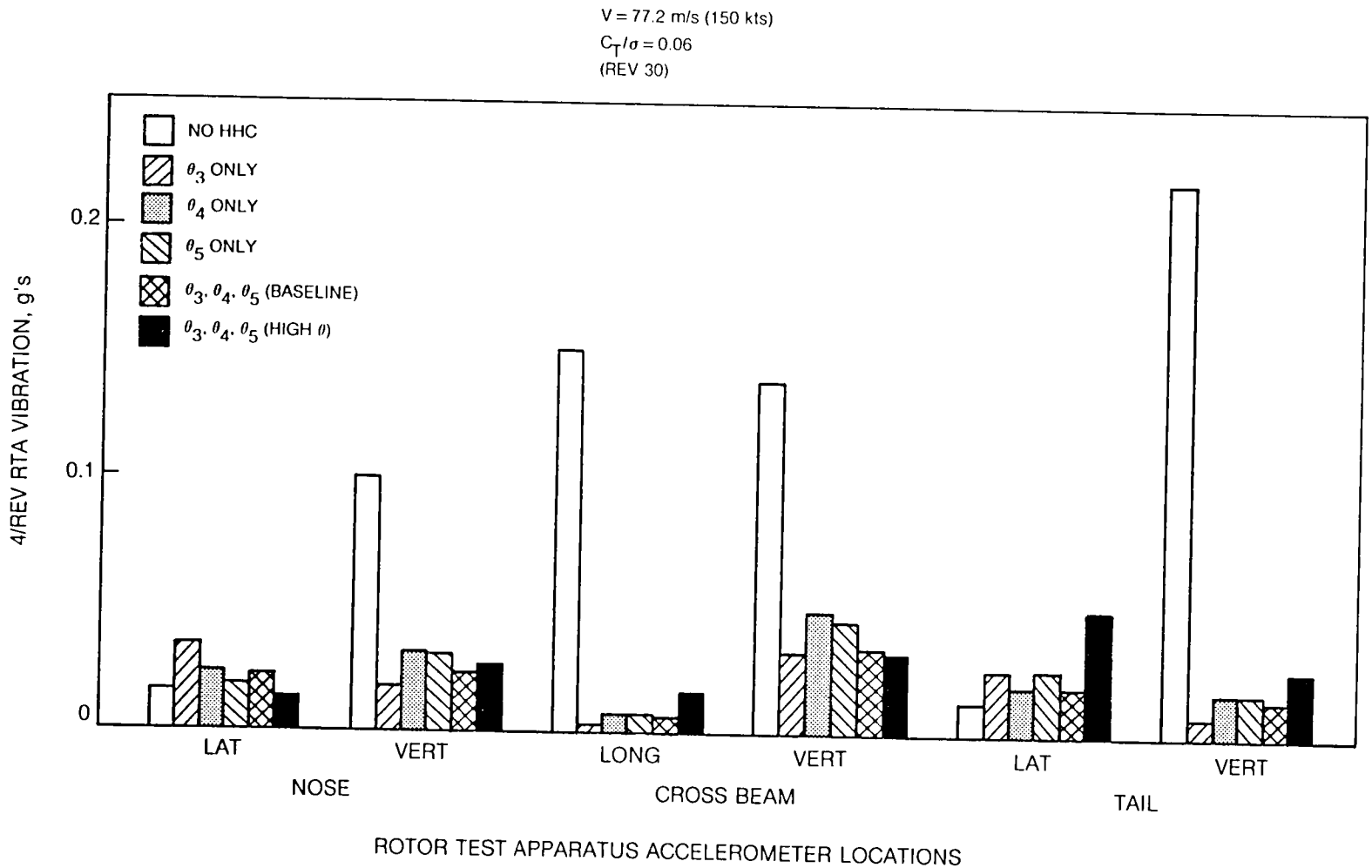

Fig. 40 Comparison of Vibration Reduction for Different Control Solutions at Baseline Flight Condition

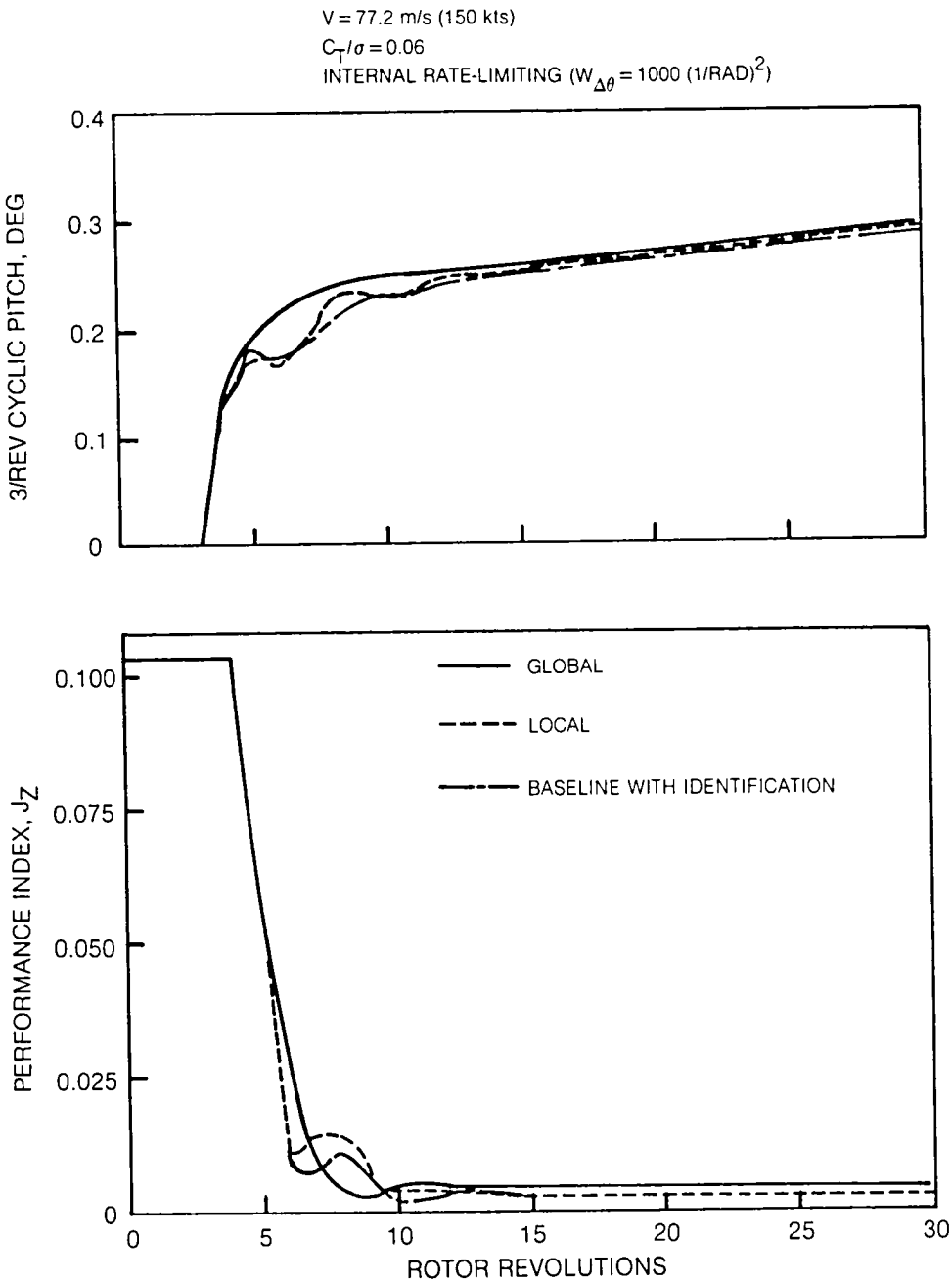

Fig. 41 Deterministic Controller Performance with System Identification Inhibited by Low Kalman Filter Gains

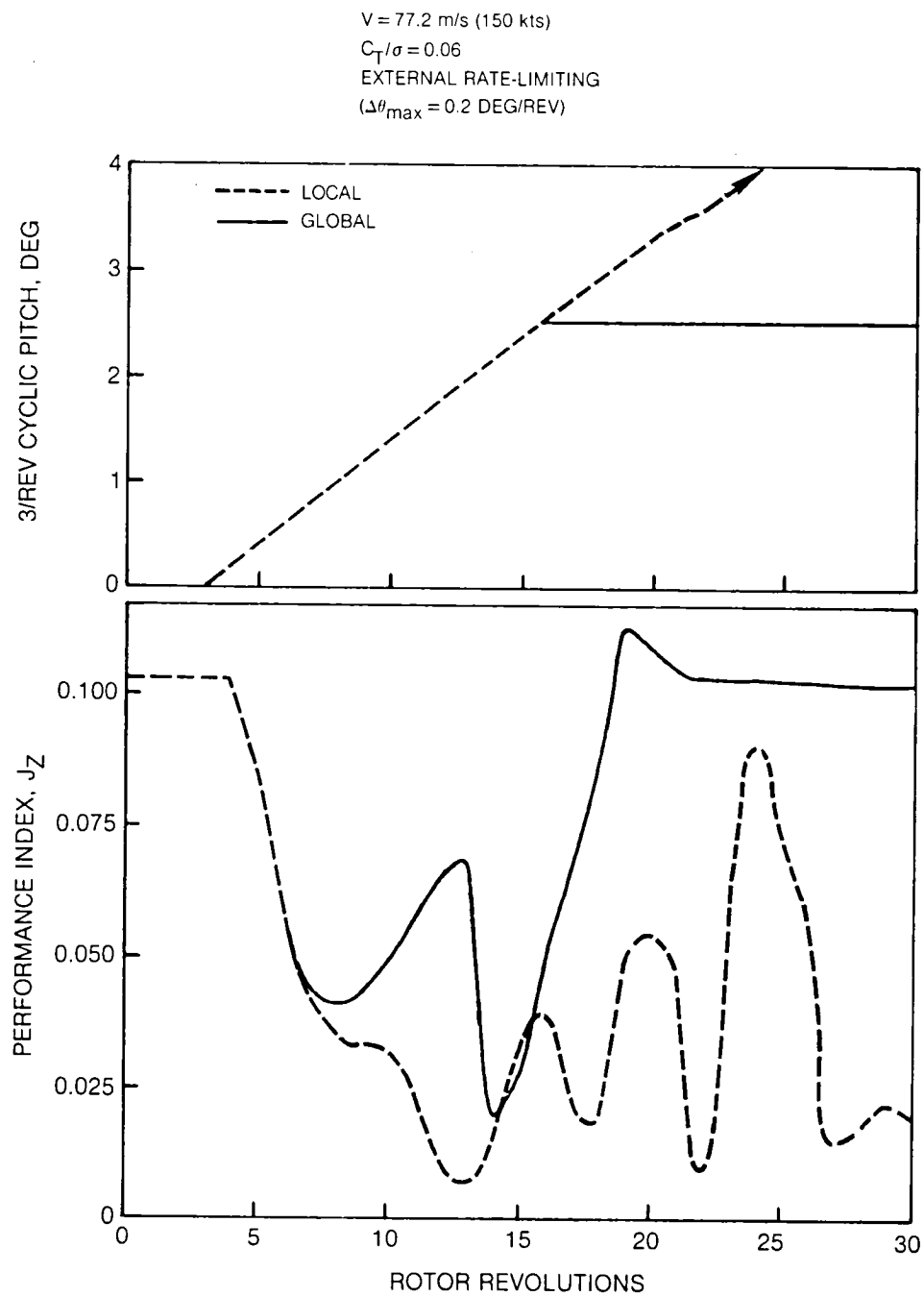

Fig. 42 Deterministic Controller Performance with System Identification Inhibited by Low Kalman Filter Gains

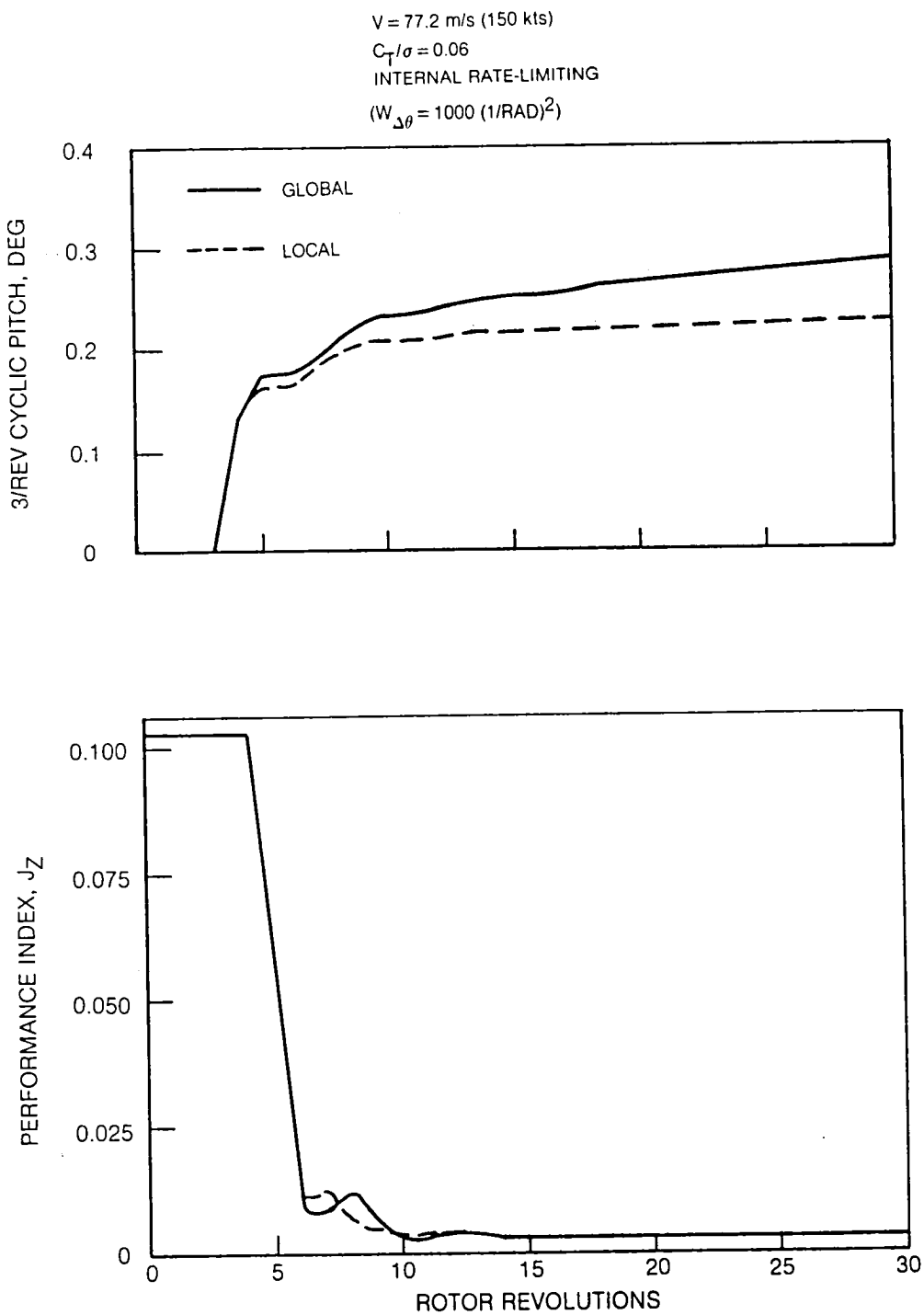

Fig. 43 Comparison of Deterministic Controller Performance with Local and Global System Models

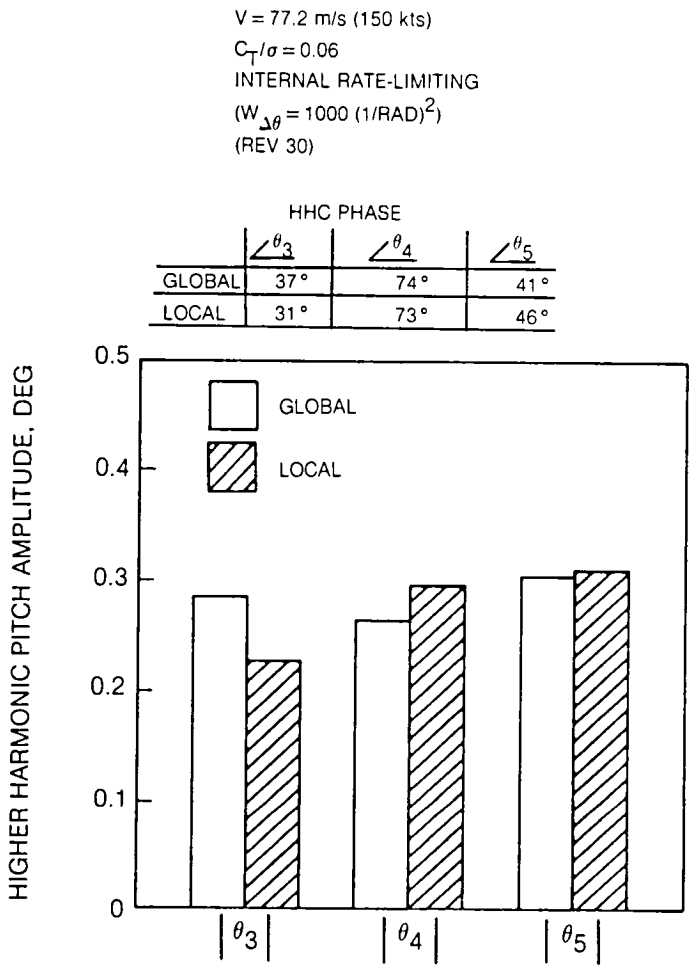

Fig. 44 Comparison of Deterministic Controller Performance with Local and Global System Models

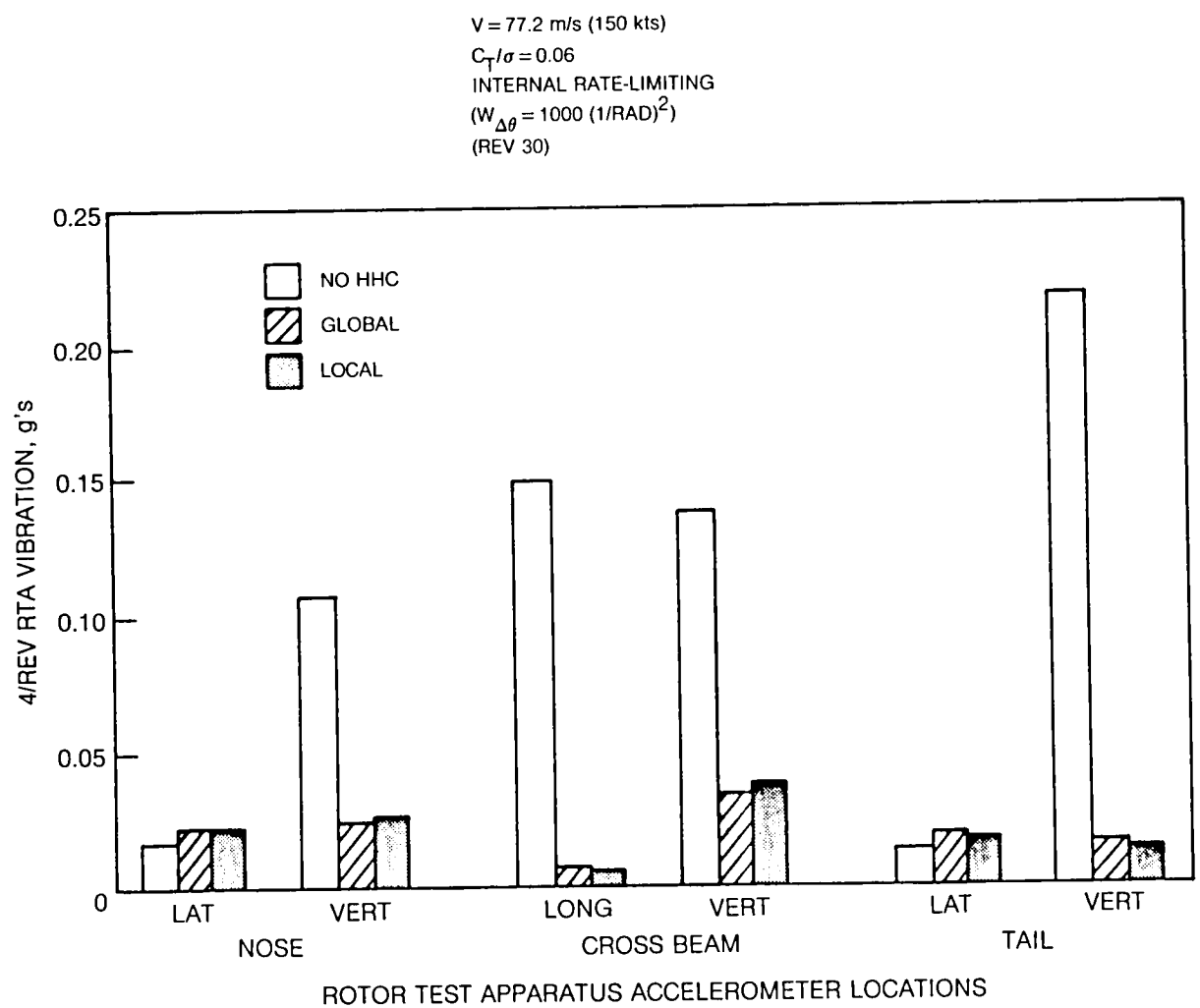

Fig. 45 Comparison of Deterministic Controller Performance with Local and Global System Models

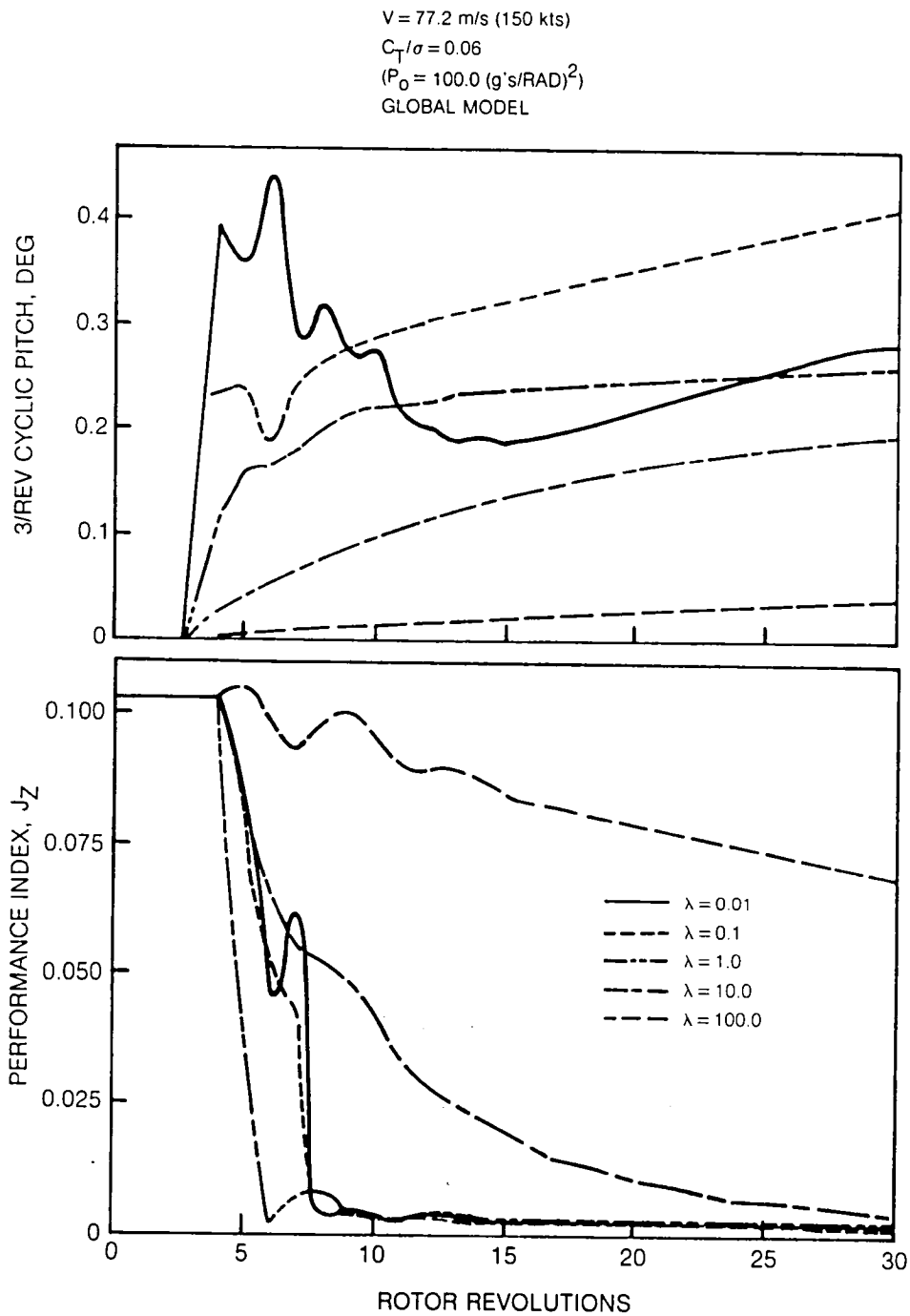

Fig. 46 Effect of Stochastic Control Constant on Cautious Controller Performance at Baseline Flight Condition

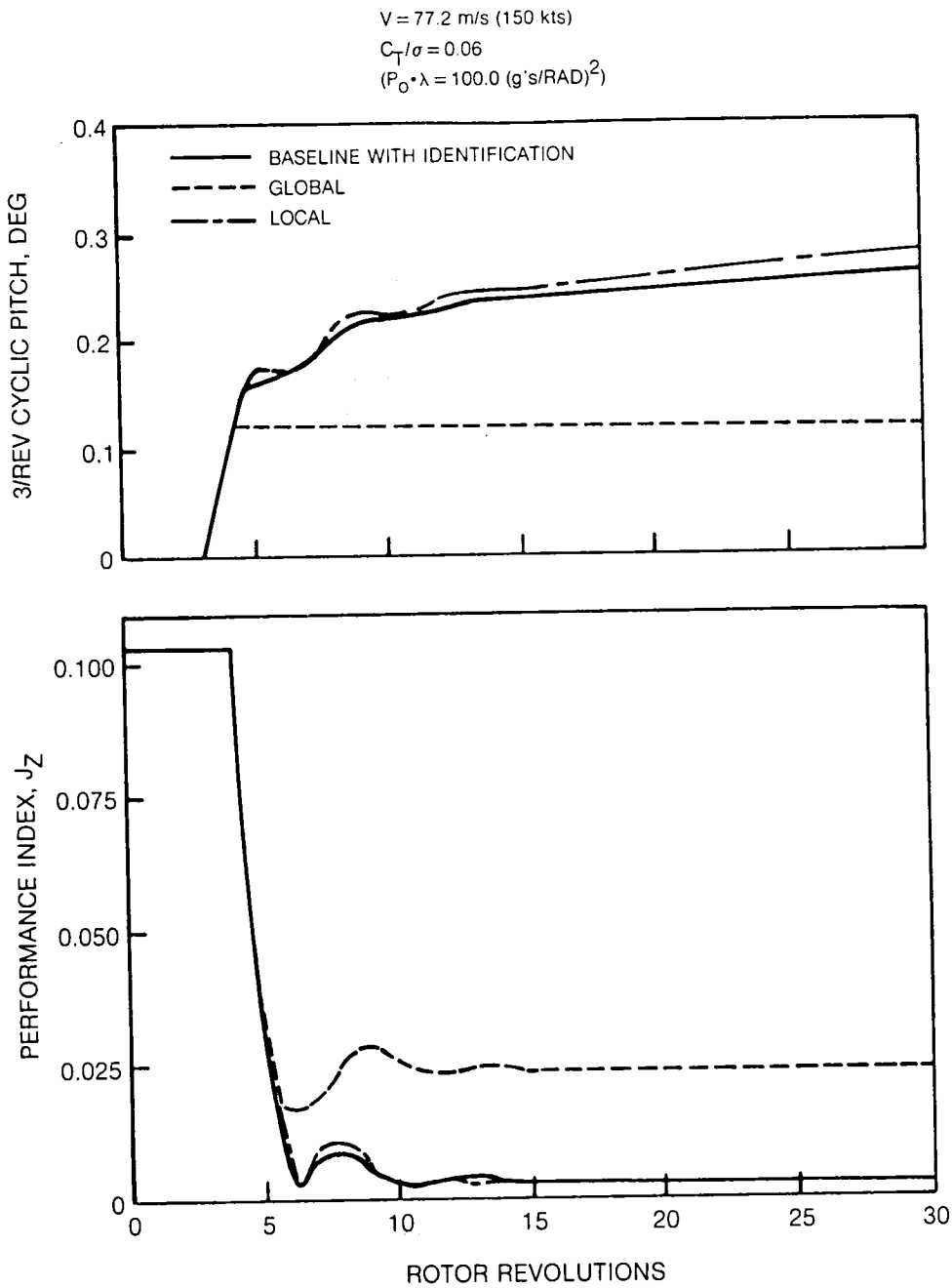

Fig. 47 Cautious Controller Performance with System Identification Inhibited by Low Kalman Filter Gains

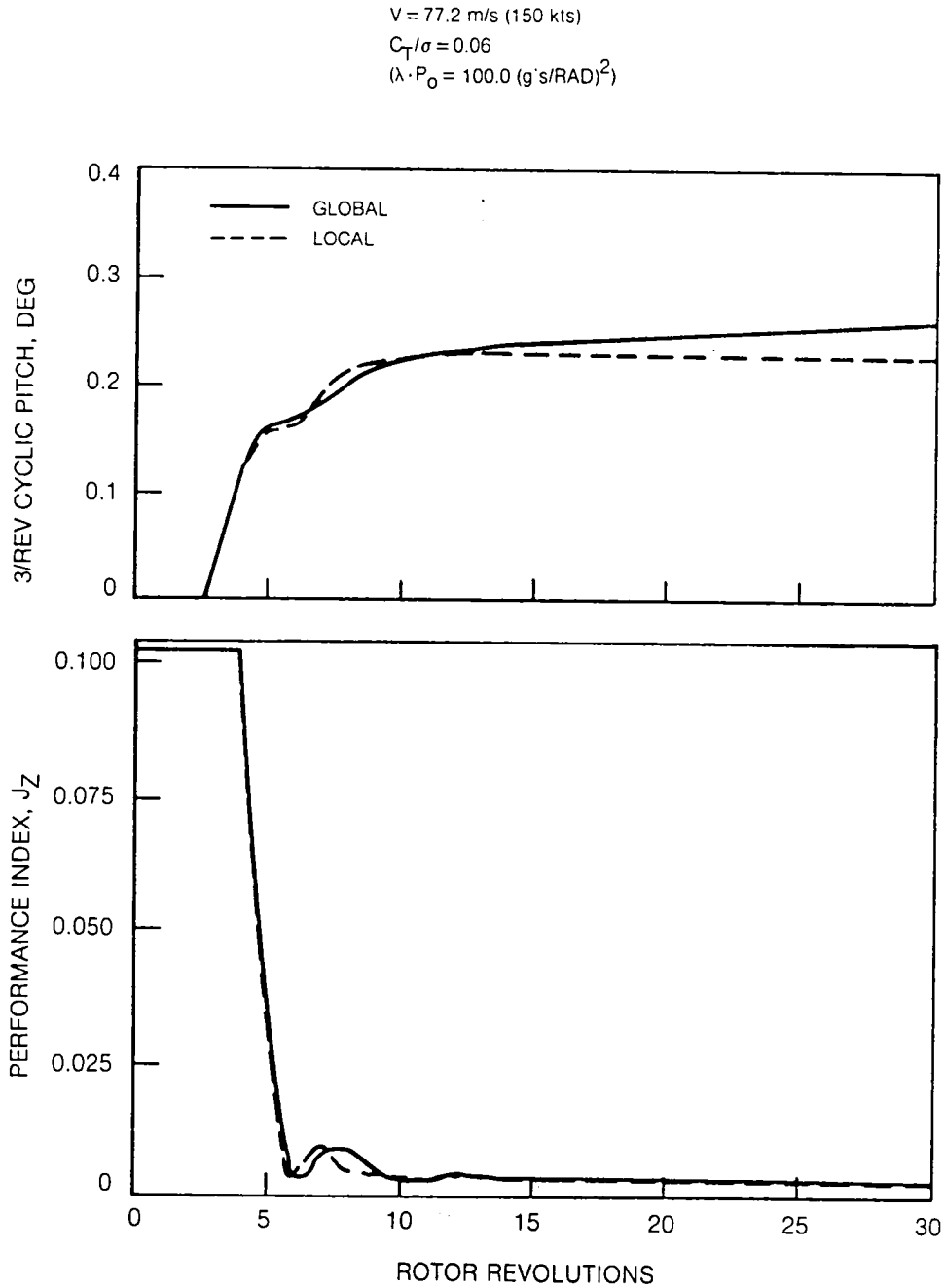

Fig. 48 Comparison of Cautious Controller Performance with Local and Global System Models

V = 77.2 m/s (150 kts)
$C_T/\sigma = 0.06$
$(\lambda \cdot P_0 = 100.0\ (g \cdot s/RAD)^2)$
(REV 30)

HHC PHASE

	θ_3	θ_4	θ_5
GLOBAL	34°	72°	44°
LOCAL	31°	71°	48°

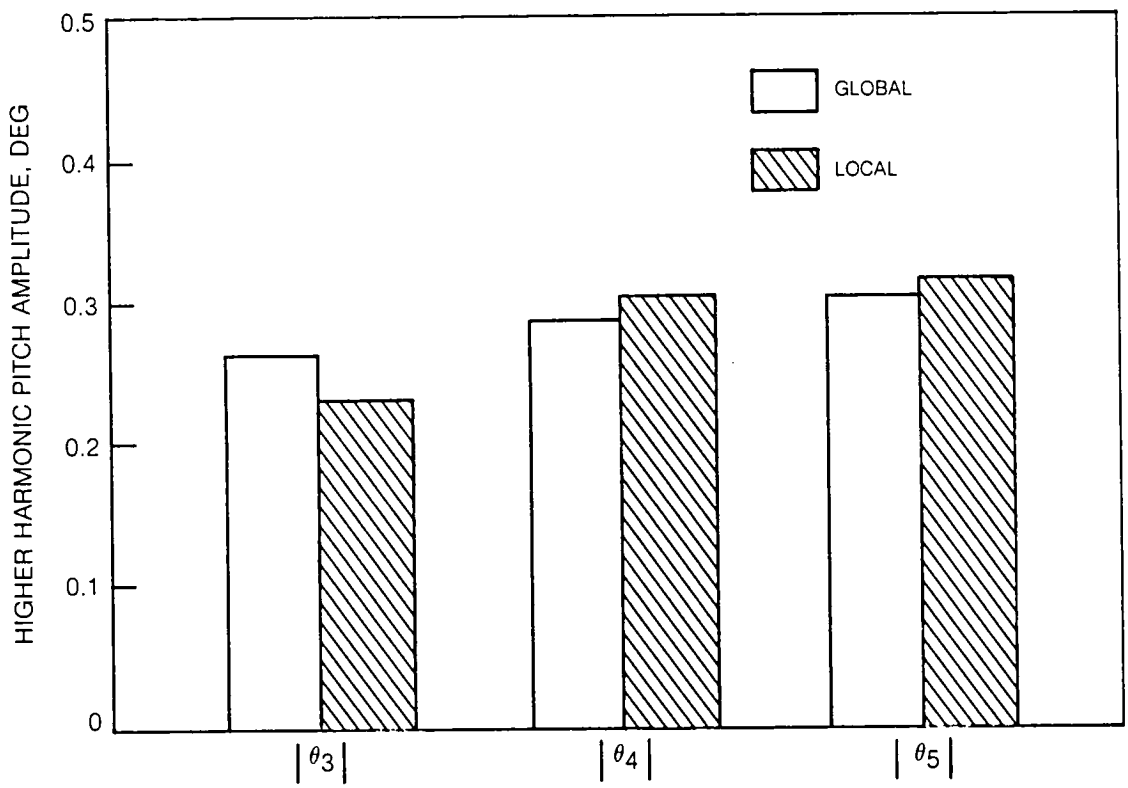

Fig. 49 Comparison of Cautious Controller Performance with Local and Global System Models

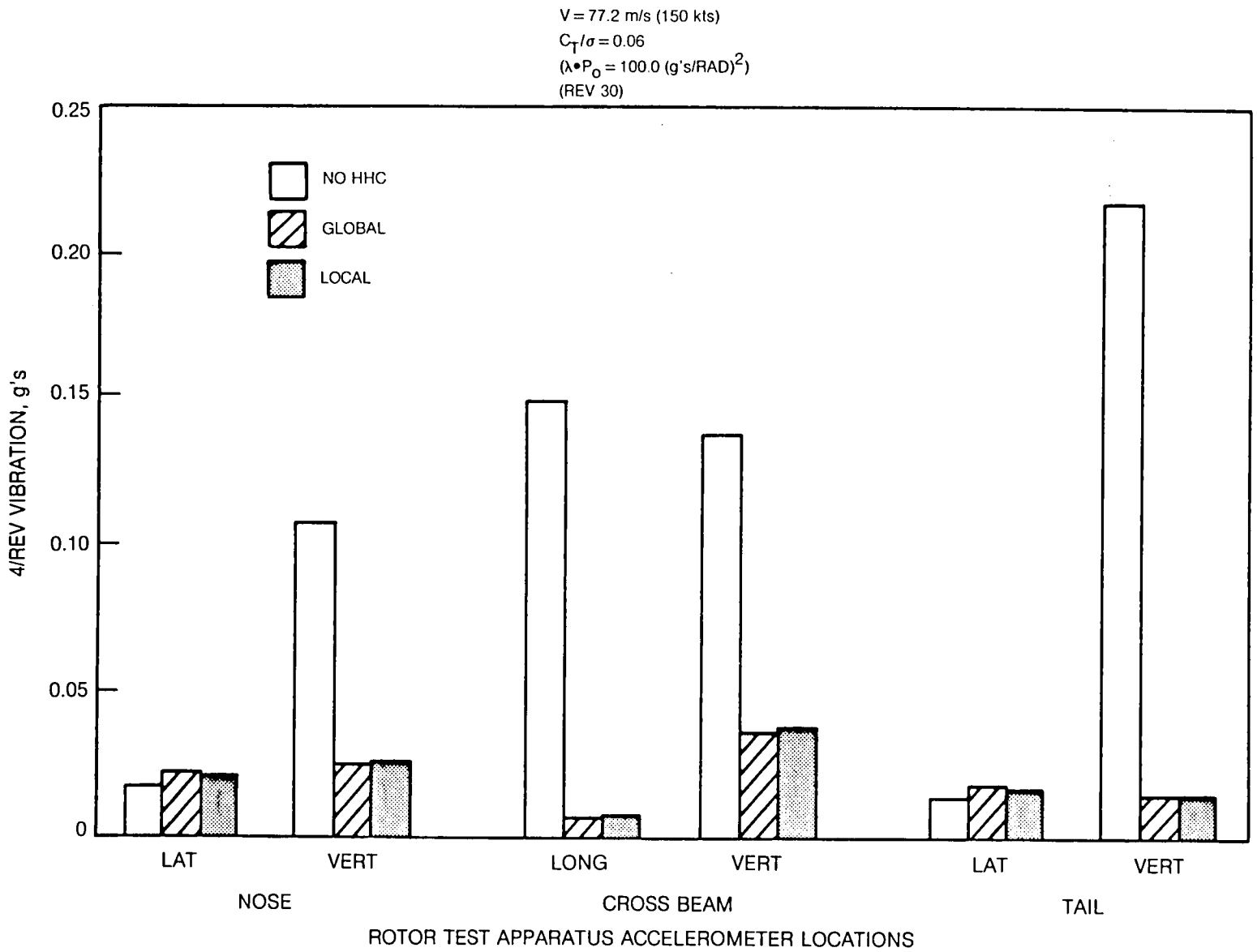

Fig. 50 Comparison of Cautious Controller Performance with Local and Global System Models

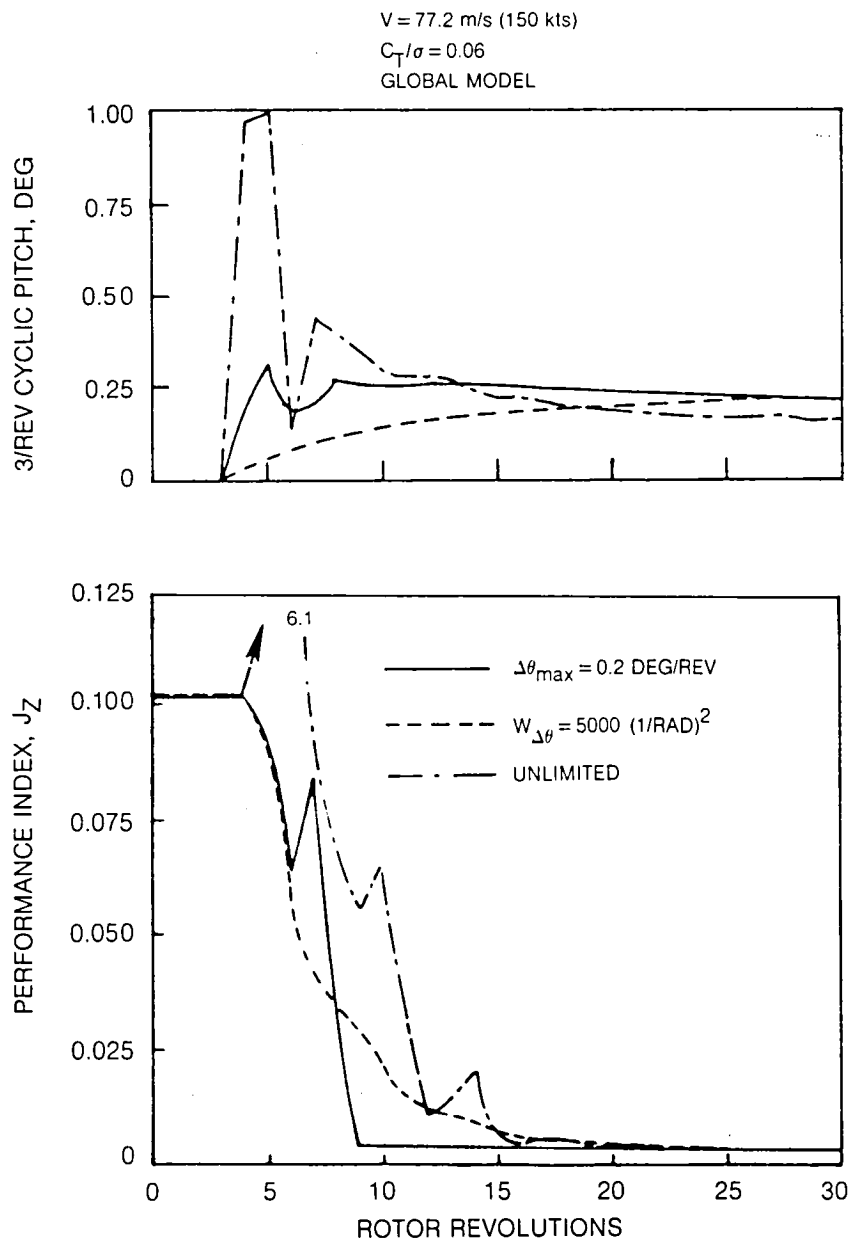

Fig. 51 Effect of Rate-Limiting on Dual Controller Performance at Baseline Flight Condition

V = 77.2 m/s (150 kts)
$C_T/\sigma = 0.06$
GLOBAL MODEL
(REV 30)

HHC PHASE

	$\angle\theta_3$	$\angle\theta_4$	$\angle\theta_5$
$\Delta\theta_{max}$	19°	67°	56°
$W_{\Delta\theta}$	32°	70°	47°
UNLIMITED	13°	64°	59°

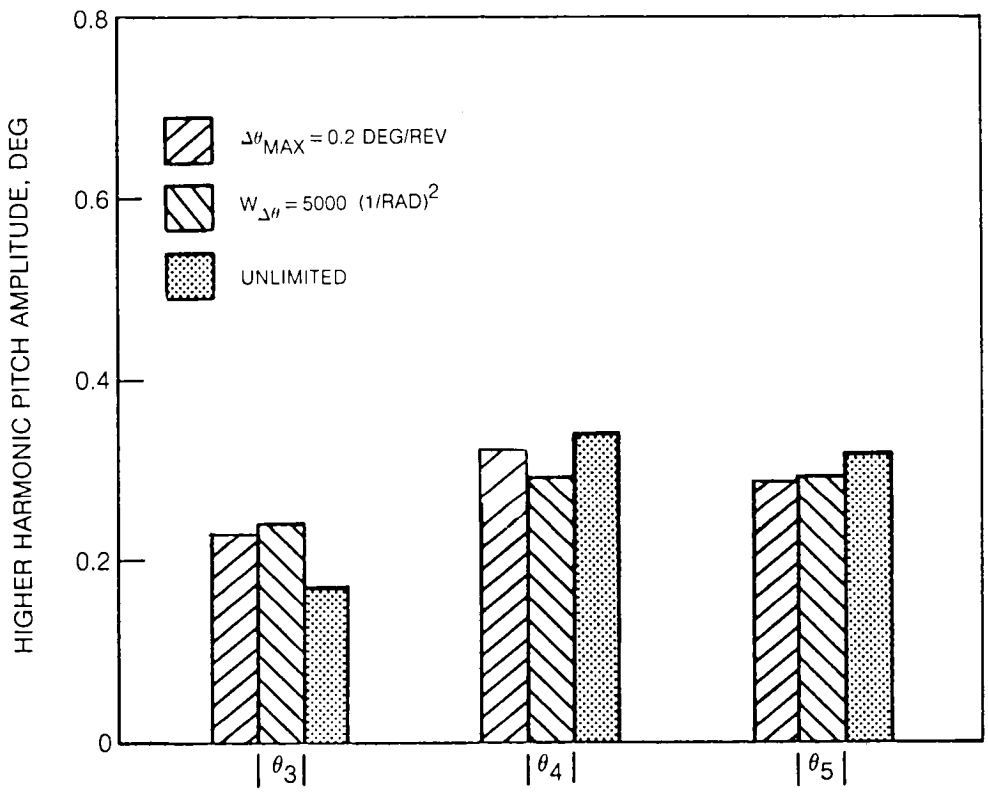

Fig. 52 Effect of Rate-Limiting on Final Control Solution Commanded by Dual Controller

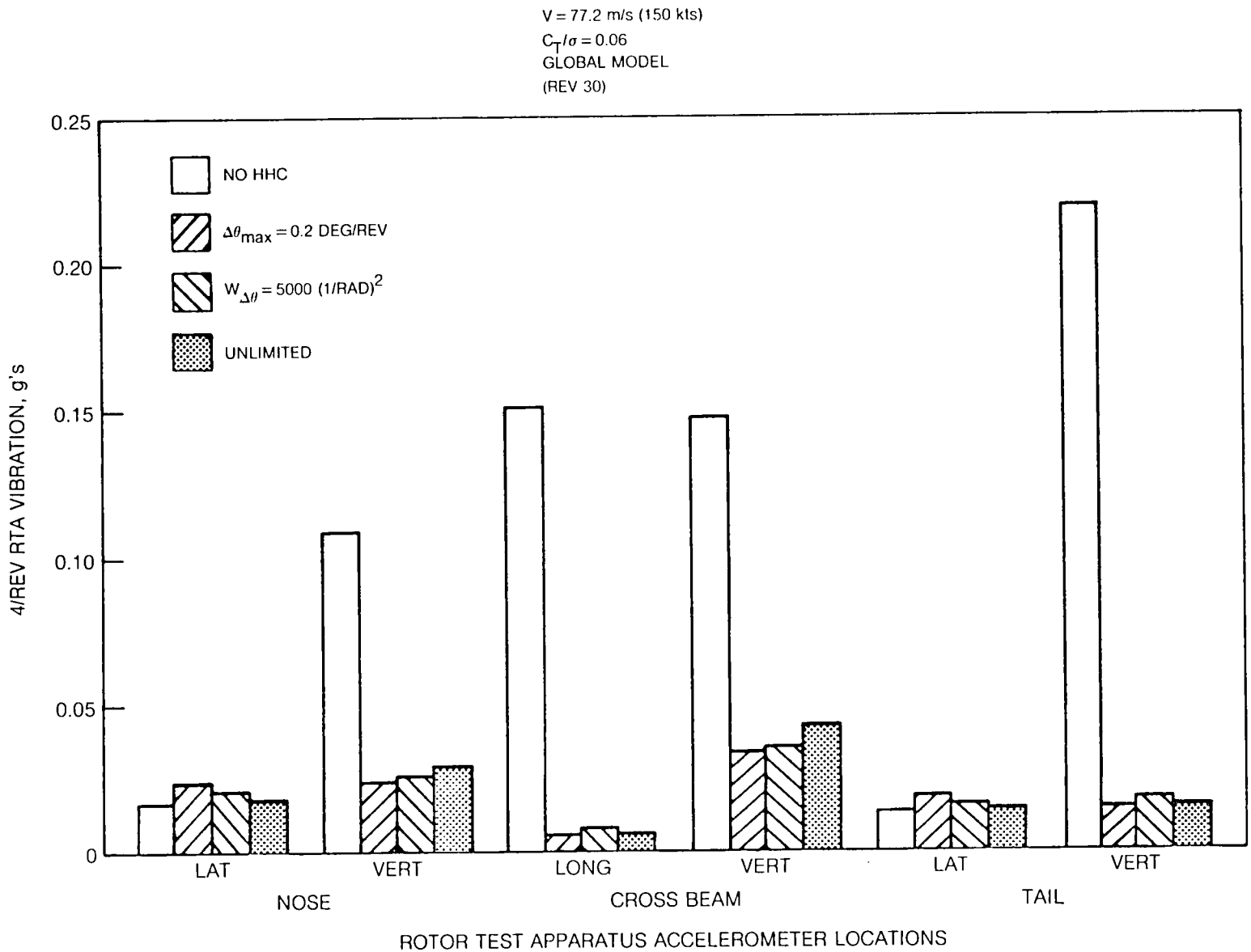

Fig. 53 Effect of Rate-Limiting on Dual Controller Performance

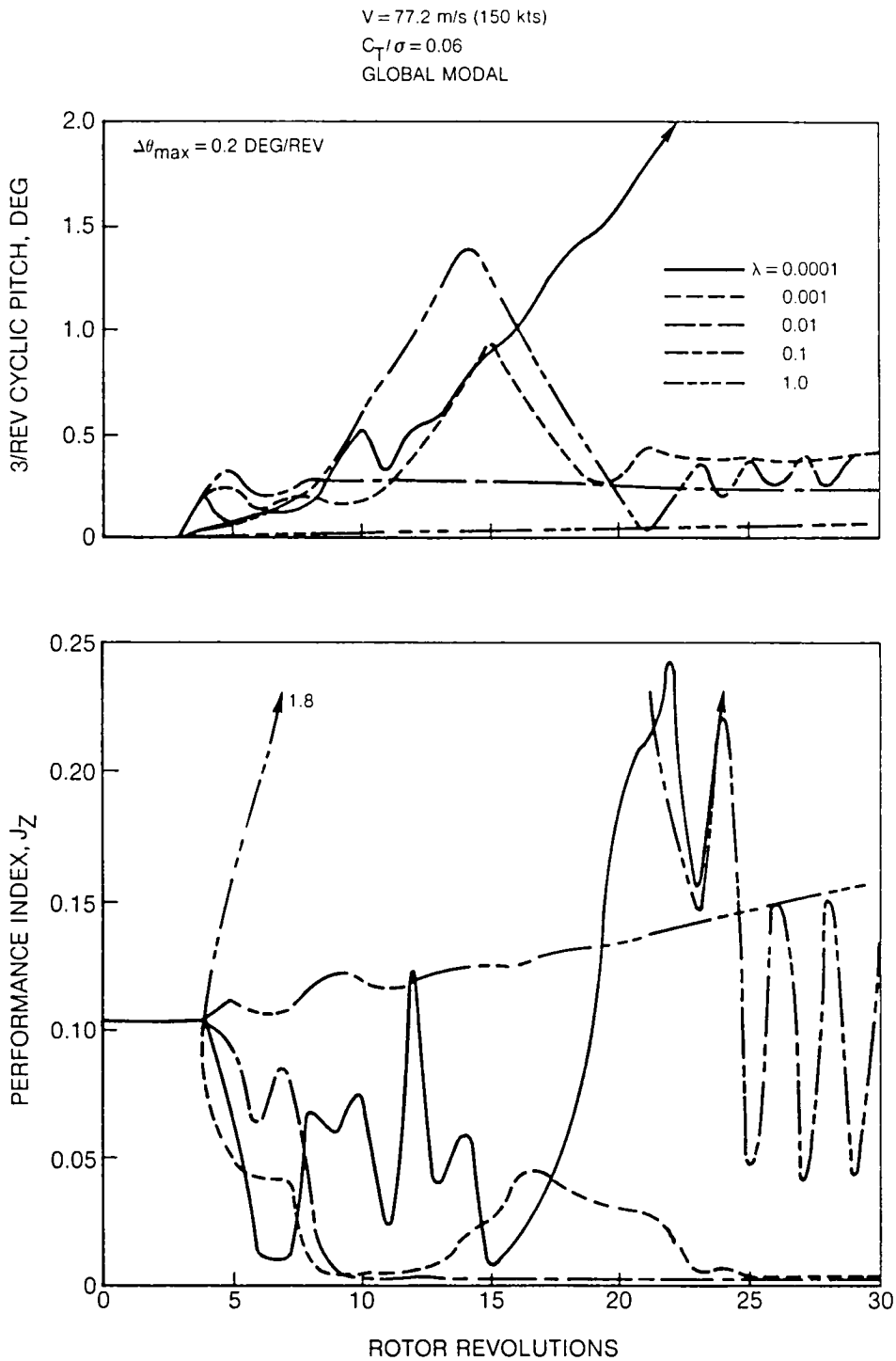

Fig. 54 Effect of Stochastic Control Constant on Dual Controller Performance at Baseline Flight Condition

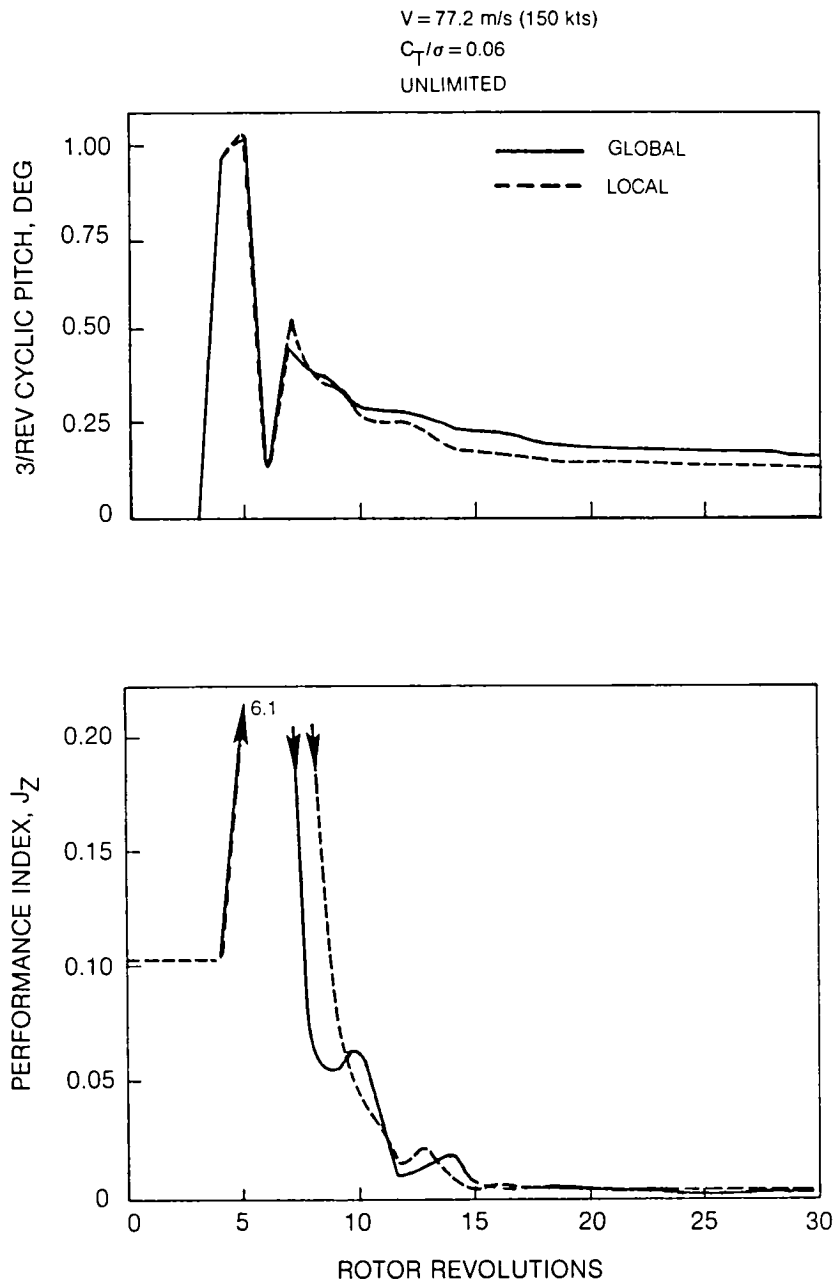

Fig. 55 Comparison of Dual Controller Performance with Local and Global System Models (No Limiting on Control Inputs)

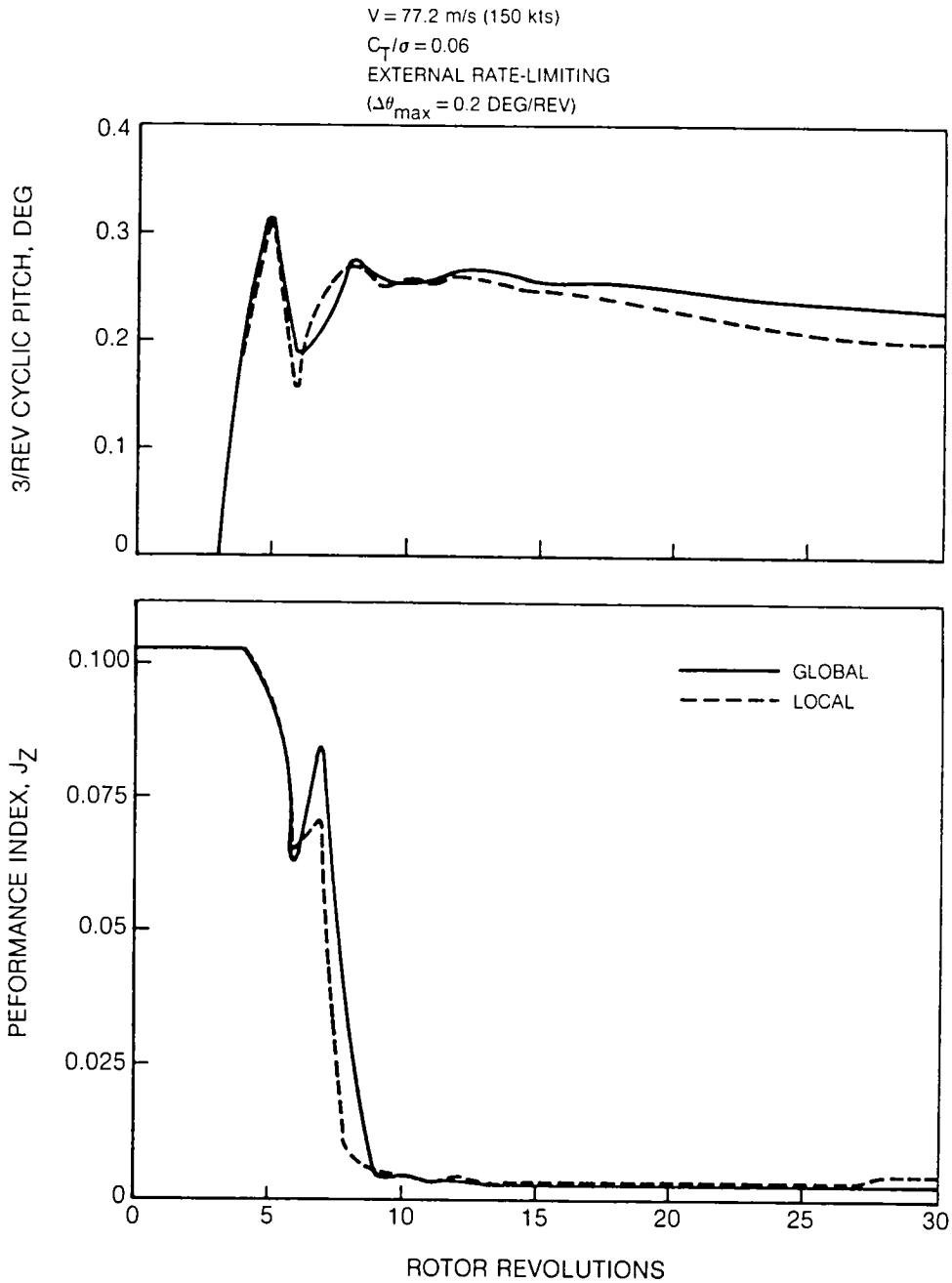

Fig. 56 Comparison of Dual Controller Performance with Local and Global System Models (External Rate-Limiting)

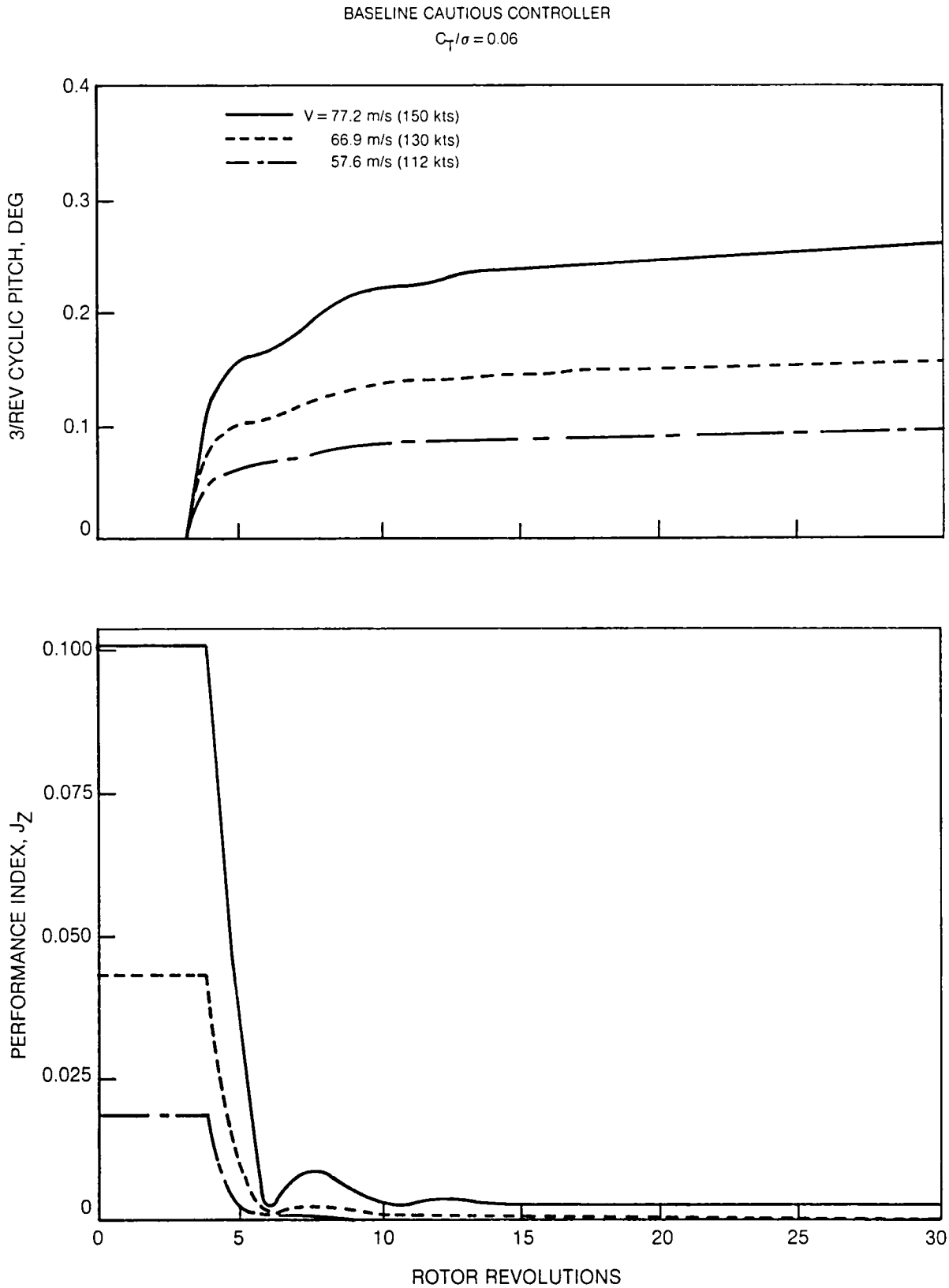

Fig. 57 Effect of Forward Velocity on Controller Performance

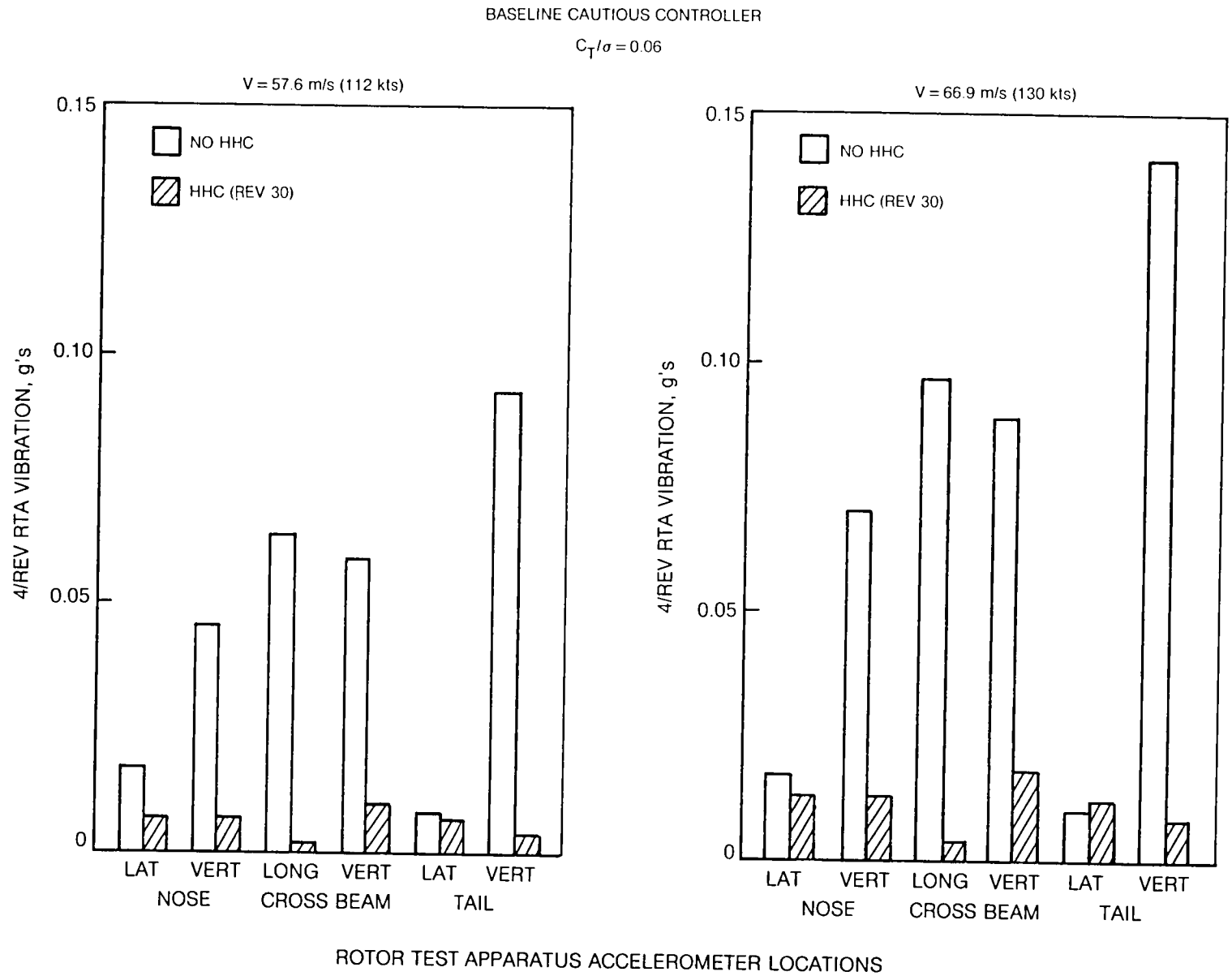

Fig. 58 Effect of Forward Velocity on Controller Performance

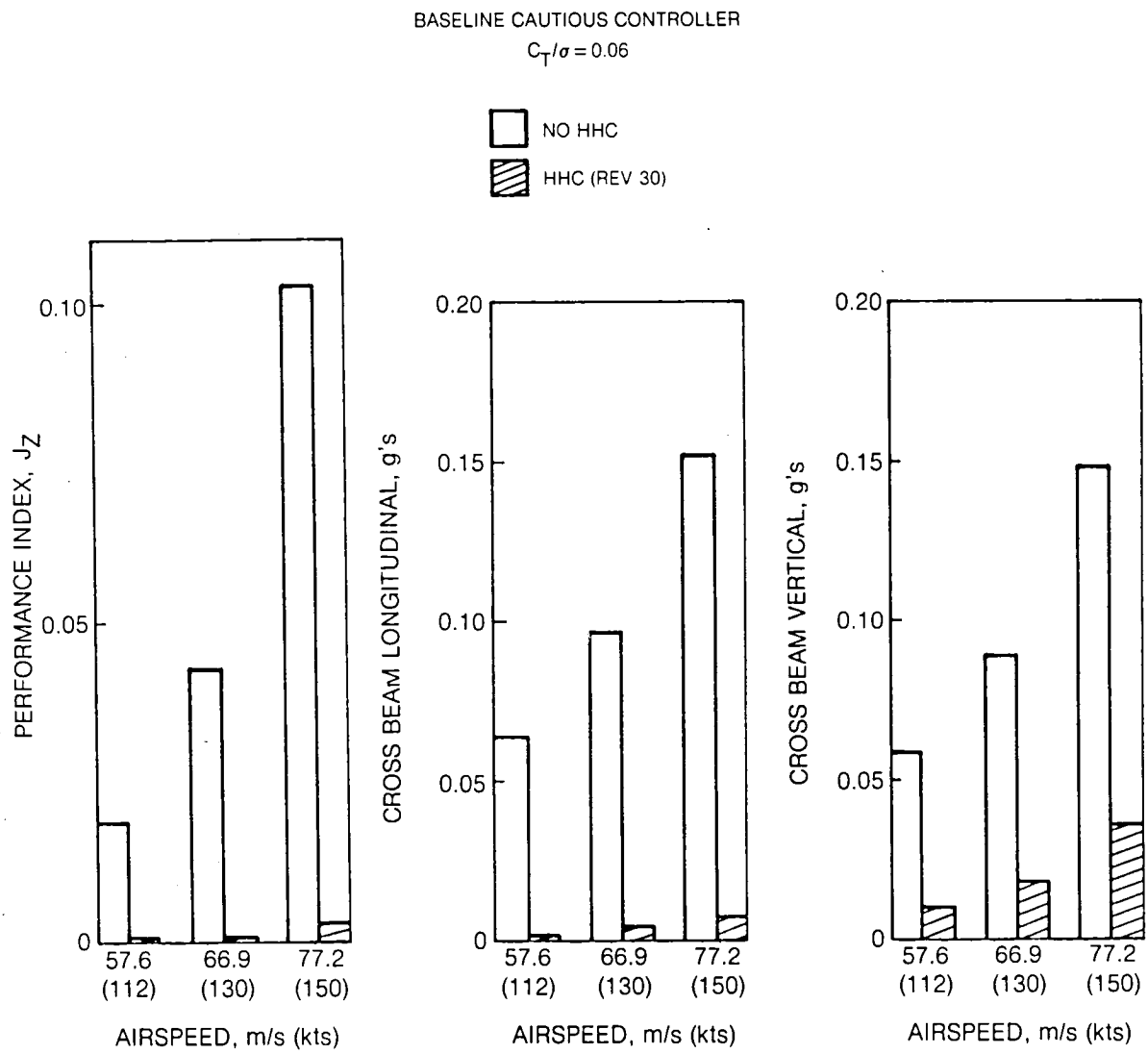

Fig. 59 Effect of Forward Velocity on Controller Performance

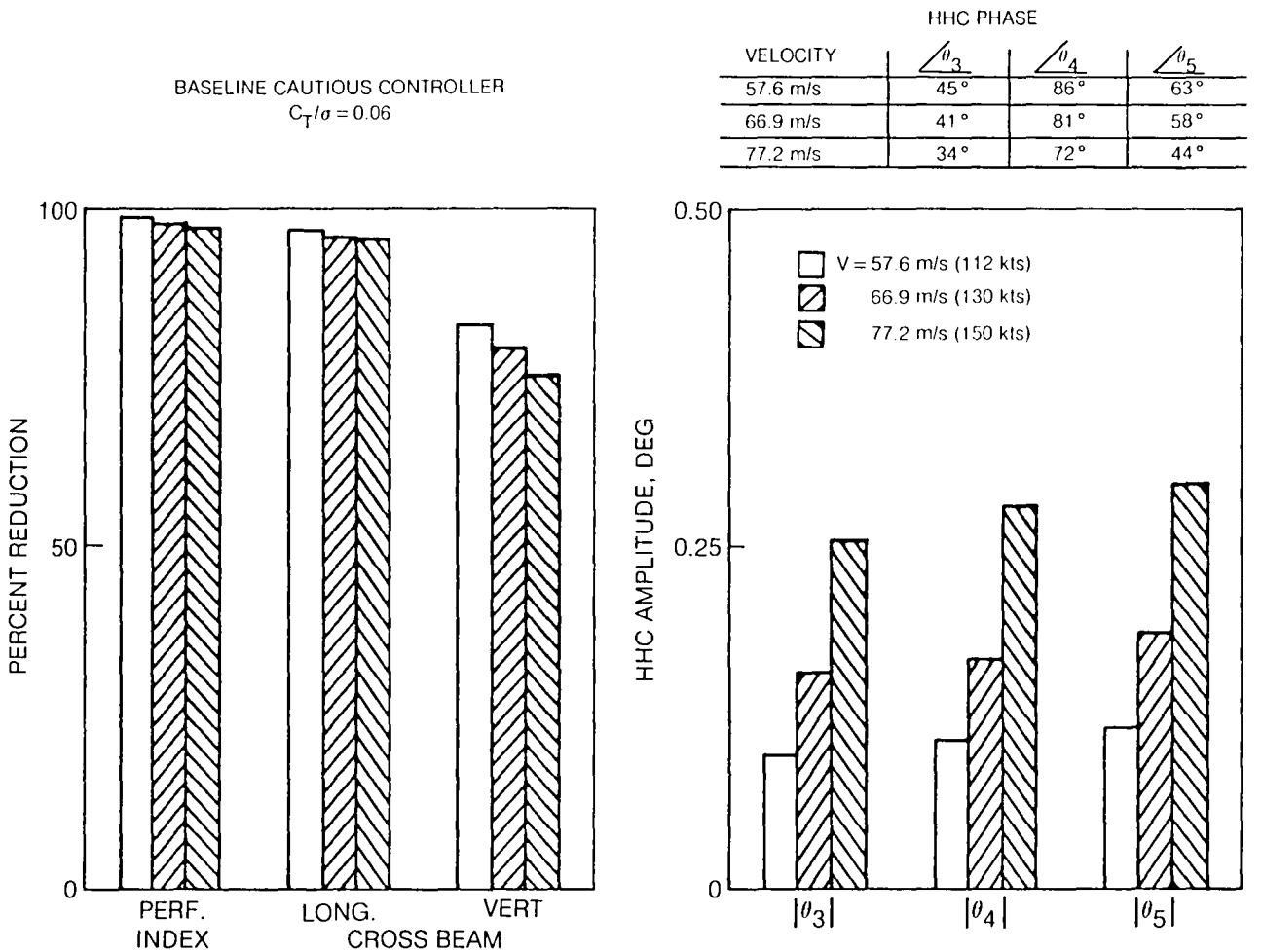

Fig. 60 Effect of Forward Velocity on Controller Performance

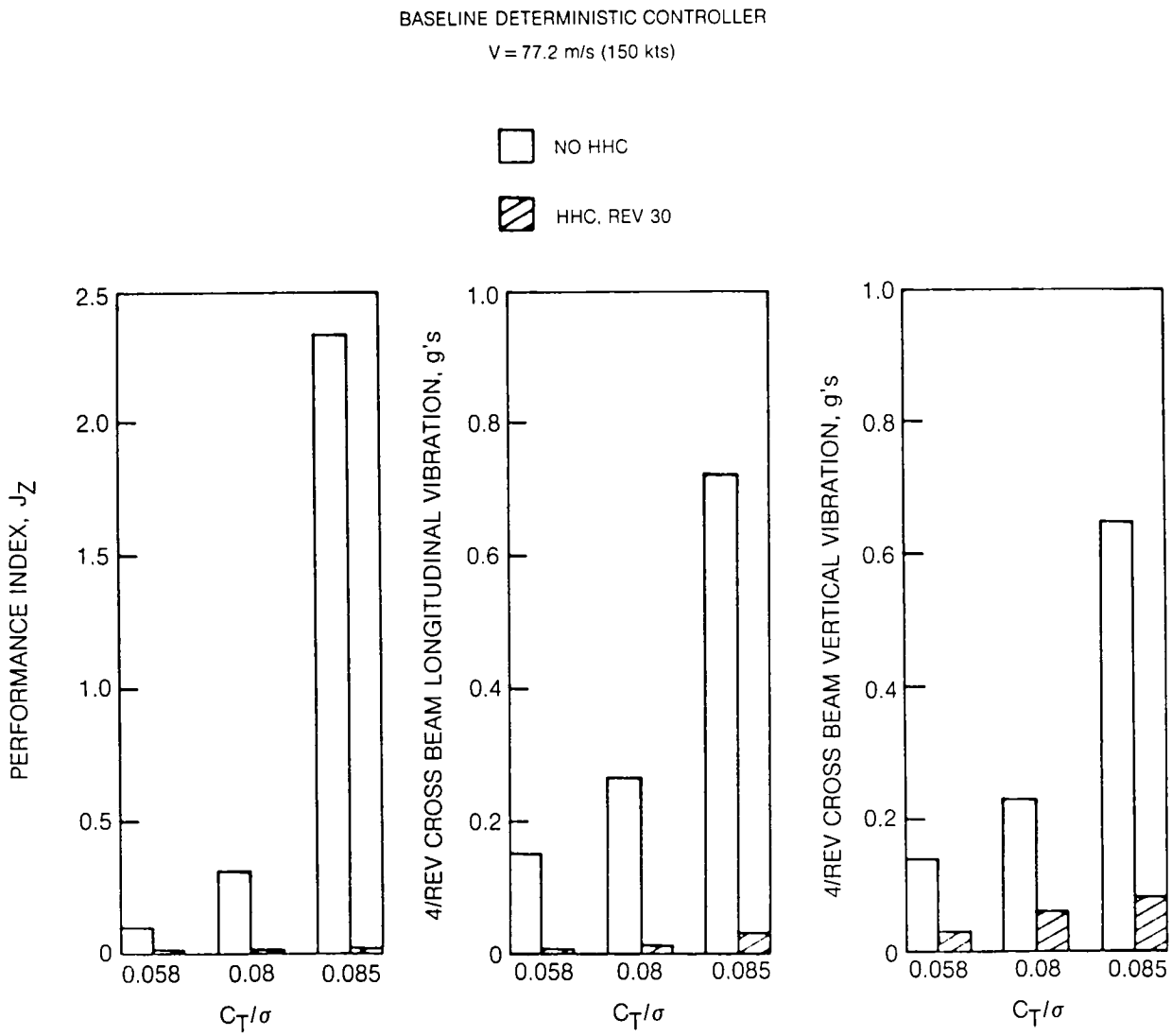

Fig. 61 Effect of Rotor Thrust on Controller Performance

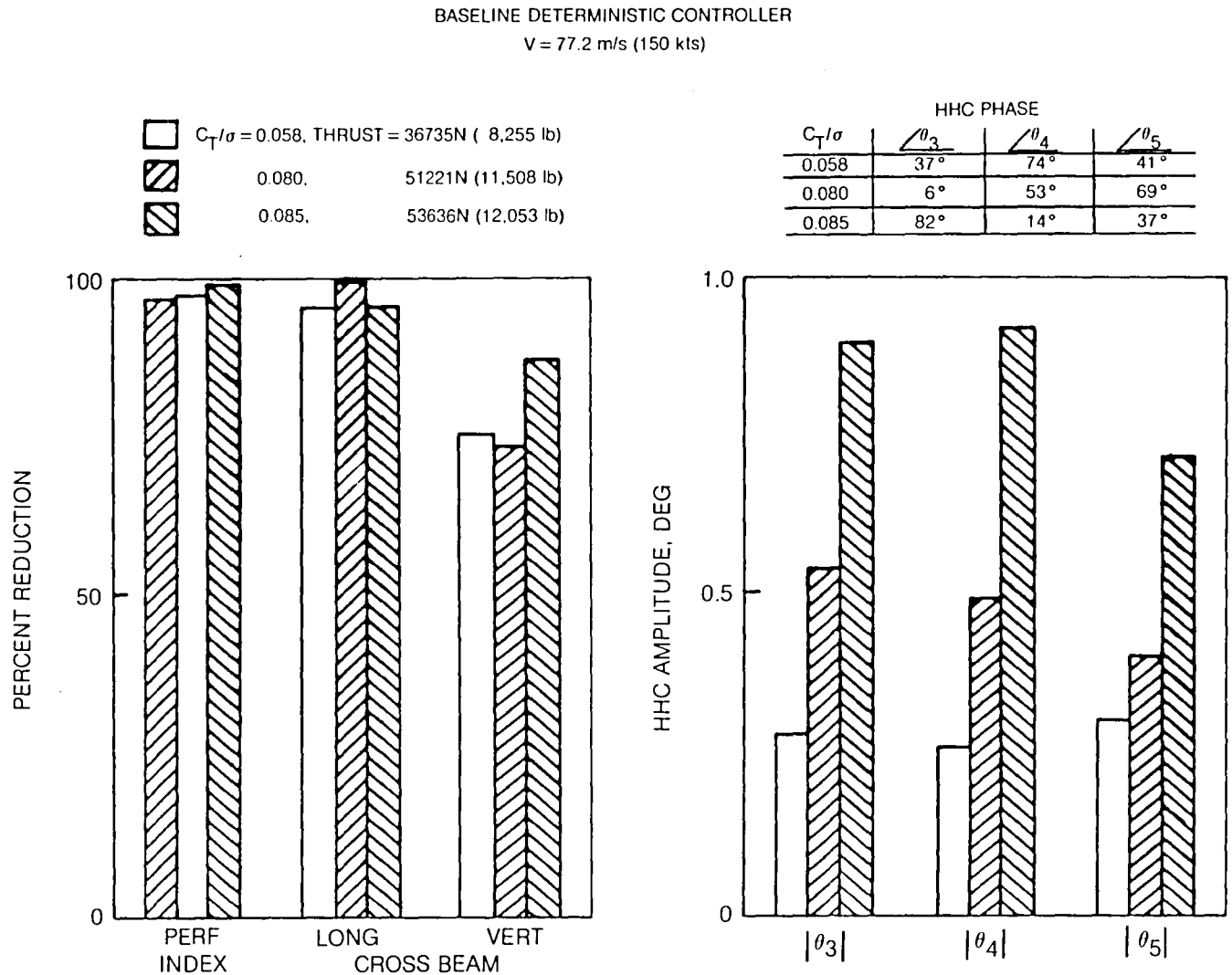

Fig. 62 Effect of Rotor Thrust on Controller Performance

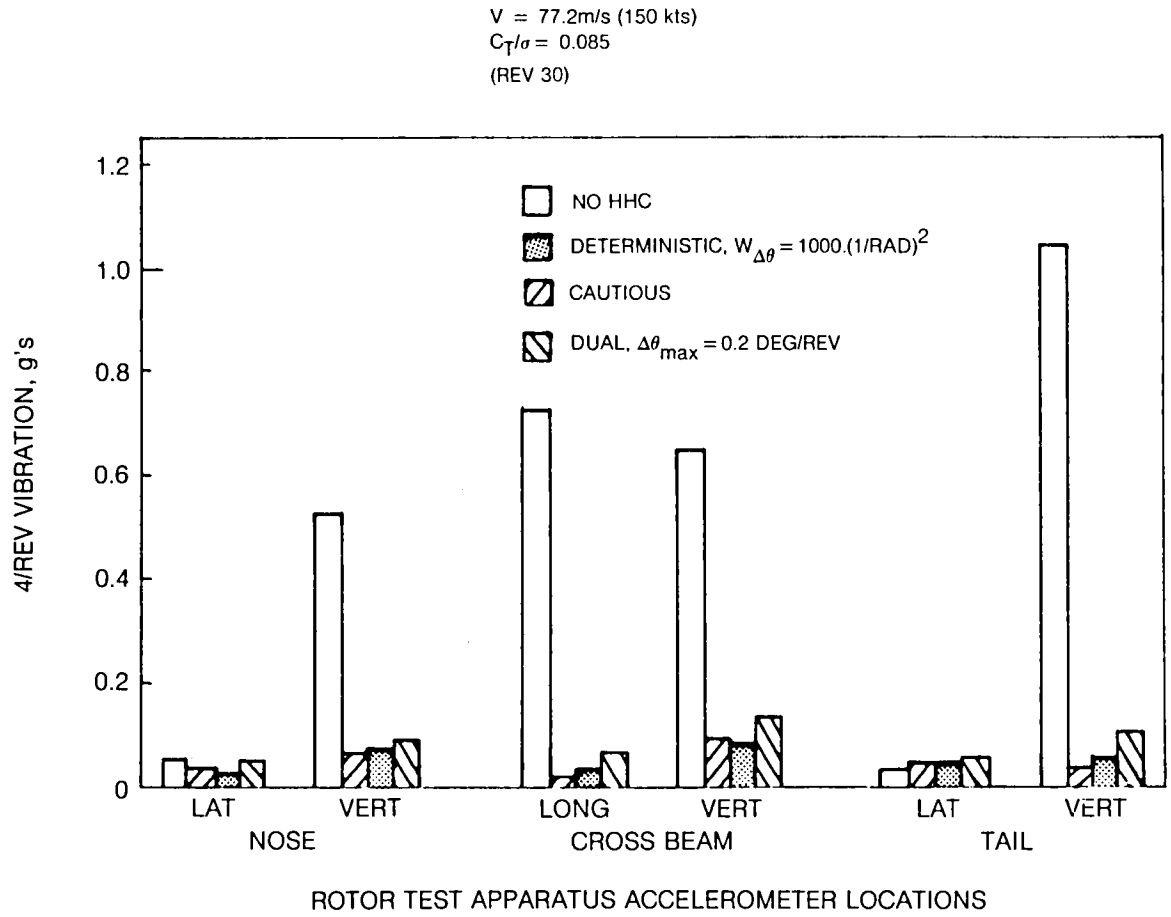

Fig. 63 Effect of Active Control on Predicted RTA Vibrations at High Thrust Flight Condition

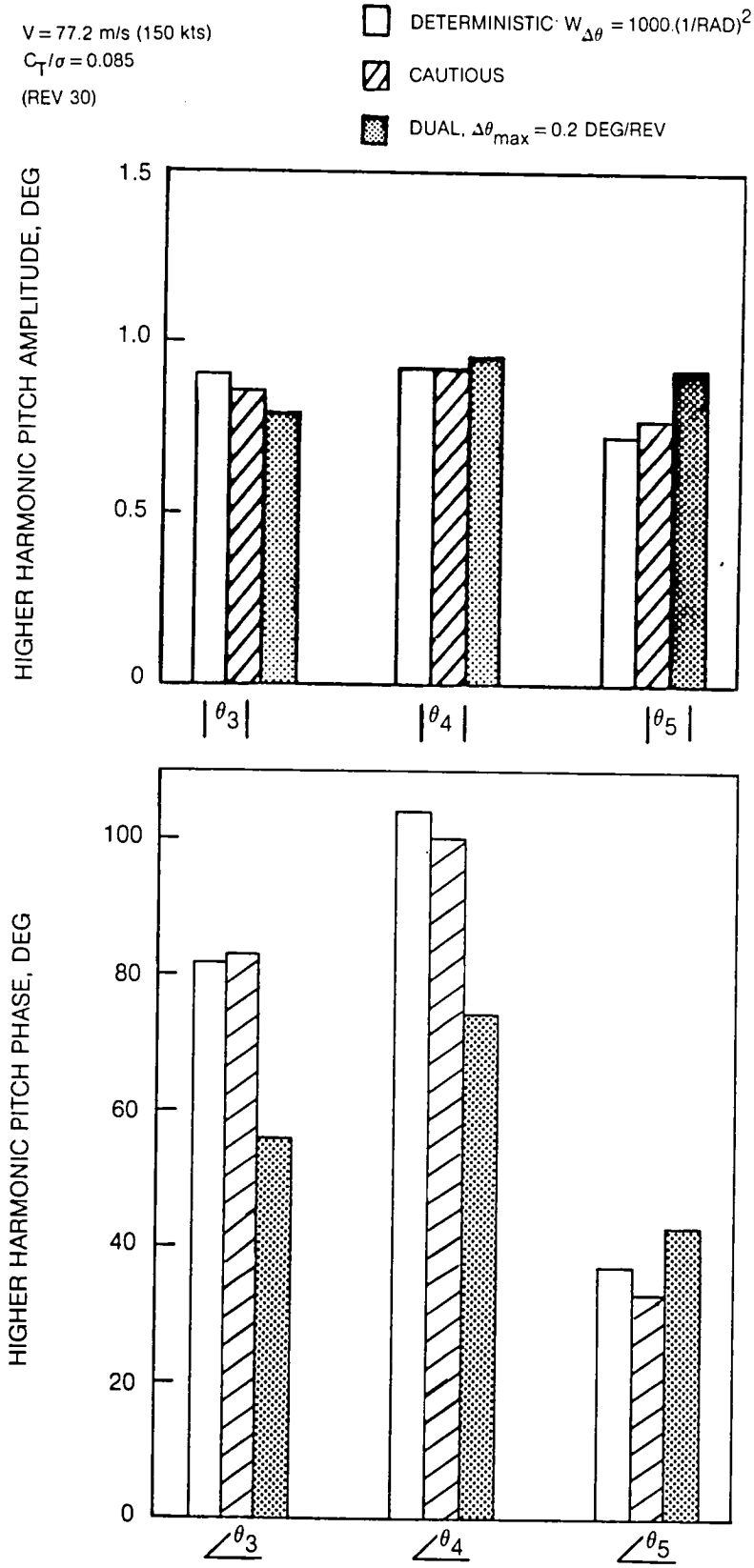

Fig. 64 Higher Harmonic Pitch Required at High Thrust Flight Condition

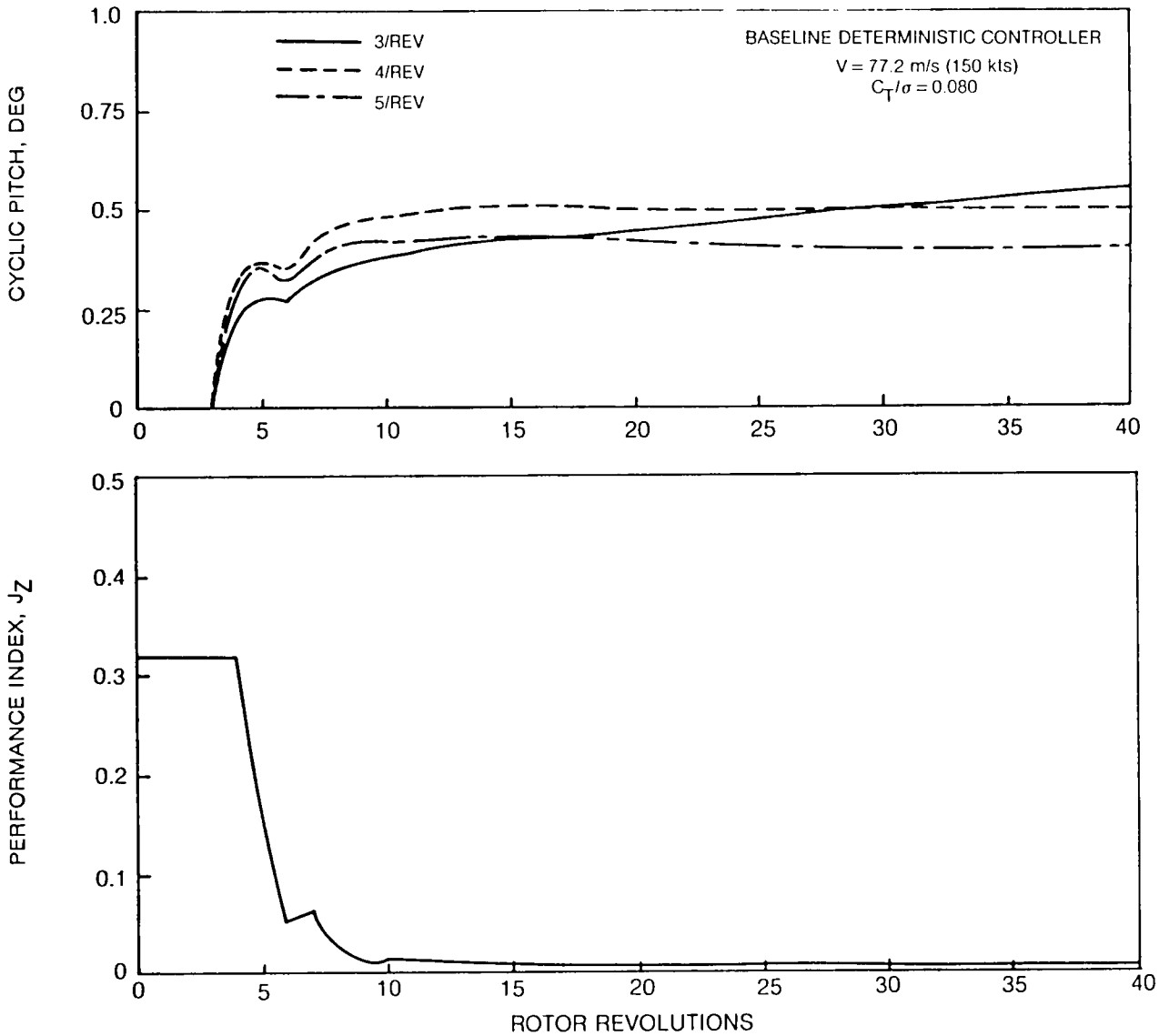

Fig. 65 Time History of Vibration Controller at High Thrust Condition

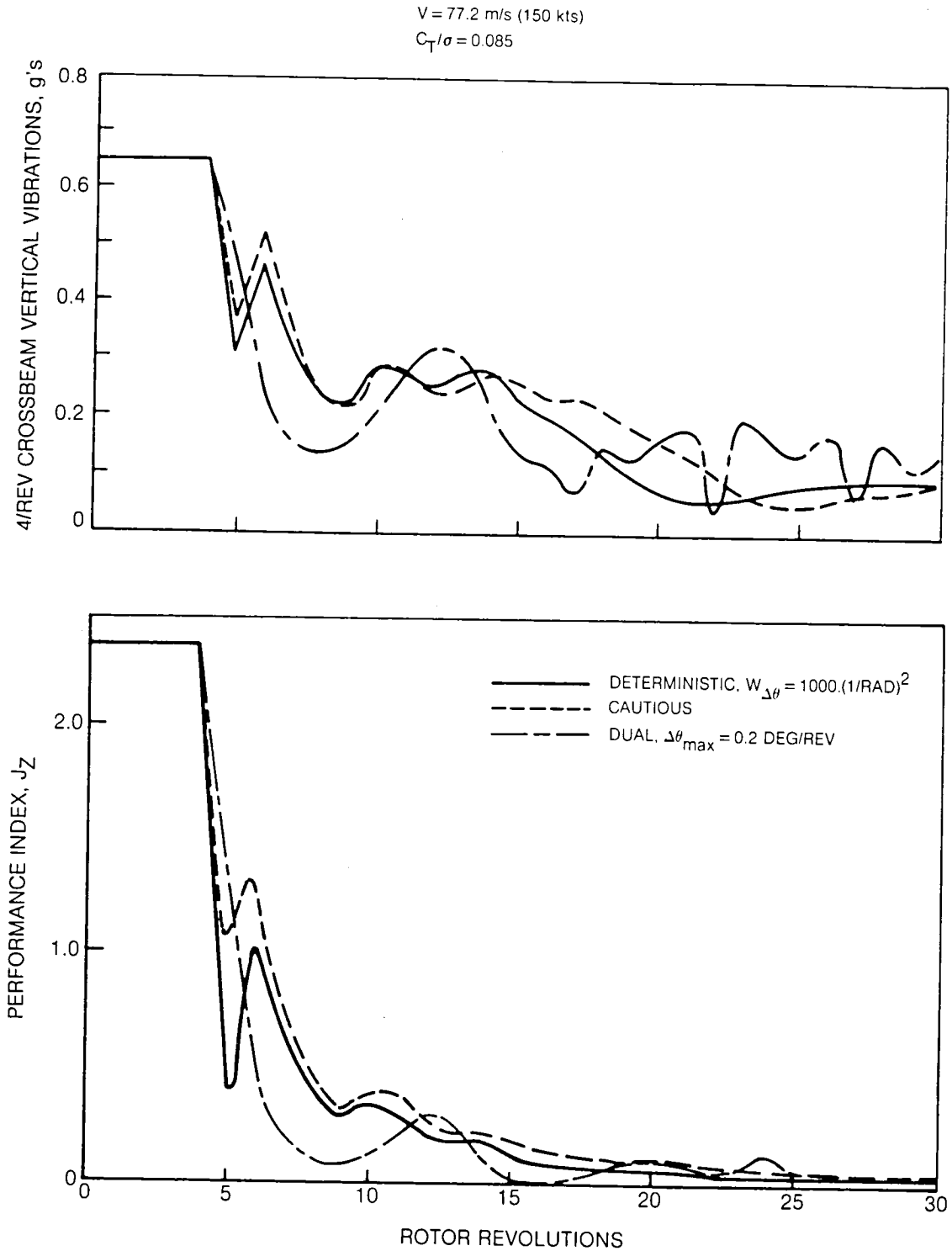

Fig. 66 Time History of Vibration Controller at High Thrust Flight Condition

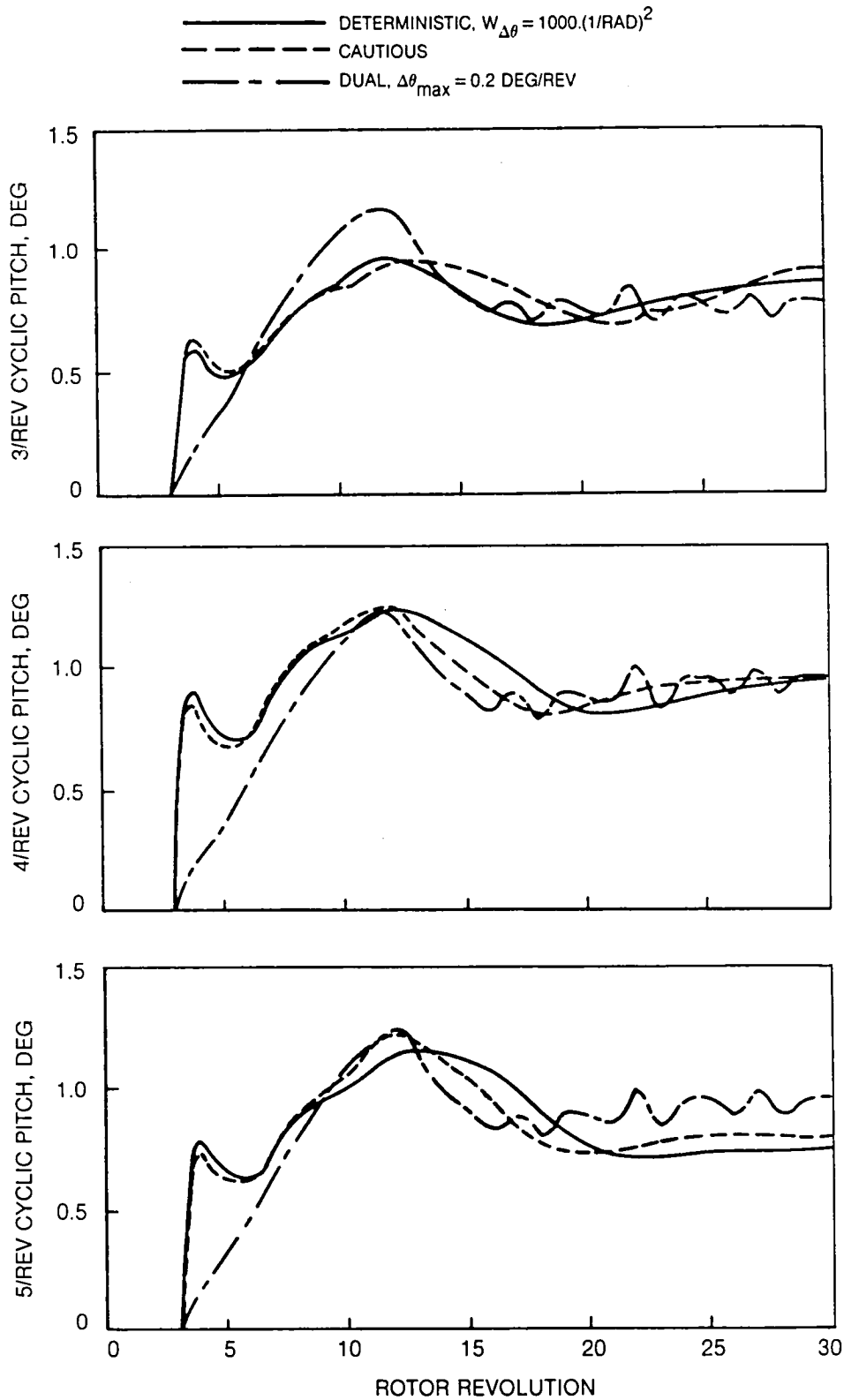

Fig. 67 Time History of Vibration Control at High Thrust Condition

			θ_{3C}	θ_{3S}	θ_{4C}	θ_{4S}	θ_{5C}	θ_{5S}
NOSE	LAT	C	1.262	0.881	-0.699	0.470	0.617	0.144
		S	-0.962	1.394	-0.717	-0.635	-0.317	0.787
NOSE	VERT	C	1.246	-5.046	5.844	0.755	-1.867	5.302
		S	4.662	1.175	0.145	5.103	-4.133	-3.170
CROSS-BEAM	LONG	C	3.139	-7.282	10.410	2.638	-3.034	10.251
		S	6.772	2.999	-1.637	9.486	-8.741	-4.879
CROSS-BEAM	VERT	C	-4.949	7.026	-12.874	-4.761	3.412	-13.613
		S	-6.595	-4.762	4.224	-12.190	12.408	5.142
TAIL	LAT	C	-1.356	-0.643	0.552	-0.449	-1.032	-0.027
		S	0.711	-1.443	0.655	0.621	0.047	-1.036
TAIL	VERT	C	-4.292	10.514	-14.675	-3.530	4.319	-14.333
		S	-9.770	-4.096	2.032	-13.315	12.121	6.990

a) OPEN-LOOP PERTURBATION AT BASELINE FLIGHT CONDITION ABOUT ZERO CONTROL ($\theta_3 = 0\angle 0°$, $\theta_4 = 0\angle 0°$, $\theta_5 = 0\angle 0°$)

			θ_{3C}	θ_{3S}	θ_{4C}	θ_{4S}	θ_{5C}	θ_{5S}
NOSE	LAT	C	0.696	-0.492	-0.262	-0.618	1.011	1.463
		S	1.488	1.886	1.558	1.402	-0.946	1.648
NOSE	VERT	C	0.959	-1.076	6.278	11.462	-15.938	2.926
		S	-0.253	1.331	-8.887	0.057	6.288	-13.614
CROSS-BEAM	LONG	C	3.002	-2.879	9.584	16.807	-22.622	6.038
		S	0.423	3.588	-13.312	1.230	5.643	-19.304
CROSS-BEAM	VERT	C	-5.217	4.681	-10.023	-16.648	21.356	-8.439
		S	-1.538	-5.852	13.538	-2.832	-0.532	18.134
TAIL	LAT	C	-0.387	0.104	0.280	0.609	-2.337	-0.983
		S	-1.125	-1.005	-0.682	-0.469	-0.119	-0.963
TAIL	VERT	C	-4.044	3.918	-13.217	-24.217	32.729	-8.392
		S	-0.469	-4.881	19.132	-1.570	-8.765	27.934

b) OPEN-LOOP PERTURBATION AT HIGH THRUST FLIGHT CONDITION ABOUT OPTIMAL CONTROL SOLUTION ($\theta_3 = 0.90\angle 82°$, $\theta_4 = 0.92\angle 14°$, $\theta_5 = 0.72\angle 253°$)

Fig. 68 Comparison of Initial and Final Transfer Matrix at High Thrust Flight Condition

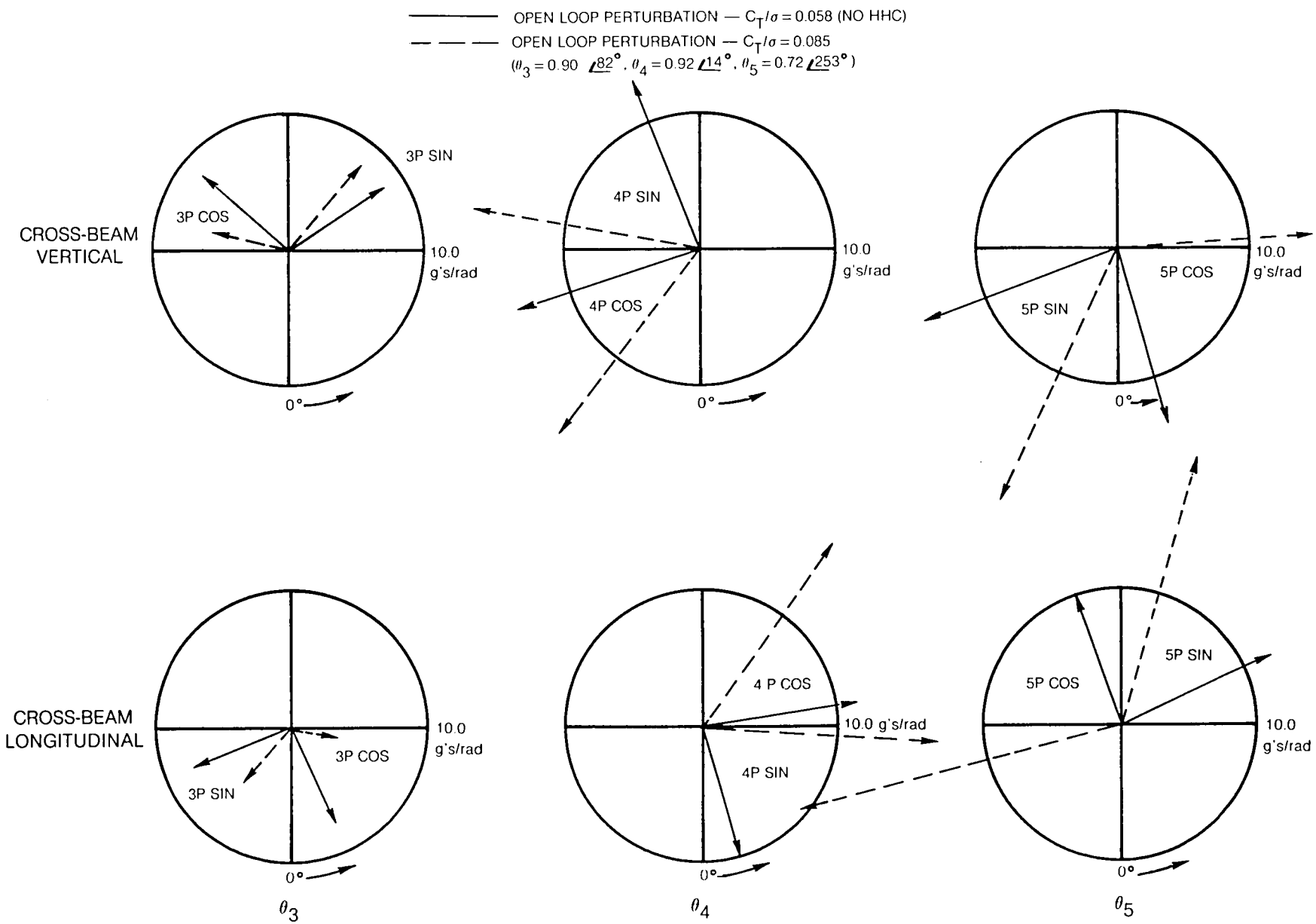

Fig. 69 Effect of Rotor Thrust on Sensitivity of Cross-Beam Vibrations to Higher Harmonic Control

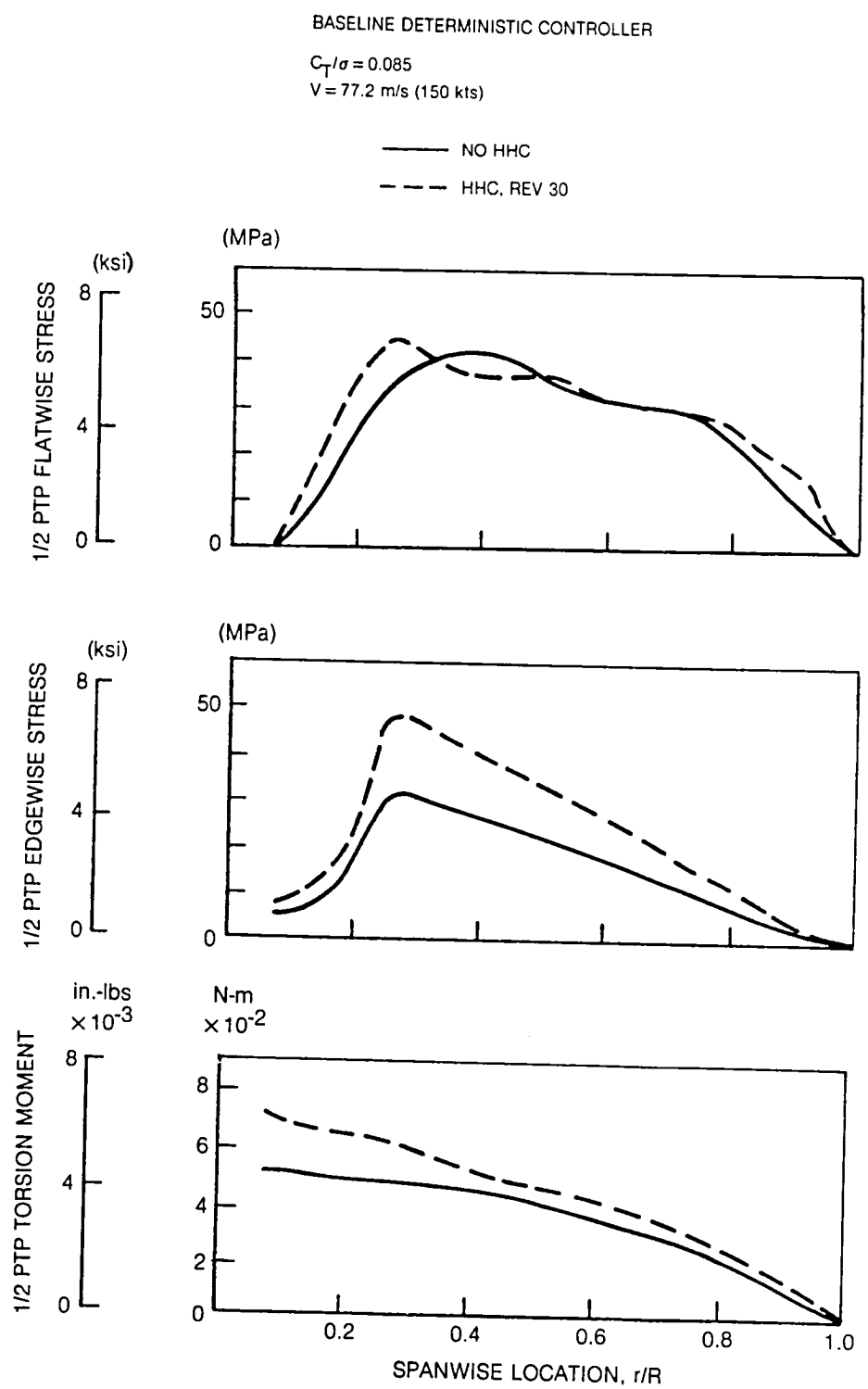

Fig. 70 Effect of Active Vibration Control on Rotor Blade Vibratory Moments and Stresses at High Thrust Flight Condition

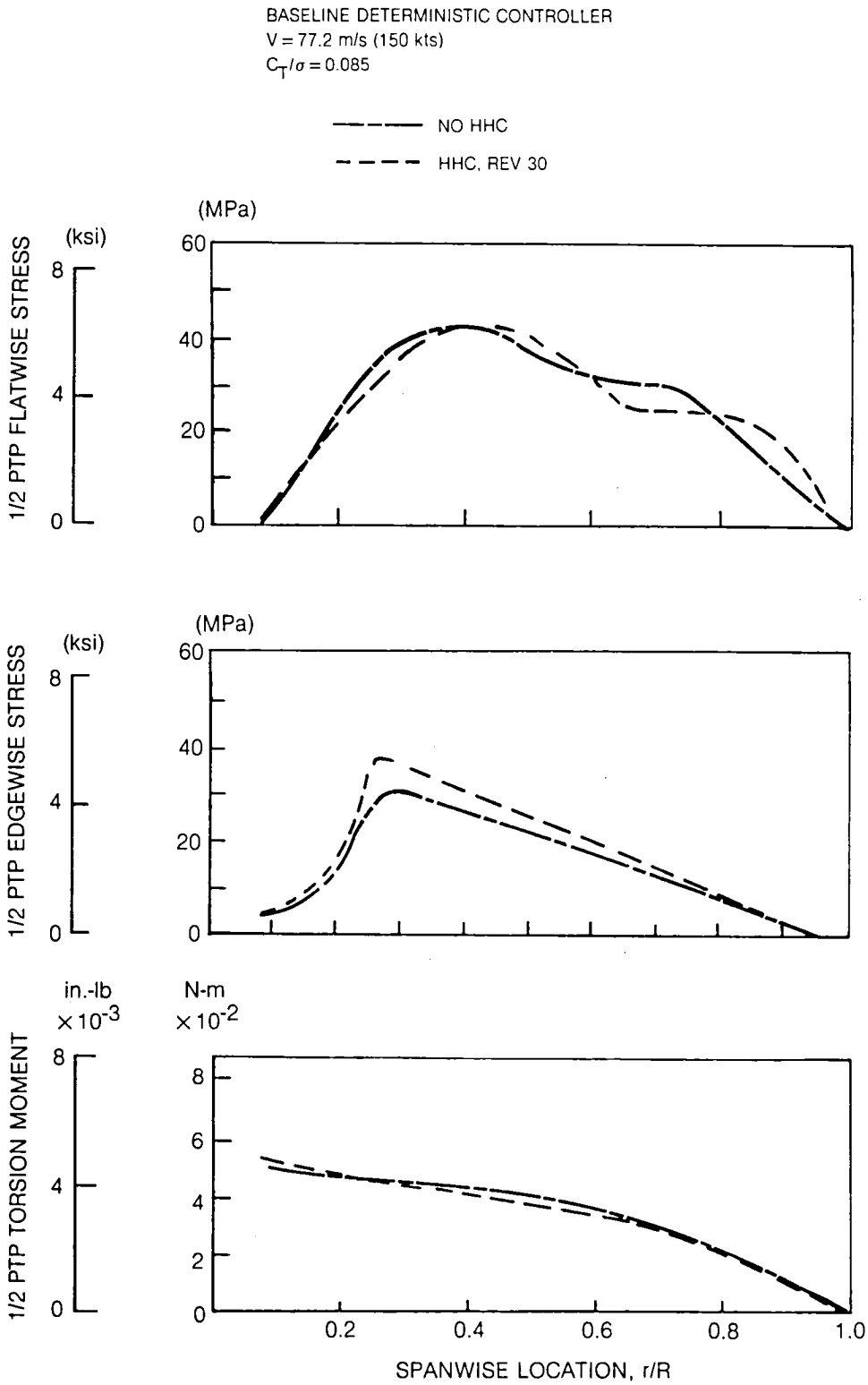

Fig. 71 Effect of Active Vibration Control on Rotor Blade Vibratory Moments and Stresses at High Thrust Flight Condition (No 5/Rev Control)

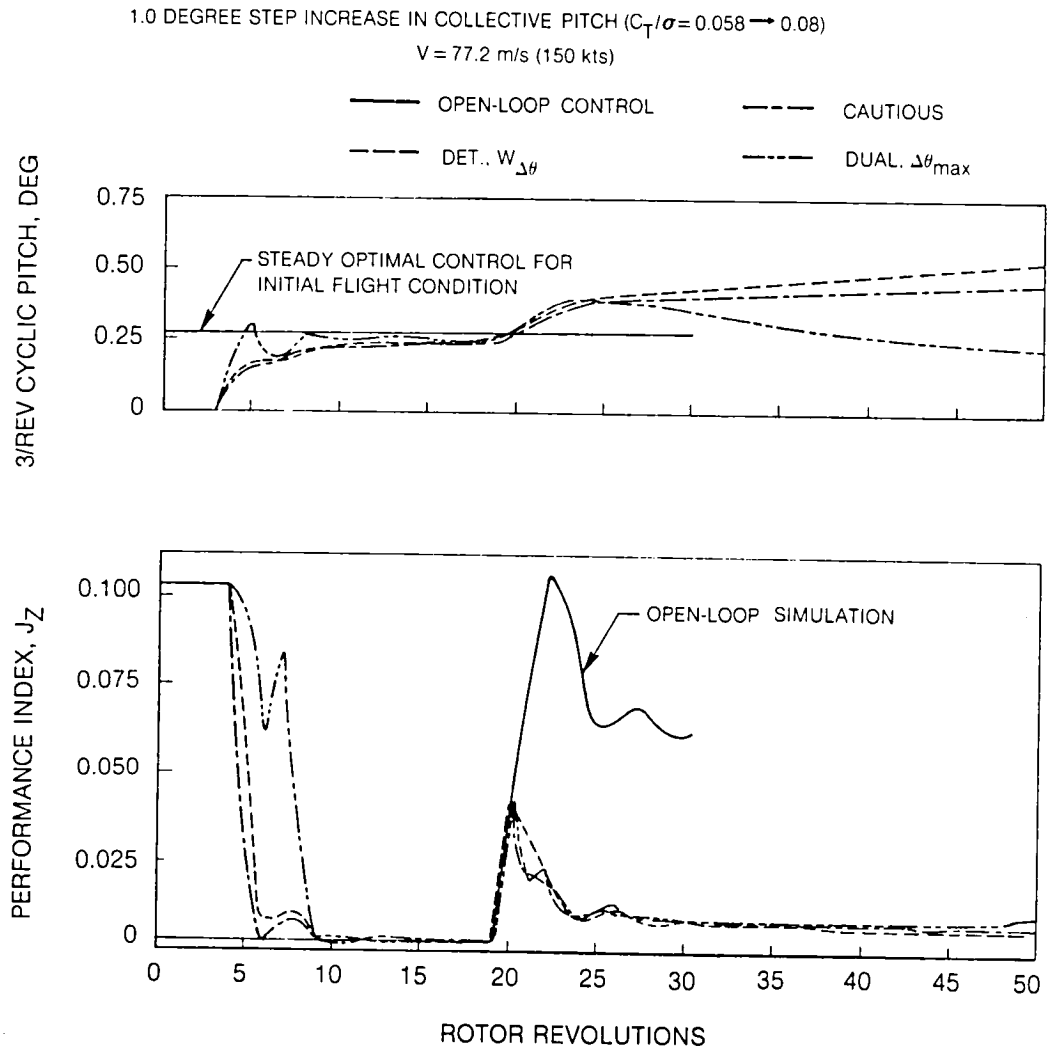

Fig. 72 Controller Performance During Transient Maneuver

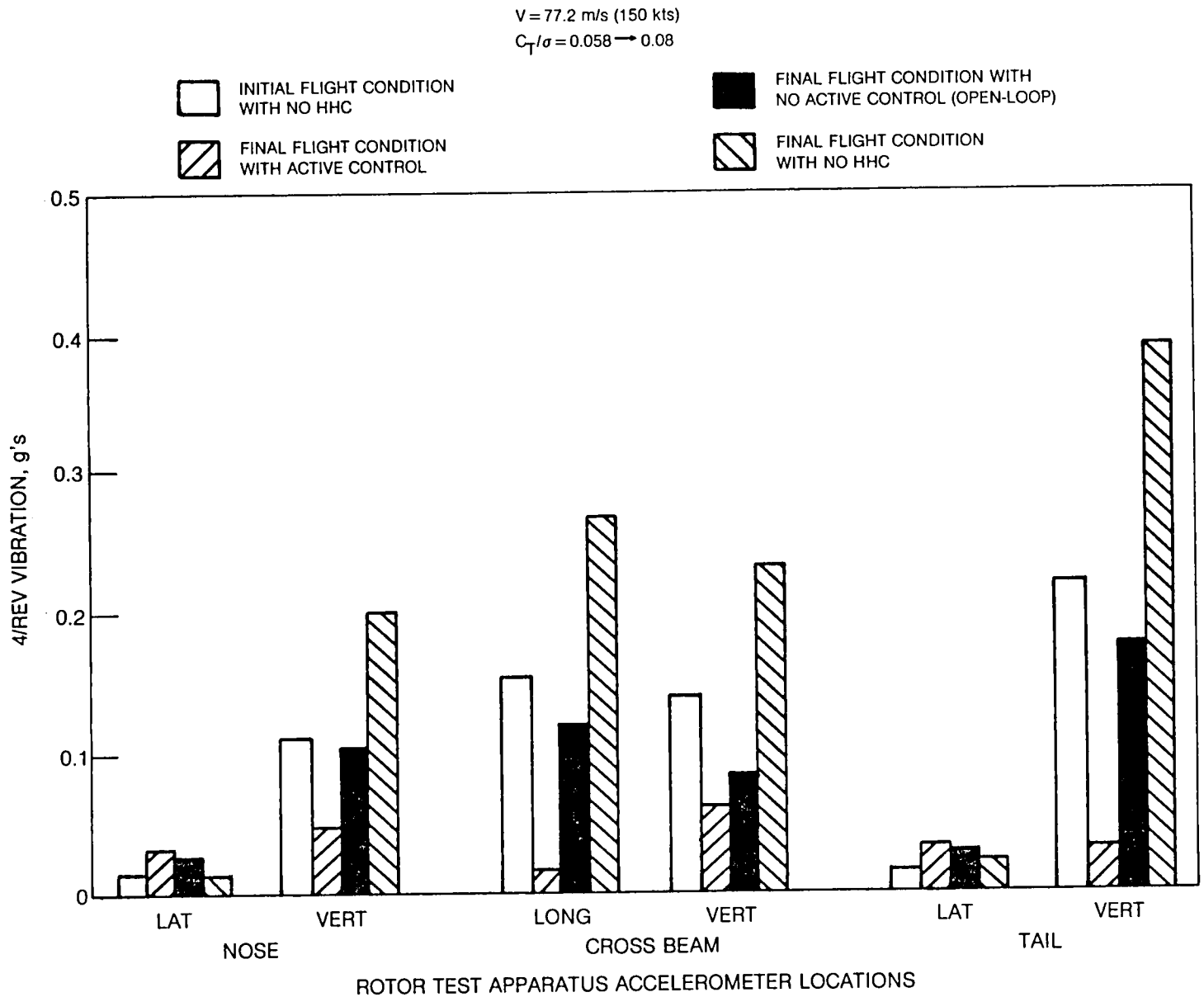

Fig. 73 Predicted RTA 4/Rev Vibrations for 1.0 Degree Step Increase in Collective Pitch

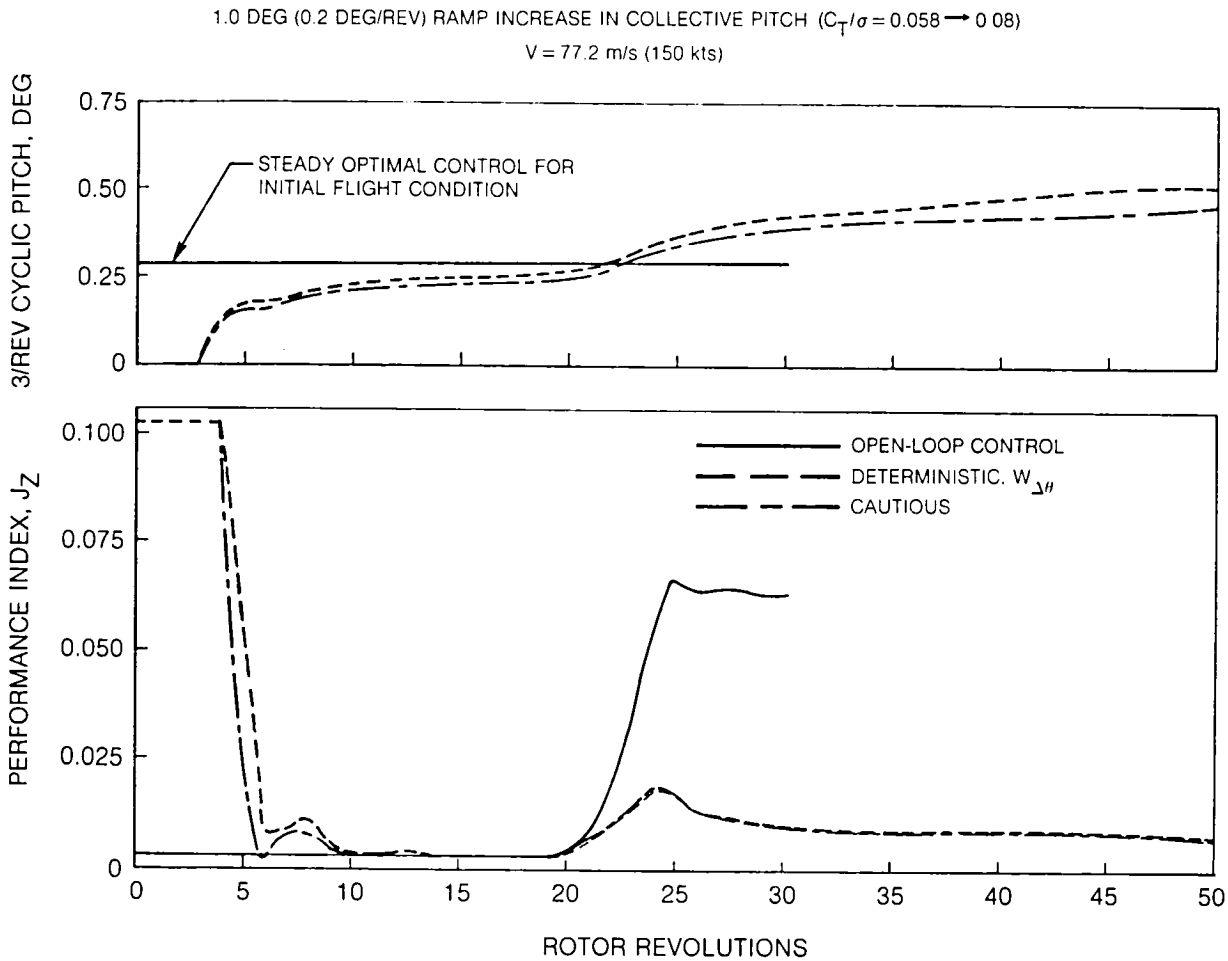

Fig. 74 Controller Performance During Transient Maneuver

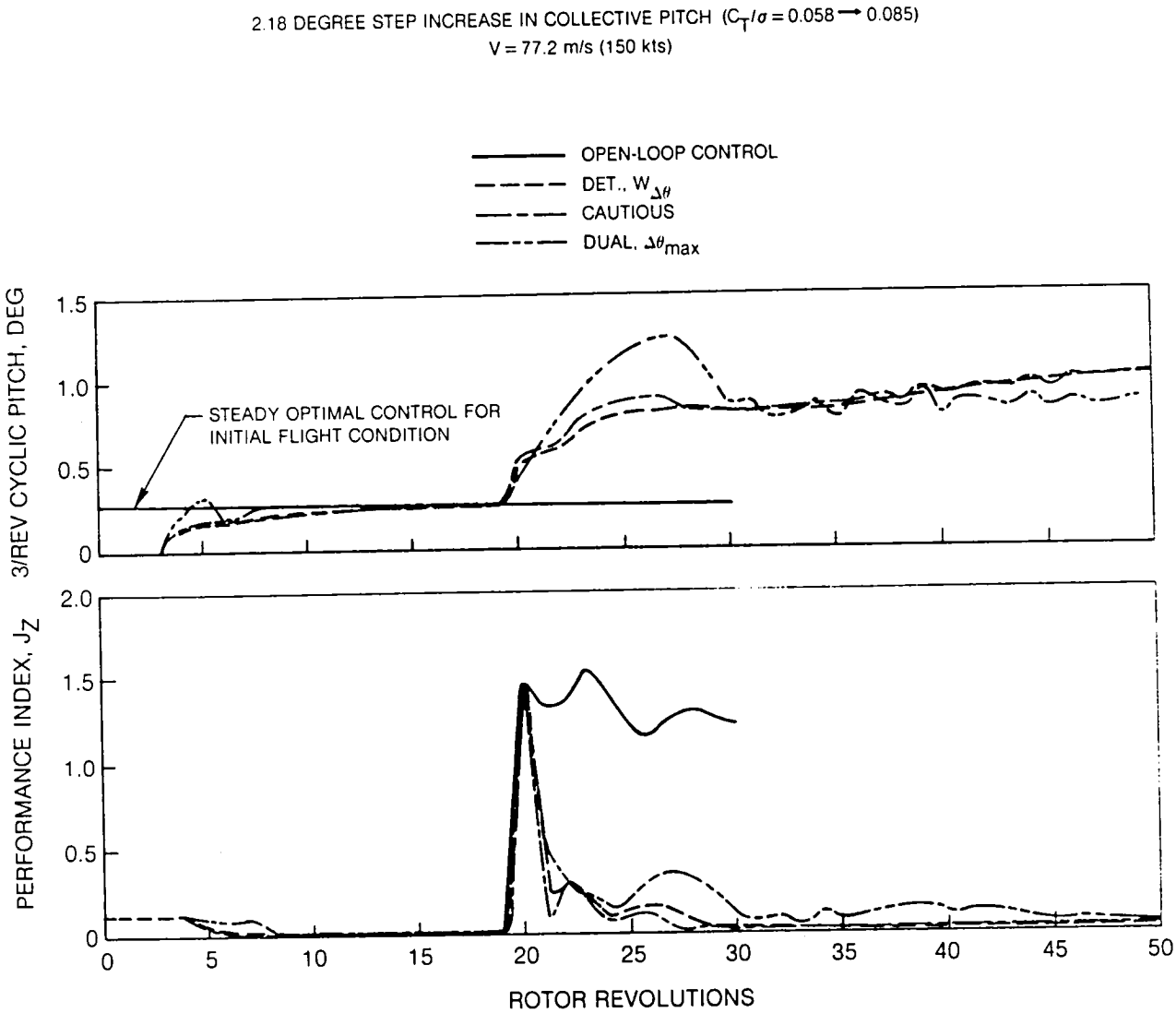

Fig. 75 Controller Performance During Transient Maneuver

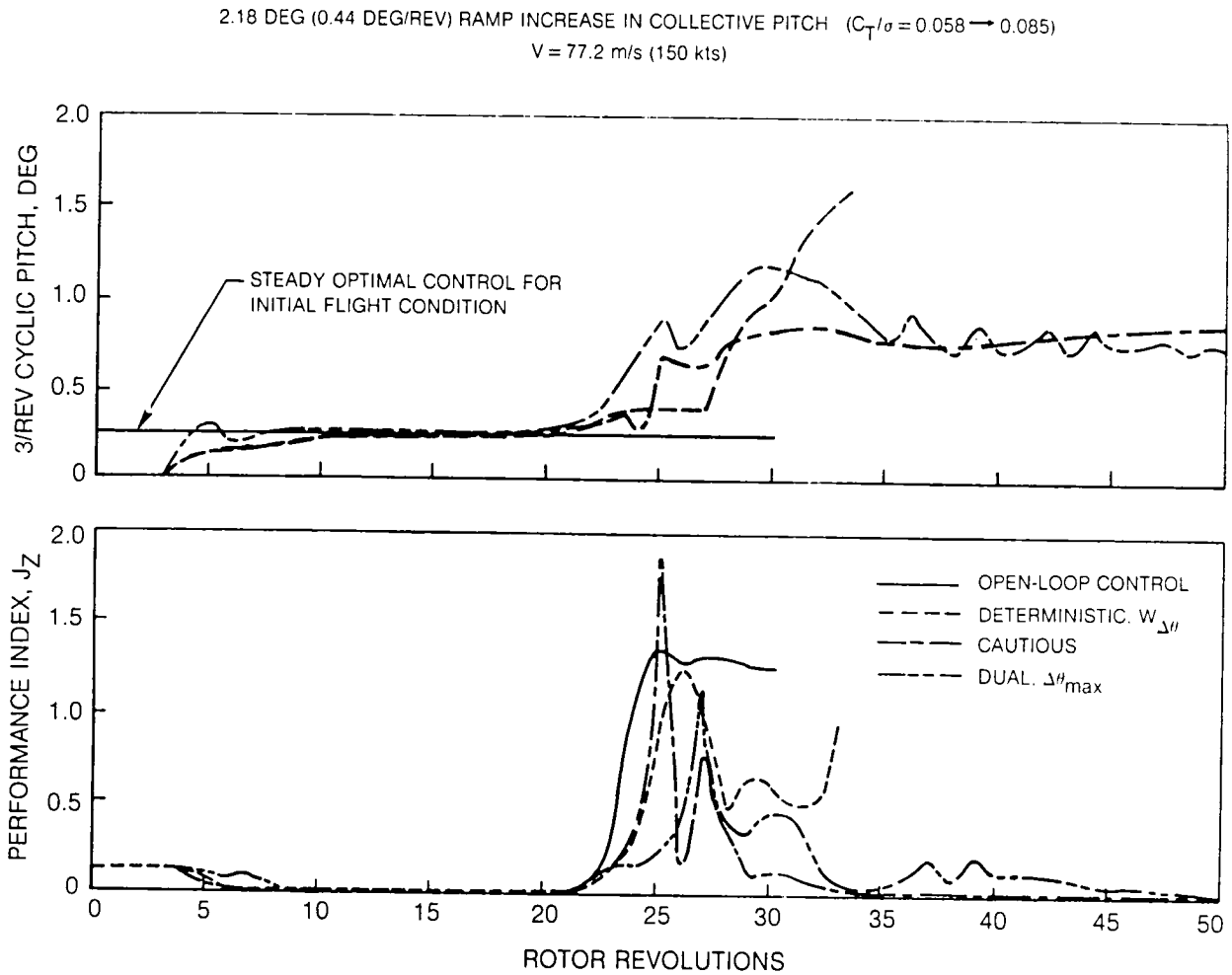

Fig. 76 Controller Performance During Transient Maneuver

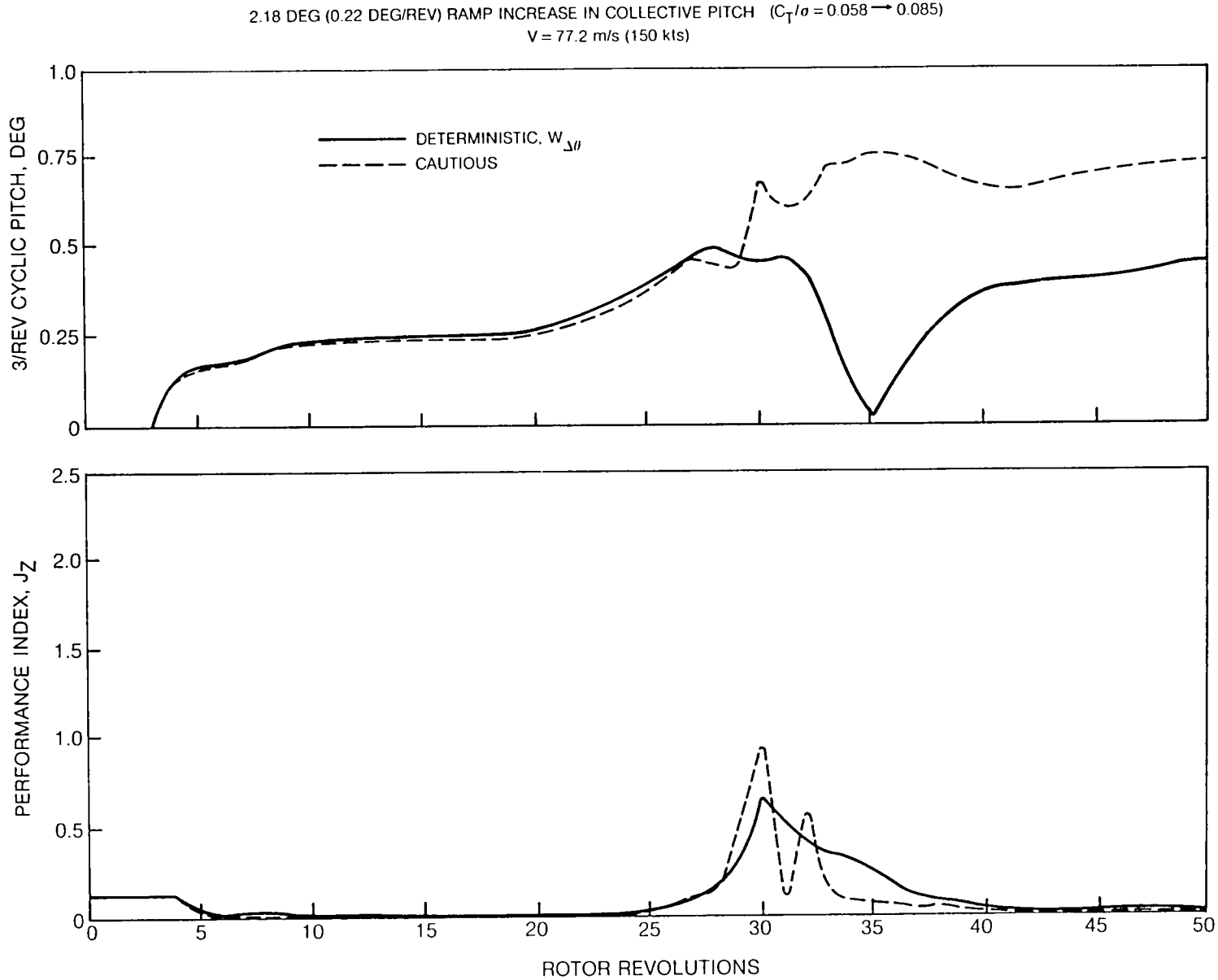

Fig. 77 Controller Performance During Transient Maneuver

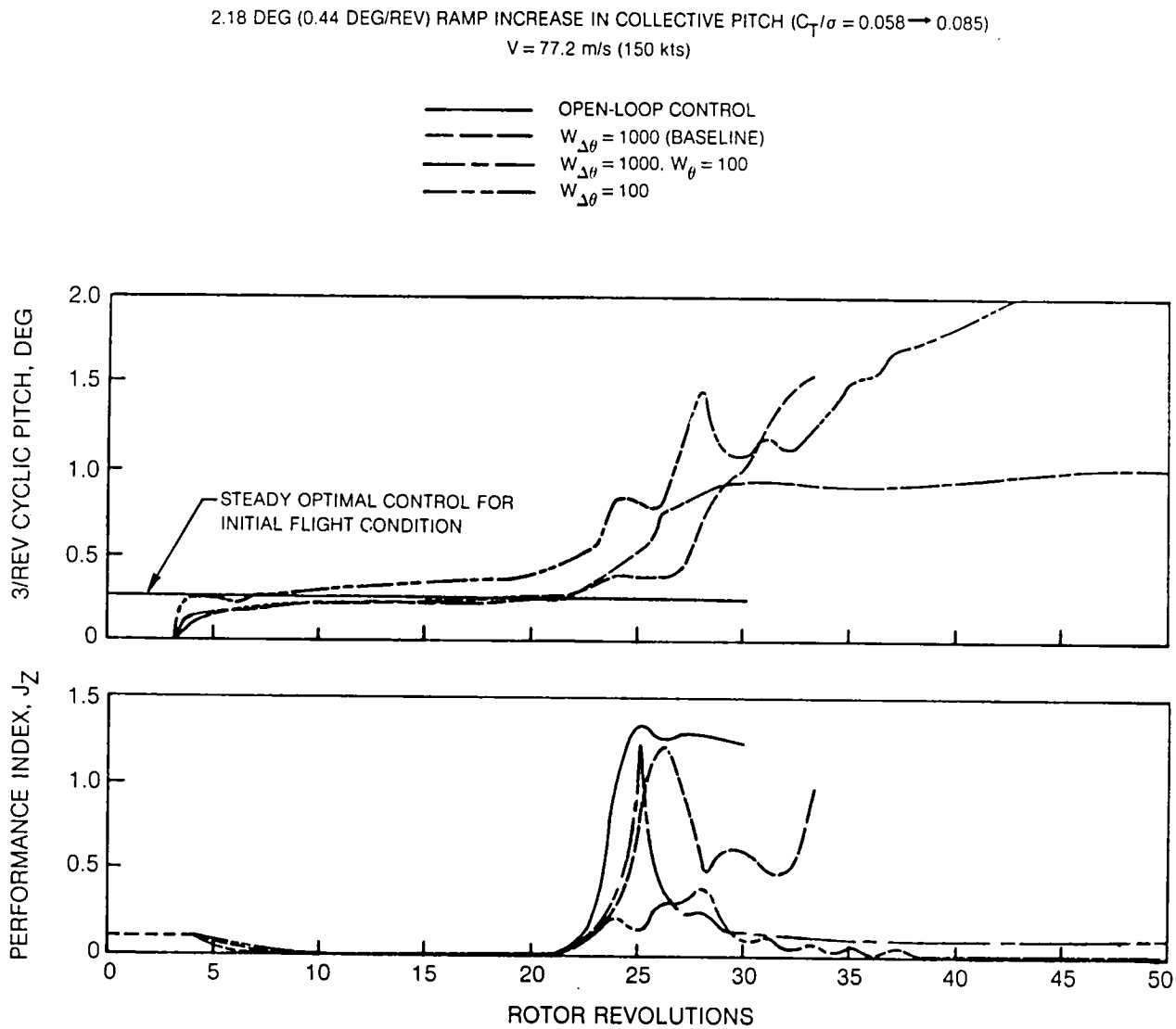

Fig. 78 Deterministic Controller Performance During Transient Maneuver

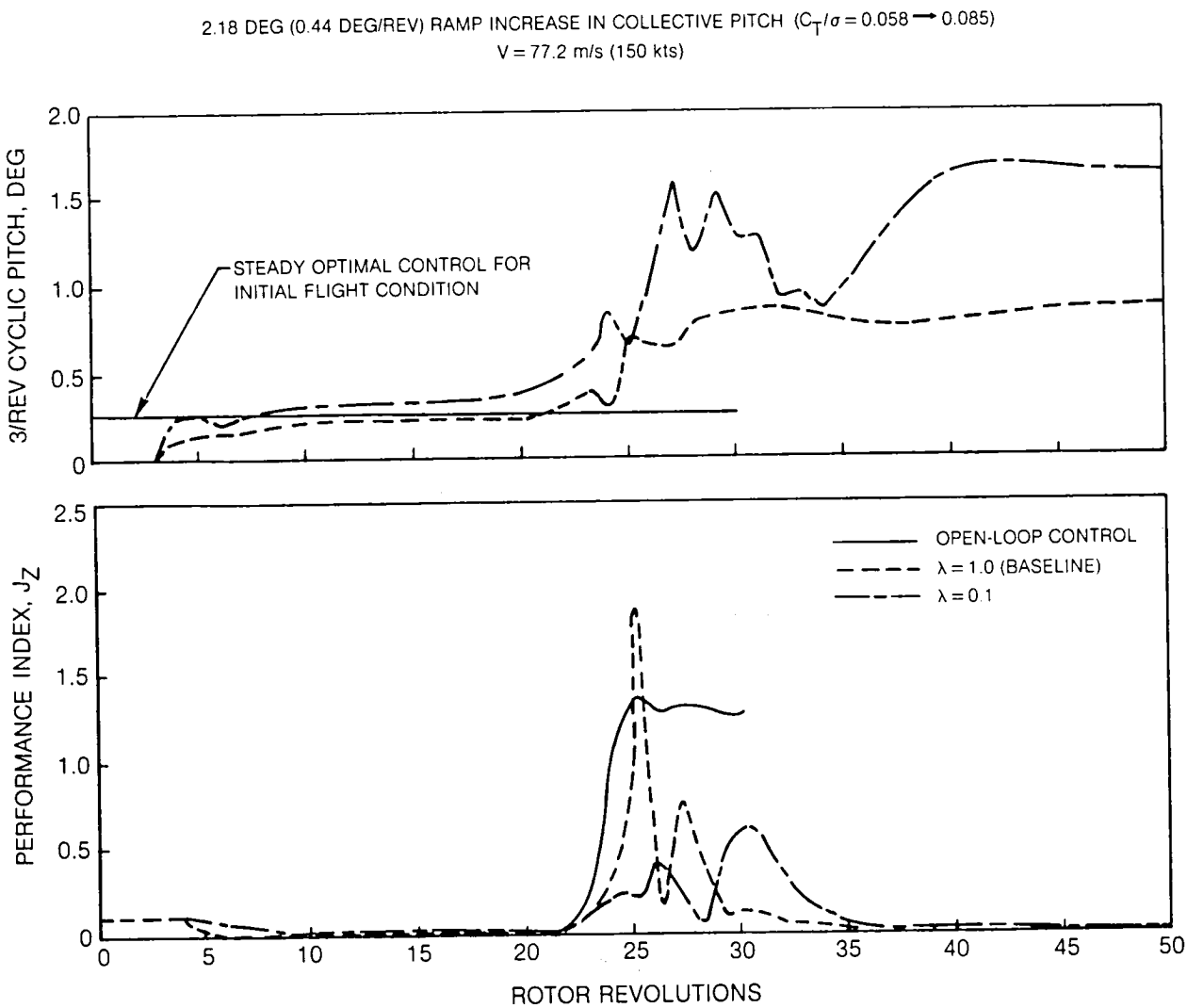

Fig. 79 Cautious Controller Performance During Transient Maneuver

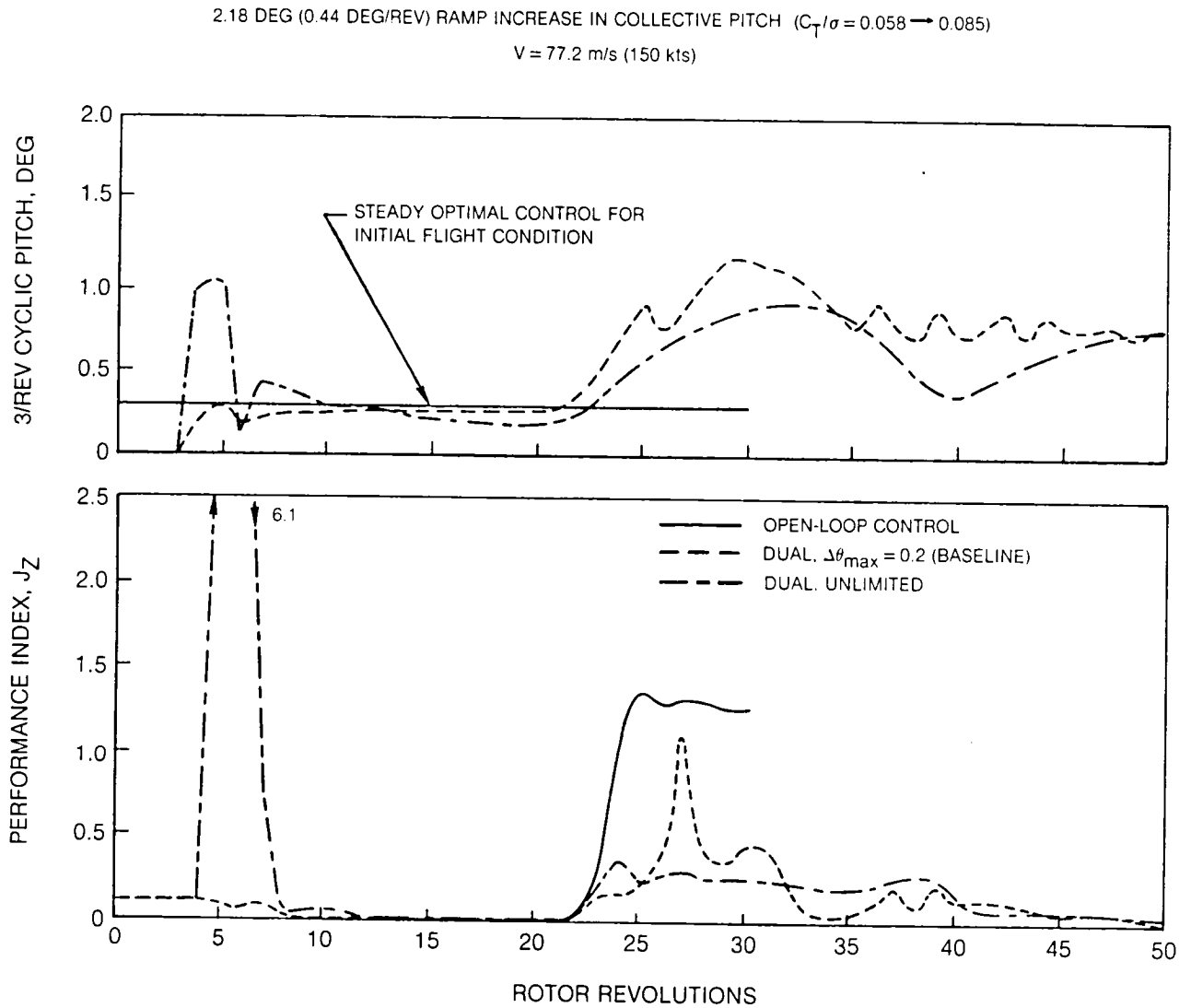

Fig. 80 Dual Controller Performance During Transient Maneuver

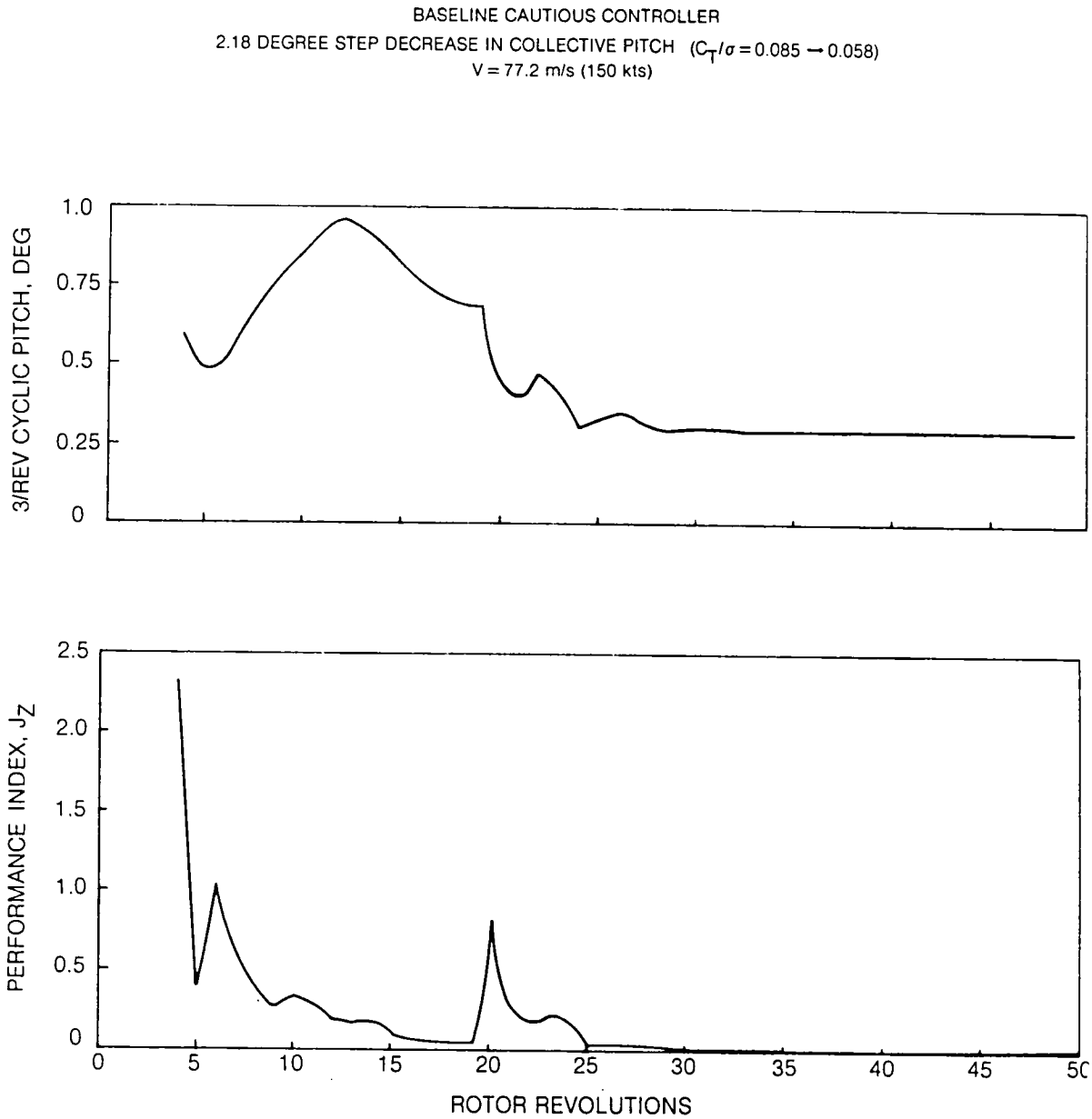

Fig. 81 Controller Performance During Transient Maneuver

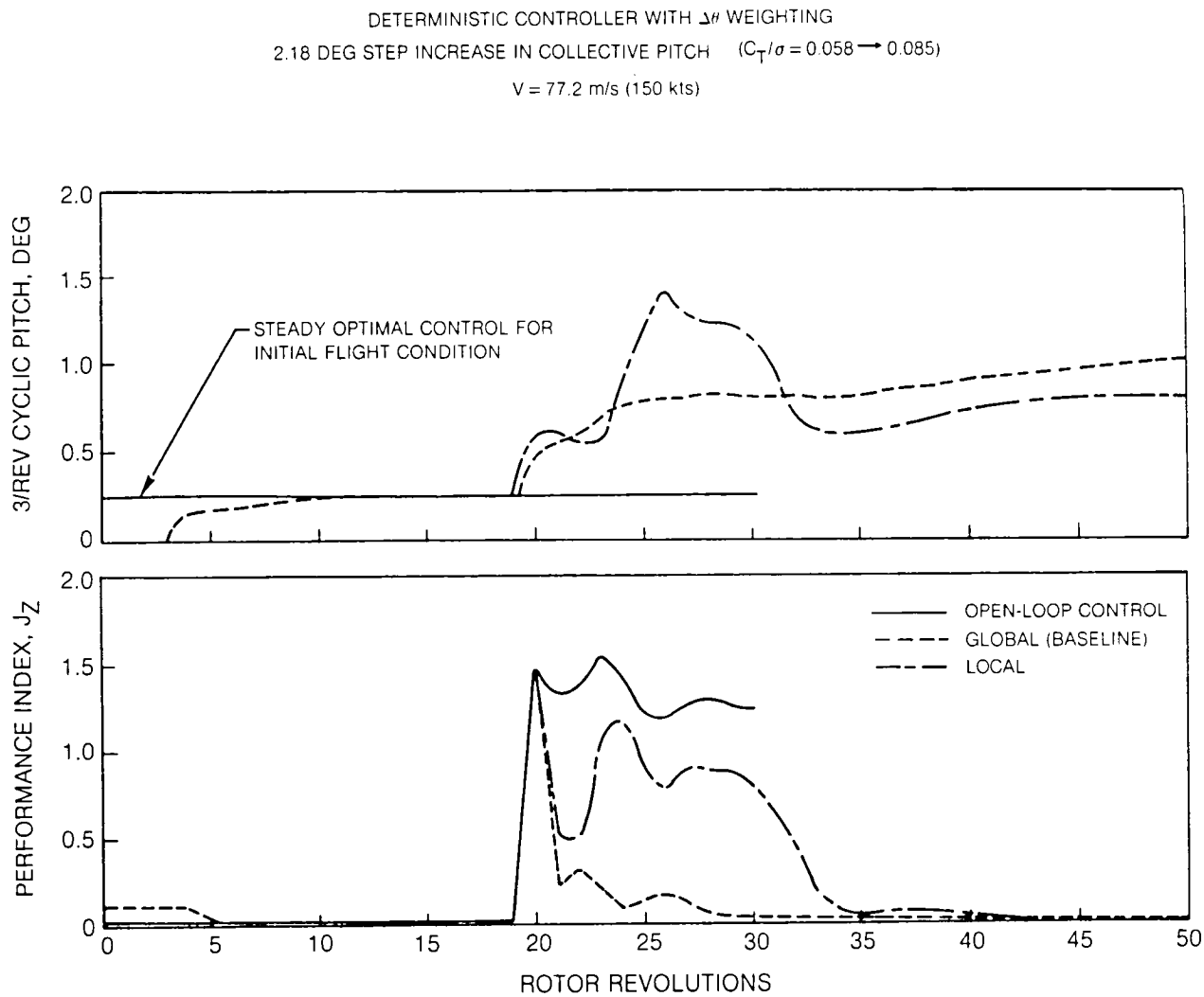

Fig. 82 Comparison of Global and Local Controller Performance During Transient Maneuver

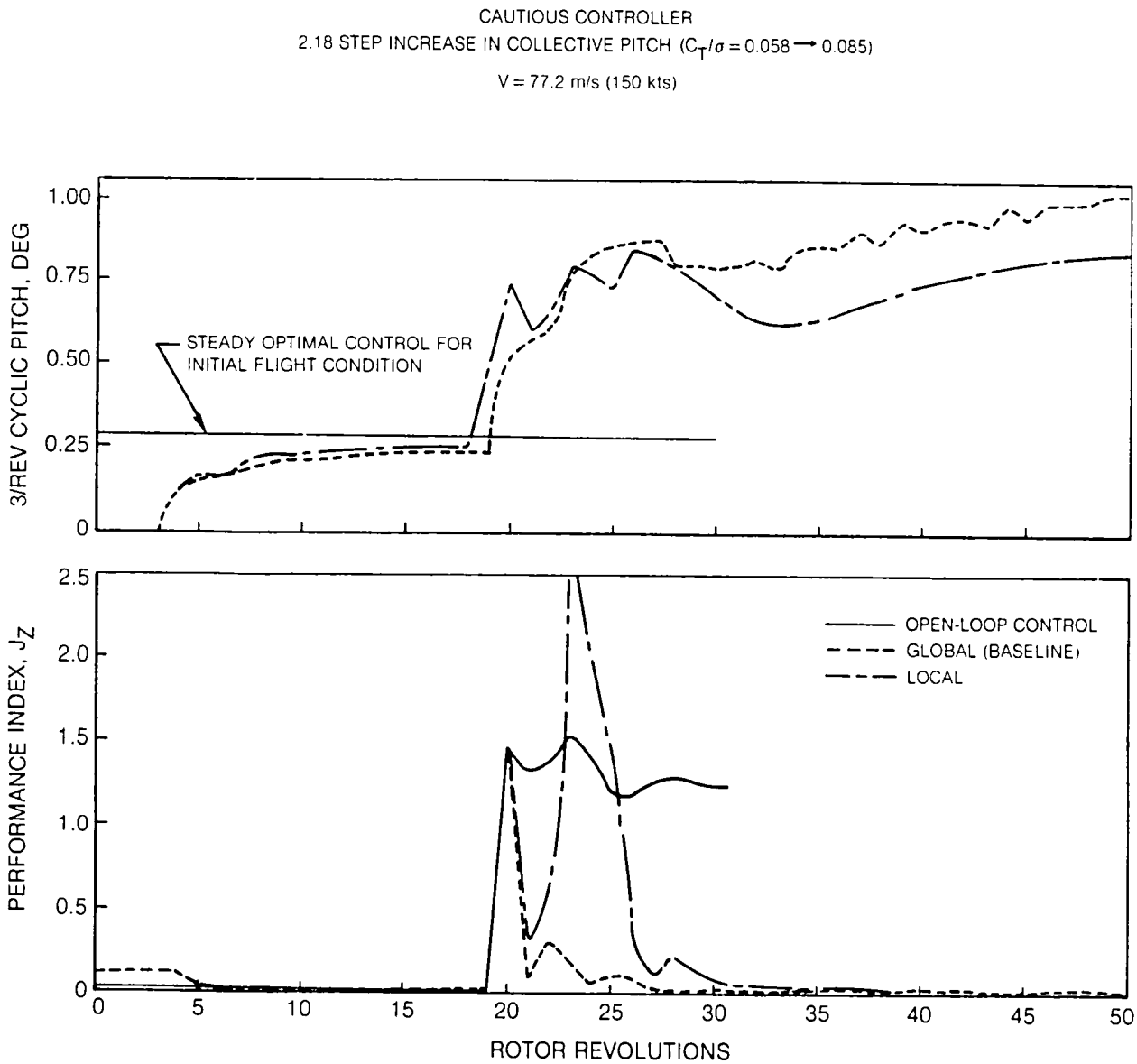

Fig. 83 Comparison of Global and Local Controller Performance During Transient Maneuver

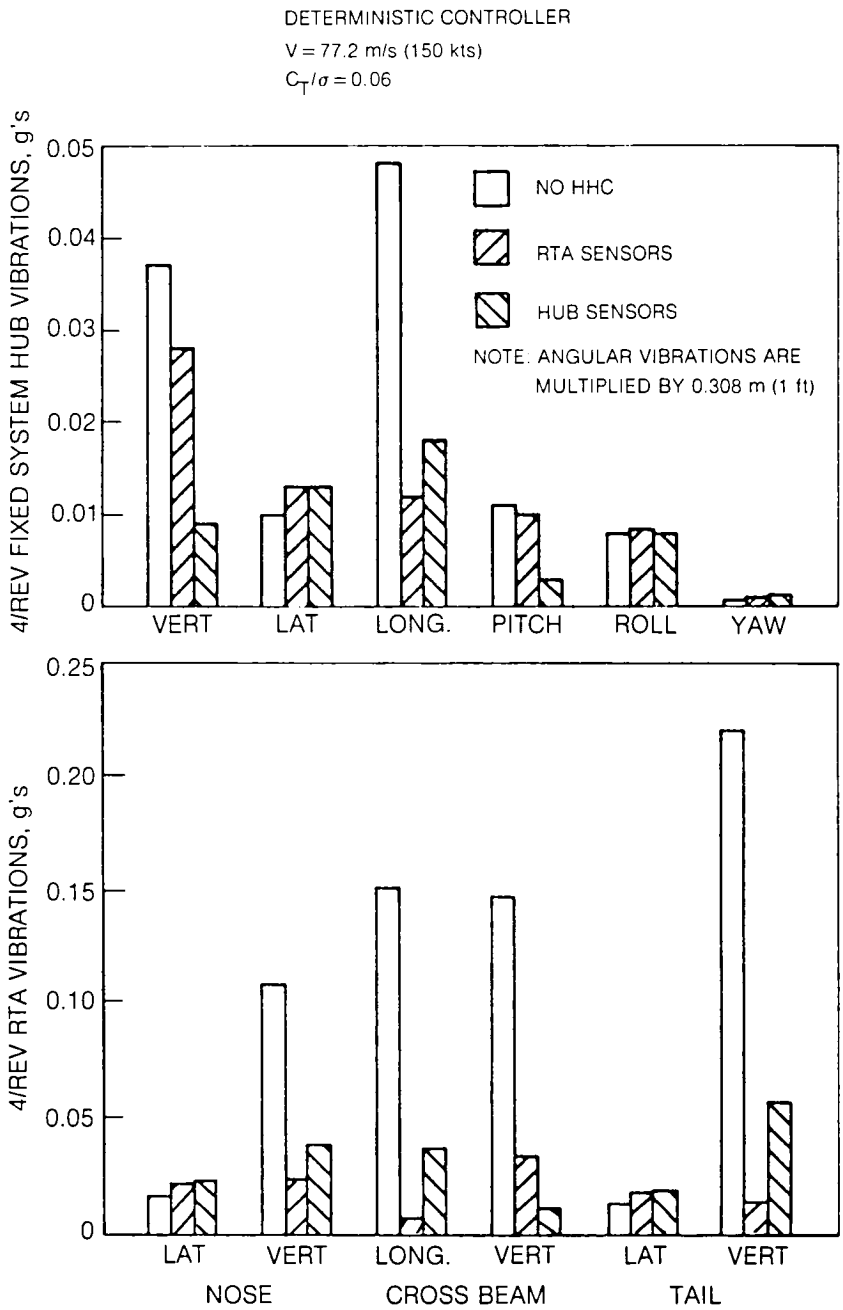

Fig. 84 Effect of Hub Vibration Sensors on Vibration Reduction at Baseline Flight Condition

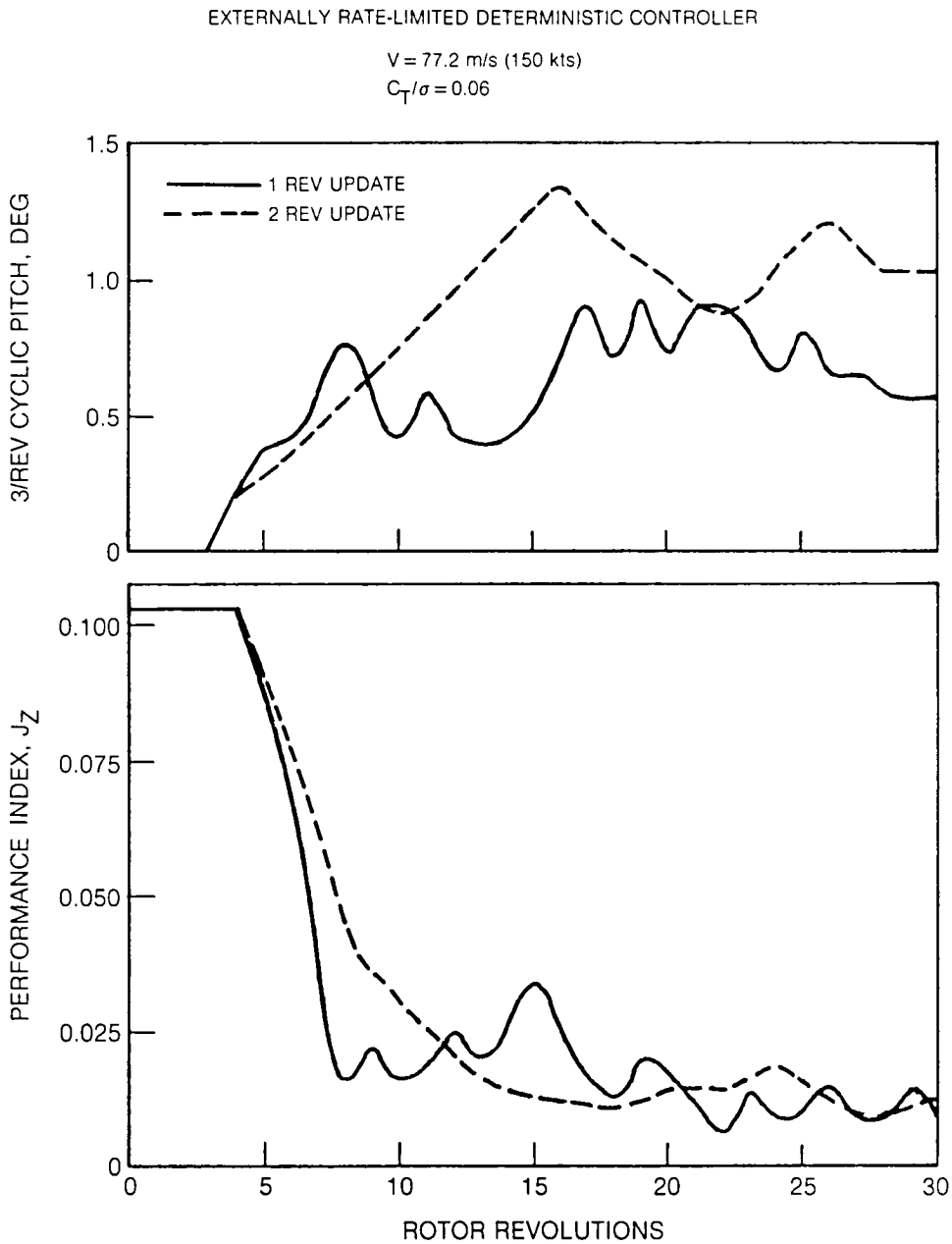

Fig. 85 Comparison of Controller Performance for One and Two Revs Between Controller Updates at Baseline Flight Condition

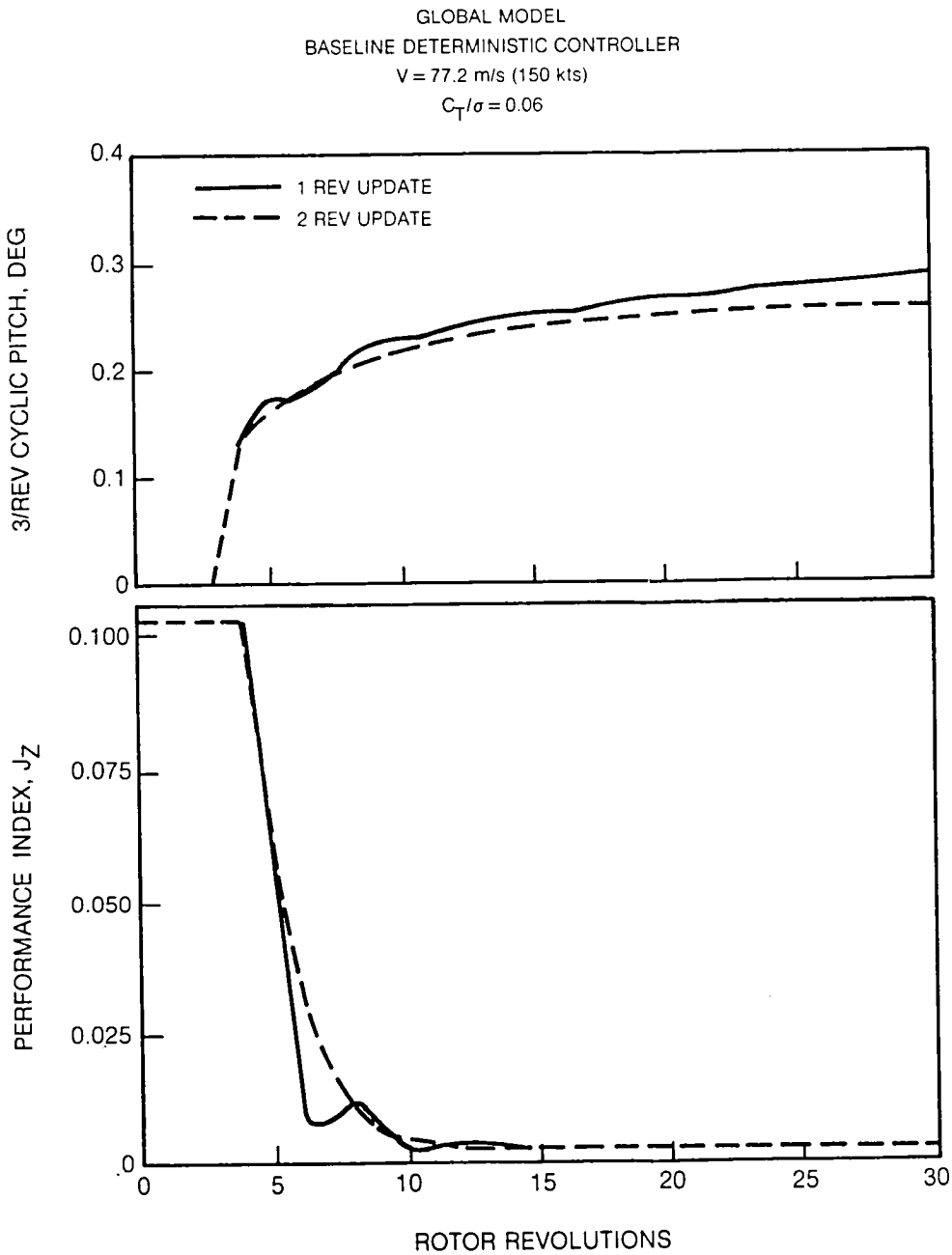

Fig. 86 Comparison of Controller Performance for One and Two Revs Between Controller Updates at Baseline Flight Condition

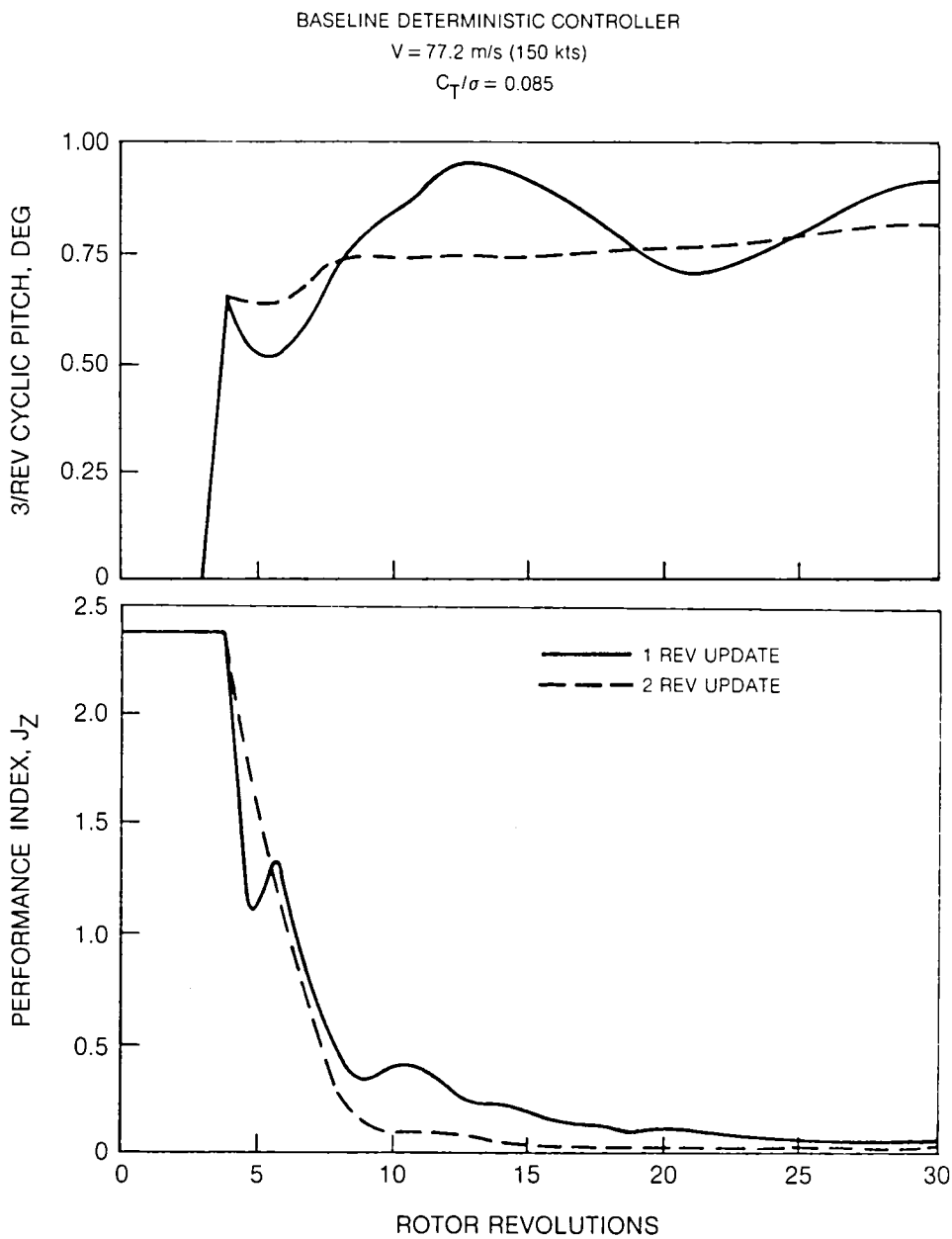

Fig. 87 Comparison of Controller Performance for One and Two Revs Between Controller Updates at High Thrust Condition

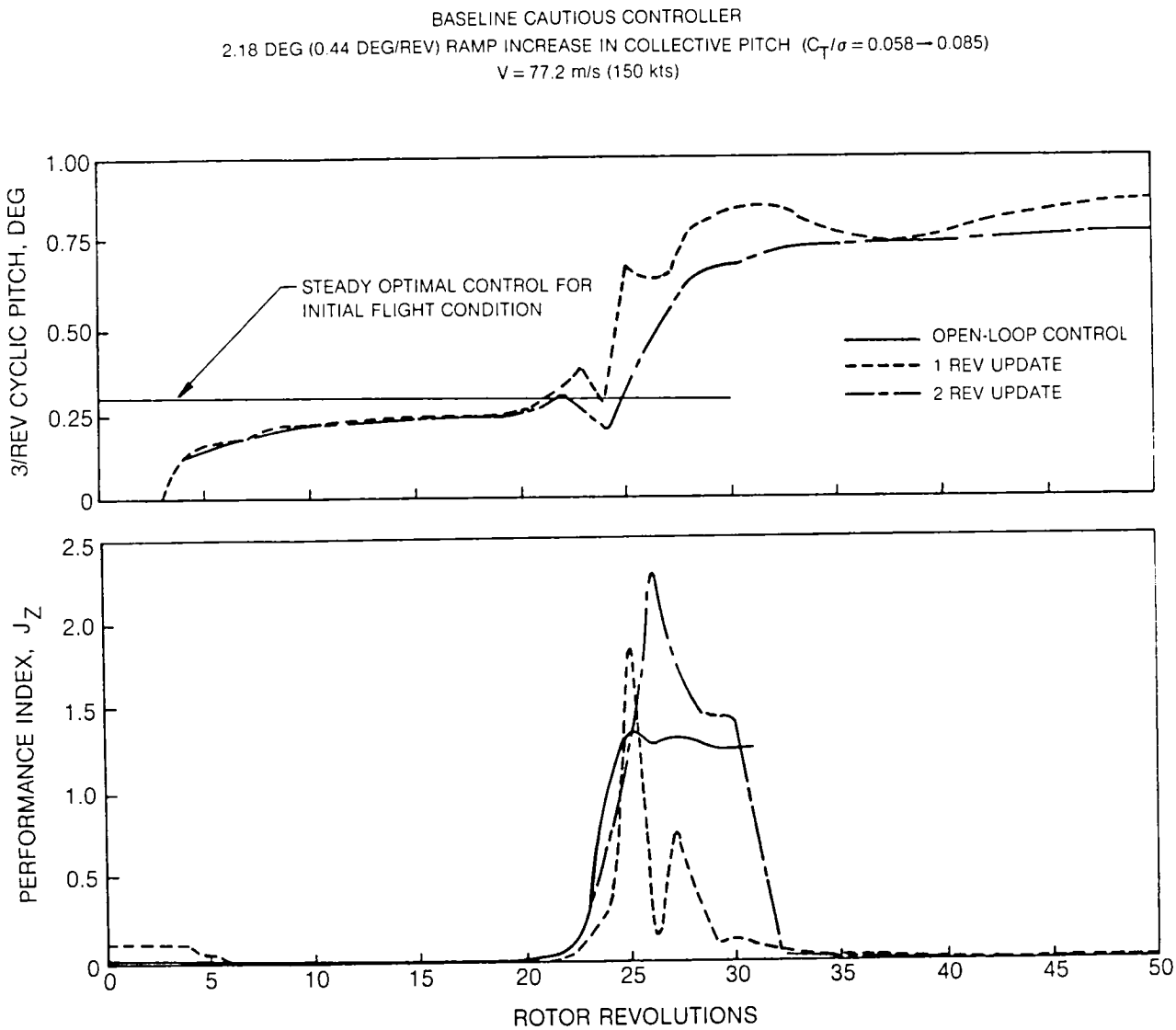

Fig 88 Comparison of Controller Performance for One and Two Revs Between Updates During Transient Maneuver

APPENDIX A

OPEN-LOOP NONLINEAR AND INTERHARMONIC RESPONSE

Charles Niebanck
Sikorsky Aircraft

Background

It is fairly well known from previous higher harmonic control (HHC) studies that rotor response to HHC has a degree of nonlinearity and interharmonic coupling (i.e., the rotor response perturbations are not strictly proportional to HHC inputs, and HHC input at a certain harmonic will create rotor responses at other harmonics). Despite this, in order to avoid undue mathematical complexity, the controller algorithms are designed on the basis of a rotor whose response is essentially linear, at least for a practically useful range of HHC increment size. The real-time self-adaptive controller configurations investigated herein do not consider the degree of interharmonic coupling as a controlled parameter. The interharmonic coupling that arises in the rotor is therefore combined with the response at the HHC frequencies in the G400 time history solution.

It is apparent that nonlinearity and interharmonic coupling may degrade the performance of the existing controllers. Nonlinearity will decrease the accuracy of the linearized calculations used by the controller to update HHC inputs and reduce vibration. The effects of interharmonic coupling combine with HHC frequency rotor response and are transmitted to the airframe or rotor support system where they appear as blade passage frequency vibrations. Therefore, it is possible for interharmonic coupling response from one HHC harmonic frequency to oppose the effects of HHC at the other two HHC frequency inputs. This creates the possibility of HHC amplitude requirements for vibration reduction which are higher than they would be without interharmonic coupling.

Objective of Open-Loop Nonlinearity and Interharmonic Coupling Study

The objective of the open-loop (i.e., controller inactive) study is to further understand the nonlinearity and interharmonic coupling characteristics of rotor response, and to provide a basis for possible definition of practicable criteria on the selection of controller or rotor parameters which could minimize degrading effects of these phenomena.

Specific concerns to be addressed in the pursuit of the above objective are:

- Understanding of the extent and source of nonlinearity and interharmonic coupling.
- Assessment of the degree to which nonlinearity and interharmonic coupling change between sample operating conditions of the rotor.
- Exploration of the extent to which nonlinearity and interharmonic coupling vary between different components of input HHC.

Description of Open-Loop Higher Harmonic Control (HHC) Cases for Nonlinearity and Interharmonic Coupling Investigation

Table A-1 presents the set of G400 Rotor Aeroelastic Analysis open-loop HHC cases chosen for this analytical study of nonlinearity and interharmonic coupling. A description of this analysis appears elsewhere in this report. HHC at the indicated amplitudes and phases was applied, and the G400 time history solution was allowed to settle to a steady state. Note that each case defined by a line in Table A-1 designates a group of several G400 runs. The cases were assigned to investigate the variation of nonlinearity and interharmonic coupling with various amplitudes and phases and with single and multicyclic HHC inputs. Two rotor operating conditions were investigated as shown. These were consistent with the conditions chosen for the closed-loop adaptive controller investigation. Cases 1 through 9 were HHC perturbations about zero HHC amplitude. Cases 10 through 12 are HHC perturbations superimposed on the optimal HHC case shown with Table A-1. Cases 10 through 12 examine the extent of nonlinearity and interharmonic coupling as the controller achieves such a solution, for comparison with perturbations about zero HHC, which represent conditions at controller turn-on.

Description of Parameters and Presentation Format for Evaluation of Nonlinearity and Interharmonic Coupling

The parameters examined for evidence of nonlinearity and interharmonic coupling were accelerations of the Rotor Systems Test Apparatus (RTA) at blade passage frequency (4P), single blade vertical root shears, blade flatwise, edgewise, and torsion modal responses, and blade out-of-plane airloads at a selected radial position.

Nonlinearity of RTA and nonlinearity and interharmonic coupling of rotor response were examined in terms of the cosine and sine amplitude response of

the various parameters. The polar response plots, represented by Fig. A-1, present the cosine versus sine parts of a stated response parameter at some stated frequency. For example, Fig. A-3 presents the cosine versus sine response of tail vertical vibration at the 4P blade passage frequency. An HHC input at some stated amplitude and phase will result in sine and cosine values of the response parameter, which will appear as a point on the polar plot. Returning to the Fig. A-1 example, hypothetical points for an HHC input of 1.5, 0, and -1.5 degrees are indicated, for some phase angle ϕ. Note that the -1.5 degree input is equivalent to a +1.5 degree input with a ±180 degree phase shift.

In order to indicate the degree of nonlinearity, a series of separate HHC conditions were run at a given flight condition. A constant increment in amplitude or phase of HHC was applied between each condition. For example, a series of cases at -1.5, -1.0, -0.5, 0, 0.5, 1.0, 1.5 degrees and a constant phase angle ϕ might be run. Connecting these points results in a contour such as the sample in Fig. A-1. In similar fashion, a series of HHC conditions at constant amplitude and phase angles of 0, 45, 90, 135, 180, 225, 270, 315, and 360 degrees might be run. This results, of course, in a closed contour. The degree of nonlinearity present affects the shape of the constant phase and constant amplitude contours.

If the coupled rotor-airframe/RTA system is completely linear, the changes in the various response parameters from the zero HHC baseline state could be obtained by multiplying the complex HHC input value by some complex constant. If one considers the polar form of the complex quantities involved, the mapping on the polar plot of the change in the response parameter due to a certain HHC increment can be expresed in the following way:

$$Z,\ \phi_Z = (k,\ \phi_k) * (\theta,\ \phi_\theta)$$

$$Z,\ \phi_Z = (k * \theta),\ (\phi_k + \phi_\theta)$$

where $Z,\ \phi_Z$ is the complex response with amplitude Z and phase angle ϕ_Z; $k,\ \phi_k$ is a complex constant with magnitude k and angle ϕ_k; and $\theta,\ \phi_\theta$ is the complex input component of HHC. Thus, the response amplitude change from zero HHC is proportional to the HHC amplitude, and the phase angle of the response is equal to the HHC phase angle plus a constant.

Therefore, equal increments of HHC amplitudes at a constant phase would map as equidistant points along a radial straight line starting at the zero HHC point in the response polar plot. On the other hand, equal increments of HHC phase at constant HHC amplitude would map on the response plot as points

at constant angular increments along circles with the zero HHC response at the center. Note that this mapping or transformation between HHC input and system response is equivalent to multiplying by a constant T-matrix.

The above obervations lead to the notion of judging the degree of system nonlinearity by comparing response tracks on the polar plots to radial straight lines or circles, as a series of appropriate HHC amplitudes at constant phase, or phases at constant amplitude are input to the system, respectively. Therefore, an immediate qualitative feel for the degree of nonlinearity is available merely by inspecting a series of such plots, generated for various responses within the system for various baseline flight conditions.

Although the above means of qualitative evaluation is valuable, some less subjective and more concise method is required for evaluation of the large number of polar plots that are generated by a detailed study. A means of quantifying the degree of nonlinearity is indicated in Fig. A-1, in terms of two numbers which quantify the departure of the response amplitude and phase from what would result from a linear system. An HHC amplitude of 1.5 degrees was selected arbitrarily for this purpose. Referring to Fig. A-1, a response due to HHC at +1.5, 0, and -1.5 degrees at some phase angle ϕ is plotted. The magnitude (distance on the polar plot) of the response change due to +1.5 degrees is divided by the similar quantity due to -1.5 degrees. The departure of this result from unity provides a quantitative measure of amplitude nonlinearity. A measure of the angle nonlinearity is provided by the angle between a line from the zero HHC response point to the respective +1.5 degree and -1.5 degree response points as indicated.

Interharmonic coupling refers to the generation of responses in the rotor at harmonic frequencies different from the HHC blade pitch frequency. The polar response plot was also used as a means of evaluating the degree and character of interharmonic coupling due to HHC. Figure A-2 provides a generalized sample of such a plot, which is analogous to Fig. A-1, except for inclusion of responses at frequencies other than the HHC frequency. As with Fig. A-1, inspection of the plot provides a qualitative impression of the degree and character of the interharmonic coupling. If interharmonic coupling is small, little change from the baseline zero HHC response will be noted at frequencies other than the specific input HHC frequency. As explained in connection with Fig. A-1, the degree of nonlinearity of the interharmonic coupling can be judged qualitatively or quantitatively from the departure of the tracks from radial straight lines or circles as, respectively, HHC amplitude is varied at constant phase, or HHC phase is varied at constant amplitude.

A quantitative evaluation of interharmonic coupling is also required, to facilitate comparisons and overviews when multiple response parameters and flight conditions are to be studied. Thus, evaluation parameters are formed by using the distances on the polar plots between the response points for +1.5 degrees and -1.5 degrees. As indicated on Fig. A-2, I_{43} is the evaluation parameter for 3P response due to 4P HHC input, and I_{45} is the parameter for 5P response due to 4P HHC input. The parameter I_{43} is the ratio of the distance between the ends of the 3P track divided by the distance between the ends of the 4P track, as indicated in Fig. A-2. In similar fashion, five other interharmonic coupling parameters are defined. These reflect 5P response due to 4P HHC, 4P and 5P response due to 3P HHC, and 3P and 4P response due to 5P HHC.

Evaluation of nonlinearity with respect to HHC input will proceed by first examining an RTA control point (namely the tail vertical accelerometer) as a sample system output parameter. Similarly, evidence of interharmonic coupling in the rotating system will be examined by starting with single blade vertical root shear vibratory loadings. Subsequently, blade bending and torsion mode response and aerodynamic loadings will be examined to provide insight on the source of nonlinearity and interharmonic coupling.

Presentation and Discussion of Open-Loop Results

An overview of the nonlinearity results for the response of the RTA to HHC inputs appears in Table A-2, in terms of the blade passage frequency acceleration at the tail vertical control point. The nonlinearity, expressed in terms of the parameters defined in Fig. A-1, is considered mild, at least in terms of the results of perturbations about the zero open-loop HHC condition. Some increase in nonlinearity is evident for the 5P HHC input, and as the rotor lift is increased from the $C_T/\sigma = 0.058$ condition to the $C_T/\sigma = 0.085$ condition.

An overview of the interharmonic coupling results appears in Table A-3, in terms of the single-blade vertical root shear response to HHC inputs, and the parameters defined in Fig. A-2. It appears that interharmonic coupling increases with rotor lift and can become quite large. For example, the 3P vertical shear force increment due to ±1.5 degree 4P sine HHC is 1.7 times as high as the corresponding 4P vertical force increment. Substantial coupling can exist not only between adjacent harmonics, but also between 3P response due to 5P HHC and 5P response due to 3P HHC.

Samples of the G400 Aeroelastic Analysis results in terms of the polar plots used to prepare Table A-2 are provided in Figs. A-3 through A-7. Figure A-3 shows tail vertical response for the $C_T/\sigma = 0.058$ condition as a function of 5P HHC amplitude and phase input. The response is considered mildly

nonlinear, as indicated by variations in spacing between lines of constant HHC amplitude, and curvature in the constant phase HHC tracks. Figure A-4 shows the effect of multi-harmonic HHC for an input of 1.5 degrees of 3P HHC. Adding the indicated ±1 degree of 5P HHC changes the shape of the constant amplitude HHC track, showing some mild nonlinearity. Figure A-5 presents simplified plots showing the effects of rotor lift condition on the response to 3P sine HHC input. The increase in lift causes the response to HHC to become more nonlinear, as shown by the curvature in the track of pure sine HHC input. Figure A-6 exhibits simplified plots showing the effect of the controller-determined optimal HHC on the response to open-loop 5P sine HHC. Note at zero open-loop input, the vibration response is much smaller in the right-hand plot because of the optimal HHC applied by the closed loop system. The incremental response due to the open-loop HHC appears reasonably similar, indicating no gross effects of nonlinearity. Figure A-7 shows results that are somewhat different for 3P open-loop HHC inputs. The plots in Fig. A-7 show tracks of constant HHC input phase at 0-180 and 90-270 degrees with varying amplitude, and a track of constant HHC amplitudes at 1.5 degrees for a phase sweep of 0 to 360 degrees. The incremental change in response due to 3P HHC is considerably smaller in the presence of the pre-existing optimal HHC, and a larger amount of nonlinearity is indicated.

Samples of the G400 Aeroelastic Analysis results, in terms of the polar plots used to prepare Table A-3, are provided in Figs. A-8 through A-10. Figure A-8 shows the single-blade vertical root shear load harmonic response variation as various amounts of 4P sine HHC are applied at the $C_T/\sigma = 0.058$ condition. The response is reasonably linear, but the variation of 3P and 5P loadings compare in magnitude to the 4P loadings. Figure A-9 shows similar data for the $C_T/\sigma = 0.085$ condition. Some similarities with Fig. A-8 may be noted. The trajectory of the 4P response is similar in length and direction, for example. The size of the 3P and the 5P responses have, however, increased and the 3P response to 4P HHC is larger than the 4P response. Figure A-10 presents the same type of data when the open-loop HHC is applied as a perturbation about the controller-defined optimal HHC. The general trend of the three harmonic response components is similar, but the relative amount of 5P response is even larger.

Diagnostic Investigation of Sources of Nonlinearity and Interharmonic Coupling of HHC

The previous paragraphs provided an overview of nonlinear and interharmonic coupling behavior at the appropriate system output points - namely an RTA acceleration control point and the rotating system hub shears.

In the following, a search for the sources of the nonlinear and interharmonic coupling behavior will be conducted, using system internal dynamic response data available from the G400 runs. Because of the nonlinear effects evident in Fig. A-7 for 3P HHC and 3P HHC plus optimal HHC, Figs. A-11 through A-13 (similar to A-8 through A-10 except for HHC frequency) have been presented. At $C_T/\sigma=0.058$ vertical root shear response (VRSR) due to 3P is linear with significant 4P coupling, as shown in Fig. A-11. At $C_T/\sigma=0.085$ VRSR at 3P due to 3P is still essentially linear, as shown in Fig. A-12. The length of the 3P track is still unchanged, but interharmonic coupling has become nonlinear. At $C_T/\sigma=0.085$ with optimum HHC (Fig. A-13), VRSR at 3P due to 3P is more nonlinear, and the length of the track is only about 30 percent of the length in the two preceding plots for cases without optimal HHC. This indicates that the rotating rather than the fixed system contains the source of the reduction in sensitivity to 3P HHC that appears on the right hand side of Fig. A-7. It also appears that nonlinearity is most evident in the interharmonic coupling response, at least for 3P HHC.

Figures A-14 through A-21 present details of the modal and airloads response to 3P HHC alone. First, flatwise bending mode 3P response to 3P is comparatively linear, with small though nonlinear interharmonic coupling, as shown in Fig. A-14. Second, flatwise bending mode response (Fig. A-15) exhibits large and nonlinear interharmonic coupling in its response, as does the third flatwise bending mode (Fig. A-16). The first edgewise bending mode response shown in Fig. A-17 is, like the first flatwise bending mode, comparatively linear with relatively minor interharmonic coupling. The torsion mode response shown in Fig. A-18 is relatively linear, with substantial coupling of 4P response. The out-of-plane airloads are also relatively linear, with substantial coupling of 4P response, as shown in Fig. A-19.

The flatwise airloads are the principal forces entering the rotor system as a result of HHC. Since these are comparatively linear with HHC input, it is indicated that the increased nonlinearity of the vertical root shear response (see Fig. A-12) is due to the inherent nonlinearities present in the blade dynamic response.

The flatwise airloads display considerable interharmonic coupling. In terms of Fig. A-19, considerable 4P loads result from 3P HHC inputs. An overview of airloads interharmonic coupling ratios is given in Table A-4, in a manner similar to Table A-3. The interharmonic coupling increases with lift and other HHC components, but remains milder in comparison to vertical root shears harmonic interaction shown in Table A-3. Review of Figs. A-14 through A-18 for relative amounts of interharmonic coupling suggest that the second and third flatwise bending mode response is the principal source of interharmonic coupling increase between the airloads and the root shears. Simplified analytical considerations were employed to assess the source of the interharmonic coupling present in the airloads response to HHC.

Local blade lift loading due to HHC can be expressed simply by:

$$L_{HHC} = \frac{\rho c}{2} (\Omega r + V\sin\psi)^2 \, C_{L\alpha} \, \alpha_{HHC}$$

where r is the blade radius
V is forward velocity of the helicopter
ψ is the blade azimuth angle
$C_{L\alpha}$ is the lift curve slope
α_{HHC} is angle of attack due to HHC

By letting $\alpha_{HHC}=\theta_3\sin 3\psi$, $\theta_4\sin 4\psi$, $\theta_5\sin 5\psi$ and expanding the expression with common trigonometric identities, one obtains expressions for harmonic parts of L_{HHC}. These were evaluated numerically and ratios formed, similar to those from the G400 results in Table A-3. These analytical ratios are presented in Table A-5.

Comparison of Table A-5 with the results from Table A-4 at the $C_T/\sigma = 0.058$ condition indicates that most (70 or 80 percent) of the low lift interharmonic coupling airload is attributable to the above basic term. Departure of the airload versus angle of attack from the above linear relationship and harmonic blade deflections will add additional interharmonic coupling. This could explain the increase in interharmonic coupling shown in Table A-4 for the higher lift conditions.

In addition to local nonlinearity revealed by curvature and increment spacing on the polar plots, a second type is evident by the disparity in magnitude of system response to 3P inputs, as shown in Fig. A-7, as a result of adding the multicyclic optimal HHC input. This tendency is also revealed in the single-blade vertical root shear plots, by comparing the 3P response in Figs. A-12 and A-13. Adding the optimal controller HHC reduces the 3P HHC incremental root shear response to close to 1/3 of its former value as measured by the length of the 3P track. Comparing the corresponding 3P airloads tracks on Figs. A-19 and A-20, one finds that addition of the optimal multicyclic input reduces the airloads to the blade to about 80 percent of its former value.

The disparity is apparently primarily due to a difference in blade modal response. Figures A-21 and A-22 show 3P first flatwise and edgewise bending mode responses that are, respectively, about 1/2 and 1/5 of their magnitudes without the multicyclic input.

Concluding Remarks - Nonlinearity and Interharmonic Coupling

At relatively low lift (C_T/σ=0.058) 4P airframe acceleration response to HHC is essentially linear for 3P and 4P inputs, and moderately nonlinear for 5P inputs. At moderate lift (C_T/σ=0.085) 4P airframe acceleration response to HHC is moderately nonlinear in character for all three HHC frequency components (3P, 4P, 5P).

The response per unit input of HHC perturbation changes significantly with flight condition and with co-existing multicyclic HHC input. This is true even though response is essentially linear with respect to those localized perturbations. Multicyclic optimal HHC was found to have a particularly severe effect on the amplitude and linearity of the vibration response to superimposed 3P open-loop HHC inputs. In general, blade mode bending response appears to be the source of most of the nonlinearity in the response. Airloads interharmonic coupling is principally between adjacent harmonics (i.e., 3P HHC produces significant 4P, 4P HHC produces significant 3P and 4P, 5P produces significant 4P). It appears that airload interharmonic coupling is basically of a magnitude that could be expected from the product of local dynamic pressure, lift curve slope, chord, density, and HHC angle varying at 3, 4, or 5P.

Actual blade response interharmonic coupling is generally substantially greater than the airload interharmonic coupling. This additional interharmonic coupling was greater at the higher lift conditions, and appears to be due to blade bending mode response. Interharmonic coupled response can be very large (substantially higher than response at the HHC perturbation input frequency). Its amplitude and phase vary substantially with rotor operating condition and with superimposed multicyclic HHC. Interharmonic coupling between 5P response to 3P HHC and between 3P response to 5P HHC can also be substantial, and variable with different flight conditions and superimposed multicyclic HHC.

From the above, it can be expected that interharmonic coupling can cause a substantial increase or decrease in the HHC amplitude that would otherwise be required.

From the cases considered in this study, no systematic relationship of HHC response nonlinearity and interharmonic coupling with flight condition can be ascertained. It appears that nonlinearity and interharmonic coupling are inherent in the rotor response, principally in blade aeroelastic response. The levels of nonlinearity and interharmonic coupling present for the flight conditions considered in this study did not prevent successful controller operation. It is believed that controller operation can be enhanced with respect to HHC amplitude required and convergence rates if the degrading

effects of nonlinearity and interharmonic coupling could be minimized. It is also believed that the degrading effects of nonlinearity and interharmonic coupling will be best minimized by using a systematic series of trial weighting factors on the HHC amplitude components of the performance function, applied and evaluated over a representative series of flight conditions during the controller tuning process.

TABLE A-1 - OPEN-LOOP HHC CASES FOR NONLINEARITY AND INTERHARMONIC COUPLING STUDY

FORWARD SPEED V = 150 kts

CASE	C_T/σ	3P INPUT		4P INPUT		5P INPUT	
		AMP (deg)	PHASE (deg)	AMP (deg)	PHASE (deg)	AMP (deg)	PHASE (deg)
1	0.058	0-2.5	0-360				
2	0.085	0-1.5	90,270				
3	0.058			0-2.5	0-360		
4	0.085			0-1.5	90,270		
5	0.058					0-2.5	0-360
6	0.085					0-1.5	90,270
7	0.058	1.5	0-360	1	0,180		
8	0.058	1.5	0-360			1	0,180
9	0.058	1.5	0-360	1	0,180	1	0,180
10	0.085	0-1.5	0-360				
11	0.085			0-1.5	0-360		
12	0.085					0-1.5	0-360

NOTES - TABLE A-1

1. Indicated amplitude variations were generally at intervals of 1/2 degree.

2. Indicated phase variations were at intervals of 90° or 45° as appropriate.

3. Cases 1-9 are perturbations about zero HHC inputs. Cases 10-12 are perturbations about a controller-defined optimal HHC input listed below:

HARMONIC	COSINE PART	SINE PART
3	.89	.12
4	.22	.90
5	-.69	-.20

TABLE A-2 - OVERVIEW OF NONLINEARITY OF RESPONSE OF RTA TO OPEN-LOOP HHC INPUTS

RTA 4P TAIL VERTICAL ACCELERATION

CASE	C_T/σ	HHC INPUT	RESPONSE NONLINEARITY	
			MAG	ϕ_Δ (deg)
1	0.058	3P SIN	.97	14
3	0.058	4P SIN	1.12	25
5	0.058	5P SIN	1.42	19
7	0.058	3P SIN, 1° 4P COS	1.00	8
7	0.058	3P SIN, -1° 4P COS	1.08	-8
8	0.058	3P SIN, 1° 5P COS	1.08	10
8	0.058	3P SIN, -1° 5P COS	1.19	-25
9	0.058	3P SIN, 1° 4P COS, 5P COS	.92	25
9	0.058	3P SIN, -1° 4P COS, 5P COS	1.3	25
2	0.085	3P SIN	.89	-32
4	0.085	4P SIN	.75	2
6	0.085	5P SIN	1.45	29
10	0.085	3P SIN + OPTIMAL HHC	1.67	-9
11	0.085	4P SIN + OPTIMAL HHC	.78	-13
12	0.085	5P SIN + OPTIMAL HHC	1.19	23

TABLE A-3 - OVERVIEW OF INTERHARMONIC COUPLING OF RESPONSE OF SINGLE-BLADE VERTICAL SHEAR TO HHC

CASE	C_T/σ	HHC INPUT	INTERHARMONIC COUPLING RATIO		
			3P	4P	5P
1	0.058	3P SIN	1.0	0.57	0.09
3	0.058	4P SIN	0.83	1.0	0.44
5	0.058	5P SIN	0.30	0.59	1.0
2	0.085	3P SIN	1.0	0.83	0.36
4	0.085	4P SIN	1.7	1.0	1.2
6	0.085	5P SIN	0.61	0.65	1.0
10	0.085	3P SIN + OPTIMAL HHC	1.0	1.8	0.71
11	0.085	4P SIN + OPTIMAL HHC	1.5	1.0	1.1
12	0.085	5P SIN + OPTIMAL HHC	0.76	0.64	1.0

TABLE A-4 - OVERVIEW OF INTERHARMONIC COUPLING OF OUT-OF-PLANE AIRLOADS RESPONSE (.78R) TO HHC

CASE	C_T/σ	HHC INPUT	INTERHARMONIC COUPLING RATIO 3P	4P	5P
1	0.058	3P SIN	1.0	.42	.06
3	0.058	4P SIN	.50	1.0	.49
5	0.058	5P SIN	.09	.50	1.0
2	0.085	3P SIN	1.0	.73	.17
4	0.085	4P SIN	.75	1.0	.92
6	0.085	5P SIN	.19	.71	1.0
10	0.085	3P SIN+OPTIMAL HHC	1.0	.88	.43
11	0.085	4P SIN+OPTIMAL HHC	.69	1.0	.86
12	0.085	5P SIN+OPTIMAL HHC	.42	.75	1.0

TABLE A-5 - INTERHARMONIC COUPLING RATIOS FROM TANGENTIAL VELOCITY HHC FREQUENCY PRODUCT

$$\frac{\rho c}{2} (\Omega r + V \sin \psi)^2 \cdot C_{L\alpha} \cdot \alpha_{HHC}$$

$r = .78R$ $\quad \Omega r = 650$ FT/SEC $\quad V = 150$ kts

HHC INPUT	INTERHARMONIC COUPLING RATIO		
	3P	4P	5P
3P SIN	1.0	.35	.01
4P SIN	.36	1.0	.36
5P SIN	.04	.36	1.0

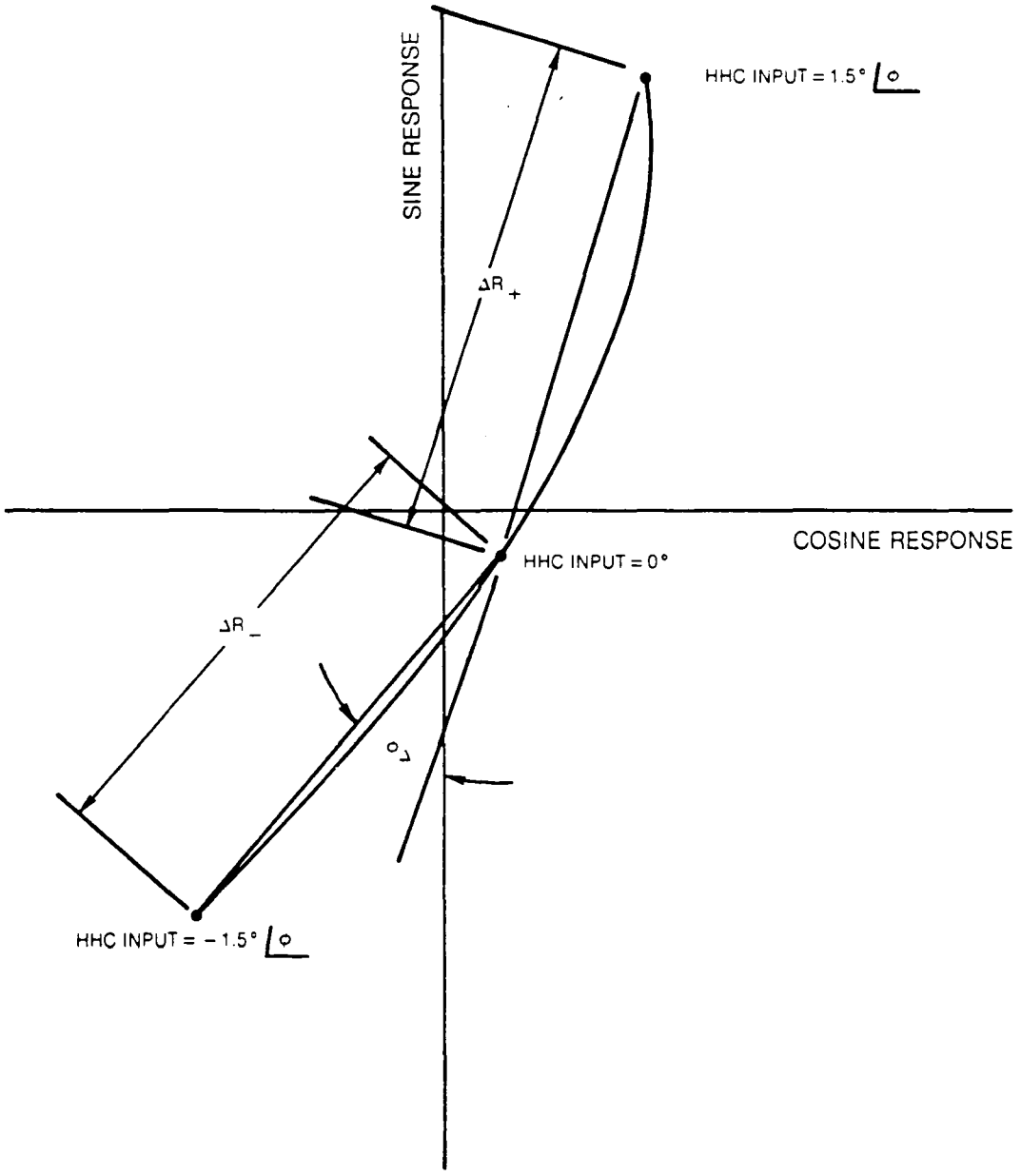

Fig. A-1 Diagram Characterizing Nonlinearities of Response to Higher Harmonic Control

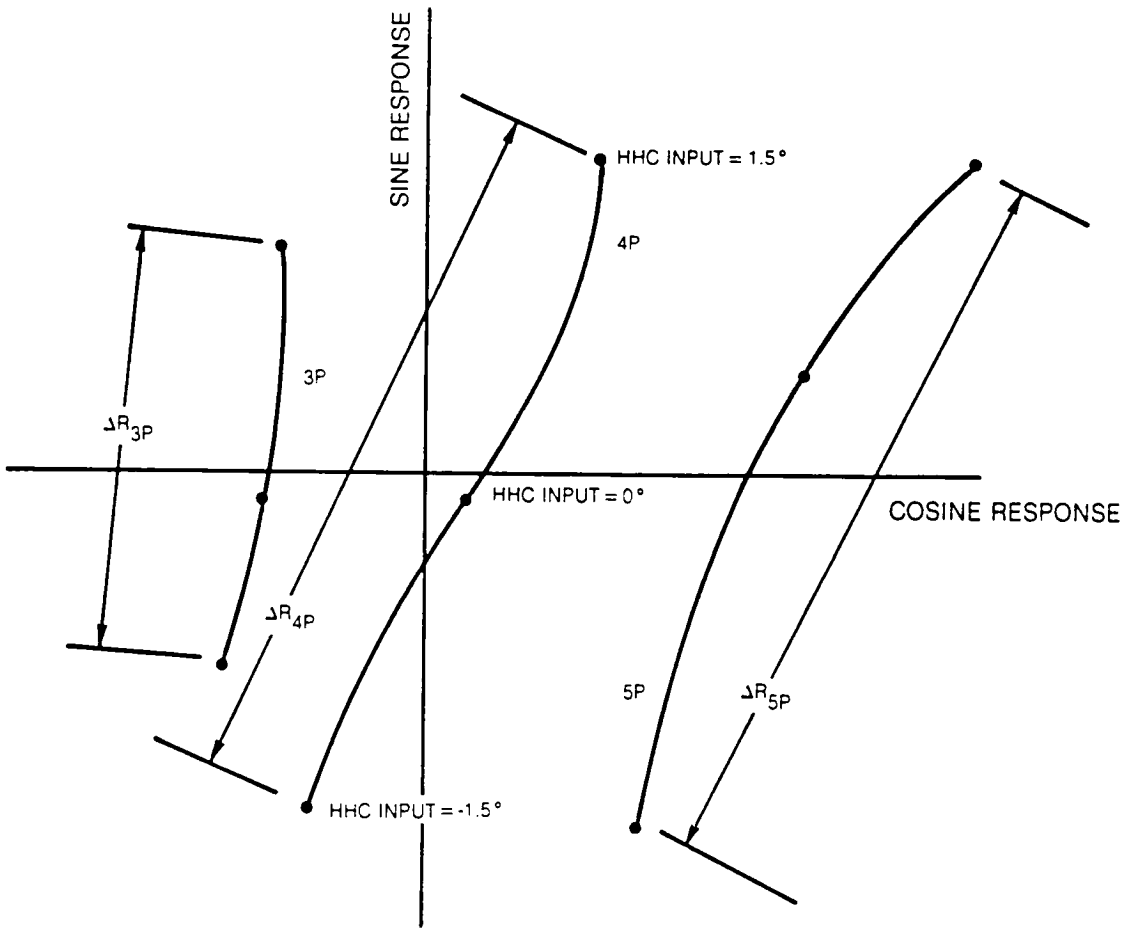

FOR CASE OF 4P HHC

$I_{43} = \Delta R_{3P}/\Delta R_{4P}$
$I_{45} = \Delta R_{5P}/\Delta R_{4P}$

SIMILARLY FOR 3P AND 5P HHC

$I_{34} = \Delta R_{4P}/\Delta R_{3P}$ $I_{53} = \Delta R_{3P}/\Delta R_{5P}$
$I_{35} = \Delta R_{5P}/\Delta R_{3P}$ $I_{54} = \Delta R_{4P}/\Delta R_{5P}$

Fig. A-2 Diagram of Interharmonic Coupling Characterization

V = 77.2 m/s (150 kts)
$C_T/\sigma = 0.058$

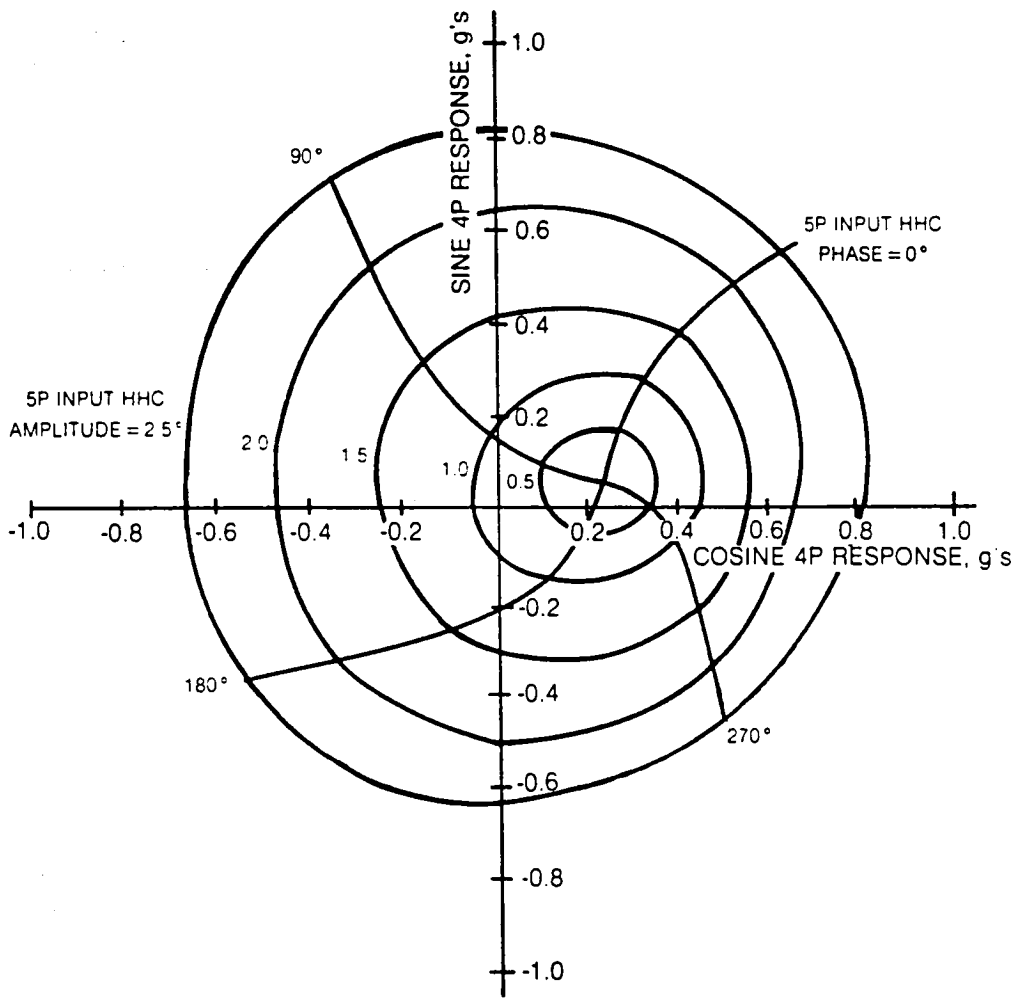

Fig. A-3 RTA Tail Vertical Vibration Due to Open-Loop 5P Input (Case 5)

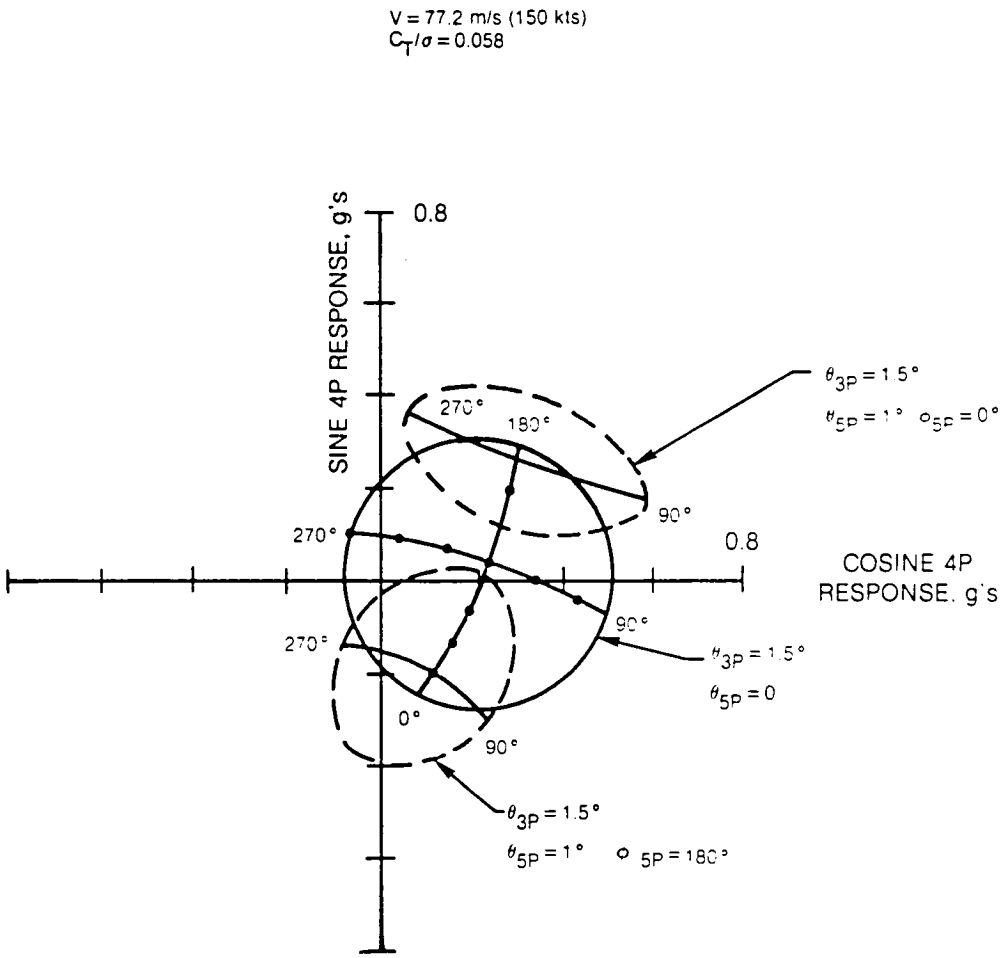

Fig. A-4 RTA Tail Vertical Vibration Due to Open-Loop 3P and Multi-Harmonic 3P and 5P HHC Input (Cases 1 and 8)

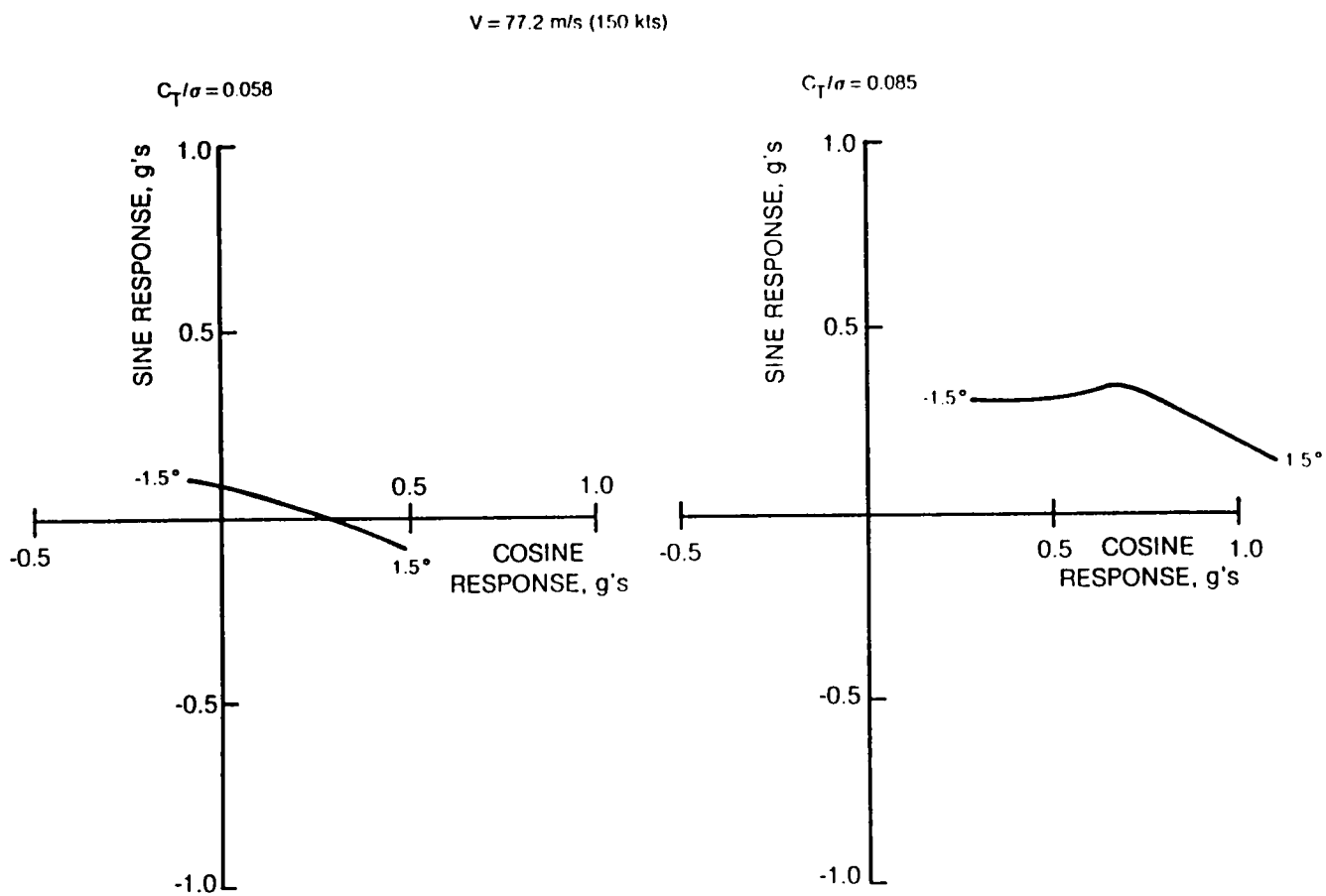

Fig. A-5 RTA Tail Vertical Vibration Due to Open-Loop 3P Sine HHC Input (Cases 1 and 2)

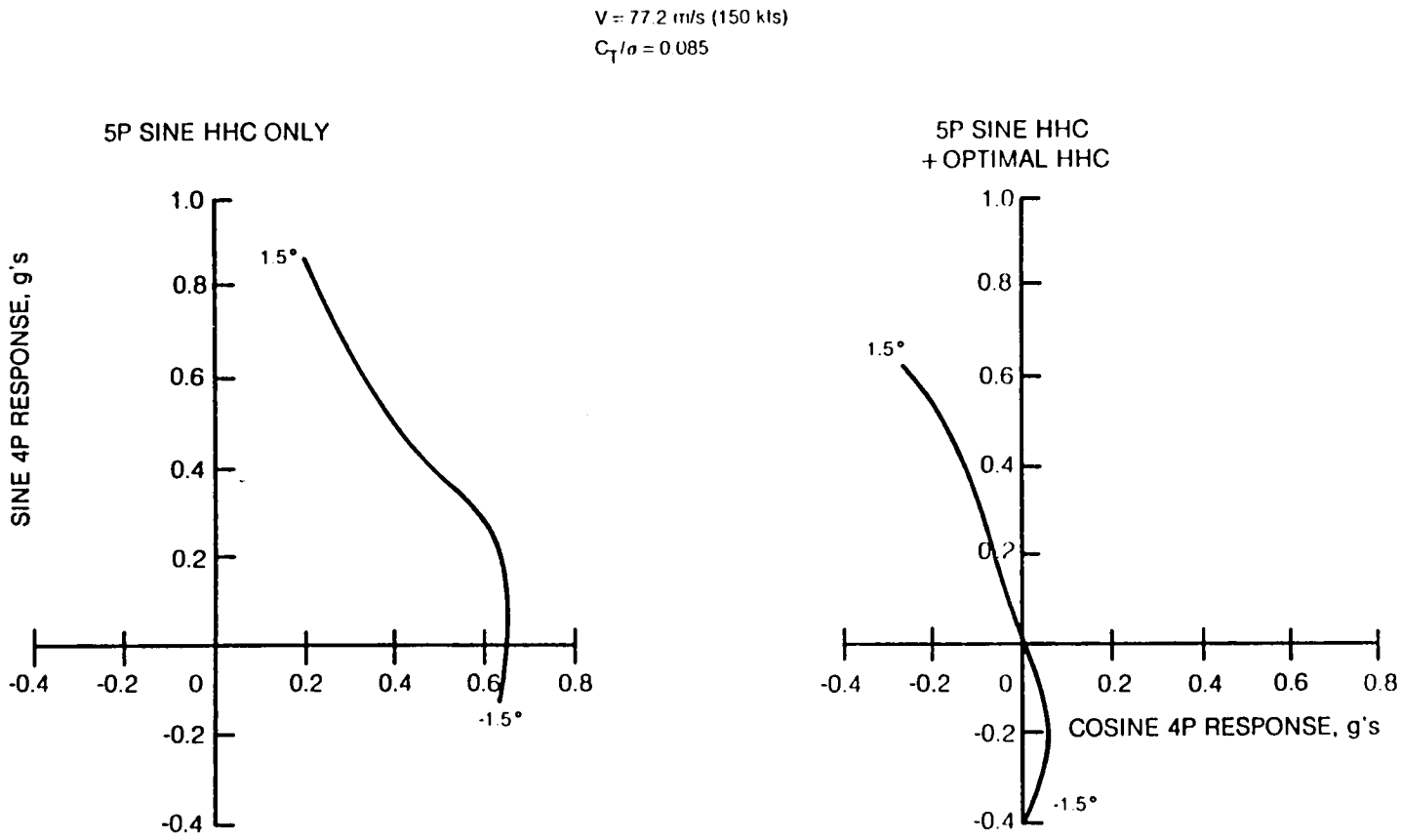

Fig. A-6 RTA Tail Vertical Vibration Due to Open-Loop 5P Sine HHC Input (Cases 6 and 12)

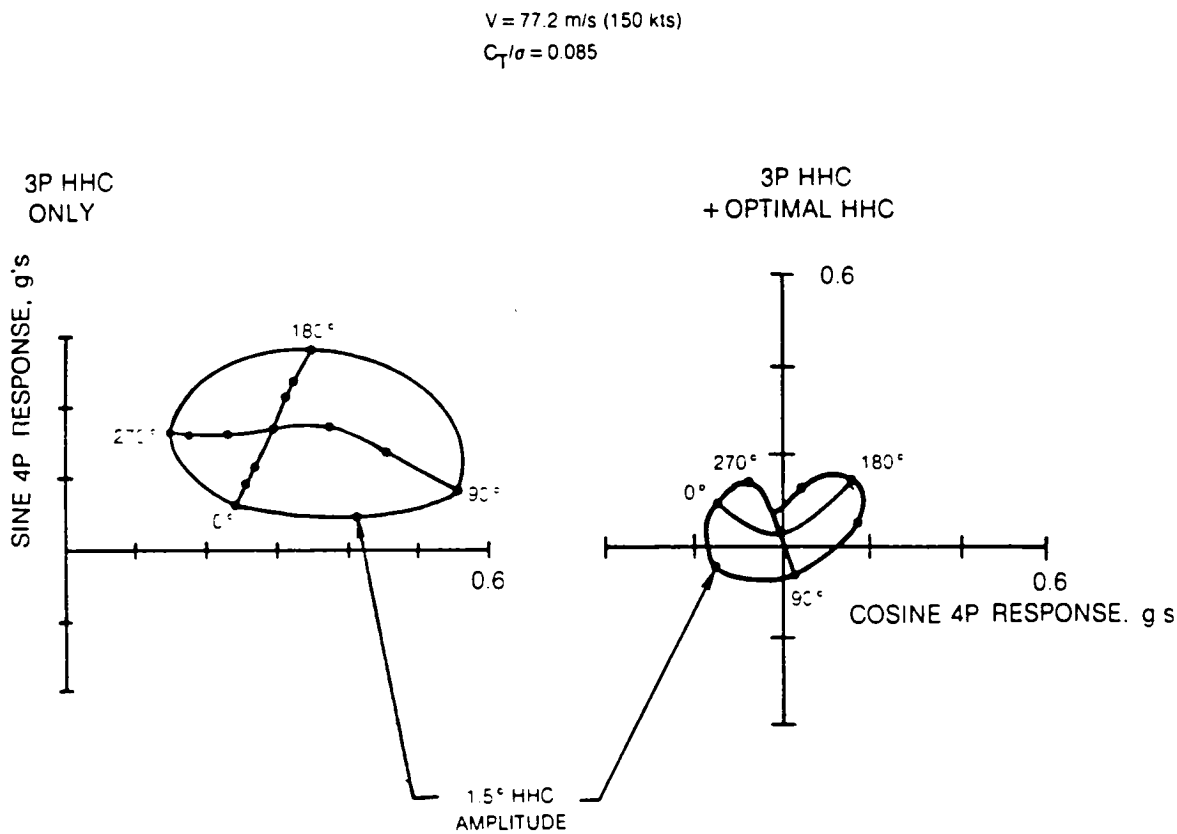

Fig. A-7 RTA Tail Vertical Vibration Due to Open-Loop 3P HHC (Cases 2 and 10)

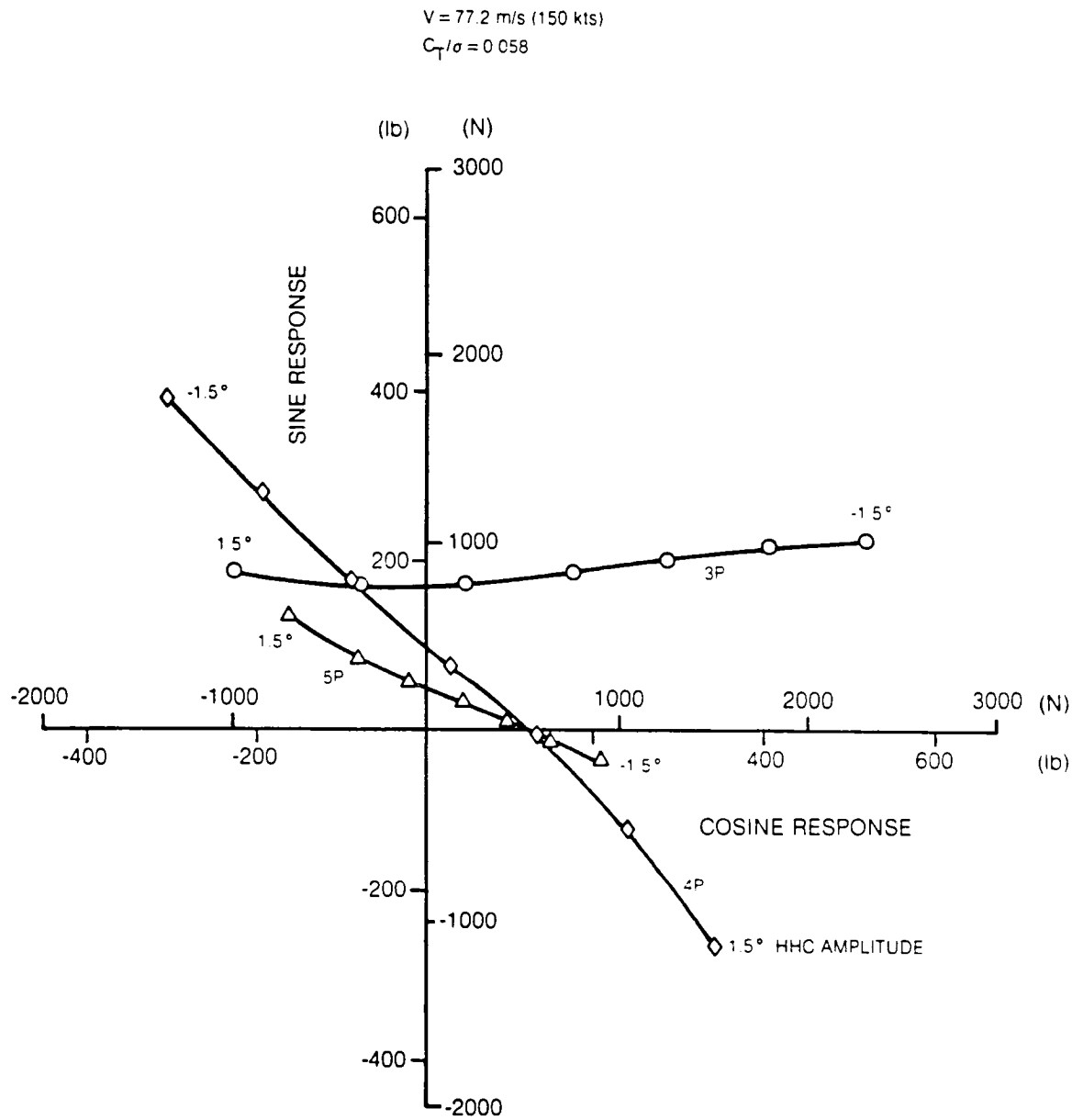

Fig. A-8 Single Blade Vertical Root Shear Response to 4P Sine HHC (Case 3)

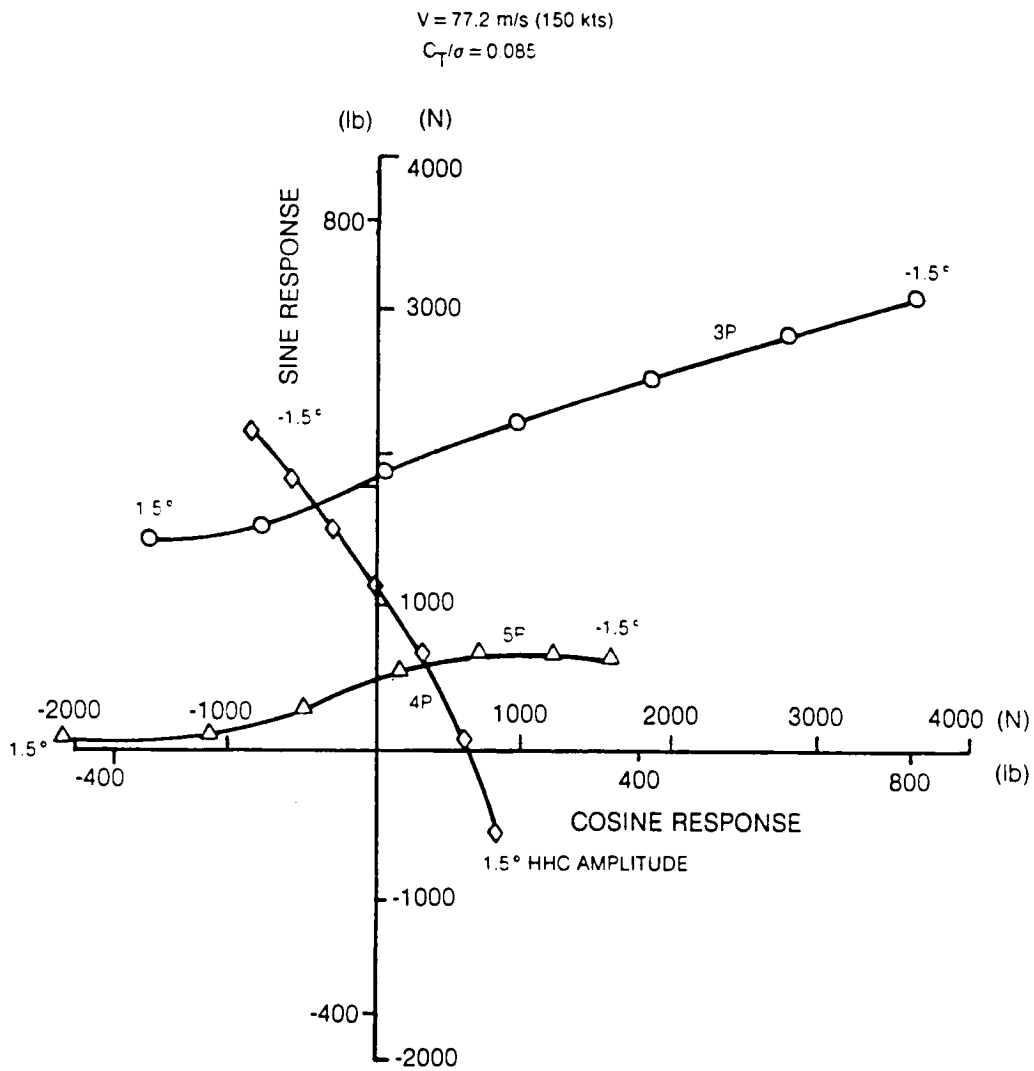

Fig. A-9 Single Blade Vertical Root Shear Response to 4P Sine HHC (Case 4)

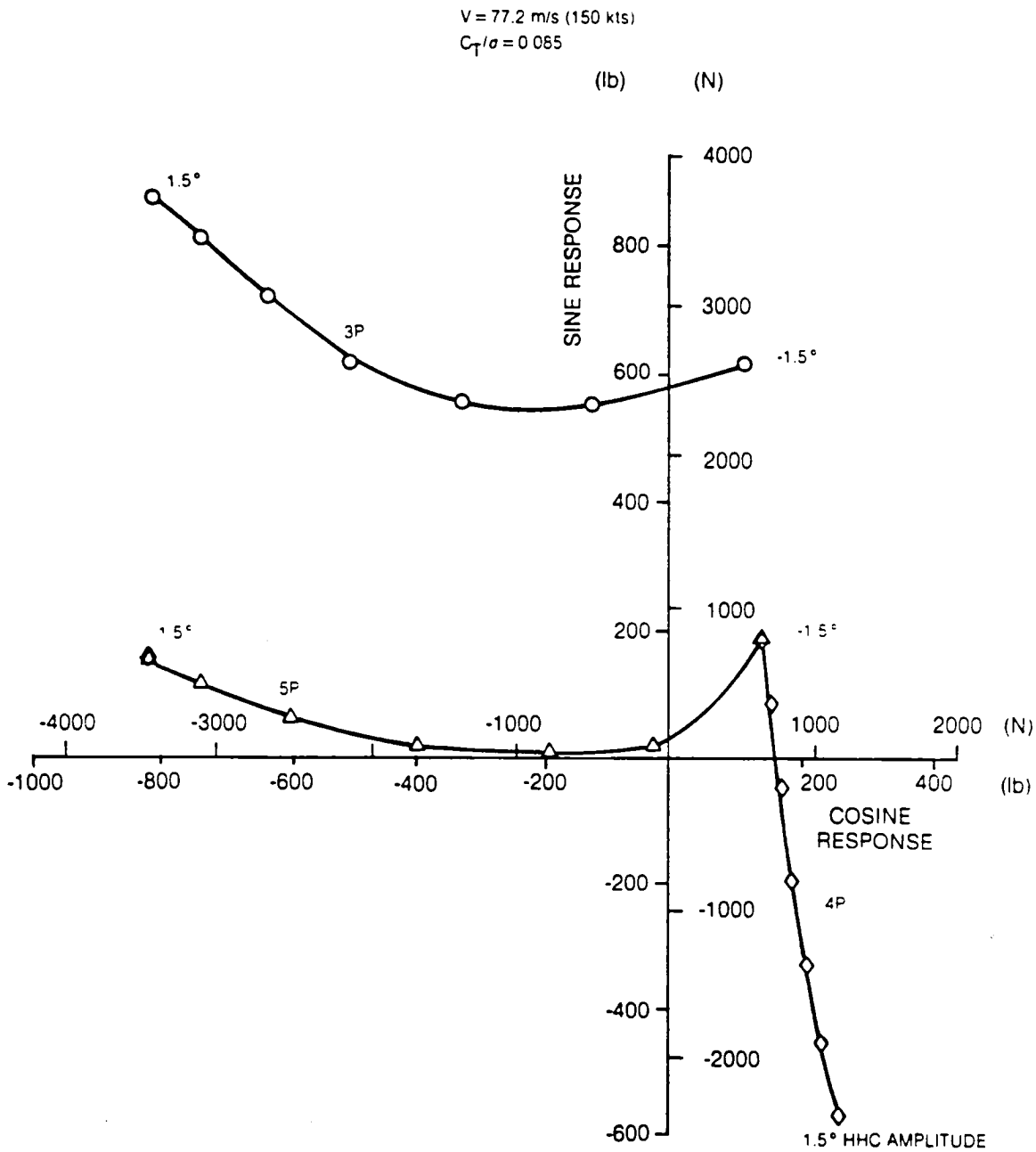

Fig. A-10 Single Blade Vertical Root Shear Response to 4P Sine HHC + Optimal Controller HHC (Case 11)

V = 77.2 m/s (150 kts)
$C_T/\sigma = 0.058$

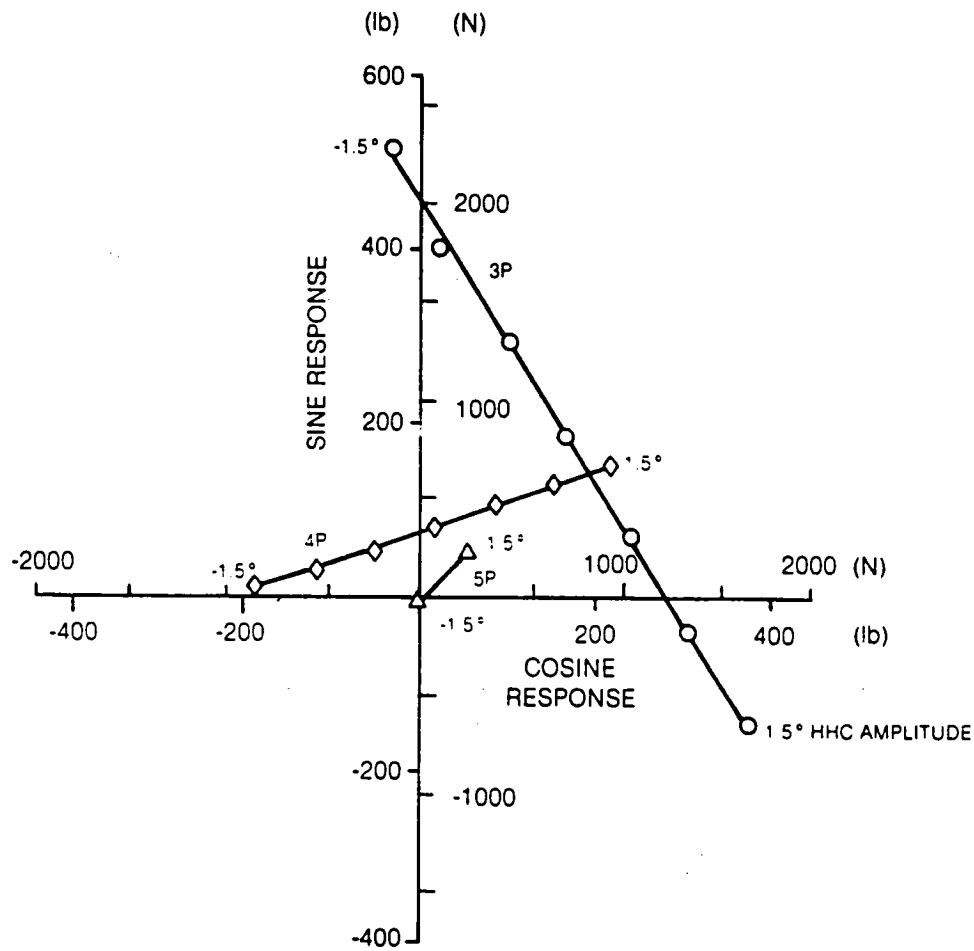

Fig. A-11 Single Blade Vertical Root Shear Response to 3P Sine HHC (Case 1)

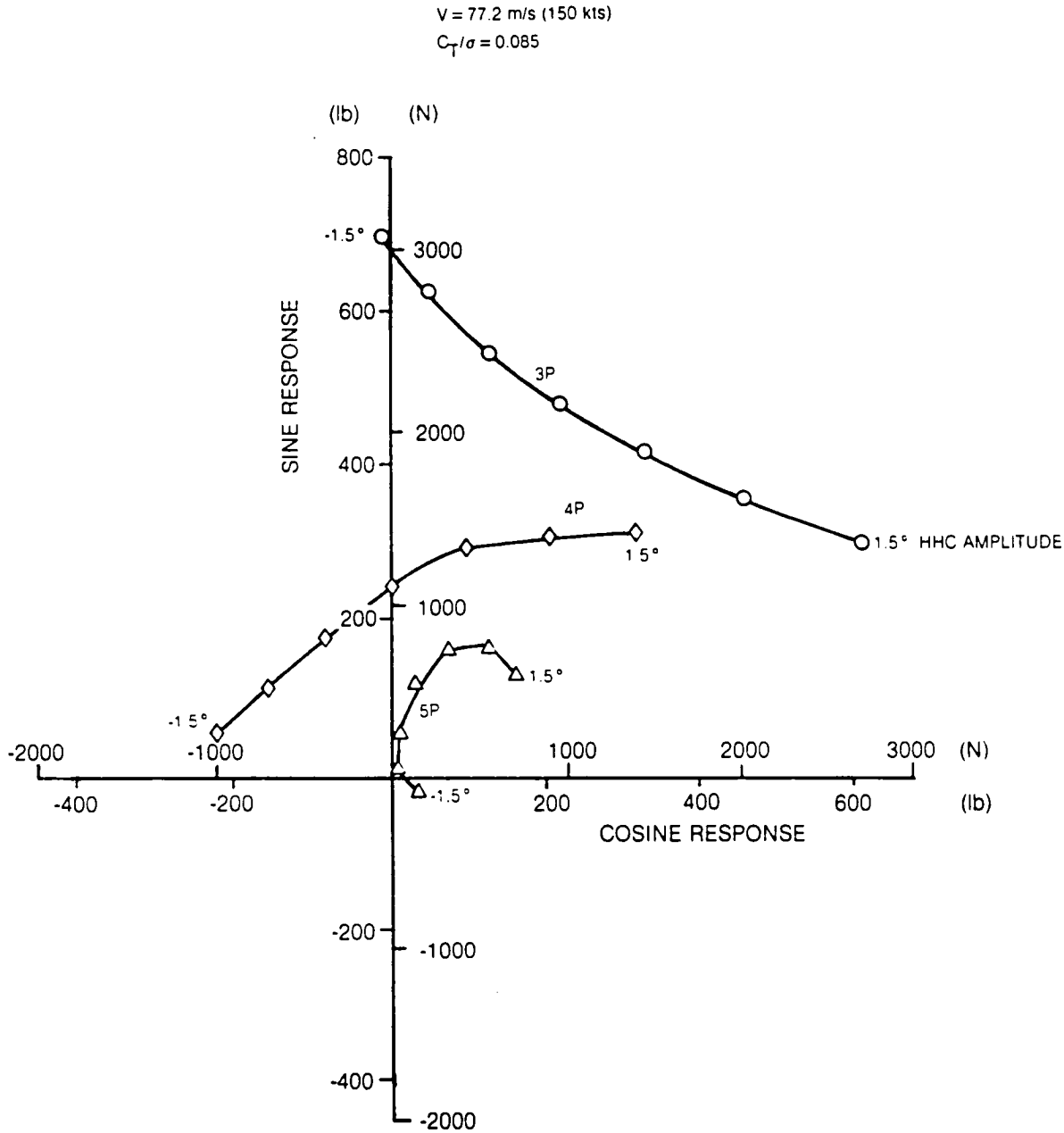

Fig. A-12 Single Blade Vertical Root Shear Response to 3P Sine HHC (Case 2)

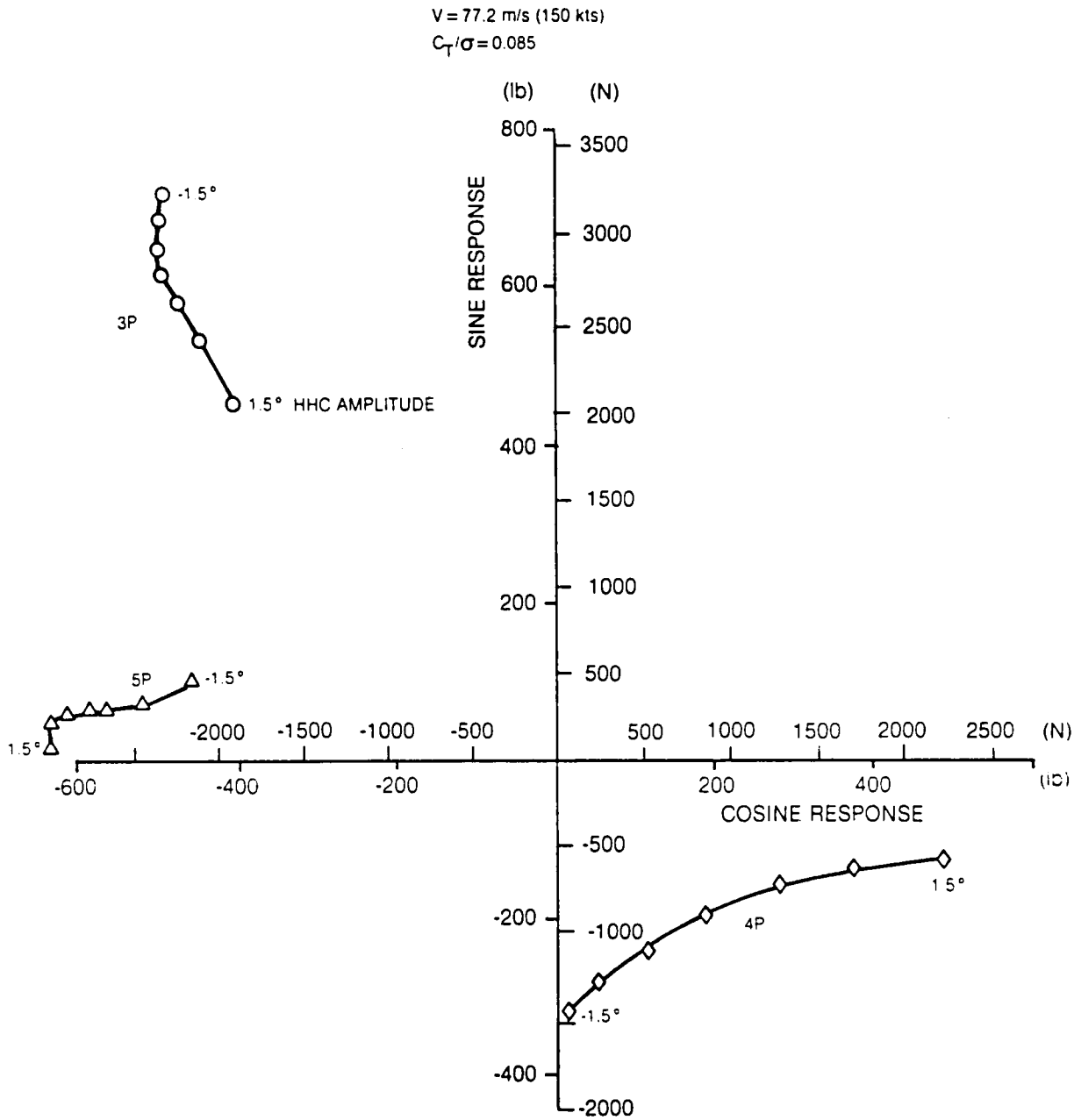

Fig. A-13 Single Blade Vertical Root Shear Response to 3P Sine HHC + Optimal Controller HHC (Case 10)

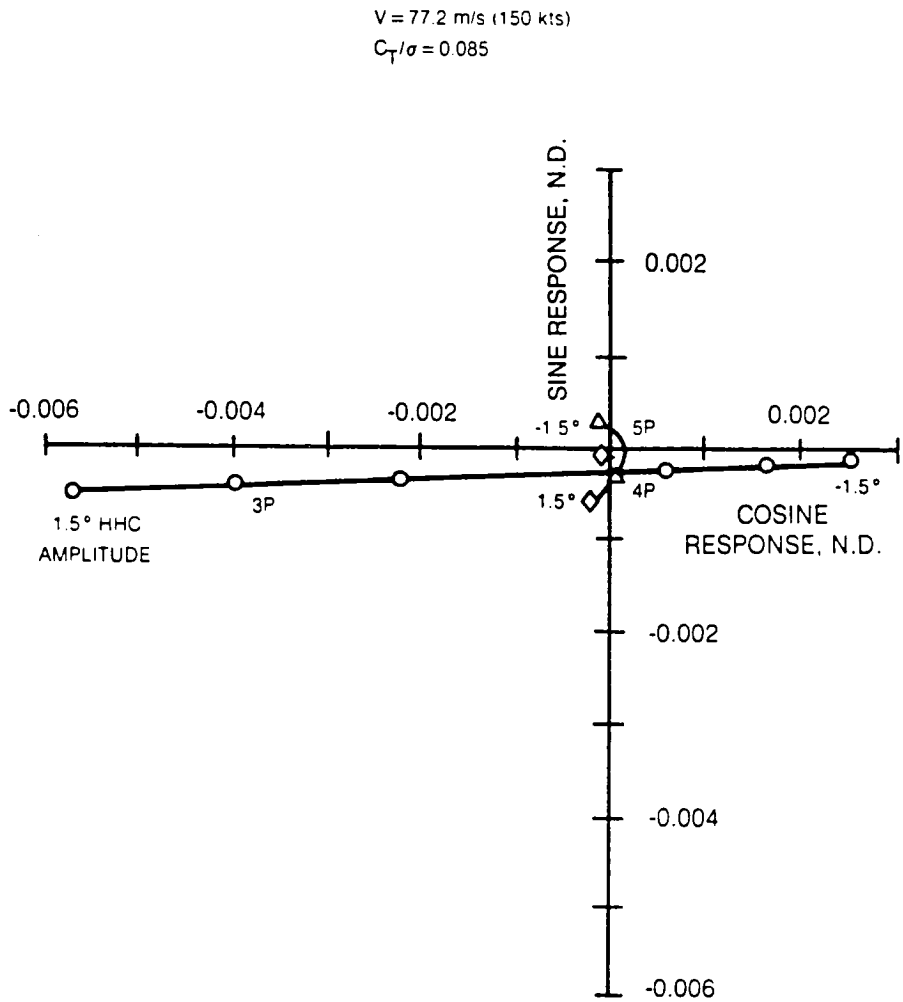

Fig. A-14 Blade First Flatwise Bending Mode (Q_{W_1}) Response to 3P Sine HHC (Case 2)

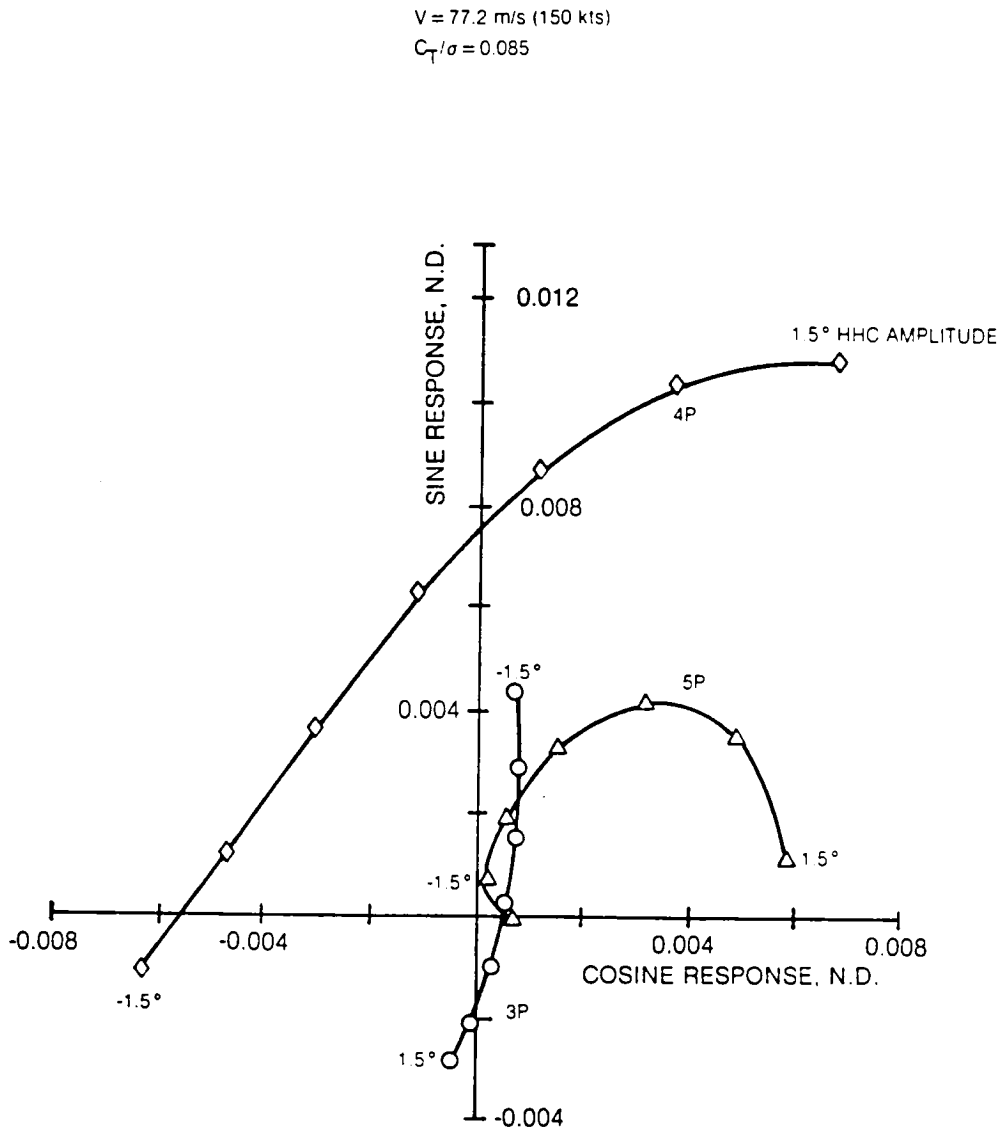

Fig. A-15 Blade Second Flatwise Bending Mode (Q_{w_2}) Response to 3P Sine HHC (Case 2)

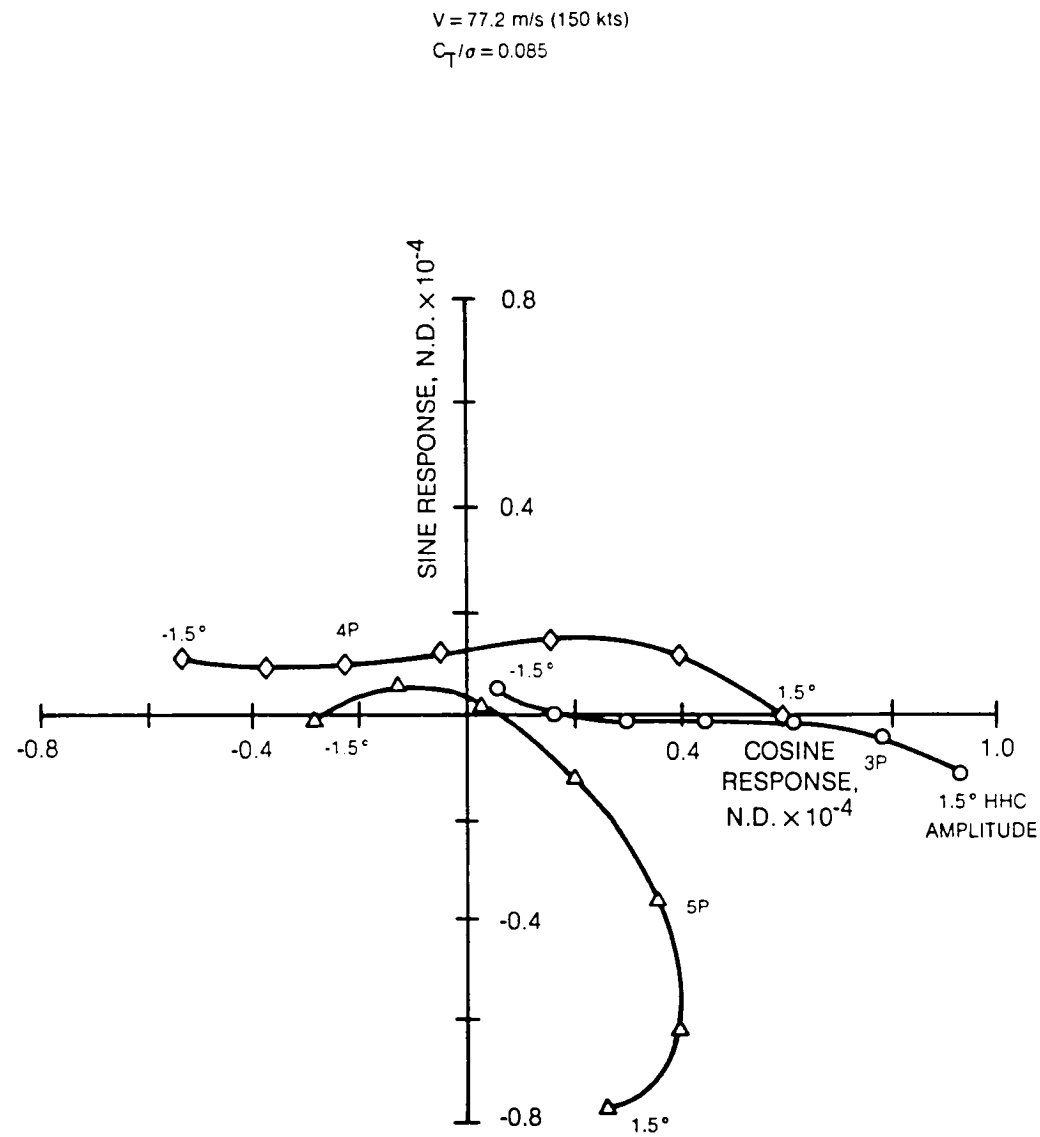

Fig. A-16 Blade Third Flatwise Bending Mode (Q_{w_3}) Response to 3P Sine HHC (Case 2)

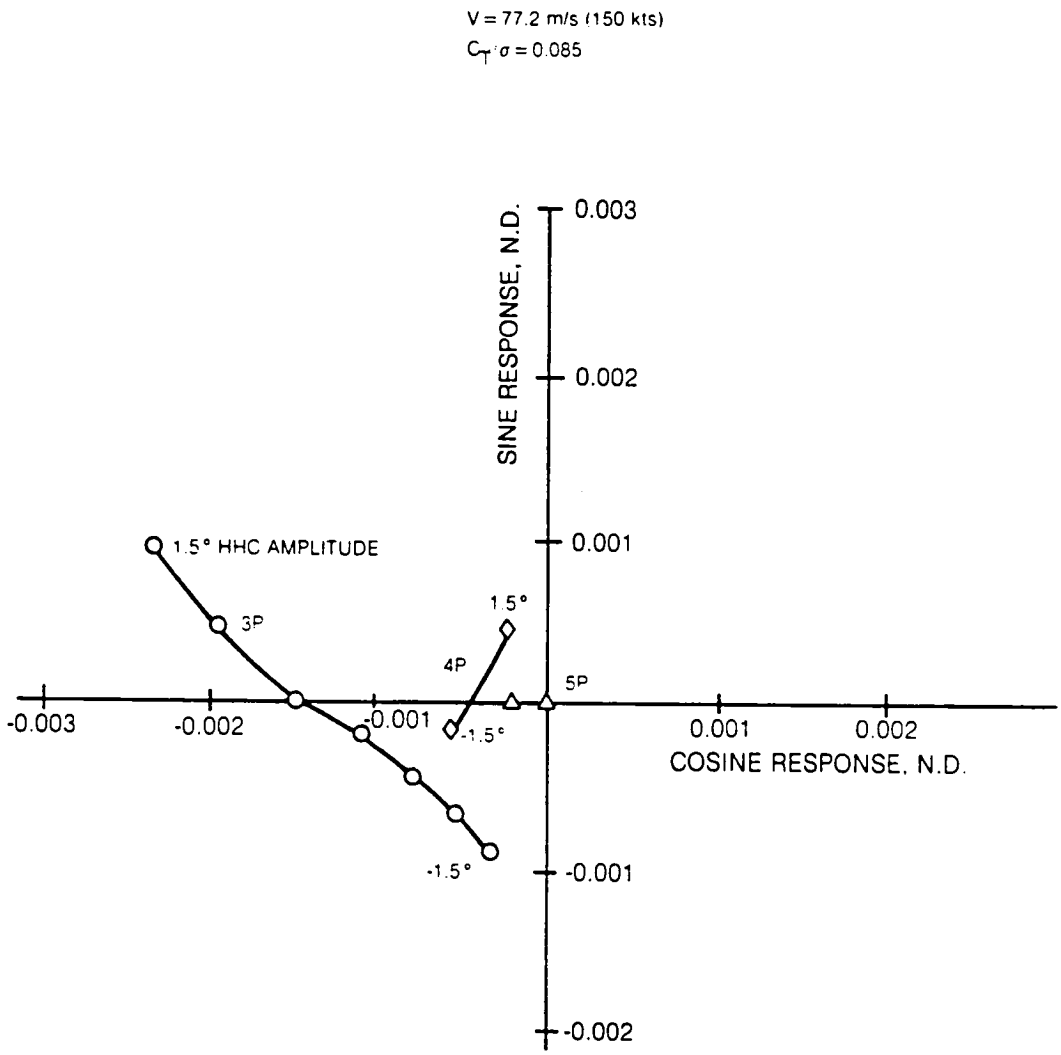

Fig. A-17 Blade First Edgewise Mode (Q_{v_1}) Response to 3P Sine HHC (Case 2)

V = 77.2 m/s (150 kts)
$C_T/\sigma = 0.085$

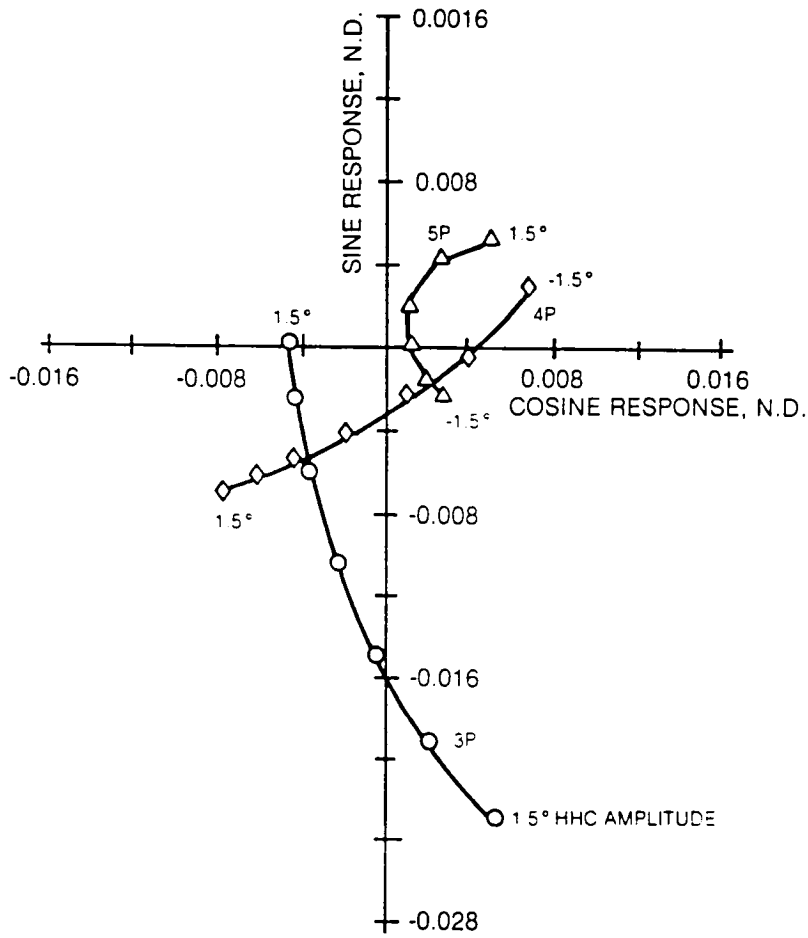

Fig. A-18 Blade 1st Torsion Mode (Q_{t_1}) Response to 3P Sine HHC (Case 2)

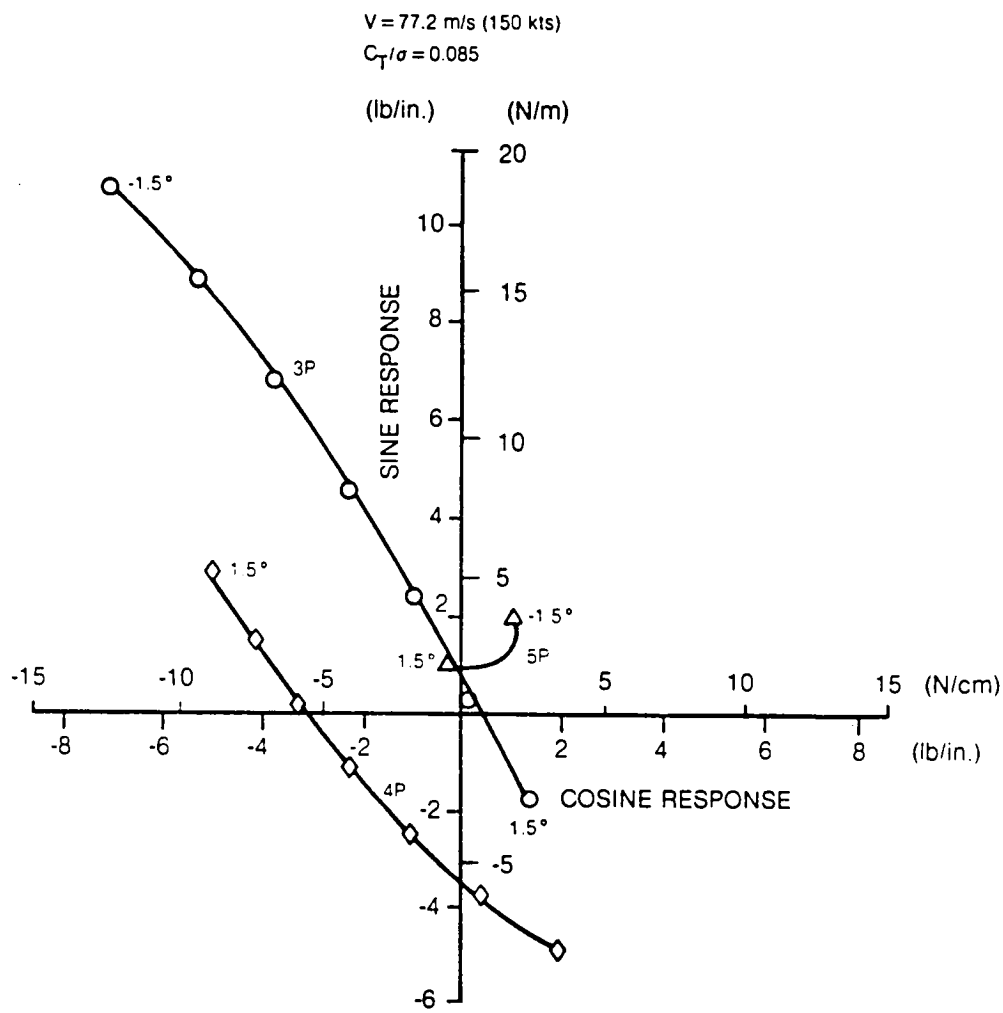

Fig. A-19 Blade Out-Of-Plane (0.78R) Airloads Response to 3P Sine HHC (Case 2)

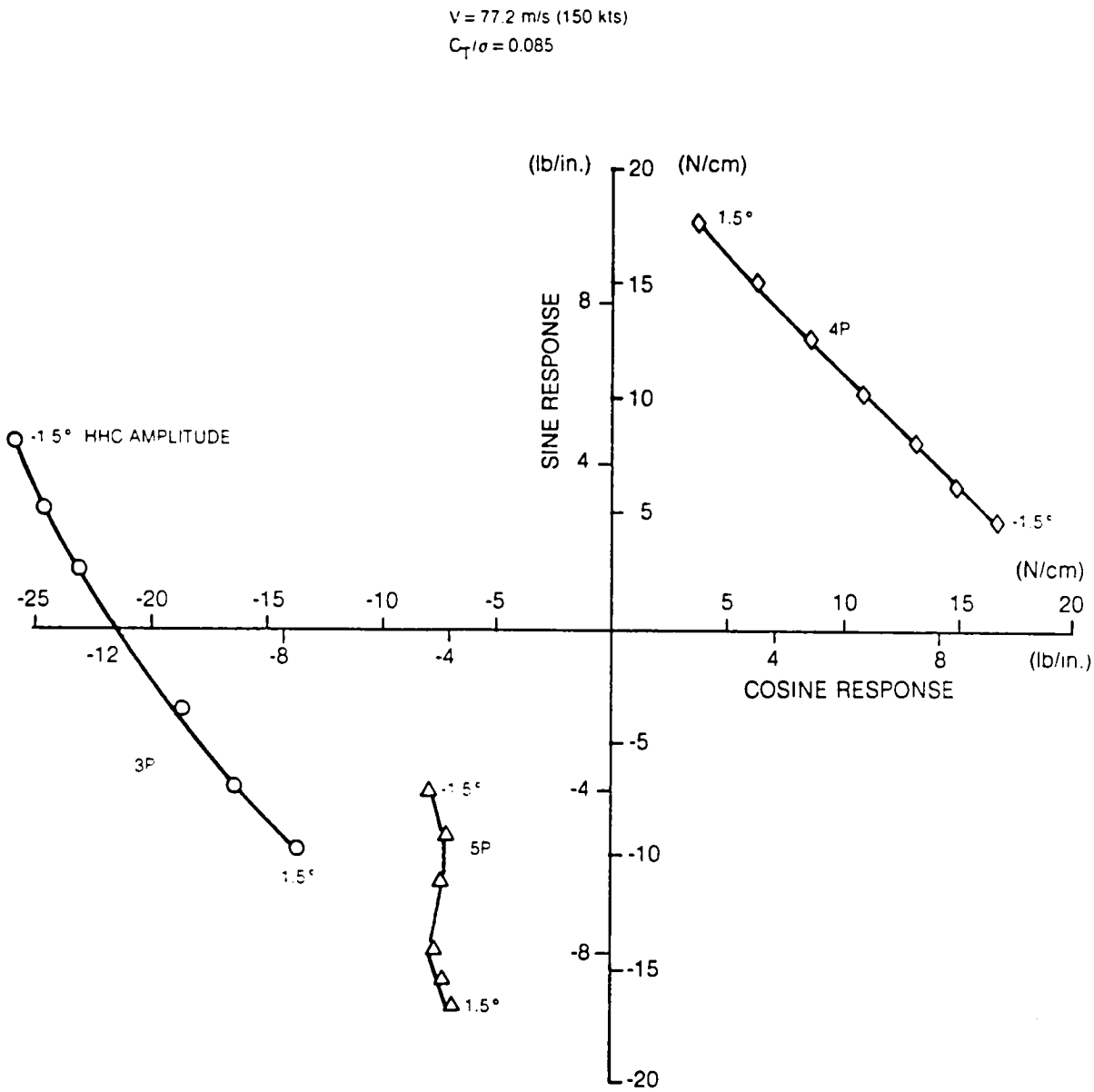

Fig. A-20 Blade Out-Of-Plane (0.78R) Airloads Response to 3P Sine HHC + Controller-Optimized HHC (Case 10)

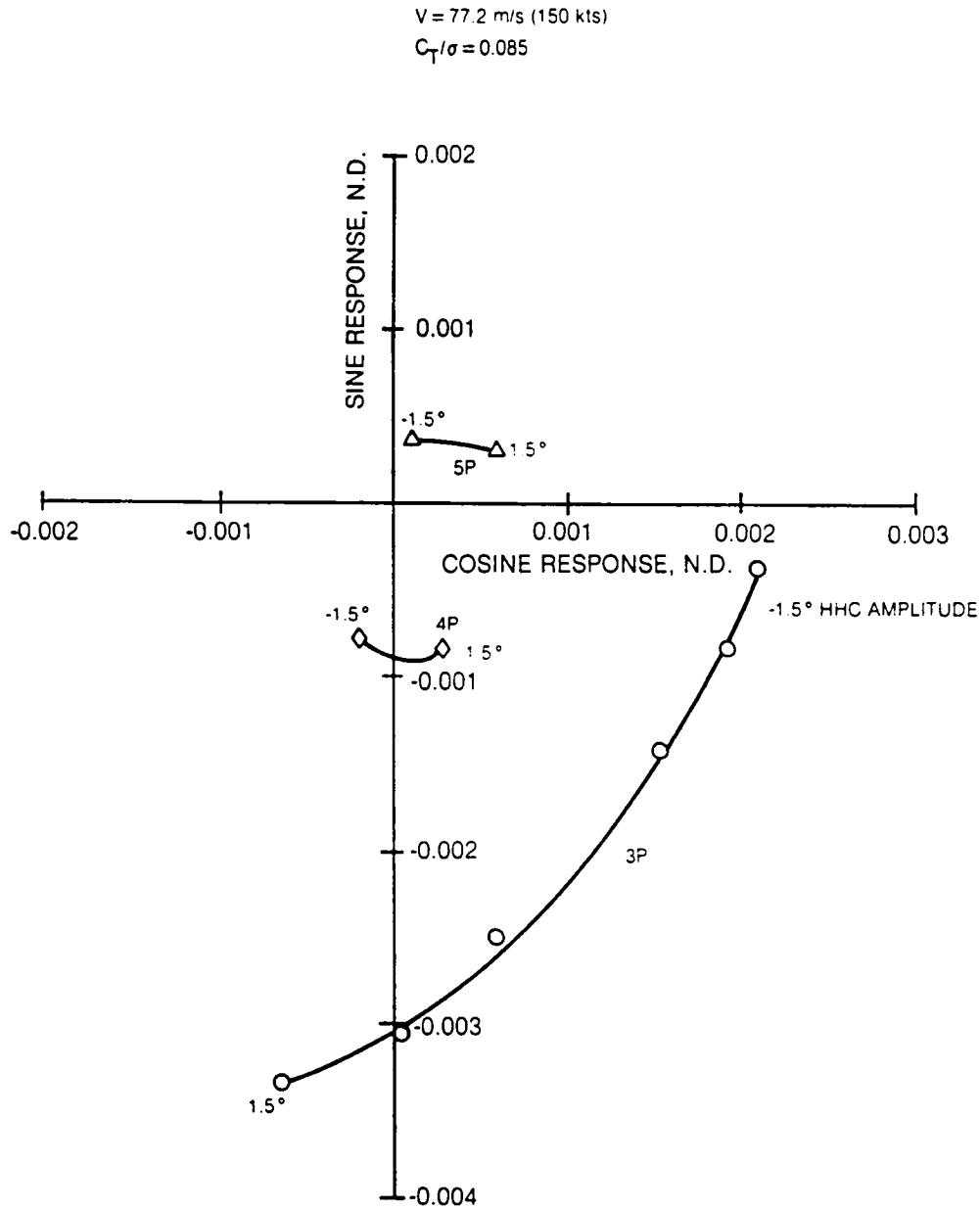

Fig. A-21 Blade First Flatwise Bending Mode (Q_{W_1}) Response to 3P Sine HHC + Controller Optimized HHC (Case 10)

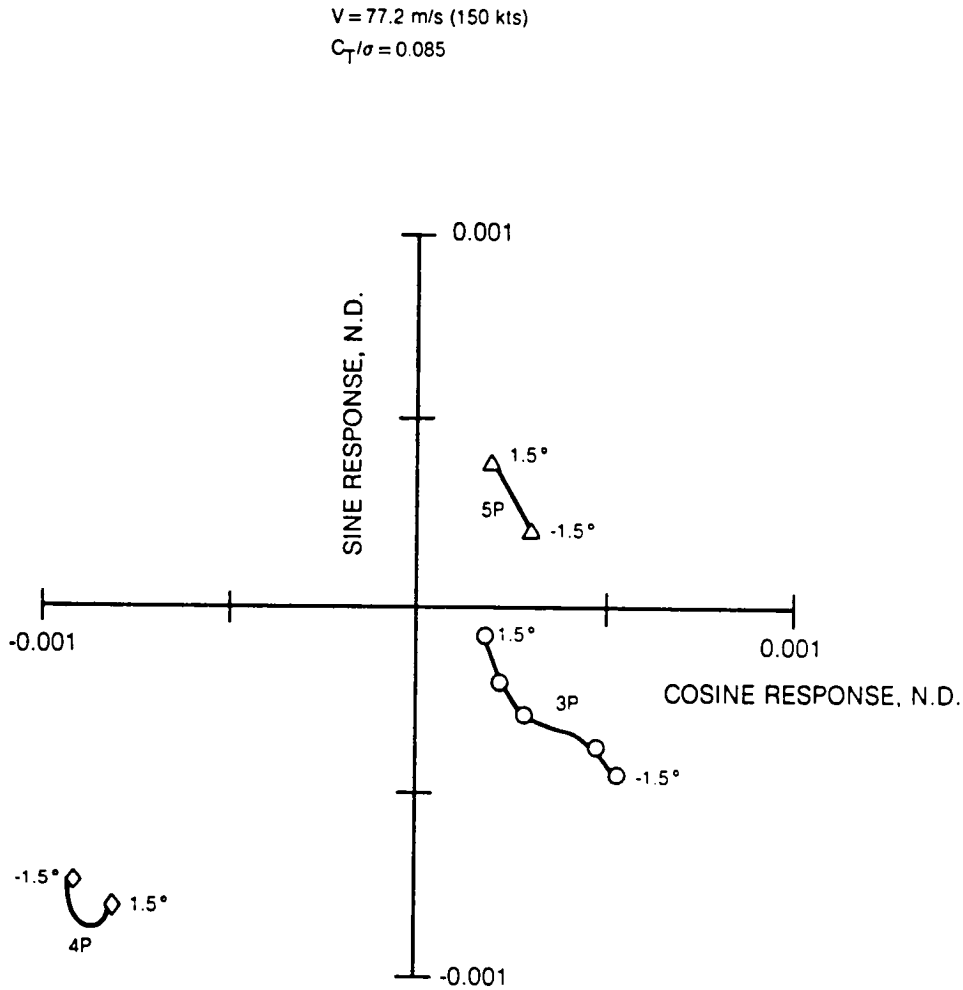

Fig. A-22 Blade First Edgewise Bending Mode (Q_{v_1}) Response to 3P Sine HHC + Controller–Optimized HHC (Case 10)

1. Report No.	2. Government Accession No.	3. Recipient's Catalog No.
NASA CR-3821		

4. Title and Subtitle	5. Report Date
Refinement and Evaluation of Helicopter Real Time Self-Adaptive Active Vibration Controller Algorithms	August 1984
	6. Performing Organization Code

7. Author(s)	8. Performing Organization Report No.
Mark W. Davis	R83-956149-16

9. Performing Organization Name and Address	10. Work Unit No.
United Technologies Research Center East Hartford, Connecticut 06108	(J.O. #) T3520
	11. Contract or Grant No. NAS2-11260

12. Sponsoring Agency Name and Address	13. Type of Report and Period Covered
National Aeronautics and Space Administration Washington, D.C. 20546	Contractor Report
	14. Sponsoring Agency Code (RTOP) 505-42-11

15. Supplementary Notes

Point of Contact: Stephen A. Jacklin, Technical Monitor (415) 965-6668
Ames Research Center, Moffett Field, CA 94035

16. Abstract

A Real-Time Self-Adaptive (RTSA) active vibration controller was used as the framework in developing a computer program for a generic controller that can be used to alleviate helicopter vibration. Based upon on-line identification of system parameters, the generic controller minimizes vibration in the fuselage by closed-loop implementation of higher harmonic control in the main rotor system. The new generic controller incorporates a set of improved algorithms that gives the capability to readily define many different configurations by selecting one of three different controller types (deterministic, cautious, and dual), one of two linear system models (local and global), and one or more of several methods of applying limits on control inputs (external and/or internal limits on higher harmonic pitch amplitude and rate). A helicopter rotor simulation analysis was used to evaluate the algorithms associated with the alternative controller types as applied to the four-bladed H-34 rotor mounted on the NASA Ames Rotor Test Apparatus (RTA) which represents the fuselage. After proper tuning all three controllers provide more effective vibration reduction and converge more quickly and smoothly with smaller control inputs than the initial RTSA controller (deterministic with external pitch-rate limiting). It is demonstrated that internal limiting of the control inputs significantly improves the overall performance of the deterministic controller. Excellent controller performance is demonstrated for all three controllers throughout a range of steady flight conditions representing moderate to high flight speeds and thrust values. Reduction in vibration from 75 to 95 percent is achieved with amplitudes of higher harmonic control (3, 4, and 5 per rev) of less than one degree. Good transient performance and vibration alleviation is exhibited for short term transient maneuvers involving a sudden change in collective pitch; however, some retuning is required. Also, the existence of multiple higher harmonic control solutions for low vibration indicates the potential for the selection of control inputs that reduce the negative impact on blade stresses and rotor performance.

17. Key Words (Suggested by Author(s))	18. Distribution Statement
Higher Harmonic Control Adaptive Active Helicopter Vibration Control Helicopter Controller Algorithms	Unclassified - Unlimited Subject Category 02

19. Security Classif. (of this report)	20. Security Classif. (of this page)	21. No. of Pages	22. Price*
Unclassified	Unclassified	284	A13

*For sale by the National Technical Information Service, Springfield, Virginia 22161

☆U.S. GOVERNMENT PRINTING OFFICE:1984 -739 -010/ 22

National Aeronautics and
Space Administration

Washington, D.C.
20546

Official Business
Penalty for Private Use, $300

SPECIAL FOURTH CLASS MAIL
BOOK

Postage
National Aeronautics and
Space Administration
NASA

U.S.MAIL

NASA

POSTMASTER: If Undeliverable (Section 158
Postal Manual) Do Not Return